

Modeling, Robust and Distributed Model Predictive Control for Freeway Networks

Shuai Liu

Cover illustration: Inspired by the picture 'A1-Hoog Buurlo.jpg' on Wikimedia.

Modeling, Robust and Distributed Model Predictive Control for Freeway Networks

Proefschrift

ter verkrijging van de graad van doctor
aan de Technische Universiteit Delft,
op gezag van de Rector Magnificus prof. ir. K.C.A.M. Luyben,
voorzitter van het College voor Promoties,
in het openbaar te verdedigen op maandag 30 mei 2016 om 15.00 uur
door **Shuai LIU**,
Master of Science in Aeronautical and Astronautical Science and Technology,
National University of Defence Technology,
geboren te Zhoukou, Henan, China.

This dissertation has been approved by the promotor:

Prof. dr. ir. B. De Schutter
Prof. dr. ir. J. Hellendoorn

Composition of the doctoral committee:

Rector Magnificus	chairperson
Prof. dr. ir. B. De Schutter	Technische Universiteit Delft, promotor
Prof. dr. ir. J. Hellendoorn	Technische Universiteit Delft, promotor

Independent members:

Prof. dr. S. Sacone	Università degli Studi di Genova
Prof. dr. F. Viti	Université du Luxembourg
Dr. ir. J. Sijs	TNO
Prof. dr. ir. S. Hoogendoorn	Technische Universiteit Delft
Prof. dr. R. Babuška, M.Sc	Technische Universiteit Delft

Research described in this thesis was supported by the China Scholarship Council (CSC), the Delft Center for Systems and Control, and the European COST Action TU1102.

TRAIL Thesis Series T2016/7, the Netherlands TRAIL Research School

P.O. Box 5017
2600 GA Delft, The Netherlands
T: +31 (0) 15 278 6046
T: +31 (0) 15 278 4333
E: info@rstrail.nl

Published and distributed by: Shuai Liu
E-mail: shuailiu.tud@gmail.com

ISBN 978-90-5584-199-8

Keywords: freeway networks, model predictive control, multi-class macroscopic traffic models, scenario-based receding-horizon parameterized control, scenario-based distributed model predictive control

Copyright © 2016 by Shuai Liu

All rights reserved. No part of the material protected by this copyright notice may be reproduced or utilized in any form or by any means, electronic or mechanical, including photocopying, recording or by any information storage and retrieval system, without written permission of the author.

Printed in the Netherlands

Preface

After working on my PhD project for several years, finally it is time to write the preface of my dissertation. I cannot help looking back upon the past several years in the Netherlands. Many people have helped me during my journey pursuing the doctoral degree.

First of all, I would like to express my deepest appreciation to my supervisors Prof. Bart De Schutter and Prof. Hans Hellendoorn. Bart has always been nice and patient with me. He helped me both on my research and on other difficulties that I experienced. He encouraged me a lot when things were not going so well. I also appreciate Hans very much for the discussions with him and for encouraging me with nice words.

Then, I would like to sincerely thank my supervisor Prof. Yulin Zhang in National University of Defense Technology, China. Under the supervision of Prof. Zhang, I started to learn how to do research during my master period. Moreover, I appreciate Prof. Zhang very much for supporting me on studying overseas.

Next, my gratitude goes to Anna, José, and Alfredo for their helps on my research. I appreciate them for their suggestions on improving my papers. Moreover, I thank Goof and Andreas for providing me a freeway network in VISSIM and necessary data for one of my case studies. I appreciate Zhe a lot for providing me the C codes for METANET.

I would like to thank the PTV group in Germany for providing me a licence for VISSIM and the TNO group in the Netherlands for providing me a license for ENVIVER. I gratefully acknowledge the China Scholarship Council for sponsoring me during my PhD period.

I would also like to express my gratitude to my PhD committee members for their time on reviewing my dissertation and for their valuable suggestions on improving my dissertation.

I have enjoyed working together with my colleagues at the Delft Center for Systems and Control for the past several years. For the nice working environment, I would like to thank Anahita, Anqi, Amir, Bart, Chengpu, Esmaeil, Edwin, Farid, Hai, Jia, Kim, Laura, Le, Mohammad, Noortje, Patricio, Reinier, Renshi, Shahrzad, Subramanya, Shuai Yuan, Vahab, Yashar, Yihui, Yiming, Yu, and Zhou, et al. I am also grateful to the secretaries for their helps.

I would like to thank all my friends in the Netherlands and in China. Your friendship makes my life much easier and more enjoyable.

At last, I would like to thank all my family members for consistently supporting me. My heartfelt thanks go to my parents for supporting me with their unconditional love. I thank my husband Huijiao Bu for understanding and encouraging me, and I never feel alone even we have been thousands of kilometers away from each other for most of the past four and half years.

Shuai Liu
Delft, May 2016

Contents

Preface	i
1 Introduction	1
1.1 Road Traffic Management	1
1.2 Problem Statement	2
1.2.1 Research Goals	2
1.2.2 Methodology	3
1.3 Contributions of the Thesis	4
1.4 Outline of the Thesis	4
2 Traffic Models and Model Predictive Control	9
2.1 Traffic Flow Models	9
2.1.1 Microscopic Traffic Flow Models	9
2.1.2 Single-Class Macroscopic Traffic Flow Models	9
2.1.3 Multi-Class Macroscopic Traffic Flow Models	10
2.1.4 Single-Class METANET Model	11
2.1.5 Basic FASTLANE Model	13
2.2 Traffic Emission and Fuel Consumption Models	15
2.2.1 Microscopic Emission and Fuel Consumption Models	15
2.2.2 Macroscopic Emission and Fuel Consumption Models	16
2.2.3 VERSIT+ Model	16
2.2.4 VT-Macro Model	17
2.3 Model Predictive Control	18
2.3.1 General Model Predictive Control	18
2.3.2 Model Predictive Control for Traffic Networks	20
2.3.3 Receding-Horizon Parameterized Control for Traffic Networks	20
2.4 Robust Model-Based Control	21
2.4.1 General Robust Model Predictive Control	21
2.4.2 Robust Model-Based Control for Traffic Networks	21
2.5 Robust Distributed Model Predictive Control	22
2.5.1 Distributed Model Predictive Control	22
2.5.2 Robust Distributed Model Predictive Control	23
2.6 Summary	24
3 Model Predictive Control Based on Multi-Class Macroscopic Traffic Models	25
3.1 Multi-Class Macroscopic Traffic Flow Models	25
3.1.1 Extensions of FASTLANE	25
3.1.2 Multi-Class METANET Model	26
3.2 Multi-Class Macroscopic Traffic Emission Models	31

3.2.1	Multi-Class VT-Macro Model	31
3.2.2	Multi-Class VERSIT+	32
3.3	MPC with End-Point Penalties	33
3.3.1	Performance Criteria	33
3.3.2	End-Point Penalties	34
3.3.3	Overall Objective Function for MPC	35
3.4	Case Study: Comparison of Multi-Class Macroscopic Traffic Models	36
3.4.1	Benchmark Network	36
3.4.2	Identification of the Model Parameters	38
3.4.3	Control Set-up	40
3.4.4	Simulation Results and Analysis	43
3.5	Summary	53
4	Scenario-Based Receding-Horizon Parameterized Control for Traffic Networks	55
4.1	RHPC Based on Multi-Class Traffic Models	55
4.1.1	RHPC Laws for Variable Speed Limits	55
4.1.2	RHPC Laws for Ramp Metering Rates	57
4.1.3	Discussions on RHPC Laws	57
4.2	Scenario-Based RHPC	58
4.2.1	Uncertainties in Demands and Traffic Compositions for Traffic Networks	58
4.2.2	Motivation for Scenario-Based RHPC	60
4.2.3	Scenario-Based RHPC Based on Multi-Class Traffic Models	61
4.3	Case Study: Assessments of Scenario-Based RHPC	62
4.3.1	Benchmark Network	62
4.3.2	Control Set-up	63
4.3.3	Simulation Results and Analysis	65
4.4	Summary	86
5	Scenario-Based Distributed Model Predictive Control for Traffic Networks	89
5.1	Global Uncertainties and Local Uncertainties in Large-Scale Traffic Networks .	89
5.1.1	Uncertainties in Large-Scale Traffic Networks	89
5.1.2	Global Uncertainties and Local Uncertainties	90
5.2	DMPC for Large-Scale Traffic Networks	91
5.2.1	Model Predictive Control for Large-Scale Traffic Networks	91
5.2.2	Decomposition of the MPC Problem for Large-Scale Traffic Networks . .	93
5.3	Scenario-Based DMPC with Global Uncertainties	93
5.3.1	Scenario-Based DMPC with Global Uncertainties on the Basis of an Expected-Value Setting	94
5.3.2	Scenario-Based DMPC with Global Uncertainties on the Basis of a Min- Max Setting	96
5.4	Scenario-Based DMPC on the Basis of a Reduced Scenario Tree of Global and Local Uncertainties	96
5.4.1	Reduced Scenario Tree of Global and Local Uncertainties	97
5.4.2	Scenario-Based DMPC on the Basis of a Reduced Scenario Tree and an Expected-Value Setting	97
5.4.3	Scenario-Based DMPC on the Basis of a Reduced Scenario Tree and a Min-Max Setting	98

5.5	Alternating Direction Method of Multipliers for Scenario-Based DMPC	99
5.5.1	Couplings between Subnetworks in ADMM	100
5.5.2	Algorithm for Scenario-Based DMPC on the Basis of ADMM	100
5.6	Case Study: Assessment of Scenario-Based DMPC	102
5.6.1	Benchmark Network	102
5.6.2	Control Settings	102
5.6.3	Results and Analysis	105
5.7	Summary	117
6	Conclusions and Future Work	119
6.1	Conclusions of the Thesis	119
6.2	Recommendations for Future Work	123
A	Computation of Jerks for Multi-Class Macroscopic Traffic Flow Models	125
B	Scenario-Based DMPC on the Basis of a Complete Scenario Tree and an Expected-Value Setting	127
	Bibliography	129
	Glossary	141
	Summary	149
	Samenvatting	151
	Curriculum Vitae	155
	TRAIL Thesis Series Publications	157

Chapter 1

Introduction

1.1 Road Traffic Management

With the development of the global economy, the amount of motor vehicles worldwide has been rapidly increasing, while the traffic infrastructure could not be easily extended due to high costs and space limitations. The large amount of motor vehicles can cause various problems in traffic networks, such as traffic accidents, traffic congestion, air pollution, etc. Traffic accidents cause safety problems, traffic congestion leads to a waste of time, and air pollution harms human health. Road traffic management [9, 91, 114] is one of the methods that can be used to address various problems in traffic networks. Road traffic management [9, 91, 114] consists of obtaining traffic information, applying traffic control, managing traffic demands and incidents, monitoring and supporting drivers, etc. Considering that travel and transportation through freeway networks are quite crucial in people's daily life, in this thesis we focus on the traffic control problem of freeway networks, where the main goal is to reduce traffic congestion and traffic emissions.

The control measures for freeway networks include speed limits, ramp metering, route guidance, and so on [47, 58, 97, 116]. Speed limits can limit the maximum speeds on freeway stretches, ramp metering can limit on-ramp traffic flows entering the mainstream roads, and route guidance can provide advices for choosing routes. In this thesis, we mainly consider Variable Speed Limits (VSL) and Ramp Metering (RM) for controlling traffic flows to reduce traffic congestion and traffic emissions for freeway networks, since VSL and RM are efficient in reducing traffic congestion and traffic emissions, and they are relatively easy to realize [94, 102, 116]. The VSL and RM rates (i.e. the control inputs) can be determined according to different traffic conditions, by means of various approaches, e.g. feedback control, optimal control, model predictive control, and so on. In conventional feedback control [57, 96], the control inputs for freeway networks are determined by feedback control laws, with parameters for the control laws computed a priori. In optimal control approaches [5, 61, 90], the control inputs for freeway networks are determined by solving optimization problems, i.e. the optimization of performance criteria defined over some period. In model predictive control [22, 37, 50, 79, 85, 98] for freeway networks, the control inputs are determined by solving an optimization problem with an objective function defined over some prediction period, with the latest measurements of traffic variables taken into account and a receding-horizon scheme applied.

1.2 Problem Statement

1.2.1 Research Goals

In order to reduce traffic congestion and traffic emissions in freeway networks by means of traffic control, it is helpful to improve the accuracy of traffic models that describe traffic dynamics and traffic emissions. Traffic flows comprise of individual vehicles, and the dynamics and emissions of individual vehicles could be described according to the characteristics of individual vehicles. However, due to the large amount of vehicles, it is time consuming to describe the dynamics and emissions of individual vehicles. The computational complexity can be reduced by describing the dynamics and emissions of multiple vehicles in an aggregated way, instead of considering individual vehicles. Traffic dynamics and traffic emissions can be aggregated for all classes of vehicles (e.g. cars, and trucks). However, in this case the differences between different classes of vehicles cannot be described. Thus dynamical characteristics (e.g. free flow speed, and capacity) that differ for different vehicle classes cannot be captured. In this thesis, we aim to extend several traffic flow models and traffic emission models so that the specific characteristics of each vehicle class can be captured.

Various uncertainties exist in freeway networks, and the uncertainties affect the performance of the freeway networks. Robust control approaches take into account uncertainties when determining the control inputs, and they can be used to handle uncertainties in freeway networks. Since the dynamics of traffic flows are usually considered to be nonlinear and nonconvex, it is challenging to develop robust control approaches for freeway networks, due to the complexity of the nonlinear-nonconvex dynamics. Furthermore, the computational complexity will be high for large-scale freeway networks. However, they can be divided into small subnetworks for reducing the computational complexity. In this case, developing robust approaches will involve extra challenges, such as accounting for the effects of uncertainties for neighboring subnetworks. In this thesis, we aim to develop a robust control approach that can handle uncertainties for freeway networks, and a robust control approach based on multiple controllers for large-scale freeway networks that takes into account uncertainties for the entire freeway networks.

The research goals are listed as follows:

- Improve the accuracy of traffic flow models and traffic emission models by extending multi-class traffic flow models and traffic emission models, where the characteristics of each vehicle class can be captured.
- Improve the performance of freeway networks by developing a robust control approach with uncertainties being taken into account in the control procedure, considering schemes that can reduce the computational complexity of the robust control problem.
- Improve the performance of a large-scale freeway network by developing a robust distributed control approach, where uncertainties in freeway networks and the computational load of the robust distributed control problem are taken into account in the control design process.

1.2.2 Methodology

For reaching the research goals, the methodologies that are considered in this thesis are listed next:

- **Model Predictive Control**

In this thesis, the basic approach that is used for controlling freeway networks is Model Predictive Control (MPC) [22, 79, 85]. The MPC approach is based on dynamic prediction and a receding-horizon scheme. The future performance of the controlled system over a prediction period is predicted through traffic models, and the predicted performance is optimized by solving an optimization problem, yielding an optimal control input sequence over a control period, which is covered by the prediction period. After that, the first element of the optimal control input sequence is applied to the controlled system, and the prediction period is shifted one control step ahead. In MPC, the measurements of traffic variables are taken into account for determining the optimal control input sequence; thus MPC could be considered to be a closed-loop control approach. MPC can be used for nonlinear-nonconvex systems, and for handling multi-objective optimization problems and constrained optimization problems.

- **Parameterized Model Predictive Control**

Parameterized MPC [34, 86, 130] is an extension of standard MPC. More specifically, in parameterized MPC, the control inputs are described using control laws that are functions of the system states and outputs. In the control procedure, the parameters of the control laws are optimized so as to optimize the predicted performance. The time step length for updating the parameters of the control laws can be different from the time step length for updating the control inputs; thus the parameters can be considered to be constant over the prediction period, while the control inputs can still vary due to the variations of system states and outputs. The Parameterized MPC approach can be applied for the sake of reducing the number of optimization variables in optimization problems to be solved, so that the computational load can be reduced w.r.t. the standard MPC approach.

- **Scenario Approach for Robust Control**

In the scenario approach for robust control [19], only a finite number of scenarios for uncertainties are accounted for when designing robust control approaches. For linear systems with convex constraints, Calafiore and Campi [19] established a bound on the number of uncertainty scenarios needed for achieving a specified probabilistic robustness level, which is defined as an upper bound of the probability of violation of constraints; moreover, they showed that the bound only increases slowly with the increase of the specified probabilistic robustness level. The scenario approach is an efficient way for reducing the computational complexity in robust control problems. Further analyses and applications of the scenario-based scheme can be found in [13, 20, 111, 131]. In this thesis, we apply the scenario approach for designing robust control approaches for freeway networks.

- **Distributed Model Predictive Control**

Distributed Model Predictive Control (DMPC) [24, 27] involves multiple controllers for controlling a large-scale system that can be divided into multiple subsystems.

Each of these controllers is used for controlling a subsystem, which is a part of the considered large-scale system. Particularly, the large optimization problem for a large-scale system is decomposed into small local optimization problems, which are solved by local controllers. By adopting the DMPC approach, the computational complexity of the control problem for large-scale systems can be reduced. In this thesis, we apply DMPC for controlling large-scale freeway networks, in combination with the scenario approach for handling uncertainties.

1.3 Contributions of the Thesis

The main contributions of this thesis are listed below:

- We extend several multi-class macroscopic traffic flow models and traffic emission models. In particular, we extend a multi-class version of METANET, extend FASTLANE with variable speed limits and ramp metering, integrate VT-macro with multi-class traffic flow models, and extend a multi-class macroscopic version of VERSIT+. Moreover, we compare these models by means of a case study.
- End-point penalties, which are included in the objective function for MPC to take into account the control performance beyond the prediction period, are developed for Model Predictive Control (MPC) of freeway networks, and the effectiveness of the end-point penalties is evaluated by simulations.
- A scenario-based Receding-Horizon Parameterized Control (RHPC) approach is proposed for controlling freeway networks in the presence of uncertainties, and the effectiveness of the scenario-based RHPC approach is investigated via a simulation experiment.
- We develop a scenario-based Distributed Model Predictive Control (DMPC) approach for large-scale freeway networks based on a reduced scenario tree, and evaluate the effectiveness of the proposed scenario-based DMPC approach by a numerical experiment.

1.4 Outline of the Thesis

For a brief overview, the structure of this thesis is shown in Figure 1.1. There are 6 chapters in this thesis, including the current chapter about the introduction of this thesis. Chapter 2 reviews traffic models, MPC, robust model-based control, and robust DMPC. In Chapter 3, several multi-class macroscopic traffic flow models and traffic emission models are extended. Chapter 4 proposes a scenario-based RHPC approach for freeway networks. Although the scenario-based RHPC approach is developed based on the multi-class METANET model of Chapter 3, it can also be used for other multi-class traffic flow models, even for single-class traffic flow models; thus, we consider Chapter 4 to be independent of Chapter 3. In Chapter 5, we propose a scenario-based DMPC approach in order to control large-scale freeway networks in the presence of uncertainties, based on the scenario scheme that is also used in Chapter 4. Thus, Chapter 5 is considered to be an extension of the scenario scheme used in Chapter 4 to a distributed setting.

More specifically, the thesis is organized as follows:

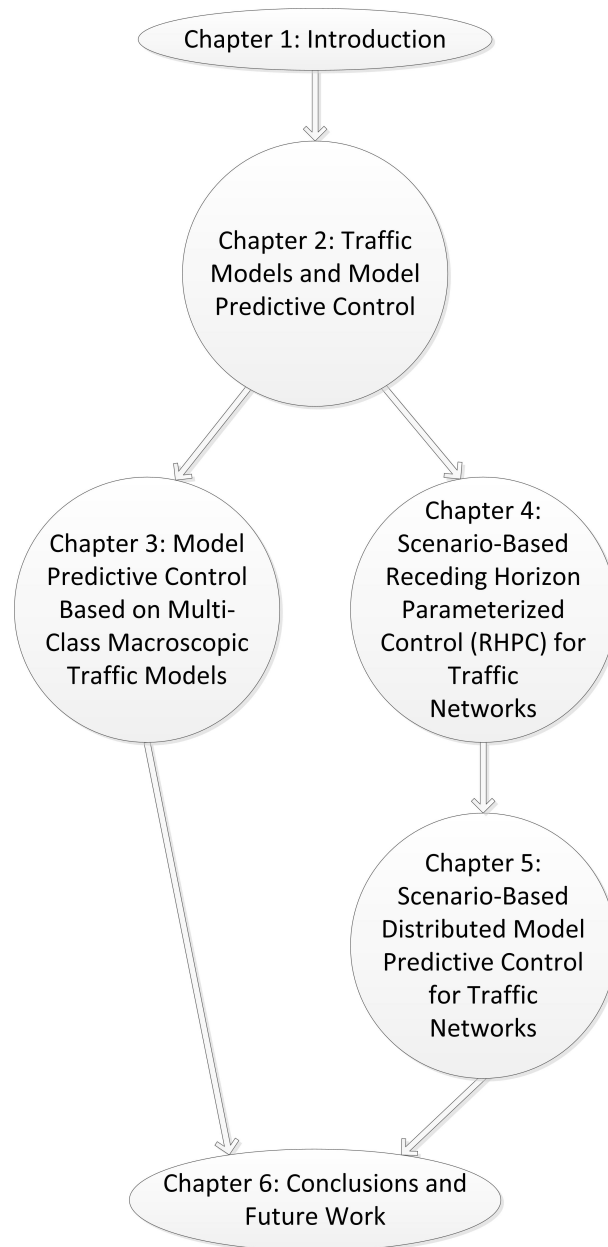


Figure 1.1: Structure of the thesis

- Chapter 2 reviews traffic models, MPC, robust model-based control, and robust DMPC. We first discuss different types of traffic flow models: microscopic traffic flow models, single-class macroscopic traffic flow models, and multi-class macroscopic traffic flow models. We also introduce the single-class macroscopic traffic flow model METANET and the multi-class macroscopic traffic flow model FASTLANE, which are used as the basis for the extensions in Chapter 3. Then we review different types of traffic emission models: microscopic traffic emission models and macroscopic traffic emission models. Moreover, we introduce the microscopic traffic emission model VERSIT+ and the macroscopic traffic emission model VT-macro, which are also used as the basis for the extensions in Chapter 3. Next, we introduce the basic concepts of MPC, recent work on MPC for traffic networks, and RHPC (i.e. parameterized MPC) for traffic networks. We also review recent work on robust model-based control, both in general and for traffic networks. After that, we review recent work on DMPC and robust DMPC, both in general and for traffic networks.
- In Chapter 3, several multi-class macroscopic traffic flow models and traffic emission models are extended. More specifically, we incorporate variable speed limits and ramp metering into the first-order multi-class traffic flow model FASTLANE, extend the second-order single-class traffic flow model METANET to a multi-class version, combine VT-macro with multi-class traffic flow models, and extend VERSIT+ to a multi-class macroscopic version. We also propose to include end-point penalties in the objective function of MPC for the considered freeway network, in order to improve the control effectiveness without significantly increasing the computational load. After that, we present a case study for evaluating the extended multi-class traffic flow models and multi-class traffic emission models, with both the total time spent and the total emissions included in the MPC objective function. In this case study, the effectiveness of the end-point penalties is also evaluated by simulations. The simulation results show that for multi-class METANET in combination with emission models, the weighted sum of the TTS and the TE can be reduced, with the maximum queue length dynamics being captured better than for FASTLANE; moreover, including the end-point penalties can further improve the total performance. However, for FASTLANE in combination with emission models, even when the end-point penalties are included, the performance for the TTS and the TE is still worse than that for the no-control case, and the queue length constraint violations are still relatively large. Our publications relating to this chapter include [68–70, 72, 101].
- In Chapter 4, a scenario-based RHPC approach for freeway networks is proposed in order to handle uncertainties. We first develop several RHPC laws for variable speed limits and ramp metering rates based on the multi-class setting, and present some considerations for the RHPC laws. Next, we describe uncertainties in demands and traffic compositions for traffic networks, and present the motivations for proposing the scenario-based RHPC approach. After that, we propose the scenario-based RHPC approach by considering a limited number of uncertainty scenarios for dealing with the robust control problem. In the scenario-based RHPC approach, a queue length constraint penalty is considered to avoid infeasibility problems. Moreover, the scenario-based RHPC approach is based on a min-max setting, in which the worst case of the sum of the control objective function and the queue length constraint violation penalty is optimized. At last, we include a case study for evaluating the

effectiveness of scenario-based RHPC, by comparing it with nominal RHPC and standard control. The simulation results show that scenario-based RHPC is effective in improving the control performance, with minor queue length constraint violations, while for nominal RHPC and standard control in general there are either relatively large queue length constraint violations or only minor performance improvements. The work presented in this chapter has been published in [71, 73].

- In Chapter 5, a scenario-based DMPC approach is proposed for controlling large-scale freeway networks with uncertainties taken into account. We first describe uncertainties in large-scale traffic networks, and distinguish global uncertainties for the overall network from local uncertainties for individual subnetworks. Then, we present DMPC for large-scale traffic networks, including MPC for large-scale traffic networks and the decomposition of MPC for large-scale traffic networks. Next, based on an expected-value setting and a min-max setting, we first include global uncertainties into the scenario-based DMPC problem, and then we propose to include local uncertainties in the scenario-based DMPC problem by defining a reduced scenario tree instead of a complete scenario tree. Afterwards, we embed the DMPC algorithm Alternating Direction Method of Multipliers (ADMM) into the scenario-based DMPC approach based on the reduced scenario tree. In the end of Chapter 5, we present a case study for investigating the effectiveness of the scenario-based DMPC approach based on the reduced scenario tree, in comparison with nominal DMPC and the scenario-based DMPC approach based on the complete scenario tree. The simulation results indicate that for both the expected-value setting and the min-max setting, scenario-based DMPC based on the reduced scenario tree can improve the total performance w.r.t. the no-control case, with the queue length constraints being satisfied. However, nominal DMPC could not improve the total performance w.r.t. to the no-control case, owing to violation of the queue length constraints. The work of this chapter has been summarized in [74].
- In Chapter 6, we conclude the thesis, and give some recommendations for future work.

Chapter 2

Traffic Models and Model Predictive Control

In this chapter we review some previous work on traffic flow models, traffic emission models, model predictive control, robust model-based control, and robust distributed model predictive control.

2.1 Traffic Flow Models

2.1.1 Microscopic Traffic Flow Models

Microscopic traffic flow models [10, 120] describe the dynamical behaviors of individual driver-vehicle pairs, including accelerating, decelerating, maintaining speeds and gaps to leading vehicles, lane changing, and so on. In the past several decades, many microscopic traffic flow models have been developed for describing traffic phenomena occurring in reality, and a lot of effort has been focused on the calibration and validation of microscopic traffic flow models, such as in [8, 18, 53, 106]. Based on microscopic traffic flow models, some traffic flow simulators have been developed by different institutions, e.g. VISSIM developed by PTV Group, Germany, and SUMO developed by the German Aerospace Center, Germany.

Microscopic traffic flow models are capable of describing the characteristics of individual vehicles; thus they can simulate flow dynamics in traffic networks in a detailed way. Microscopic traffic flow models are often used as process models for evaluating the effectiveness of the control approaches for traffic networks. However, when online model-based control is applied, the computational burden for using microscopic traffic flow models for determining the control inputs is quite large, making the implementation of model-based control intractable. Instead, macroscopic traffic flow models, which describe traffic flows in a macroscopic way, are often used for determining the control inputs in model-based control for traffic networks.

2.1.2 Single-Class Macroscopic Traffic Flow Models

In macroscopic models, traffic flows are often considered to be similar to fluid or gas flows; thus, the dynamics of traffic flows are described through aggregated traffic variables for vehicles, including density, mean speed, flow, and so on, and the aggregated traffic variables

vary with space and time [10, 120]. Macroscopic traffic flow models can reproduce some collective phenomena occurring in real traffic networks, such as the propagation of shock waves [120]. In the past decades, various single-class macroscopic models have been developed for describing traffic flows, by assuming that all vehicles in the considered traffic network have the same physical characteristics, i.e. the difference between different classes of vehicles is ignored. The different classes of vehicles refer to cars, buses, vans, trucks, and so on. According to the number of independent state variables (i.e. the order of a traffic flow model), the existing single-class macroscopic traffic flow models can be classified as first-order models [65, 109, 124], second-order models [103, 124], or models with even higher orders [52, 54]. In this thesis we mainly focus on first-order models and second-order models. Therefore, we only review some previous work on first-order models and second-order models in the following two paragraphs.

First-order traffic flow models describe the relationship between flow (or speed) and density through static fundamental functions, which were first proposed in the Lighthill-Whitham-Richards (LWR) model [65, 109]. In the LWR model, flow (or speed) is assumed to be uniquely determined by density, i.e. once density is known, flow (or speed) can be determined from a static fundamental function. Some other first-order traffic flow models are also available in the literature, e.g. the Cell Transmission Model (CTM) [30, 31]. For example, the CTM model of [30] is a discrete approximation of the LWR model, including a set of difference equations for updating traffic variables at every time step; the shape of the flow-density fundamental diagram is an isosceles trapezoid.

In second-order traffic flow models, there are two independent state variables: the speed and the density. The earliest second-order macroscopic traffic flow model is the Payne-Whitham (PW) model [103, 124], where compared to the LWR model one more equation (i.e. an acceleration equation) is included for computing the speed. The METANET model [60, 84] is another second-order macroscopic traffic flow model, where a relaxation term, a convection term, and an anticipation term are used for updating the speed. According to the literature [7, 49, 51, 93], in general second-order models are more accurate than first-order models, due to the fact that second-order models can avoid certain non-realistic phenomena generated in first-order models. For instance, at the head and tail of shock waves (or traffic jams), the abrupt change in speed resulting from the large change in density in first-order traffic flow models does not correspond to reality; however, this abrupt change can be avoided in second-order traffic flow models. Besides, in first-order traffic flow models the tail of a shock wave has a higher speed than the high-density body of the shock wave, and the tail will catch up with the body, causing an unrealistically sharp rear end of the shock wave, which can be avoided in second-order traffic flow models. In addition, first-order models cannot reproduce capacity drop near on-ramps and in shock waves, while second-order models can reproduce this capacity drop.

2.1.3 Multi-Class Macroscopic Traffic Flow Models

Some first-order multi-class macroscopic traffic flow models have been developed by researchers. Wong and Wong [125] extended the LWR model [65, 109] to a multi-class version, in which the essential characteristics of each vehicle class remain unchanged, i.e. the states of a vehicle class depend on the fundamental diagram of that vehicle class and the total density. Wong and Wong [125] validated that the multi-class LWR model can

reproduce some traffic phenomena that the single-class LWR model cannot reproduce, e.g. two-capacity phenomena, hysteresis phenomena of phase transition, and platoon dispersion. Logghe [75, 76] also developed a multi-class version of the LWR model, where each class is subject to its own fundamental diagram, and is considered to be limited within an assigned space of the road. Van Lint et al. [122, 123] proposed the FASTLANE model, which is a first-order multi-class macroscopic model. Here dynamic passenger car equivalents are used to describe different vehicle classes, taking into account the differences in the space occupied by a vehicle class under different traffic conditions (e.g. different densities). Schreiter et al. [112] proposed a multi-class controller based on FASTLANE, specifically rerouting the different traffic classes, and showed that a multi-class controller can improve the control performance more than a single-class controller.

The second-order model METANET has also been extended to multi-class by some researchers. Caligaris et al. [21] extended the macroscopic model described in [92] by accounting for two different vehicle classes. They used the steady-state relation between speed and density for representing the interference between these two vehicle classes they used. Deo et al. [35] proposed a multi-class version of the METANET model [60, 84] in which passenger car equivalents are used to represent different vehicle classes. For the multi-class METANET model of Deo et al. [35], the total effective density, the joint maximum density, and the joint critical density are considered to be the same for all vehicle classes. Two options are considered by Deo et al. [35] for computing the desired speeds for different vehicle classes. *One option* is to use the convex combination of all class-dependent fundamental diagrams, limited by the desired speed of the given vehicle class; *the other option* is to use the same approach as in FASTLANE: when the total effective density is larger than the joint critical density, the fundamental diagrams are the same for all vehicle classes; otherwise, the fundamental diagrams for different vehicle classes depend on class-dependent free-flow speeds. Pasquale et al. [102] extended the METANET model to a two-class version, where a conversion factor between cars and trucks, which is analogous to passenger car equivalents, is used for describing different vehicle classes. Similarly to [35], the total density, the maximum density, and the critical density in terms of cars are considered to be the same for both cars and trucks. However, in [102] the desired speed of a vehicle class is defined by means of the desired speed function of that vehicle class, based on class-specific parameters, the maximum density, and the total density; this is different from the above two options for defining the fundamental relationship between the desired speed and density for a vehicle class in [35].

2.1.4 Single-Class METANET Model

The METANET model [60, 84] is a second-order macroscopic model that describes traffic flows in traffic networks. In METANET, links (indexed by m) are used for representing freeway stretches without major change in road geometry, and each link is divided into several homogenous segments (indexed by i). Traffic flows enter the considered traffic network through origins (e.g. mainstream origins and on-ramps), and leave the considered traffic network by arriving at destinations (e.g. mainstream destinations and off-ramps). Moreover, nodes (indexed by o) include more than one upstream links (e.g. on-ramps) or more than one downstream links (e.g. off-ramps).

In single-class METANET [60, 84], all vehicles are assumed to belong to the same class with the same characteristics. The traffic dynamics of segments are described through *flows*

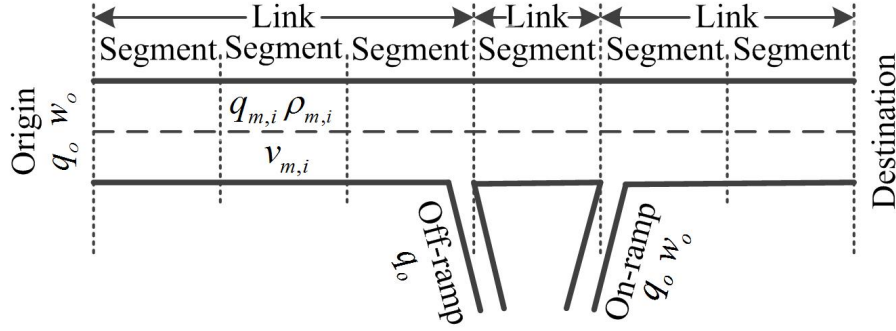


Figure 2.1: An illustrative freeway network

($q_{m,i}$), densities ($\rho_{m,i}$), and speeds ($v_{m,i}$). The traffic dynamics of origins are described through *origin flows* (q_o) and *queue lengths* (w_o) at origins, etc. Figure 2.1 shows an illustrative freeway network consisting of several links, one mainstream origin, one mainstream destination, one on-ramp, and one off-ramp, including the corresponding traffic variables.

Remark 2.1 Note that the METANET model involves a time and space discretization. For traffic flow models based on discrete space and time, the Courant-Friedrichs-Lewy (CFL) condition [28] is often considered in order to ensure the stability. In particular, no vehicle should cross a segment in one simulation time step T [49], i.e.

$$T \leq \min_{m \in I_{\text{link}}} \frac{L_m}{v_m^{\text{free}}} \quad (2.1)$$

where v_m^{free} is the free flow speed in link m , L_m represents the length of the segments of link m , and I_{link} is the set of all links. \square

The dynamic equations for segment i of link m are as follows:

$$q_{m,i}(k) = \mu_m \rho_{m,i}(k) v_{m,i}(k) \quad (2.2)$$

$$\rho_{m,i}(k+1) = \rho_{m,i}(k) + \frac{T}{L_m \mu_m} (q_{m,i-1}(k) - q_{m,i}(k)) \quad (2.3)$$

$$\begin{aligned} v_{m,i}(k+1) = & v_{m,i}(k) + \frac{T}{\tau_m} (V_m(\rho_{m,i}(k)) - v_{m,i}(k)) \\ & + \frac{T}{L_m} v_{m,i}(k) (v_{m,i-1}(k) - v_{m,i}(k)) \\ & - \frac{T \eta_m}{L_m \tau_m} \frac{\rho_{m,i+1}(k) - \rho_{m,i}(k)}{\rho_{m,i}(k) + \kappa_m} \end{aligned} \quad (2.4)$$

$$V_m(\rho_{m,i}(k)) = v_m^{\text{free}} \exp\left(-\frac{1}{a_m} \left(\frac{\rho_{m,i}(k)}{\rho_m^{\text{crit}}}\right)^{a_m}\right) \quad (2.5)$$

in which k is the time step counter corresponding to the time instant $t = kT$, T is the simulation time interval, μ_m is the number of lanes of link m , V_m represents the desired speed for link m , ρ_m^{crit} is the critical density in link m , and τ_m , η_m , κ_m , and a_m are model parameters. The desired speed equation including a variable speed limit can be defined as

follows [50]:

$$V_m(\rho_{m,i}(k)) = \min \left(v_m^{\text{free}} \exp \left(-\frac{1}{a_m} \left(\frac{\rho_{m,i}(k)}{\rho_m^{\text{crit}}} \right)^{a_m} \right), (1 + \delta_m) v_{m,i}^{\text{SL}}(k) \right) \quad (2.6)$$

where $v_{m,i}^{\text{SL}}$ is the speed limit that is applied in segment i of link m , and $1 + \delta_m$ is the non-compliance factor in link m , which allows for modeling enforced and unenforced variable speed limits.

The flow q_o for an on-ramp origin o is described as:

$$q_o(k) = \min \left[d_o(k) + \frac{w_o(k)}{T}, C_o r_o(k), C_o \left(\frac{\rho_m^{\text{max}} - \rho_{m,1}(k)}{\rho_m^{\text{max}} - \rho_m^{\text{crit}}} \right) \right] \quad (2.7)$$

in which d_o is the demand at mainstream origin o , w_o is the queue length at mainstream origin o , C_o is the capacity of on-ramp o , r_o is the ramp metering rate at on-ramp o , $\rho_{m,1}$ is the density of the first segment of the link m that is connected to on-ramp o , and ρ_m^{max} is the maximum density of link m .

According to [50], the flow q_o for a mainstream origin o is

$$q_o(k) = \min \left(d_o(k) + \frac{w_o(k)}{T}, q_{m,1}^{\text{lim}}(k) \right) \quad (2.8)$$

with

$$q_{m,1}^{\text{lim}}(k) = \begin{cases} \mu_m \rho_m^{\text{crit}} v_{m,1}^{\text{lim}}(k) \left(-a_m \ln \left(\frac{v_{m,1}^{\text{lim}}(k)}{v_m^{\text{free}}} \right) \right)^{\frac{1}{a_m}} & \text{if } v_{m,1}^{\text{lim}}(k) < V_m(\rho_m^{\text{crit}}) \\ \mu_m \rho_m^{\text{crit}} V_m(\rho_m^{\text{crit}}) & \text{if } v_{m,1}^{\text{lim}}(k) \geq V_m(\rho_m^{\text{crit}}) \end{cases} \quad (2.9)$$

where $q_{m,1}^{\text{lim}}$ is the maximum inflow of the first segment of the link m that is connected to the mainstream origin o , $v_{m,1}^{\text{lim}}(k) = \min(v_{m,1}^{\text{SL}}(k), v_{m,1}(k))$ is the speed that limits the flow in the first segment of link m at time step k .

The queue length at a mainstream origin o or an on-ramp origin o is described through the following equation:

$$w_o(k+1) = w_o(k) + T(d_o(k) - q_o(k)) \quad (2.10)$$

In addition, we refer to [50, 60, 84] for more details about METANET and its extensions.

2.1.5 Basic FASTLANE Model

FASTLANE [122, 123] is a first-order multi-class macroscopic traffic flow model that is represented by links (indexed by m), and each link is divided into several homogeneous cells (indexed by i), which are similar with segments in METANET. Other components of traffic networks are similar as those for METANET: origins, on-ramps, off-ramps, and destinations, etc.

The main feature of FASTLANE is that it uses dynamic passenger car equivalents (pce) for representing different vehicle classes by means of a representative vehicle class. Based on the dynamic pce, the different space occupied by vehicles under different traffic conditions (different traffic densities) is taken into account. In FASTLANE, the dynamic pce ($\Theta_{m,i,c}$) for

a vehicle class (indexed by c) in cell i of link m is defined as

$$\Theta_{m,i,c} = \frac{s_c + T_{h,c} \cdot v_{m,i,c}}{s_1 + T_{h,1} \cdot v_{m,i,1}} \quad (2.11)$$

in which $v_{m,i,c}$ represents the speed of vehicle class c in cell (m, i) , s_c is the gross stopping distance¹ of vehicle class c , and $T_{h,c}$ is the minimum time headway² of vehicle class c . The index 1 denotes the reference vehicle class.

Based on the dynamic pce, the effective density³ ($\rho_{m,i}^{\text{efc}}$) in cell i of link m is defined as

$$\rho_{m,i}^{\text{efc}} = \sum_{c=1}^{n_c} \Theta_{m,i,c} \rho_{m,i,c} \quad (2.12)$$

where $\rho_{m,i,c}$ is the density of vehicle class c in cell (m, i) , and n_c is the total number of all vehicle classes.

Since we use the FASTLANE model within a MPC framework in this thesis, we present the discrete-time form of FASTLANE as follows. The discrete-time forms of (2.11) and (2.12) are given as follows⁴:

$$\Theta_{m,i,c}(k) = \frac{s_c + T_{h,c} \cdot v_{m,i,c}(k)}{s_1 + T_{h,1} \cdot v_{m,i,1}(k)} \quad (2.13)$$

$$\rho_{m,i}^{\text{efc}}(k) = \sum_{c=1}^{n_c} \Theta_{m,i,c}(k-1) \rho_{m,i,c}(k) \quad (2.14)$$

The basic equations for computing the flow, density, and speed of vehicle class c in cell i of link m are

$$q_{m,i,c}(k) = \mu_m \rho_{m,i,c}(k) v_{m,i,c}(k) \quad (2.15)$$

$$\rho_{m,i,c}(k+1) = \rho_{m,i,c}(k) + \frac{T}{L_m \mu_m} \left(q_{m,c}^{i-1,i}(k) - q_{m,c}^{i,i+1}(k) \right) \quad (2.16)$$

$$v_{m,i,c}(k) = V_{m,c}(\rho_{m,i}^{\text{efc}}(k)) = \begin{cases} v_{m,c}^{\text{free}} - \rho_{m,i}^{\text{efc}}(k) \frac{(v_{m,c}^{\text{free}} - v_{m,jt}^{\text{crit}})}{\rho_{m,jt}^{\text{crit}}} & \text{for } \rho_{m,i}^{\text{efc}}(k) < \rho_{m,jt}^{\text{crit}} \\ \frac{v_{m,jt}^{\text{crit}} \rho_{m,jt}^{\text{crit}}}{\rho_{m,i}^{\text{efc}}(k)} \left(1 - \frac{\rho_{m,i}^{\text{efc}}(k) - \rho_{m,jt}^{\text{crit}}}{\rho_{m,\text{efc}}^{\text{max}} - \rho_{m,jt}^{\text{crit}}} \right) & \text{for } \rho_{m,i}^{\text{efc}}(k) \geq \rho_{m,jt}^{\text{crit}} \end{cases} \quad (2.17)$$

where $q_{m,i,c}$ is the flow of vehicle class c in cell i of link m , $q_{m,c}^{i,i+1}$ is the flow of vehicle class c from cell i to cell $i+1$ of link m , $v_{m,c}^{\text{free}}$ is the free-flow speed for vehicle class c in link m , $v_{m,jt}^{\text{crit}}$ is the joint critical speed for all vehicle classes in link m , $\rho_{m,jt}^{\text{crit}}$ is the joint critical density³ for

¹The gross stopping distance is the sum of the length of a vehicle and the distance to the lead vehicle [122].

²The minimum time headway is equal to the minimum allowed distance between two vehicles driving in series divided by the speed of the following vehicle [118].

³The effective density $\rho_{m,i}^{\text{efc}}$, the joint critical density $\rho_{m,jt}^{\text{crit}}$, and the effective maximum density $\rho_{m,\text{efc}}^{\text{max}}$ in link m are expressed in pce/km/lane, the density $\rho_{m,i,c}$ of vehicle class c in cell i of link m is expressed in vehicle/km/lane.

⁴Note that in (2.14) the dynamic pce at time step $k-1$ is used: $\Theta_{m,i,c}(k-1)$. According to (2.13), $\Theta_{m,i,c}$ depends on $v_{m,i,c}$, which is determined by $\rho_{m,i}^{\text{efc}}$ according to (2.17); thus, $\Theta_{m,i,c}(k)$ cannot be computed before $\rho_{m,i}^{\text{efc}}(k)$ is computed. This is why $\Theta_{m,i,c}(k-1)$ is used in (2.14).

all vehicle classes in link m , and $\rho_{m,\text{efc}}^{\max}$ is the effective maximum density³ in link m . Note that $v_{m,\text{jt}}^{\text{crit}}$, $\rho_{m,\text{jt}}^{\text{crit}}$, and $\rho_{m,\text{efc}}^{\max}$ are joint parameters for all vehicle classes, and they can be determined through parameter identification for FASTLANE based on class-specific measurements.

The traffic demand of cell i of link m needs to be distributed among different vehicle classes, according to the traffic composition in cell i of link m . This composition is represented by the flow ratio $\lambda_{m,i,c}$ of vehicle class c in cell i of link m :

$$\lambda_{m,i,c}(k) = \frac{\Theta_{m,i,c}(k)q_{m,i,c}(k)}{\sum_{j=1}^{n_c} \Theta_{m,i,j}(k)q_{m,i,j}(k)} \quad (2.18)$$

The flow of vehicle class c from cell i to cell $i+1$ of link m is described as follows:

$$q_{m,c}^{i,i+1}(k) = \frac{1}{\Theta_{m,i,c}(k)} \min\left(D_{m,i,c}(k), \lambda_{m,i,c}(k)S_{m,i+1}(k)\right) \quad (2.19)$$

where the demand $D_{m,i,c}$ of vehicle class c and the supply $S_{m,i}$ for all vehicle classes in cell i of link m are defined as

$$D_{m,i,c}(\rho_{m,i}^{\text{efc}}(k)) = \begin{cases} \mu_m \Theta_{m,i,c}(k) \rho_{m,i,c}(k) V_{m,c}(\rho_{m,i}^{\text{efc}}(k)) & \text{for } \rho_{m,i}^{\text{efc}}(k) < \rho_{m,\text{jt}}^{\text{crit}} \\ \mu_m \lambda_{m,i,c}(k) \rho_{m,\text{jt}}^{\text{crit}} v_{m,\text{jt}}^{\text{crit}} & \text{for } \rho_{m,i}^{\text{efc}}(k) \geq \rho_{m,\text{jt}}^{\text{crit}} \end{cases} \quad (2.20)$$

$$S_{m,i}(\rho_{m,i}^{\text{efc}}(k)) = \begin{cases} \mu_m \rho_{m,\text{jt}}^{\text{crit}} v_{m,\text{jt}}^{\text{crit}} & \text{for } \rho_{m,i}^{\text{efc}}(k) < \rho_{m,\text{jt}}^{\text{crit}} \\ \mu_m \rho_{m,i}^{\text{efc}}(k) V_{m,c}(\rho_{m,i}^{\text{efc}}(k)) & \text{for } \rho_{m,i}^{\text{efc}}(k) \geq \rho_{m,\text{jt}}^{\text{crit}} \end{cases} \quad (2.21)$$

For more details about FASTLANE, we refer to [122, 123].

2.2 Traffic Emission and Fuel Consumption Models

2.2.1 Microscopic Emission and Fuel Consumption Models

Microscopic emission and fuel consumption models describe the emissions and fuel consumption of individual vehicles, based on vehicle dynamics over time and space. Some microscopic emission models have been developed in the literature [4, 6, 66, 128]. The CMEM model in [6] uses sec-by-sec velocity, or distribution of modal activity, or average traffic characteristics for computing emission rates or fuel consumption rates. In COPERT [128], the travel speeds of individual vehicles are used as inputs for estimating emission rates and fuel consumption rates. In VT-micro [4] and VERSIT+ [66], both the travel speeds and accelerations of individual vehicles are used as inputs for estimating emission rates and fuel consumption rates. Some simulators for microscopic emission models are also available, e.g. EnViver, which is developed based on VERSIT+ by TNO, Netherlands, and the module for emissions and fuel consumption in SUMO [11], which is based on a continuous model derived from values stored in the HBEFA database [1].

Microscopic emission and fuel consumption models can simulate emissions and fuel consumption in traffic networks in a detailed way, and they can be used as process models for estimating emissions and fuel consumption in traffic networks. In model-based control

for reducing emissions and fuel consumption in traffic networks, macroscopic emission models can be used for determining the control inputs, with the computational burden reduced w.r.t. the case that microscopic emission models are used.

2.2.2 Macroscopic Emission and Fuel Consumption Models

Macroscopic emission and fuel consumption models describe emissions and fuel consumption for aggregated vehicles, instead of individual vehicles. According to [120], emission factors can be aggregated for all vehicles in the considered traffic network over the entire period, yielding global emission factors independent of time and space; emission factors can also be aggregated for vehicles in individual links over the entire period, yielding local emission factors depending on space; moreover, emission factors can be aggregated for vehicles over distance and time, yielding instantaneous emission factors depending on space and time.

Some macroscopic emission models have been developed in the literature [29, 102, 107, 127, 130]. As introduced in [107], macroscopic emission model MOBILE5a is based on average-trip speeds, and macroscopic emission model MOBILE6 is based on vehicle testing over facility cycles for different facility types and average speeds. In [127] Yu et al. developed a macroscopic emission model for China, based on real-world emission measurements in China and supplementary data modeled by MOBILE6. In [127], emission factors are based on vehicle age distribution, and vehicle-specific power (which depends on speed and acceleration), etc. Zegeye et al. [130] developed the VT-macro model by integrating the VT-micro model with the METANET model. The VT-micro model uses the speeds and accelerations of individual vehicles as inputs. In [130], two types of accelerations were proposed, i.e. the inter-segment acceleration corresponding to those vehicles stay in one segment within one time step, and the cross-segment acceleration corresponding to those vehicles moving from one segment to the next segment within one time step. Next, these two types of accelerations are used for computing emission rates and fuel consumption rates in [130]. For example, Csikós et al. [29] extended the COPERT model into a macroscopic version by introducing the concept of the spatiotemporal window; the average speeds over individual spatiotemporal windows are used as the inputs for the COPERT model for estimating emission factors for different vehicle classes. In [102], Pasquale et al. combined a multi-class version of METANET with COPERT for reducing traffic congestion and traffic emissions through nonlinear optimization control.

2.2.3 VERSIT+ Model

The VERSIT+ model [66, 115] is a microscopic emission model developed based on a large number of emission tests. The VERSIT+ model requires speed-data profiles as inputs. In the VERSIT+ model, the emission rate EM_y (expressed in g/s) of a single vehicle is estimated as follows [66]:

$$EM_y(k) = \begin{cases} u_{0,y} & \text{if } v(k) \leq 5, a(k) \leq 0.5 \\ u_{1,y} + u_{2,y}(z(k))_+ + u_{3,y}(z(k) - 1)_+ & \text{if } 5 < v(k) \leq 50 \text{ or } v(k) \leq 5, a(k) > 0.5 \\ u_{4,y} + u_{5,y}(z(k))_+ + u_{6,y}(z(k) - 1)_+ & \text{if } 50 < v(k) \leq 80 \\ u_{7,y} + u_{8,y}(z(k) - 0.5)_+ + u_{9,y}(z(k) - 1.5)_+ & \text{if } v(k) > 80 \end{cases} \quad (2.22)$$

where y represents the emission category (e.g. CO₂, NO_x, and ⁵PM10), $u_{0,y}, \dots, u_{9,y}$ are model parameters, v is the speed of the vehicle in km/h, a is the acceleration of the vehicle in m/s², and z is defined as

$$z(k) = a(k) + 0.014v(k) \quad (2.23)$$

In addition, the function $(x)_+$ is defined as

$$(x)_+ = \begin{cases} 0 & \text{if } x < 0 \\ x & \text{if } x > 0 \end{cases} \quad (2.24)$$

2.2.4 VT-Macro Model

The VT-macro model [130] is a macroscopic emission and fuel consumption model. It has been developed based on an integration of the VT-micro model [4] and the METANET model [60, 84]. However, it is possible to use the VT-macro model together with other macroscopic traffic flow models. VT-micro is a microscopic emissions and fuel consumption model, i.e., it yields the emissions and fuel consumption rate of an individual vehicle. So this model requires the speed and the acceleration of a single vehicle as inputs. However, the METANET model only yields the space-mean speeds of segments. The accelerations can be derived from the METANET model as follows [130].

For each segment, two acceleration components are considered: inter-segment acceleration and cross-segment acceleration. They are defined as follows:

$$a_{m,i}^{\text{inter}}(k) = \frac{v_{m,i}(k) - v_{m,i}(k-1)}{T} \quad (2.25)$$

$$a_{\alpha,\beta}^{\text{cross}}(k) = \frac{v_{\beta}(k) - v_{\alpha}(k-1)}{T} \quad (2.26)$$

where the indices α and β represent different adjacent segments, on-ramps, or off-ramps. The numbers of vehicles that correspond to these two accelerations are

$$n_{m,i}^{\text{inter}}(k) = L_m \mu_m \rho_{m,i}(k) - T q_{m,i}(k) \quad (2.27)$$

$$n_{\alpha,\beta}^{\text{cross}}(k) = T q_{\alpha}(k) \quad (2.28)$$

Based on the accelerations, the VT-macro model yields estimates of the emission rates and the fuel consumption rates for segments:

$$\text{EM}_{y,m,i}^{\text{inter}}(k) = n_{m,i}^{\text{inter}}(k) \exp\left(\tilde{v}_{m,i}^T(k) P_y \tilde{a}_{m,i}^{\text{inter}}(k)\right) \quad (2.29)$$

$$\text{EM}_{y,\alpha,\beta}^{\text{cross}}(k) = n_{\alpha,\beta}^{\text{cross}}(k) \exp\left(\tilde{v}_{\alpha}^T(k) P_y \tilde{a}_{\alpha,\beta}^{\text{cross}}(k)\right) \quad (2.30)$$

where P_y is a model parameter matrix, $y \in Y = \{\text{CO}, \text{NO}_x, \text{HC}, \text{fuel}\}$, and $\tilde{v}_{m,i}$, $\tilde{a}_{m,i}^{\text{inter}}$, \tilde{v}_{α} , and $\tilde{a}_{\alpha,\beta}^{\text{cross}}$ are vectors in the form of $\tilde{x} = [1 \ x \ x^2 \ x^3]^T$.

The VT-macro model does not yield the emission rate of CO₂. According to [104, 129], an approximate affine relationship exists between the emission rate for CO₂ and the fuel

⁵PM10 represents respirable suspended particle in the atmosphere, i.e., particles with diameter of 10 micrometres or less.

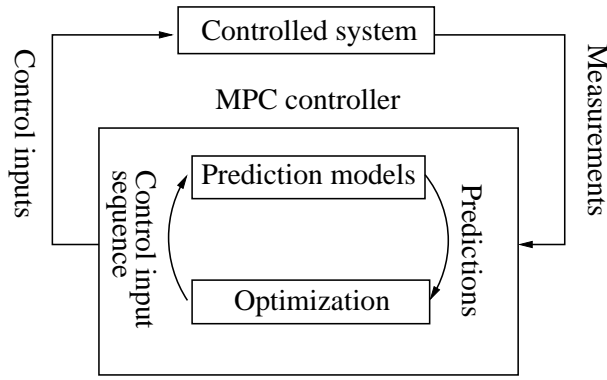


Figure 2.2: Model predictive control

consumption rate. Thus, the CO₂ emission rate ($EM_{CO_2,m,i}$) can be estimated as

$$EM_{CO_2,m,i}(k) = \gamma_1 v_{m,i}(k) + \gamma_2 EM_{fuel,m,i}(k) \quad (2.31)$$

where γ_1 and γ_2 are model parameters, and $EM_{fuel,m,i}$ is the fuel consumption rate given by

$$EM_{fuel,m,i}(k) = EM_{fuel,m,i}^{inter}(k) + \sum_{\alpha \in I_{m,i}^{up}} EM_{fuel,\alpha,(m,i)}^{cross}(k) \quad (2.32)$$

where $I_{m,i}^{up}$ is the set that includes all the upstream segments and origins that directly connect to segment (m, i) .

2.3 Model Predictive Control

2.3.1 General Model Predictive Control

Model Predictive Control (MPC) [22, 79, 85] is a control approach that is based on dynamic prediction and a receding-horizon scheme. Figure 2.2 is a representation for a closed-loop MPC process, including the controlled system and the MPC controller.

Assume that the controlled system is described by a discrete-time nonlinear model of the following form⁶:

$$x(k+1) = f(x(k), u(k), D(k)) \quad (2.33)$$

$$y(k) = h(x(k)) \quad (2.34)$$

where f is the state function, h is the output function, x represents the state vector, y represents the output vector, u represents the control input vector, and D represents the uncontrollable input vector.

In MPC, the predicted performance of the controlled system over the prediction period ($(kT, (k + N_p)T)$) is evaluated using an objective function, based on prediction models. The objective function of the MPC problem is in general a function of the predicted state vector $\tilde{x}(k)$, the predicted output vector $\tilde{y}(k)$, the control input sequence vector $\tilde{u}(k)$, and the

⁶Note that in Chapter 2 we assume $T_c = T$ for the sake of simplicity of notation, with T_c the control time interval.

predicted external uncontrollable input vector $\tilde{D}(k)$, which are defined as follows:

$$\tilde{x}(k) = [x^T(k+1), \dots, x^T(k+N_p)]^T \quad (2.35)$$

$$\tilde{y}(k) = [y^T(k+1), \dots, y^T(k+N_p)]^T \quad (2.36)$$

$$\tilde{u}(k) = [u^T(k), \dots, u^T(k+N_c-1)]^T \quad (2.37)$$

$$\tilde{D}(k) = [D^T(k), \dots, D^T(k+N_p-1)]^T \quad (2.38)$$

Note that for reducing the number of variables in the optimization problem of MPC, a control horizon (N_c) can be chosen as less than or equal to the prediction horizon (N_p), i.e. $N_c \leq N_p$. Then the control input $u(k+l)$ equals $u(k+N_c-1)$ for $l = N_c, \dots, N_p-1$.

The MPC problem is defined as follows:

$$\min_{\tilde{u}(k)} J(\tilde{x}(k), \tilde{y}(k), \tilde{u}(k)) \quad (2.39)$$

$$\text{s.t. } x(k+l+1) = f(x(k+l), u(k+l), D(k+l)) \quad l = 0, \dots, N_p-1 \quad (2.40)$$

$$y(k+l) = h(x(k+l)) \quad l = 1, \dots, N_p \quad (2.41)$$

$$x(k) = x_k \quad (2.42)$$

$$u(k+l) = u(k+N_c-1), \quad l = N_c, \dots, N_p-1 \quad (2.43)$$

$$x(k+l) \in \mathbb{X}, \quad l = 1, \dots, N_p \quad (2.44)$$

$$y(k+l) \in \mathbb{Y}, \quad l = 1, \dots, N_p \quad (2.45)$$

$$u(k+l) \in \mathbb{U}, \quad l = 0, \dots, N_c-1 \quad (2.46)$$

where J is the objective function, x_k represents the measured state vector at time step k , \mathbb{X} is the set of all the feasible states, \mathbb{Y} is the set of all the feasible outputs, and \mathbb{U} is the set of all the feasible control inputs.

The controller determines the control input sequence $\tilde{u}(k)$ that optimizes the value of the objective function subject to the constraints. According to the receding-horizon scheme, only the first element of the optimal control input sequence is applied to the controlled system. After that, the prediction period shifts to the next control step, and the control inputs are optimized again. In addition, an end-point penalty [15, 26, 99], which is based on the system states at the end of the prediction period, can be added to the objective function for ensuring stability:

$$J(\tilde{x}(k), \tilde{y}(k), \tilde{u}(k)) + \Phi(x(N_p)) \quad (2.47)$$

where $\Phi(x(N_p))$ represents the end-point penalty.

2.3.2 Model Predictive Control for Traffic Networks

MPC can be used for on-line traffic management, considering its capability to deal with nonlinear systems, multi-criteria optimization, and constraints, and it has been successfully tested in simulations of traffic systems [2, 37, 40, 46, 50, 77, 81, 98].

Hegyi et al. [50] applied MPC for freeway networks to reduce the total time spent, i.e. the total time that all vehicle spend in the considered network, with variable speed limits and ramp metering as control measures. Hegyi et al. [50] showed by a case study that MPC with variable speed limits and ramp metering can significantly reduce the total time spent.

Papamichail et al. [98] proposed a nonlinear MPC approach for coordinating ramp metering, in combination with AMOC (Advanced Motorway Optimal Control)[61] and the feedback control approach ALINEA [96]; Papamichail et al. showed by a simulation experiment that the proposed approach can perform better than uncoordinated ramp metering. Aboudolas et al. [2] proposed a rolling-horizon quadratic-programming approach for large-scale urban networks, with traffic flows being modeled based on the store-and-forward modeling paradigm, and the effectiveness of the proposed approach in [2] was demonstrated by a simulation experiment. Lu et al. [77] proposed a control approach for maximizing bottleneck flows for freeway networks, with variable speed limits and ramp metering as control measures. In that approach, variable speed limits are first determined by control laws, based on mainstream flow, on-ramp demand, and the characteristics of drivers; next, ramp metering rates are determined by means of MPC. Moreover, it was shown by a numerical experiment that this approach could significantly improve the traffic performance w.r.t. the no-control case. Hadiuzzaman et al. [46] proposed a variable speed limit strategy with fundamental diagrams at bottlenecks explicitly considered, and Hadiuzzaman et al. showed by a case study that the proposed approach in [46] together with the MPC approach can effectively reduce traffic congestion. Frejo et al. [40] proposed a MPC approach for freeway networks based on discrete signals for variable speed limits, and showed by a case study that the proposed method in [40] can result in a good performance, with the computation time decreased. Maggi et al. [81] proposed different MPC approaches, which differ for the prediction models (CTM and modified CTM) and the objective functions, and the different approaches in [81] was compared by means of simulations. With ramp metering as the control measure for freeway networks, Ferrara et al. [37] developed an event-triggered MPC approach, in which the control inputs are not computed at every control time step, but based on an event-triggered rule. In [37], the event-triggered MPC problem is formulated in a mixed-integer linear form; thus the optimization problem can be solved by efficient solvers. Moreover, Ferrara et al. [37] showed the effectiveness of their approach by numerical simulations.

2.3.3 Receding-Horizon Parameterized Control for Traffic Networks

A Receding-Horizon Parameterized Control (RHPC) approach for traffic networks has been developed by Zegeye et al. [130] based on a receding-horizon control scheme and parameterized control laws for single-class traffic models. RHPC is a variation of standard MPC: in MPC the control inputs are directly optimized for the whole control period, and the number of variables in the optimization problem is determined by the length of the control period. In contrast, in RHPC the control inputs are parameterized and only the parameters of the control laws are optimized instead of all control inputs. These parameters can be time-varying or constant over the control period, and therefore the number of variables in the optimization problem can be decreased with respect to that of standard MPC. Zegeye et al. validated by a case study that the performance improvement for RHPC can be almost the same as standard MPC, and the computational load for RHPC is much lower than that for standard MPC.

Hart [117] also investigated some parameterized MPC laws for freeway networks based on single-class traffic model. In [117], eleven parameterized control laws were considered in total, and it was shown that seven of the considered parameterized MPC laws could result in similar performance as standard MPC, with relatively low computational burden w.r.t.

standard MPC.

For more details about the RHPC approach, we refer to Section 4.1.

2.4 Robust Model-Based Control

2.4.1 General Robust Model Predictive Control

Since the predictions of the future evolutions of the controlled networks are used for determining the optimal control actions in MPC, the uncertainties that affect the accuracy of the predictions will also affect the control performance and the satisfaction of constraints on states and outputs. In particular, these uncertainties include the uncertainties in measurements of states, the uncertainties in model parameters, the uncertainties in the external uncontrollable inputs, and so on, since the measured states, the model parameters, and the uncontrollable inputs are used for predicting future traffic dynamics. Robust MPC approaches [23, 33, 45, 83, 113] take into account uncertainties in the control design procedure in order to improve the control performance and to ensure the satisfaction of constraints.

There are some robust MPC approaches available in the literature for handling uncertainties for MPC. For instance, one type of approach is based on Lyapunov functions, see e.g. [33, 113]. Another type of approach is tube-based MPC, see e.g. [83], where a model predictive controller forces the trajectories of the disturbed system to be within a tube around a central reference trajectory, which is obtained by a nominal control approach with tightened constraints on states and inputs. Moreover, a min-max scheme is used for handling uncertainties in [23, 45], where the worst-case control objective functions among all the considered uncertainties are optimized. In addition, in [23] constraints on the control inputs and system outputs are taken into account for all possible uncertainties, and in [45] only constraints on the control inputs are considered.

2.4.2 Robust Model-Based Control for Traffic Networks

Various uncertainties exist in model-based control procedures for traffic networks. In particular, demand uncertainties, model uncertainties, missing samples, sensor errors, and delays are all significant factors in model-based traffic control. In multi-class traffic models, the fractions of different vehicle classes in the demands at the origins of the network are required. Thus, the uncertainties in the estimation of these fractions will affect the control performance. Considering these uncertainties in the model-based control design is important for improving the control performance and for ensuring the satisfaction of constraints.

Some robust control approaches have been developed for traffic networks. Tettamanti et al. [119] developed a min-max MPC approach for urban networks to minimize the objective function in the worst-case scenario. Ukkusuri et al. [121] proposed a robust optimal traffic signal control approach for traffic networks with the future demand assumed to be uncertain, and they developed a robust system-optimal control approach with an embedded cell transmission model. Similarly considering the uncertainties in the origin-destination (OD) demands, Jones et al. [56] proposed a near-Bayes near-Minimax method for robust traffic signal control for an urban network, and obtained a good

compromise solution between the Bayes case and the Minimax case. Zhong et al. [132] dealt with the robust control problem by using a min-max scheme, and solved the optimal control for freeway networks using a set of recursive coupled Riccati difference equations. Huang et al. [55] proposed Iterative Optimizing Control with Model Bias Correction (IOCMBC) for handling uncertainties in traffic signal control. In the IOCMBC approach, a model bias correction is included by adjusting the model output and the slope of the model based on the measurements.

2.5 Robust Distributed Model Predictive Control

2.5.1 Distributed Model Predictive Control

A large-scale traffic network is hard to control through centralized MPC due to the computational complexity. In Distributed Model Predictive Control (DMPC), a large-scale network is divided into small subnetworks, which are assigned to local agents.

Some approaches have been developed for partitioning large-scale networks into small networks in the literature [89, 110, 133]. Ocampo-Martinez et al. [89] developed a partitioning approach on the basis of graph-theory: they represent a system by means of a graph, and divided the system graph into a number of non-overlapping subgraphs by identifying the highly coupling subgraphs. By means of a simulation experiment, the partitioning approach in [89] was shown to be capable of reducing the computational complexity with negligible loss of performance w.r.t. the centralized MPC approach. Zhou et al. [133] proposed a fast network division approach based on optimizing a criterion for the quality of the partition schemes, and the fast network division approach was shown to be efficient in partitioning real-world urban traffic networks by a case study. For the anticipatory control problem for large-scale traffic networks, Rinaldi et al. [110] proposed a dynamic decomposition mechanism, which can recognize when and which controllers should be grouped in clusters, based on the sensitivity of traffic variables to the control inputs. In [110] the effectiveness of the dynamic decomposition mechanism was tested by numerical case studies involving MPC for traffic networks; the results show that the new approach outperforms both the fully centralized MPC approach where the controllers are in one group, and the fully decomposed MPC approach where all the controllers are in different groups.

After partitioning the large-scale network into small networks, the overall optimization problem is decomposed into local optimization problems for the local agents by methods such as primal decomposition or dual decomposition [27]. In the dual decomposition method [27, 87], coupling constraints between subnetworks are incorporated into the overall control objective function by Lagrangian relaxation or augmented Lagrangian relaxation, resulting in a dual problem that can be decomposed into local optimization problems. It can be shown [14, 24, 87] that when the control objective functions and the inequality constraints of subnetworks are convex and the equality constraints of subnetworks are affine, the solution of the original overall optimization problem can be retrieved by iteratively solving the dual problem in a distributed way.

Some researchers also use DMPC for nonlinear-nonconvex systems, and they use numerical experiments for investigating the control effectiveness. For instance, Frejo and Camacho applied DMPC for a nonlinear-nonconvex freeway network in [39], where they

did not include coupling terms in the control objective function, and they adopted a setting in which each local controller can negotiate with other controllers through communication about coupling variables. Frejo and Camach [39] showed by a numerical experiment that DMPC can improve the control performance w.r.t. the no-control case, albeit that the control performance is suboptimal compared to that for the centralized control approach. Ferrara et al. [38] reformulated a nonlinear traffic flow model as a mixed logical dynamical system including linear equalities and inequalities. By considering a freeway network as a system of systems, Ferrara et al. [38] developed two different DMPC approaches: a so-called partially connected noniterative independent algorithm where each local controller optimizes a local control objective function, and a so-called partially connected noniterative cooperative algorithm where each local controller optimizes the weighted sum of the control objective functions of that local controller and all neighbors. Ferrara et al. [38] showed by a case study that the control performance can be improved by DMPC compared to the no-control case, and that the DMPC approach based on the so-called partially connected noniterative cooperative algorithm leads to a control performance that is close to that for the centralized control approach.

2.5.2 Robust Distributed Model Predictive Control

In DMPC, local agents communicate with other agents to obtain solutions for the control problem of the overall network. Apart from the uncertainties of the current local agent, the uncertainties appearing in other local agents also affect the control effectiveness of DMPC. Some robust DMPC approaches have been developed in [42, 62, 63, 80, 82, 108].

For linear systems, in [42, 108] a constraint tightening scheme is used for dealing with uncertainties in DMPC. In [42], local constraint sets are tightened to account for uncertainties, and the global constraint set is taken as the Cartesian product of tightened local constraint sets, ensuring robustness w.r.t. small disturbances. In [108], constraints are tightened in a monotonic way to ensure robust feasibility, including additional margins in the coupling constraints of each local agent to account for the uncertainties for neighboring subsystems.

For nonlinear systems, some robust DMPC approaches are also available in the literature. Li and Shi [63] proposed a robust DMPC approach for continuous-time decoupled nonlinear subsystems, where coupling occurring in a global control objective function is incorporated into local control objective functions. In [63] a robustness constraint making local cost functions (Lyapunov functions) decrease was proposed to ensure robustness against external bounded disturbances. Furthermore, some robust DMPC approaches have been developed for nonlinear systems based on scenario trees for uncertainties [62, 80, 82]. In these approaches, the considered scenarios for uncertainties are distributed to different local agents, i.e. each local agent deals with one scenario for the uncertainties. Non-anticipativity constraints, which are incorporated into local control objective functions, are introduced in these approaches for ensuring that the control inputs of one agent equal the control inputs of other agents at the same time step. Note, however, that the approaches in [62, 80, 82] are not designed for multiple subsystems, but for a single system only.

2.6 Summary

In this chapter, we have reviewed some previous work about traffic flow models, traffic emission models, model predictive control both in general and for traffic networks, robust model-based control both in general and for traffic networks, and robust distributed model predictive control both in general and for traffic networks.

As prediction models for MPC, in this thesis a multi-class METANET model will be compared with the FASTLANE model in combination with multi-class macroscopic emission models extended based on VT-macro and VERSIT+; this has not yet been done in the literature. Furthermore, in this thesis we will develop a robust RHPC approach and a robust DMPC approach for freeway networks, which have not yet been developed in the literature.

Chapter 3

Model Predictive Control Based on Multi-Class Macroscopic Traffic Models

In order to describe the heterogenous nature of traffic dynamics through macroscopic models, in this chapter we extend a multi-class macroscopic traffic flow model: a new multi-class METANET model, integrate a macroscopic emission model VT-Macro with multi-class traffic flow models, and extend a new multi-class macroscopic emission model: multi-class VERSIT+. To allow for a comparison with the new multi-class METANET model, we also extend the first-order multi-class macroscopic traffic flow model FASTLANE with variable speed limits and ramp metering. These multi-class macroscopic traffic flow and emission models are used next as prediction models in online model predictive control for freeway networks. Besides, end-point penalties are also included to account for the behavior of the considered traffic system beyond the prediction period.

3.1 Multi-Class Macroscopic Traffic Flow Models

3.1.1 Extensions of FASTLANE

The FASTLANE model of [122, 123] does not yield the queue lengths at origins (indexed by o). Besides, traffic control measures such as speed limits and ramp metering are also not included. Here we extend the FASTLANE model with a queue length equation, and we also include variable speed limits and ramp metering.

Just as in METANET [60], we introduce a simple queue equation for estimating the queue lengths at origins:

$$w_{o,c}(k+1) = w_{o,c}(k) + T(d_{o,c}(k) - q_{o,c}(k)) \quad (3.1)$$

where $w_{o,c}$ is the queue length of vehicle class c at origin o , $q_{o,c}$ is the flow of vehicle class c at origin o , and $d_{o,c}$ is the external demand of vehicle class c at origin o .

Following the METANET speed equation of [50], a variable speed limit is incorporated in the speed equation as follows:

$$v_{m,i,c}(k) = \min\left(V_{m,c}\left(\rho_{m,i}^{\text{efc}}(k)\right), (1 + \delta_{m,c})v_{m,i}^{\text{SL}}(k)\right) \quad (3.2)$$

where $1 + \delta_{m,c}$ represents the non-compliance factor of vehicle class c in link m .

In order to apply ramp metering in traffic networks, the on-ramp flow equation with ramp metering is defined as

$$q_{o,c}(k) = \frac{1}{\Theta_{o,c}(k)} \min \left(r_o(k) D_{o,c}(k), \Lambda_o \lambda_{o,c}(k) S_{m,1}(k) \right) \quad (3.3)$$

in which $(m,1)$ indicates the cell to which the on-ramp connects, $\Theta_{o,c}$ is the dynamic pce for vehicle class c at on-ramp o , $D_{o,c}$ is the total demand of vehicle class c at on-ramp o , and $\lambda_{o,c}$ is equal to the traffic composition at on-ramp o set by the user, representing the share for vehicle class c among the total demand at on-ramp o . In addition, Λ_o is defined as follows:

$$\Lambda_o = \frac{C_o^{\text{efc}}}{C_o^{\text{efc}} + C_{m-1}^{\text{efc}}} \quad (3.4)$$

where C_o^{efc} represents the effective capacity for on-ramp o , and C_{m-1}^{efc} represents the effective capacity for the upstream link $m-1$ of the link m that connects to on-ramp o , and C_o^{efc} and C_{m-1}^{efc} are represented in pce/h. The effective capacities C_o^{efc} and C_{m-1}^{efc} are joint parameters for all vehicle classes, and they can be determined by parameter identification based on class-specific measurements.

3.1.2 Multi-Class METANET Model

In this section, we propose a new multi-class METANET model based on the method that is used by Logghe for developing the multi-class LWR model in [75, 76]. In particular, it is assumed that each vehicle class is constrained within an assigned space of the road, being subject to its own fundamental diagram:

$$q_{m,i,c} = \alpha_{m,i,c} Q_c \left(\frac{\rho_{m,i,c}}{\alpha_{m,i,c}} \right) \quad (3.5)$$

where $Q_c(\rho_{m,i,c}) = \mu_m \rho_{m,i,c} v_{m,i,c}$ is the flow function of vehicle class c , and $\alpha_{m,i,c}$ is the road space fraction of vehicle class c in segment i of link m , which is defined as the ratio between the assigned space and the whole road space. The road space fractions for different classes of vehicles are always nonnegative, with the sum of all fractions equal to 1:

$$\alpha_{m,i,c} \geq 0 \quad (3.6)$$

$$\sum_{c=1}^{n_c} \alpha_{m,i,c} = 1 \quad (3.7)$$

The actual density divided by the road space fraction for a vehicle class is considered to be the effective density of that vehicle class. Similarly, the actual flow divided by the road space fraction for a vehicle class is considered to be the effective flow of that vehicle class.

Traffic Flow Equations for Multi-Class METANET

Referring to single-class METANET [60, 84], the equation for computing the flow $q_{m,i,c}$ of vehicle class c in segment i of link m is the same as (2.15), and the equation for computing the queue length $w_{o,c}$ of vehicle class c at origin o is the same as (3.1). The density $\rho_{m,i,c}$ of

vehicle class c in segment i of link m is computed as follows:

$$\rho_{m,i,c}(k+1) = \rho_{m,i,c}(k) + \frac{T}{L_m \mu_m} (q_{m,i-1,c}(k) - q_{m,i,c}(k)) \quad (3.8)$$

Class-dependent parameters ($\tau_{m,c}$, $\eta_{m,c}$, $\kappa_{m,c}$, $\rho_{m,c}^{\text{crit}}$, $v_{m,c}^{\text{free}}$, and $a_{m,c}$) are necessary for computing the speed $v_{m,i,c}$ and the origin flow $q_{o,c}$. These class-dependent parameters describe different characteristics of different vehicle classes, and they can be determined by parameter identification based on class-specific measurements. The speed of vehicle class c in segment i of link m is described through the following equation:

$$\begin{aligned} v_{m,i,c}(k+1) = & v_{m,i,c}(k) + \frac{T}{\tau_{m,c}} \left(V_{m,c} \left(\frac{\rho_{m,i,c}(k)}{\alpha_{m,i,c}(k)} \right) - v_{m,i,c}(k) \right) \\ & + \frac{T}{L_m} v_{m,i,c}(k) (v_{m,i-1,c}(k) - v_{m,i,c}(k)) \\ & - \frac{T \eta_{m,c}}{L_m \tau_{m,c}} \frac{\rho_{m,i+1,c}(k) - \rho_{m,i,c}(k)}{\rho_{m,i,c}(k) + \kappa_{m,c}} \end{aligned} \quad (3.9)$$

where $\tau_{m,c}$, $\eta_{m,c}$, and $\kappa_{m,c}$ are model parameters for vehicle class c in link m , and the desired speed function $V_{m,c}$ for vehicle class c in link m is defined as:

$$V_{m,c} \left(\frac{\rho_{m,i,c}(k)}{\alpha_{m,i,c}(k)} \right) = v_{m,c}^{\text{free}} \exp \left(\frac{-1}{a_{m,c}} \left(\frac{\rho_{m,i,c}(k)}{\alpha_{m,i,c}(k) \rho_{m,c}^{\text{crit}}} \right)^{a_{m,c}} \right) \quad (3.10)$$

in which $a_{m,c}$ is a model parameter of vehicle class c in link m , and $\rho_{m,c}^{\text{crit}}$ is the critical density of vehicle class c in link m .

According to Hegyi et al. [50], a variable speed limit is included in the desired speed function $V_{m,c}$ for vehicle class c similarly to (3.2):

$$V_{m,c} \left(\frac{\rho_{m,i,c}(k)}{\alpha_{m,i,c}(k)} \right) = \min \left(V_{m,c} \left(\frac{\rho_{m,i,c}(k)}{\alpha_{m,i,c}(k)} \right), (1 + \delta_{m,c}) v_{m,i}^{\text{SL}}(k) \right) \quad (3.11)$$

The flow $q_{o,c}$ of vehicle class c at on-ramp o is

$$q_{o,c}(k) = \min \left[d_{o,c}(k) + \frac{w_{o,c}(k)}{T}, r_o(k) \alpha_{m,1,c}(k) C_{o,c}, \alpha_{m,1,c}(k) C_{o,c} \left(\frac{\rho_{m,c}^{\text{max}} - \frac{\rho_{m,1,c}(k)}{\alpha_{m,1,c}(k)}}{\rho_{m,c}^{\text{max}} - \rho_{m,c}^{\text{crit}}} \right) \right] \quad (3.12)$$

where the index 1 represents the segment that the on-ramp is connected to in link m , $\alpha_{m,1,c}$ is the road space fraction of vehicle class c in segment 1 of link m , $C_{o,c}$ is the theoretical maximum capacity of on-ramp o if there would be only vehicle class c , $\rho_{m,c}^{\text{max}}$ is the theoretical maximum density of link m if there would be only vehicle class c , and $\rho_{m,1,c}$ is the density of vehicle class c in segment 1 of link m .

For a mainstream origin o , the flow equation of vehicle class c is similar to the single-class equation developed in [50]:

$$q_{o,c}(k) = \min \left[d_{o,c}(k) + \frac{w_{o,c}(k)}{T}, q_{m,1,c}^{\text{lim}}(k) \right] \quad (3.13)$$

where $q_{m,1,c}^{\text{lim}}$ is the maximum inflow of vehicle class c for the first segment of link m that is

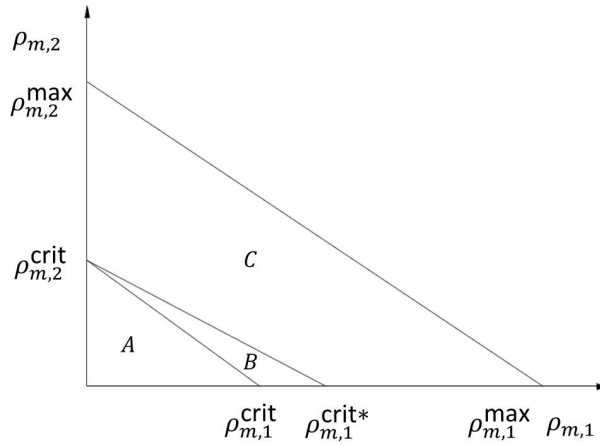


Figure 3.1: Traffic regimes for two vehicle classes

connected to the origin:

$$q_{m,1,c}^{\text{lim}}(k) = \begin{cases} \alpha_{m,i,c}(k) \mu_m \rho_{m,c}^{\text{crit}} v_{m,1,c}^{\text{lim}}(k) \left[-a_{m,c} \ln \left(\frac{v_{m,1,c}^{\text{lim}}(k)}{v_{m,c}^{\text{free}}} \right) \right]^{\frac{1}{a_{m,c}}} & \text{if } v_{m,1,c}^{\text{lim}}(k) < V_{m,c}(\rho_{m,c}^{\text{crit}}) \\ \alpha_{m,i,c}(k) \mu_m \rho_{m,c}^{\text{crit}} V_{m,c}(\rho_{m,c}^{\text{crit}}) & \text{if } v_{m,1,c}^{\text{lim}}(k) \geq V_{m,c}(\rho_{m,c}^{\text{crit}}) \end{cases} \quad (3.14)$$

in which $v_{m,1,c}^{\text{lim}}(k) = \min(v_{m,1}^{\text{SL}}(k), v_{m,1,c}(k))$ is the speed that limits the flow for vehicle class c in the first segment of link m at time step k , and $\alpha_{m,i,c}$ is used for converting effective flows to actual flows.

Road Space Fractions and Traffic Regimes

According to the densities for different vehicle classes, three traffic regimes are defined here, i.e. free-flow, semi-congestion, and congestion. The road space fractions are determined on the basis of these traffic regimes. Figure 3.1 shows the traffic regimes for the case with two vehicle classes.

- Regime A: Free-Flow

In the free-flow regime, the effective density of each vehicle class is less than or equal to its critical density. Therefore, the sufficient and necessary condition for the free-flow regime is

$$\frac{\rho_{m,i,c}(k)}{\alpha_{m,i,c}(k)} \leq \rho_{m,c}^{\text{crit}} \quad \text{for all } c \quad (3.15)$$

Based on (3.7) and (3.15), the constraint that separates the free-flow regime from the semi-congestion regime is obtained as follows:

$$\sum_{c=1}^{n_c} \frac{\rho_{m,i,c}(k)}{\rho_{m,c}^{\text{crit}}} \leq 1 \quad (3.16)$$

According to (3.15), we define the space fraction of vehicle class c as

$$\alpha_{m,i,c}(k) = \frac{\frac{\rho_{m,i,c}(k)}{\rho_{m,c}^{\text{crit}}}}{\sum_{j=1}^{n_c} \frac{\rho_{m,i,j}(k)}{\rho_{m,j}^{\text{crit}}}} \quad (3.17)$$

- Regime B: Semi-Congestion

From the macroscopic behavioral theory for traffic dynamics and empirical phenomena in [32], it could happen that slower vehicles are still in the free-flow regime, while faster vehicles are already in the congested mode. Similarly to [75, 76], in the multi-class setting faster vehicle classes are considered to get in the congested mode earlier than slower vehicle classes, and the desired speeds of the congested vehicle classes are considered to be equal. The semi-congestion regime corresponds to the case that the desired speeds of the congested vehicle classes are larger than or equal to the desired speeds of slower vehicle classes that are still in the free-flow regime. In the semi-congestion regime, the effective density of at least one vehicle class is less than or equal to its critical density, and the effective density of at least one vehicle class is larger than its critical density.

In order to obtain the boundary condition distinguishing the semi-congestion regime from the congestion regime, it is assumed that all vehicle classes are congested except for one vehicle class c_m^* that is on the verge of getting in the congested mode, i.e. the effective density of vehicle class c_m^* is equal to its critical density, resulting in the following road space fraction for vehicle class c_m^* :

$$\alpha_{m,i,c_m^*}(k) = \frac{\rho_{m,i,c_m^*}(k)}{\rho_{m,c_m^*}^{\text{crit}}} \quad (3.18)$$

Actually, c_m^* is the vehicle class with the slowest desired speed when all vehicle classes are assumed to be on the verge of getting in the congested mode:

$$c_m^* = \arg \min_{c=1,\dots,n_c} \left(v_{m,c}^{\text{free}} \exp \left(\frac{-1}{a_{m,c}} \right) \right) \quad (3.19)$$

The following relation holds according to the definition of the semi-congestion regime:

$$V_{m,c_m^*} \left(\frac{\rho_{m,i,c_m^*}(k)}{\alpha_{m,i,c_m^*}(k)} \right) \leq V_{m,c} \left(\frac{\rho_{m,i,c}(k)}{\alpha_{m,i,c}(k)} \right) \quad (3.20)$$

for $c = 1, \dots, n_c$ with $c \neq c_m^*$

Considering (3.7), (3.18), and (3.20), the boundary condition distinguishing the semi-congestion regime from the congestion regime is obtained as follows:

$$\sum_{c=1}^{n_c} \frac{\rho_{m,i,c}(k)}{\rho_{m,c}^{\text{crit}*}} \leq 1 \quad (3.21)$$

where $\rho_{m,c}^{\text{crit}*}$ is determined by the following equation:

$$\rho_{m,c}^{\text{crit}*} = \rho_{m,c}^{\text{crit}} \left[-a_{m,c} \ln \left(\frac{v_{m,c_m^*}^{\text{free}}}{v_{m,c}^{\text{free}}} \exp \left(\frac{-1}{a_{m,c_m^*}} \right) \right) \right]^{\frac{1}{a_{m,c}}} \quad (3.22)$$

The proof of (3.21) and (3.22) is as follows:

Proof. The proof is based on (3.7), (3.10), (3.18), and (3.20). Substitute (3.10) into (3.20), and consider (3.18):

$$v_{m,c_m^*}^{\text{free}} \exp \left(\frac{-1}{a_{m,c_m^*}} \right) \leq v_{m,c}^{\text{free}} \exp \left(\frac{-1}{a_{m,c}} \left(\frac{\rho_{m,i,c}(k)}{\alpha_{m,i,c}(k) \rho_{m,c}^{\text{crit}}} \right)^{a_{m,c}} \right) \quad (3.23)$$

for $c = 1, \dots, n_c$ with $c \neq c_m^*$

From (3.23), the following equation can be obtained:

$$\frac{\rho_{m,i,c}(k)}{\alpha_{m,i,c}(k)} \leq \rho_{m,c}^{\text{crit}} \left[-a_{m,c} \ln \left(\frac{v_{m,c_m^*}^{\text{free}}}{v_{m,c}^{\text{free}}} \exp \left(\frac{-1}{a_{m,c_m^*}} \right) \right) \right]^{\frac{1}{a_{m,c}}} \quad (3.24)$$

for $c = 1, \dots, n_c$ with $c \neq c_m^*$

The right-hand side of (3.24) is equal to $\rho_{m,c}^{\text{crit}*}$, cf. (3.22). Hence,

$$\frac{\rho_{m,i,c}(k)}{\rho_{m,c}^{\text{crit}*}} \leq \alpha_{m,i,c}(k) \quad (3.25)$$

for $c = 1, \dots, n_c$ with $c \neq c_m^*$

For vehicle class c_m^* , $\rho_{m,c_m^*}^{\text{crit}} = \rho_{m,c}^{\text{crit}*}$. Considering (3.7), the boundary condition for the semi-congestion regime can be obtained: $\sum_{c=1}^{n_c} \frac{\rho_{m,i,c}(k)}{\rho_{m,c}^{\text{crit}*}} \leq 1$, i.e. (3.21).

Suppose that $S_{m,i}^{\text{cong}}(k)$ denotes the set of all vehicle classes that are in the congested mode in segment i of link m at time step k , and $S_{m,i}^{\text{free}}(k)$ denotes the set of all vehicle classes that are in the free-flow mode in segment i of link m at time step k . The space fractions for the vehicle classes that are in the free-flow mode are

$$\alpha_{m,i,c}(k) = \frac{\rho_{m,i,c}(k)}{\rho_{m,c}^{\text{crit}}} \quad \text{for } c \in S_{m,i}^{\text{free}}(k) \quad (3.26)$$

The space fractions for the congested vehicle classes are obtained by solving the following system of equations:

$$\begin{cases} V_{m,c} \left(\frac{\rho_{m,i,c}(k)}{\alpha_{m,i,c}(k)} \right) = V_{m,l_{m,i}} \left(\frac{\rho_{m,i,l_{m,i}}(k)}{\alpha_{m,i,l_{m,i}}(k)} \right) & \text{for } c \in S_{m,i}^{\text{cong}}(k) / \{l_{m,i}\} \\ \sum_{c \in S_{m,i}^{\text{cong}}(k)} \alpha_{m,i,c}(k) = 1 - \sum_{\hat{c} \in S_{m,i}^{\text{free}}(k)} \alpha_{m,i,\hat{c}}(k) \end{cases} \quad (3.27)$$

where $l_{m,i}$ is an arbitrary element of $S_{m,i}^{\text{cong}}(k)$.

- Regime C: Congestion

In the congestion regime, the effective density of each vehicle class is larger than its critical density; the desired speeds of all classes of vehicles are equal.

The constraint for the congestion regime is the restriction on the maximum density:

$$\frac{\rho_{m,i,c}(k)}{\alpha_{m,i,c}} \leq \rho_{m,c}^{\max} \quad \text{for } c = 1, \dots, n_c \quad (3.28)$$

Note that $\rho_{m,c}^{\text{crit}} < \rho_{m,i,c}$

Considering (3.7) and (3.28), the boundary condition for the congestion regime is obtained as follows:

$$\sum_{c=1}^{n_c} \frac{\rho_{m,i,c}(k)}{\rho_{m,c}^{\max}} \leq 1 \quad (3.29)$$

The space fractions can be derived by equating the desired speeds of all classes of vehicles:

$$\left\{ \begin{array}{l} V_{m,1} \left(\frac{\rho_{m,i,1}(k)}{\alpha_{m,i,1}(k)} \right) = V_{m,2} \left(\frac{\rho_{m,i,2}(k)}{\alpha_{m,i,2}(k)} \right) \\ \vdots \\ V_{m,n_c-1} \left(\frac{\rho_{m,i,n_c-1}(k)}{\alpha_{m,i,n_c-1}(k)} \right) = V_{m,n_c} \left(\frac{\rho_{m,i,n_c}(k)}{\alpha_{m,i,n_c}(k)} \right) \\ \sum_{c=1}^{n_c} \alpha_{m,i,c}(k) = 1 \end{array} \right. \quad (3.30)$$

3.2 Multi-Class Macroscopic Traffic Emission Models

VT-micro and VERSIT+, which has been introduced in Section 2, are microscopic emission models, and they describe the emissions generated by individual vehicles. Considering the computational complexity, in Model Predictive Control (MPC) for traffic networks we want to describe the total emissions in a macroscopic way, not for individual vehicles. As a macroscopic version of VT-micro, VT-macro is based on the single-class METANET model. In the thesis VT-macro is integrated with multi-class traffic flow models. Similarly, we also extend the microscopic emission model VERSIT+ to a multi-class macroscopic version, which can be used together with multi-class traffic flow models.

3.2.1 Multi-Class VT-Macro Model

When the VT-macro model, which has been developed in [130] based on the single-class METANET model, is used for a multi-class setting, it is necessary to integrate it with multi-class macroscopic traffic flow models. In the ensuing part of this section, the explanations are given for multi-class METANET and FASTLANE with segments being equivalent to cells, but the multi-class VT-macro model can also be used for other multi-class macroscopic traffic flow models.

For multi-class traffic flows, the inter-segment acceleration (denoted by $a_{m,i,c}^{\text{inter}}$) and cross-segment acceleration (denoted by $a_{\alpha,\beta,c}^{\text{cross}}$) for vehicle class c are defined as follows:

$$a_{m,i,c}^{\text{inter}}(k) = \frac{v_{m,i,c}(k+1) - v_{m,i,c}(k)}{T} \quad (3.31)$$

$$a_{\alpha,\beta,c}^{\text{cross}}(k) = \frac{v_{\beta,c}(k+1) - v_{\alpha,c}(k)}{T} \quad (3.32)$$

The numbers of vehicles corresponding to the above two types of accelerations are as follows:

$$n_{m,i,c}^{\text{inter}}(k) = L_m \mu_m \rho_{m,i,c}(k) - T q_{m,i,c}(k) \quad (3.33)$$

$$n_{\alpha,\beta,c}^{\text{cross}}(k) = T q_{\alpha,c}(k) \quad (3.34)$$

where $n_{m,i,c}^{\text{inter}}$ (expressed in veh) is the number of vehicles corresponding to $a_{m,i,c}^{\text{inter}}$, and $n_{\alpha,\beta,c}^{\text{cross}}$ (expressed in veh) is the number of vehicles corresponding to $a_{\alpha,\beta,c}^{\text{cross}}$.

Two types of emission rates (denoted by $\text{EM}_{y,m,i,c}^{\text{inter}}$ and $\text{EM}_{y,\alpha,\beta,c}^{\text{cross}}$) corresponding to $a_{m,i,c}^{\text{inter}}$ and $a_{\alpha,\beta,c}^{\text{cross}}$ are as follows:

$$\text{EM}_{y,m,i,c}^{\text{inter}}(k) = n_{m,i,c}^{\text{inter}}(k) \exp\left(\tilde{v}_{m,i,c}^T(k) P_{y,c} \tilde{a}_{m,i,c}^{\text{inter}}(k)\right) \quad (3.35)$$

$$\text{EM}_{y,\alpha,\beta,c}^{\text{cross}}(k) = n_{\alpha,\beta,c}^{\text{cross}}(k) \exp\left(\tilde{v}_{\alpha,c}^T(k) P_{y,c} \tilde{a}_{\alpha,\beta,c}^{\text{cross}}(k)\right) \quad (3.36)$$

in which $P_{y,c}$ is a class-dependent parameter matrix, and $\tilde{v}_{m,i,c}^T$, $\tilde{a}_{m,i,c}^{\text{inter}}$, $\tilde{v}_{\alpha,c}^T$, and $\tilde{a}_{\alpha,\beta,c}^{\text{cross}}$ are vectors in the form of $\tilde{x} = [1 \ x \ x^2 \ x^3]^T$.

The emission rate $\text{EM}_{\text{CO}_2,m,i,c}$ for CO_2 for vehicle class c in segment i of link m can be estimated as

$$\text{EM}_{\text{CO}_2,m,i,c}(k) = \gamma_{1,c} v_{m,i,c}(k) + \gamma_{2,c} \text{EM}_{\text{fuel},m,i,c}(k) \quad (3.37)$$

where $\gamma_{1,c}$ and $\gamma_{2,c}$ are class-dependent model parameters, and $\text{EM}_{\text{fuel},m,i,c}$ is the fuel consumption rate for vehicle class c in segment i of link m given by

$$\text{EM}_{\text{fuel},m,i,c}(k) = \text{EM}_{\text{fuel},m,i,c}^{\text{inter}}(k) + \sum_{\alpha \in I_{m,i}^{\text{up}}} \text{EM}_{\text{fuel},\alpha,(m,i),c}^{\text{cross}}(k) \quad (3.38)$$

Remark 3.1 The approach for extending the multi-class VT-macro model based on multi-class macroscopic traffic flow models is general in the sense that it can be used for any emission model using car characteristics, and with speeds, accelerations, and jerks as inputs. Since the jerks are not derived above, jerk equations are included in Appendix A. \square

3.2.2 Multi-Class VERSIT+

Based on the VERSIT+ model in [66], we extend a multi-class VERSIT+ model by means of the approach for extending the multi-class VT-macro model. In particular, the inter-segment acceleration and the cross-segment acceleration are also used here. The emission rates $\text{EM}_{y,m,i,c}^{\text{inter}}$ (g/s) and $\text{EM}_{y,\alpha,\beta,c}^{\text{cross}}$ (g/s) corresponding to the inter-segment

acceleration and the cross-segment acceleration are as follows:

$$EM_{y,m,i,c}^{\text{inter}}(k) = \begin{cases} n_{m,i,c}^{\text{inter}}(k) u_{0,y,c} & \text{if } v_{m,i,c}(k) \leq 5, a_{m,i,c}^{\text{inter}}(k) \leq 0.5 \\ n_{m,i,c}^{\text{inter}}(k) (u_{1,y,c} + u_{2,y,c}(z_{m,i,c}^{\text{inter}}(k))_+ + u_{3,y,c}(z_{m,i,c}^{\text{inter}}(k) - 1)_+) & \text{if } 5 < v_{m,i,c}(k) \leq 50 \text{ or } v_{m,i,c}(k) \leq 5, a_{m,i,c}^{\text{inter}}(k) > 5 \\ n_{m,i,c}^{\text{inter}}(k) (u_{4,y,c} + u_{5,y,c}(z_{m,i,c}^{\text{inter}}(k))_+ + u_{6,y,c}(z_{m,i,c}^{\text{inter}}(k) - 1)_+) & \text{if } 50 < v_{m,i,c}(k) \leq 80 \\ n_{m,i,c}^{\text{inter}}(k) (u_{7,y,c} + u_{8,y,c}(z_{m,i,c}^{\text{inter}}(k) - 0.5)_+ + u_{9,y,c}(z_{m,i,c}^{\text{inter}}(k) - 1.5)_+) & \text{if } 80 < v_{m,i,c}(k) \end{cases} \quad (3.39)$$

$$EM_{y,\alpha,\beta,c}^{\text{cross}}(k) = \begin{cases} n_{\alpha,\beta,c}^{\text{cross}}(k) u_{0,y,c} & \text{if } v_{\alpha,c}(k) \leq 5, a_{\alpha,\beta,c}^{\text{cross}}(k) \leq 0.5 \\ n_{\alpha,\beta,c}^{\text{cross}}(k) (u_{1,y,c} + u_{2,y,c}(z_{\alpha,\beta,c}^{\text{cross}}(k))_+ + u_{3,y,c}(z_{\alpha,\beta,c}^{\text{cross}}(k) - 1)_+) & \text{if } 5 < v_{\alpha,c}(k) \leq 50 \text{ or } v_{\alpha,c}(k) \leq 5, a_{\alpha,\beta,c}^{\text{cross}}(k) > 0.5 \\ n_{\alpha,\beta,c}^{\text{cross}}(k) (u_{4,y,c} + u_{5,y,c}(z_{\alpha,\beta,c}^{\text{cross}}(k))_+ + u_{6,y,c}(z_{\alpha,\beta,c}^{\text{cross}}(k) - 1)_+) & \text{if } 50 < v_{\alpha,c}(k) \leq 80 \\ n_{\alpha,\beta,c}^{\text{cross}}(k) (u_{7,y,c} + u_{8,y,c}(z_{\alpha,\beta,c}^{\text{cross}}(k) - 0.5)_+ + u_{9,y,c}(z_{\alpha,\beta,c}^{\text{cross}}(k) - 1.5)_+) & \text{if } 80 < v_{\alpha,c}(k) \end{cases} \quad (3.40)$$

where $u_{0,y,c}, \dots, u_{9,y,c}$ are class-dependent model parameters, and $z_{m,i,c}^{\text{inter}}$ and $z_{\alpha,\beta,c}^{\text{cross}}$ are defined as

$$z_{m,i,c}^{\text{inter}}(k) = a_{m,i,c}^{\text{inter}}(k) + 0.014 v_{m,i,c}(k) \quad (3.41)$$

$$z_{\alpha,\beta,c}^{\text{cross}} = a_{\alpha,\beta,c}^{\text{cross}} + 0.014 v_{\alpha,c} \quad (3.42)$$

in which inter-segment acceleration $a_{m,i,c}^{\text{inter}}$ and the cross-segment acceleration $a_{\alpha,\beta,c}^{\text{cross}}$ are expressed in m/s^2 , and $v_{m,i,c}$ and $v_{\alpha,c}$ are expressed in km/h .

3.3 MPC with End-Point Penalties

The newly extended models (FASTLANE with extensions, multi-class METANET, multi-class VT-macro, and multi-class VERSIT+) are used as prediction models. The control measures that we choose are variable speed limits and ramp metering.

3.3.1 Performance Criteria

Various performance criteria can be considered when constructing the objective function for traffic management. As a proof of concept for reducing traffic congestion and traffic emission in an integrated way, in this chapter we consider the Total Time Spent (TTS) and the Total Emissions (TE) as performance criteria.

The total time that all vehicles spend in the considered traffic network is denoted by Total Time Spent⁷ (TTS), and defined as follows:

$$\text{TTS}(k_c) = T \sum_{j=k_c M}^{(k_c+N_p)M-1} \sum_{c=1}^{n_c} p_c \left(\sum_{(m,i) \in I_{\text{all}}} \mu_m \rho_{m,i,c}(j) L_m + \sum_{o \in O_{\text{all}}} w_{o,c}(j) \right) \quad (3.43)$$

where I_{all} is the set of all pairs of link and segment indices (m, i) in the traffic network, O_{all} is the set of the indices of all origins, k_c is the control time step counter, which corresponds to the time instant $t = k_c T_c$ (with T_c the control time interval⁸), $M = T_c / T$ is assumed to be a positive integer, p_c indicates the fixed passenger car equivalents (pce) for vehicle class c , and in this chapter $p_c = s_c / s_1$.

The TE indicates the total emissions that all vehicles in the considered traffic network generate. The TE for emission type y is defined as

$$\text{TE}_y(k_c) = T \sum_{j=k_c M}^{(k_c+N_p)M-1} \sum_{c=1}^{n_c} \left(\sum_{(m,i) \in I_{\text{all}}} \text{EM}_{y,m,i,c}^{\text{inter}}(j) + \sum_{\alpha, \beta \in P_{\text{all}}} \text{EM}_{y,\alpha,\beta,c}^{\text{cross}}(j) + \sum_{o \in O_{\text{all}}} \text{EM}_{y,o,c}^{\text{inter}}(j) \right) \quad (3.44)$$

in which P_{all} is the set of all pairs of adjacent segments and origins, and $\text{EM}_{y,o,c}^{\text{inter}}$ represents the emission rate of emission category y for vehicles in queue at origin o . The emission rate $\text{EM}_{y,o,c}^{\text{inter}}$ is computed in a similarly way as $\text{EM}_{y,m,i,c}^{\text{inter}}$, with vehicles in queue considered to have low speeds and no acceleration.

3.3.2 End-Point Penalties

In MPC for traffic networks, obtaining appropriate control performance may require a long prediction period, since it is recommended [50] to select the prediction period to be in the order of the typical travel time for a vehicle to cross the traffic network. This makes computation slow and complex for large-scale traffic networks. In this section, we propose to use end-point penalties to take into account the performance of the considered traffic network beyond the prediction period.

End-Point Penalty Derived from the TTS

Based on the definition of the TTS, we develop a TTS end-point penalty, which is an estimate of the TTS for all vehicles that are still in the network at time step $(k_c + N_p)M$. Particularly, the TTS end-point penalty consists of the following parts:

- The number of vehicles in each segment multiplied by the time $t_{m,i,c}^{\text{rem}}((k_c + N_p)M)$ that a vehicle that is present in that segment at time step $(k_c + N_p)M$ would on the average need to get to its destination.
- The number of vehicles in each origin queue multiplied by the time $t_{o,c}^{\text{rem}}((k_c + N_p)M)$ that a vehicle present in that origin queue at time step $(k_c + N_p)M$ would on the average need to get to its destination.

⁷Note that the TTS index here includes the TTS for all segments, the TTS for all origins, and the TTS for all on-ramps, and they are treated equally, i.e. their weights are equal to 1.

⁸Note that in Sections 3.1 and 3.2 we assume $T_c = T$. Now we consider the general case with $T_c \neq T$.

The formula for computing the TTS end-point penalty is

$$\begin{aligned} \text{TTS}^{\text{end}}(k_c) = & \sum_{c=1}^{n_c} \sum_{(m,i) \in I_{\text{all}}} \mu_m \rho_{m,i,c}((k_c + N_p)M) L_m t_{m,i,c}^{\text{rem}}((k_c + N_p)M) \\ & + \sum_{o \in O_{\text{all}}} w_{o,c}((k_c + N_p)M) t_{o,c}^{\text{rem}}((k_c + N_p)M) \end{aligned} \quad (3.45)$$

End-Point Penalty Derived from the TE

Based on the definition of the TE, we develop a TE end-point penalty, which is an estimate of the total emissions that the remaining vehicles at time step $(k_c + N_p)M$ generate before leaving the traffic network. The TE end-point penalty consists of the following two parts:

- The number of vehicles in each segment at time step $(k_c + N_p)M$ multiplied by the emissions $\text{TE}_{y,m,i,c}^{\text{rem}}((k_c + N_p)M)$ that a vehicle present in that segment at time step $(k_c + N_p)M$ would on the average generate before leaving the network.
- The number of vehicles in each origin queue at time step $(k_c + N_p)M$ multiplied by the emissions $\text{TE}_{y,o,c}^{\text{rem}}((k_c + N_p)M)$ that a vehicle present in that origin queue at time step $(k_c + N_p)M$ would on the average generate before leaving the network.

The formula for computing the TE end-point penalty is

$$\begin{aligned} \text{TE}_y^{\text{end}}(k_c) = & \sum_{c=1}^{n_c} \sum_{(m,i) \in I_{\text{all}}} \mu_m \rho_{m,i,c}((k_c + N_p)M) L_m \text{TE}_{y,m,i,c}^{\text{rem}}((k_c + N_p)M) \\ & + \sum_{o \in O_{\text{all}}} w_{o,c}((k_c + N_p)M) \text{TE}_{y,o,c}^{\text{rem}}((k_c + N_p)M) \end{aligned} \quad (3.46)$$

Remark 3.2 Note that Origin-Destination (OD) matrices are needed for computing the proposed end-point penalties, since they both depend on the destinations of vehicles. As reviewed in [12], OD matrices can be estimated based on traffic counts by means of both static methods [36, 78, 100] and dynamic methods [25, 48, 88]. In this chapter, we just assume that a good estimate of the OD information is available. \square

3.3.3 Overall Objective Function for MPC

For different traffic conditions, the traffic control objectives may be conflicting [3]. We aim to achieve a balanced trade-off between the TTS and the TE here. However, the approach that we develop is generic, and it can also accommodate other performance indicators. As examples, variable speed limits and ramp metering are chosen as control measures.

The overall objective function of the online traffic control in this chapter is defined as follows:

$$\begin{aligned} J(k_c) = & \xi_{\text{TTS}} \frac{\text{TTS}(k_c)}{\text{TTS}_{\text{nom}}} + \sum_{y \in Y} \xi_{\text{TE},y} \frac{\text{TE}_y(k_c)}{\text{TE}_{y,\text{nom}}} \\ & + \frac{\xi_{\text{ramp}}}{N_c N_{\text{RM}}} \sum_{l=k_c}^{k_c+N_c-1} \sum_{o \in O_{\text{ramp}}} \left(r_o^{\text{ctrl}}(l) - r_o^{\text{ctrl}}(l-1) \right)^2 \\ & + \frac{\xi_{\text{speed}}}{N_c N_{\text{VSL}}} \sum_{l=k_c}^{k_c+N_c-1} \sum_{(m,i) \in I_{\text{speed}}} \left(\frac{v_{m,i}^{\text{ctrl}}(l) - v_{m,i}^{\text{ctrl}}(l-1)}{v_{m,\text{max}}^{\text{free}}} \right)^2 \end{aligned}$$

$$+ \xi_{\text{TTS}}^{\text{end}} \frac{\text{TTS}^{\text{end}}(k_c)}{\text{TTS}_{\text{nom}}^{\text{end}}} + \sum_{y \in Y} \xi_{\text{TE},y}^{\text{end}} \frac{\text{TE}_y^{\text{end}}(k_c)}{\text{TE}_{y,\text{nom}}^{\text{end}}} \quad (3.47)$$

where ξ_{TTS} , $\xi_{\text{TE},y}$, ξ_{ramp} , ξ_{speed} , $\xi_{\text{TTS}}^{\text{end}}$, and $\xi_{\text{TE},y}^{\text{end}}$ are nonnegative weights, TTS_{nom} , $\text{TE}_{y,\text{nom}}$, $\text{TTS}_{\text{nom}}^{\text{end}}$, and $\text{TE}_{y,\text{nom}}^{\text{end}}$ are the corresponding "nominal" values for some nominal control profile (e.g. the no-control case), N_{RM} is the number of groups of metered on-ramps, and N_{VSL} is the number of groups of variable speed limits, O_{ramp} is the set of all metered on-ramps, I_{speed} is the set of all segments with speed limits, $v_{m,\text{max}}^{\text{free}} = \max_{c=1,\dots,n_c} v_{m,c}^{\text{free}}$, r_o^{ctrl} is the ramp metering rate of on-ramp o for a given control step, $v_{m,i}^{\text{ctrl}}$ is the speed limit in segment i of link m for a given control step, and for $k = M(k_c - 1) + 1, \dots, Mk_c$, $r_o(k) = r_o^{\text{ctrl}}(k_c)$ and $v_{m,i}^{\text{SL}}(k) = v_{m,i}^{\text{ctrl}}(k_c)$. In (3.47), the first term and the second term are performance indices; the third term and the fourth term are used for penalizing the variations of the control inputs; the fifth term and the sixth term are end-point penalties for taking into account the performance beyond the prediction period.

3.4 Case Study: Comparison of Multi-Class Macroscopic Traffic Models

We now present a case study for comparing the multi-class traffic flow models and traffic emission models of Sections 3.1-3.2, and for evaluating the effectiveness of the end-point penalties proposed in Section 3.3.

3.4.1 Benchmark Network

The case study is based on the Dutch freeway A13, where we consider the direction from Rijswijk to Rotterdam, as shown in Figure 3.2. The start of the considered part of the A13 is seen as the mainstream origin (O_0), and the end of the considered part of the A13 is seen as the mainstream destination (D_0). There are four on-ramps (O_1 , O_2 , O_3 , and O_4) and four off-ramps (O_5 , O_6 , O_7 , and O_8) each of which consists of a single lane, and all the on-ramps are metered. The main road subsumes three lanes, and variable speed limit signs are installed through the whole stretch. According to the location of on-ramps, off-ramps, and variable speed limit signs, the main road (7.8 km) is divided into 21 links, and in total 23 segments, i.e., most links only have 1 segment. More specifically, Table 3.1 lists the lengths of all segments (indexed from O_0 to D_0 in the form of (m, i)) and the positions of the variable speed limit signs (15 positions in total, numbered as $1, \dots, 15$).

The microscopic simulators VISSIM and ENVIVER are used as process models for representing the real traffic network. VISSIM is used for simulating the traffic flows, and ENVIVER is used for simulating the emissions. The case study can be seen as a proof of the concept for the integrated control approach for reducing traffic congestion and traffic emissions; thus the VISSIM bases are chosen so that in VISSIM relevant phenomena are present, such as capacity drop and stability of traffic flows. The multi-class traffic flow models and traffic emission models extended in Sections 3.1-3.2 are used as prediction models in MPC. In both the process models and the prediction models, we consider two classes of vehicles (i.e. cars and trucks), and the traffic variables for different vehicle classes

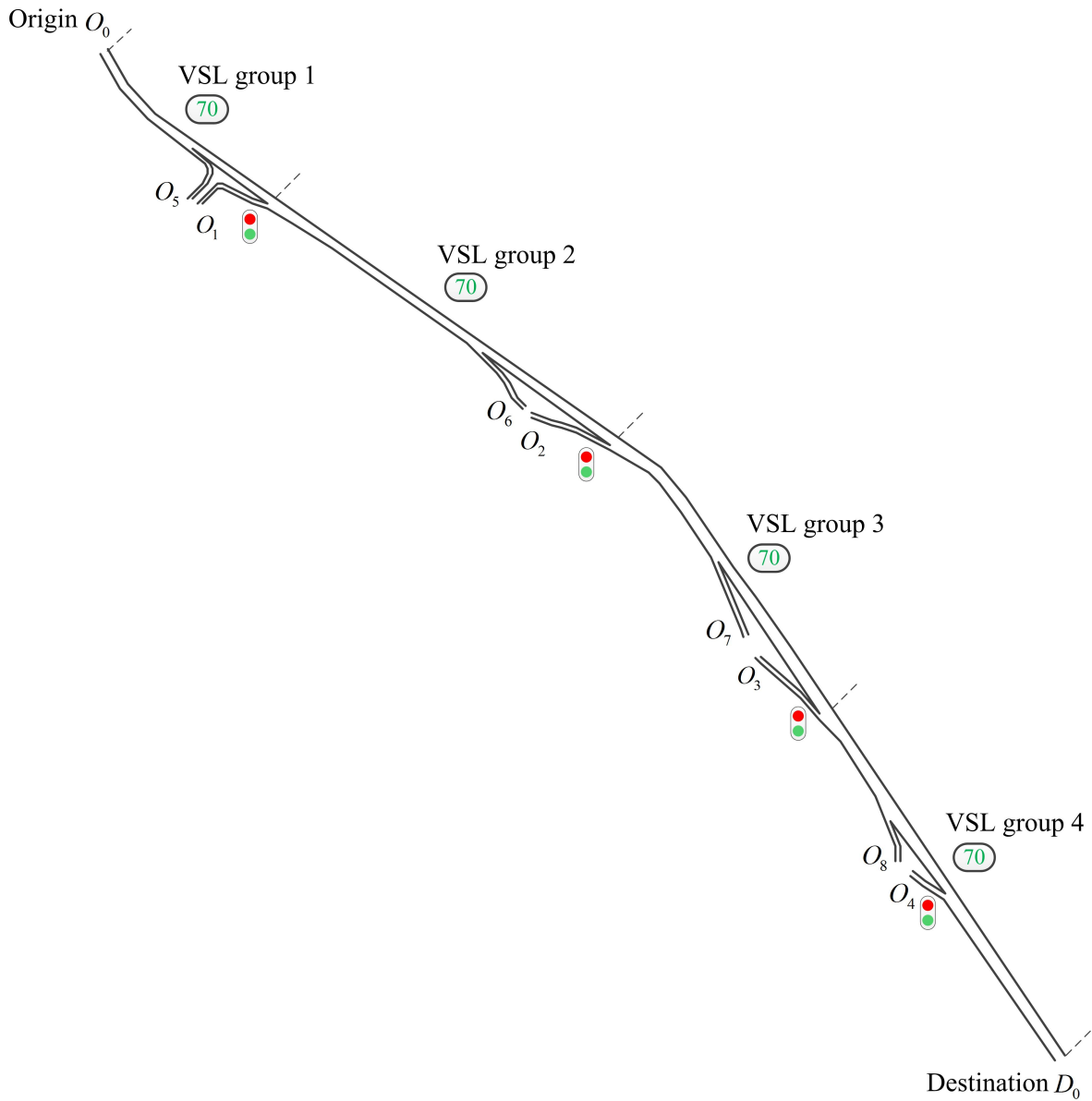


Figure 3.2: Part of the Dutch freeway A13 considered in the case study (O_0 : Rijswijk; O_1 and O_5 : Delft-Noord; O_2 and O_6 : Delft; O_3 and O_7 : Delft-Zuid; O_4 and O_8 : Service area Vrijenban.)

Table 3.1: Segments and Variable Speed Limits (VSL)

Segment	(1,1)	(2,1)	(3,1)	(4,1)	(5,1)	(6,1)	(7,1)	(8,1)
Length (km)	0.28	0.40	0.40	0.21	0.31	0.28	0.56	0.24
VSL	–	1, 2	3	4	–	–	5	6
Segment	(9,1)	(10,1)	(10,2)	(11,1)	(12,1)	(13,1)	(14,1)	(14,2)
Length (km)	0.27	0.34	0.33	0.34	0.33	0.59	0.37	0.37
VSL	–	7	–	8	9	–	10	–
Segment	(15,1)	(16,1)	(17,1)	(18,1)	(19,1)	(20,1)	(21,1)	
Length (km)	0.25	0.32	0.35	0.43	0.28	0.23	0.37	
VSL	–	11	12	13	14	–	15	

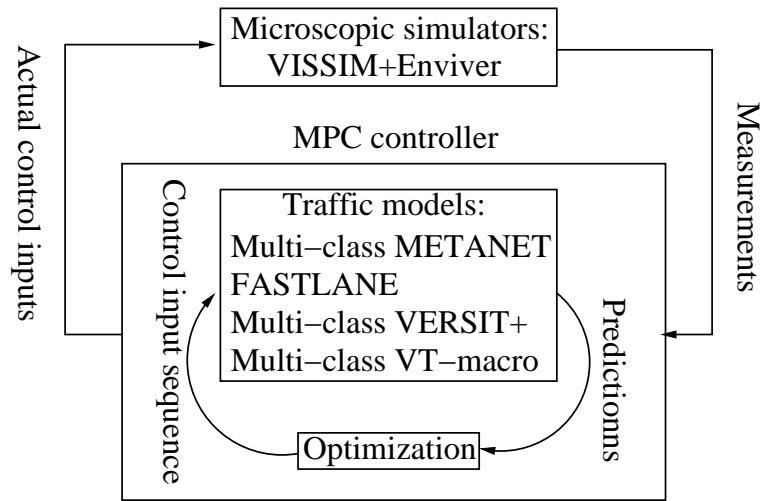


Figure 3.3: Model predictive control for A13

can be measured in VISSIM. The control procedure of MPC based on the extended multi-class models is shown in Figure 3.3.

3.4.2 Identification of the Model Parameters

In order to describe the traffic flows and emissions through the models extended in Sections 3.1 and 3.2, the parameters for these models need to be calibrated. The mainstream demand and the on-ramp demands for identification, which are shown in Figure 3.4, are generated based on the field measurements of the A13 on Feb. 18, 2014. The fraction of trucks in all the demands is taken as 0.1, considering the actual situation on the A13. These demands are used as the inputs for the microscopic simulator VISSIM, and the outputs from VISSIM are used as the inputs for ENVIVER. The simulation results of VISSIM and ENVIVER are used for identifying the parameters of the multi-class macroscopic models of Sections 3.1-3.2, and the measured mainstream speeds in VISSIM for several representative segments are plotted in Figure 3.5.

For multi-class METANET and FASTLANE, the objective for the identification procedure is to fit the TTS. Similarly, for multi-class VERSIT+ and multi-class VT-macro, the objective for the identification procedure is to fit the TE, where only CO₂ is considered. The optimizer "lsqnonlin" in MATLAB has been used for solving the calibration problem, based on the "trust-region-reflective" algorithm.

The prediction period length is chosen as 15 minutes, which corresponds to the average time needed for a vehicle to cross the freeway stretch under consideration. We consider the morning rush hours from 8.00 am to 10.00 am for the identification of the model parameters. For the period 8.00 am-10.00 am, the average calibration and validation errors within the prediction period between the measured TTS and the predicted TTS by METANET and FASTLANE are shown in Table 3.2. The calibration and validation errors for multi-class VT-macro and multi-class VERSIT+ in the period 8.00 am-10.00 am are shown in Table 3.3. Three scenarios for the traffic demands are considered for assessment:

- Scenario 1: the scenario used for identification;
- Scenario 2: Scenario 1 + sinusoidal noise (with an amplitude equal to 5% of the

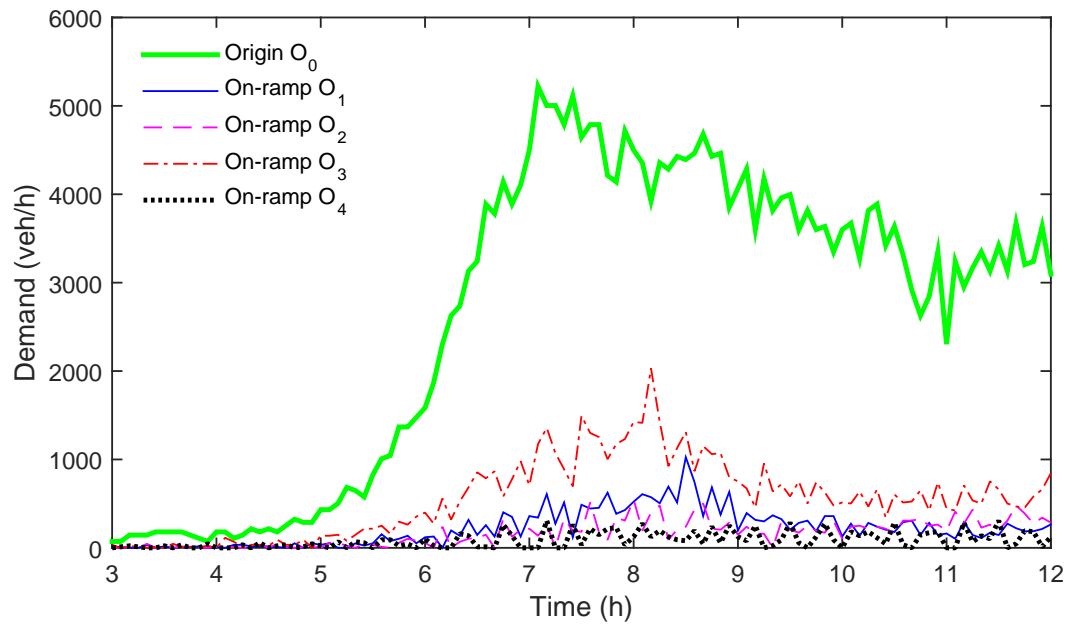


Figure 3.4: Demands for A13

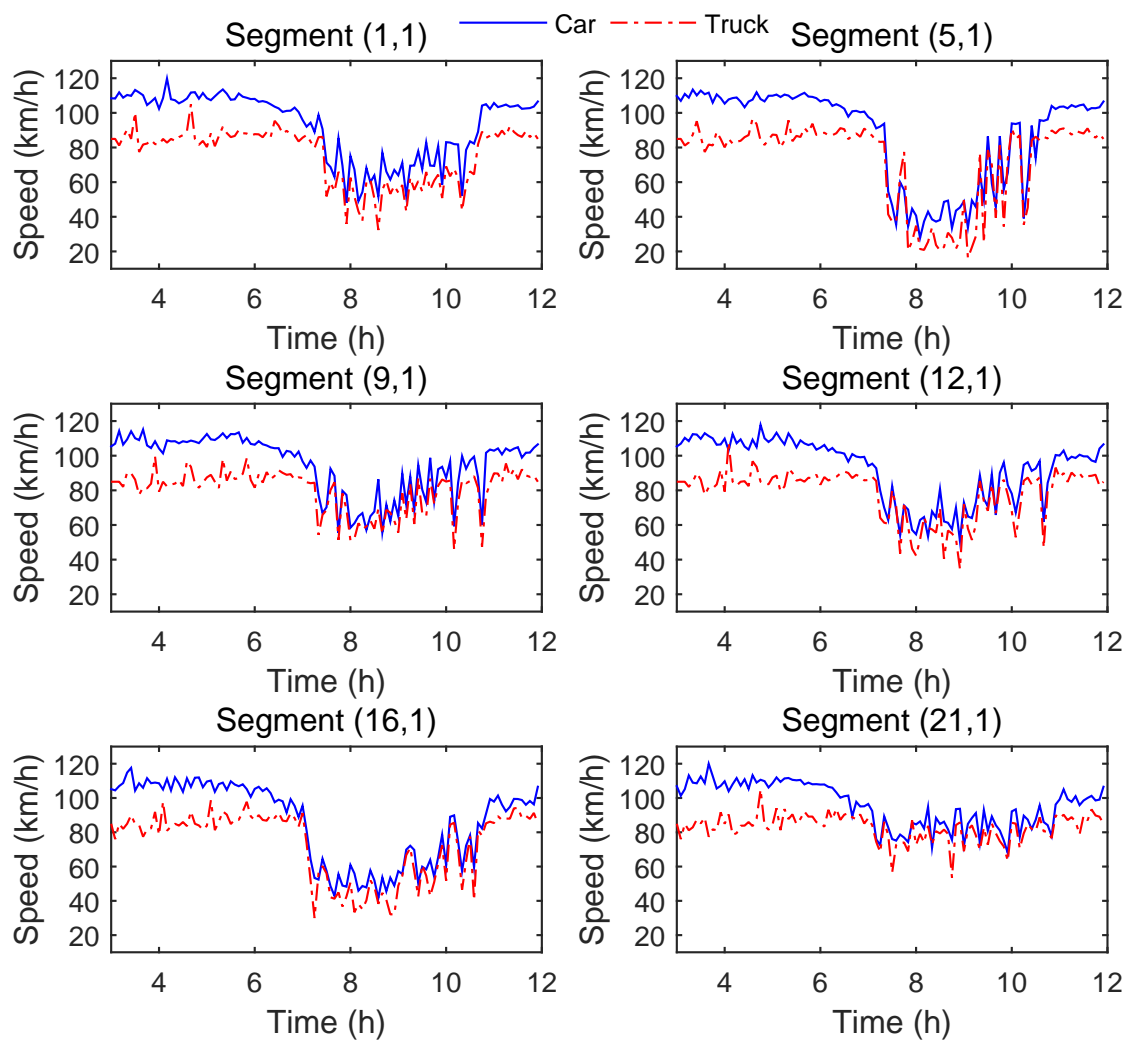


Figure 3.5: Measured mainstream speeds for A13)

Table 3.2: Calibration (Scenario 1) and validation (Scenarios 2 and 3) errors for traffic flow models

	Scenario 1	Scenario 2	Scenario 3
Multi-class METANET	8.8%	9.2%	7.7%
FASTLANE	8.1%	7.4%	6.8%

Table 3.3: Calibration (Scenario 1) and validation (Scenarios 2 and 3) errors for emission models

	Scenario 1	Scenario 2	Scenario 3
Multi-class VERSIT+	2.6%	3.3%	4.3%
Multi-class VT-macro	1.1%	1.3%	1.4%

demands for Scenario 1, and with a cycle time of 15 minutes);

- Scenario 3: Scenario 1 + white noise (with an amplitude equal to 5% of the demands for Scenario 1).

From Table 3.2, it can be noticed that for multi-class METANET the calibration error is 8.8%, and the validation error is 7.7% – 9.2%; for FASTLANE, the calibration error is 8.1%, and the validation error is 6.8% – 7.4%. Thus, both the calibration errors and the validation errors are comparable for multi-class METANET and FASTLANE. From Table 3.3, it can be seen that for multi-class VERSIT+ the calibration error is 2.6%, and the validation error is 3.3% – 4.3%; for multi-class VT-macro, the calibration error is 1.1%, and the validation error is 1.3% – 1.4%. The calibration errors and the validation errors are thus also comparable for multi-class VERSIT+ and multi-class VT-macro.

Based on the model parameters obtained, the total fundamental diagram (basic flow-density relationship) of the new multi-class METANET model is shown in Figure 3.6, and the space fractions for cars are plotted in Figure 3.7.

3.4.3 Control Set-up

Scenario 1 as shown in Figure 3.4 is considered for control in this case study. The control time interval (T_c) is chosen as 5 minutes, the control period length is chosen as 10 minutes ($N_c T_c = 10$ minutes, $N_c = 2$), and the prediction period length is chosen as 15 minutes ($N_p T_c = 15$ minutes, $N_p = 3$). The simulation time step (T) is selected to be 6 seconds, according to (2.1).

Recall that all four on-ramps are metered, i.e. $N_{RM} = 4$. According to the actual length of the on-ramps, the maximum permitted queue lengths for all vehicle classes ($w_{o,efc}^{\max}$, $o \in O_{\text{ramp}} = \{O_1, O_2, O_3, O_4\}$) are repetitively 100, 100, 200, 50 pce. We divide the 15 positions (as listed in Table 3.1) installed with variable speed limit signs into 4 groups ($N_{VSL} = 4$):

- VSL group 1: VSL 1-VSL 4, i.e. variable speed limits before O_1 ;
- VSL group 2: VSL 5-VSL 7, i.e. variable speed limits between O_1 and O_2 ;
- VSL group 3: VSL 8-VSL 10, i.e. variable speed limits between O_2 and O_3 ;
- VSL group 4: VSL 11-VSL 15, i.e. variable speed limits after O_3 .

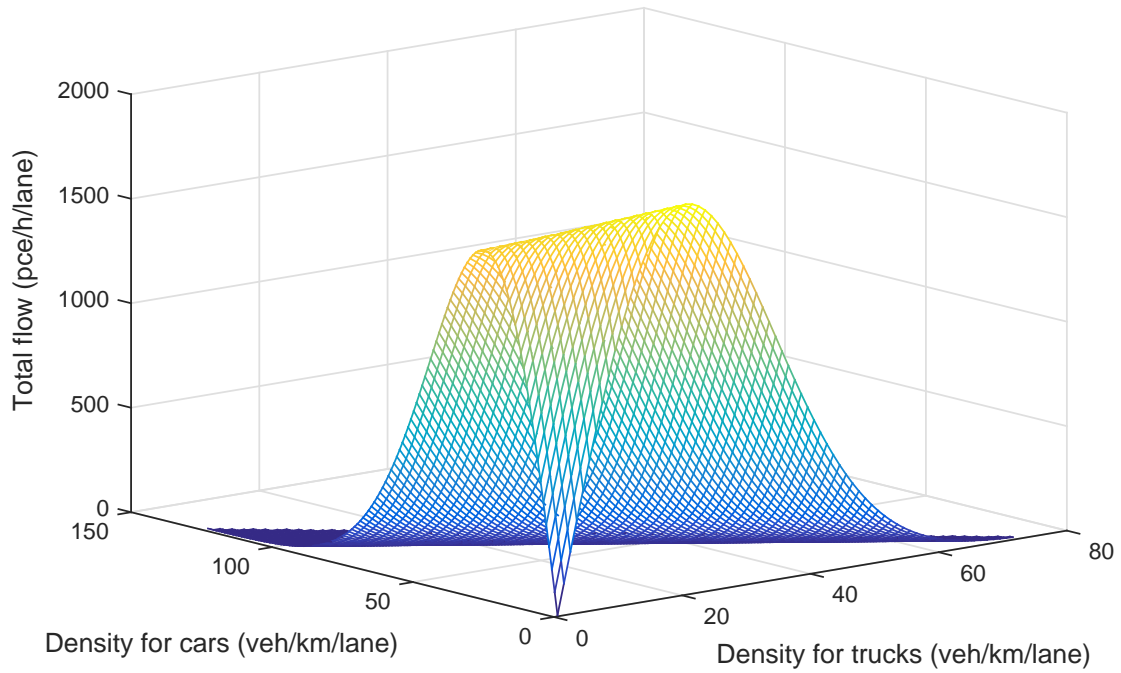


Figure 3.6: Total fundamental diagram for cars and trucks based on multi-class METANET

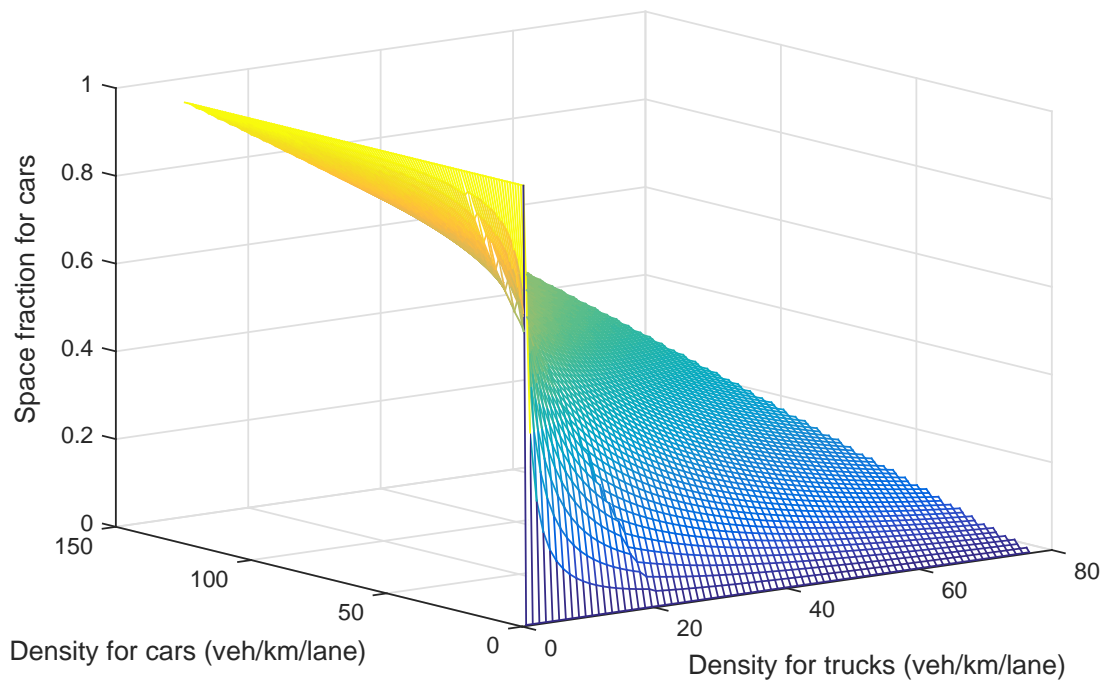


Figure 3.7: Space fraction for cars

Considering that all segments are relatively short, we assume that vehicles in a segment without a variable speed limit sign are subject to the variable speed limit for the closest upstream segment with a variable speed limit sign.

As will be explained below, two groups of approaches are implemented for comparing multi-class macroscopic traffic flow models and traffic emission models extended in Sections 3.1-3.2, and for investigating the effectiveness of the end-point penalties proposed in Section 3.3.

Comparison for multi-class traffic models

For the multi-class macroscopic traffic flow models and traffic emission models, we compare four approaches *without* end-point penalties as follows:

- Approach A: multi-class METANET and multi-class VERSIT+;
- Approach B: multi-class METANET and multi-class VT-macro;
- Approach C: FASTLANE and multi-class VERSIT+;
- Approach D: FASTLANE and multi-class VT-macro.

For each approach, we consider 3 combinations of weights *without* end-point penalties:

- Combination 1: $\xi_{TTS}=1$, $\xi_{TE,CO_2}=0.1$, $\xi_{TTS}^{end}=0$, and $\xi_{TE,CO_2}^{end}=0$;
- Combination 2: $\xi_{TTS}=0.5$, $\xi_{TE,CO_2}=0.5$, $\xi_{TTS}^{end}=0$, and $\xi_{TE,CO_2}^{end}=0$;
- Combination 3: $\xi_{TTS}=0.1$, $\xi_{TE,CO_2}=1$, $\xi_{TTS}^{end}=0$, and $\xi_{TE,CO_2}^{end}=0$.

Assessment of end-point penalties

In order to investigate the effects of the end-point penalties, we also implement the following four approaches:

- Approach E: multi-class METANET and multi-class VERSIT+ with end-point penalties;
- Approach F: multi-class METANET and multi-class VT-macro with end-point penalties;
- Approach G: FASTLANE and multi-class VERSIT+ with end-point penalties;
- Approach H: FASTLANE and multi-class VT-macro with end-point penalties.

As an illustration, we choose $\xi_{TTS}=1$ and $\xi_{TE,CO_2}=0.1$ (the same as in Combination⁹ 1) for Approaches E to H. For $\xi_{TTS}=1$ and $\xi_{TE,CO_2}=0.1$, an investigation has been done to find appropriate ξ_{TTS}^{end} and ξ_{TE,CO_2}^{end} for the end-point penalties; the values obtained are $\xi_{TTS}^{end}=0.1$ and $\xi_{TE,CO_2}^{end}=0.01$.

We solve the control problem by means of "fmincon" in Matlab based on the 'active-set' algorithm and a multi-start scheme. An investigation has been done to ensure that the

⁹Combinations 2 and 3 are not considered here, since for Approaches E to H we mainly focus on the comparison between the case with end-point penalties and the case without end-point penalties, not on the effects of different combinations of weights for the TTS and the TE.

CPU time for the approaches including multi-class METANET and the approaches including FASTLANE are roughly the same. Thus for Approaches A, B, E, and F, 50 starting points are used for every control step, and for C, D, G, and H, 70 starting points are used for every control step.

3.4.4 Simulation Results and Analysis

All simulations are implemented on a computer with 2 Intel(R) Xeon(R) CPU E5-1620 v3 @3.50GHz processors. For each approach and each combination of weights, 10 runs with different random seeds corresponding to different starting points for "fmincon" are implemented, and the average results are listed in Tables 3.4-3.7. In addition, we have also recorded the CPU time for each approach and each combination of weights, and the results are listed in Tables 3.4-3.7.

In these tables, $J_{TTS,TE}^{imp}$ represents the relative improvement for $J_{TTS,TE}$ in the entire simulation period w.r.t. the case without control:

$$J_{TTS,TE} = \xi_{TTS} \frac{TTS_{tot}}{TTS_{nom}} + \xi_{TE,CO_2} \frac{TE_{CO_2,tot}}{TE_{CO_2,nom}} \quad (3.48)$$

$$J_{TTS,TE}^{imp} = \frac{J_{TTS,TE}^{no\ control} - J_{TTS,TE}^{control}}{J_{TTS,TE}^{no\ control}} \quad (3.49)$$

where TTS_{nom} is the TTS over the prediction period for the no-control case computed at the first control step, TTS_{tot} is the total time spent over the entire simulation period, $TE_{CO_2,nom}$ is the TE of CO₂ over the prediction period for the no-control case computed at the first control step, and $TE_{CO_2,tot}$ represents the TE of CO₂ over the entire simulation period. In addition, $J_{TTS,TE}^{no\ control}$ represents $J_{TTS,TE}$ for the case without control, and $J_{TTS,TE}^{control}$ represents $J_{TTS,TE}$ for the case with control based on Approaches E-H.

We define a total objective function J_{tot} as follows:

$$J_{tot} = \xi_{TTS} \frac{TTS_{tot}}{TTS_{nom}} + \xi_{TE,CO_2} \frac{TE_{CO_2,tot}}{TE_{CO_2,nom}} + \xi_{queue} \max_{o \in O_{ramp}} \max \left(\max_{k=1, \dots, k_{end}} \sum_{c=1}^{n_c} \frac{p_c w_{o,c}(k)}{w_{o,efc}^{max}} - 1, 0 \right) \quad (3.50)$$

where k_{end} is the last simulation time step of the entire simulation period. The last term of J_{tot} represents the maximum queue length constraint violation for all on-ramps over the entire simulation period, and the weight for this term is set to be a large value aiming at evaluating the satisfaction of queue length constraints: $\xi_{queue} = 10$. This total objective function is used for comparing the total performance including the TTS, the TE, and the queue length constraint violations, where higher values indicate a worse total performance.

Results for multi-class traffic models without end-point penalties

The results for multi-class traffic models *without* end-point penalties are listed in Tables 3.4-3.6.

From Tables 3.4-3.6, it can be seen that Approach A (multi-class METANET and multi-class VERSIT+) can improve the performance for TTS and TE ($J_{TTS,TE}^{imp}$: 2.2% – 6.8%) w.r.t. the

Table 3.4: Simulation results for Combination 1

Approaches	$J_{TTS,TE}^{imp}$	J_{TTS}^{imp}	J_{TE}^{imp}	Constraint violations				J_{tot}	CPU (h)
				O_1	O_2	O_3	O_4		
A	2.2%	2.3%	1.0%	0%	0%	0%	0%	8.6	7.7
B	2.4%	2.6%	0.6%	0%	0%	0%	0%	8.6	11.4
C	-5.7%	-7.5%	12.6%	43.5%	0%	125.4%	0%	21.8	10.0
D	-8.6%	-10.8%	14.1%	48.1%	14.6%	210.2%	0%	30.6	10.7

Table 3.5: Simulation results for Combination 2

Approaches	$J_{TTS,TE}^{imp}$	J_{TTS}^{imp}	J_{TE}^{imp}	Constraint violations				J_{tot}	CPU (h)
				O_1	O_2	O_3	O_4		
A	3.9%	1.0%	6.8%	0%	0%	0%	0%	7.7	7.0
B	2.4%	2.1%	2.8%	6.6%	0%	0%	0%	8.4	10.1
C	0.6%	-12.9%	14.2%	10.2%	8.1%	229.2%	0%	30.8	10.7
D	0.2%	-14.0%	14.6%	57.4%	0%	220.9%	0%	30.0	13.3

Table 3.6: Simulation results for Combination 3

Approaches	$J_{TTS,TE}^{imp}$	J_{TTS}^{imp}	J_{TE}^{imp}	Constraint violations				J_{tot}	CPU (h)
				O_1	O_2	O_3	O_4		
A	6.8%	1.3%	7.4%	5.1%	0%	0%	0%	8.6	6.1
B	3.7%	1.8%	3.9%	26.5%	0%	0%	0%	11.0	8.9
C	13.1%	-17.3%	16.1%	37.9%	23.8%	177.0%	0%	25.3	10.3
D	12.7%	-15.0%	15.5%	107.1%	18.9%	188.7%	0%	26.5	12.9

Table 3.7: Simulation results for Combination 1 with end-point penalties

Approaches	$J_{TTS,TE}^{imp}$	J_{TTS}^{imp}	J_{TE}^{imp}	Constraint violations				J_{tot}	CPU (h)
				O_1	O_2	O_3	O_4		
E	3.5%	3.6%	1.5%	0%	0%	0%	0%	8.5	8.2
F	4.2%	4.5%	1.1%	0%	0%	0%	0%	8.4	12.4
G	-9.7%	-11.8%	11.7%	57.2%	6.3%	236.3%	0%	33.3	8.0
H	-5.9%	-7.8%	12.8%	69.0%	7.7%	157.8%	0%	25.1	10.0

no-control case, with relatively small queue length constraint violations (0% – 5.1%). The queue length constraint violations only occur for Combination 3, which has a high weight for TE. Approach B (multi-class METANET and multi-class VT-macro) can also improve the performance for TTS and TE ($J_{TTS,TE}^{imp}$: 2.4% – 3.7%) w.r.t. the no-control case, but the queue length constraint violations increase from 0% to 26.5% with the increase of the weight for TE. The queue length constraint violations for multi-class METANET increase with the weight for TE, probably due to the fact that vehicles in queues are considered to generate less emissions than vehicles that are driving, since the vehicles in the queues have low speeds and almost no acceleration. For all the combinations of weights, Approaches A and B reduce both TTS

($J_{TTS}^{imp} : 1.0\% - 2.6\%$) and TE ($J_{TE}^{imp} : 0.6\% - 7.4\%$) w.r.t. the no-control case. When the weight for TE increases, the value of TE is further reduced, with a sacrifice in the reduction for TTS. For Approach A, the values of J_{tot} are less than or equal to those for Approach B for all the combinations of weights, i.e. the total performance for Approach A is better than the total performance for Approach B.

The approaches based on FASTLANE (C and D) lead to a worse performance for TTS and TE ($J_{TTS,TE}^{imp} : -8.6\% - -5.7\%$) than the no-control case for Combination 1, but a better performance for TTS and TE ($J_{TTS,TE}^{imp} : 0.2\% - 13.1\%$) than the no-control case for Combination 2 and Combination 3. For all the combinations of weights, Approaches C and D decrease TE ($J_{TE}^{imp} : 12.6\% - 16.1\%$) but increase TTS ($J_{TTS}^{imp} : -17.3\% - -7.5\%$) w.r.t. the no-control case. When the weight for TE increases, the value of TE is further reduced, with a sacrifice in TTS. Note, however, that for all the combinations there are consistent queue length constraint violations for on-ramps O_1 (10.2% – 107.1%) and O_3 (125.4% – 229.2%). Thus the values of J_{tot} (21.8 – 30.8) for the approaches based on FASTLANE (C and D) are much higher than the values (7.7 – 11.0) for the approaches based on multi-class METANET (A and B), i.e. the total performance for the former approaches is worse than that of the latter approaches. High constraint violations can lead to traffic jams upstream of the given on-ramps, which is an important issue to be handled when a control approach is developed. For the settings of our experiment, the approaches based on multi-class METANET are more capable of dealing with the queue length constraints.

Comparing the CPU time for Approach A (which is based on multi-class METANET and multi-class VERSIT+) with that for Approach B (which is based on multi-class METANET and multi-class VT-macro), we find that Approach A is faster than Approach B for the 3 considered combinations of weights. Comparing the CPU time for Approach C (which is based on FASTLANE and multi-class VERSIT+) with that for Approach D (which is based on FASTLANE and multi-class VT-macro), we find that Approach C is faster than Approach D for the 3 considered combinations of weights.

Results for end-point penalties

The results for approaches with end-point penalties are included in Table 3.7, and these results are now compared with results in Table 3.4. In comparison with the approaches based on multi-class METANET without end-point penalties (A and B in Combination 1), including end-point penalties (E and F) can further improve the performance for TTS and TE ($J_{TTS,TE}^{imp} : 3.5\% - 4.2\%$), while there is still no queue length constraint violation. Approaches E and F further improve TTS ($J_{TTS}^{imp} : 3.6\% - 4.5\%$) and TE ($J_{TE}^{imp} : 1.1\% - 1.5\%$) w.r.t. Approaches A and B. In addition, the values of J_{tot} (8.4 – 8.5) are also further reduced w.r.t. the approaches without end-point penalties. Thus, for approaches based on multi-class METANET we can say that end-point penalties can improve both the performance for TTS and TE and the total performance.

The approaches based on FASTLANE with end-point penalties (G and H) cannot reduce the high constraint violations for on-ramps O_1 (57.2% – 69.0%) and O_3 (157.8% – 236.3%) to a low level, and the values of J_{tot} (25.1 – 33.3) are still much higher than those for the approaches based on multi-class METANET (A, B, E, and F). This might be because of the first-order characteristics of FASTLANE, which makes the estimations of end-point penalties less reliable.

Comparing the CPU time for Approaches A and B (which are based on multi-class

METANET without end-point penalties) with that for Approaches E and F (which are based on multi-class METANET with end-point penalties), we find that when the end-point penalties are included the CPU time is increased by 6.5% for Approach A, and by 8.8% for Approach B. However, for the approaches based on FASTLANE, the CPU time for Approach G (with end-point penalties) is reduced compared to Approach C (without end-point penalties), and the CPU time for Approach H (with end-point penalties) is also reduced compared to Approach D (without end-point penalties).

Control Inputs

For each of the Approaches A-D based on Combination 1 of weights and for each of the Approaches E-H, the control inputs determined by a representative run among the 10 repeated runs (cf. the first paragraph of Section 3.4.4) are plotted in Figures 3.8-3.9.

As can be seen in Figure 3.8, speed limits differ from the maximum speed limit (i.e. free-flow speed of cars) in the period 8 h-8.3 h for Approaches A and B (which are based on multi-class METANET without end-point penalties). For Approaches E and F (which are based on multi-class METANET with end-point penalties), speed limits differ from the maximum speed limit for a longer period (8 h-9 h) than Approaches A and B. For Approaches C, D, G, and H (which are based on FASTLANE), variable speed limits fluctuate much more than for Approaches A, B, E, and F (which are based on multi-class METANET).

From Figure 3.9, ramp metering rates differ from the maximum metering rate (i.e. 1) in the period 8 h-8.3 h for Approaches A and B (which are based on multi-class METANET without end-point penalties), and in a longer period (8 h-9 h) for Approaches E and F (which are based on multi-class METANET with end-point penalties). Similarly to the speed limits, for Approaches C, D, G, and H (which are based on FASTLANE), ramp metering rates fluctuate much more than for Approaches A, B, E, and F (which are based on multi-class METANET).

Analysis of Traffic Behavior

For the same settings as Figures 3.8-3.9, the densities and speeds of several representative segments are plotted in Figures 3.10-3.13.

From Figures 3.10-3.11, it can be noticed that the profiles of densities for all the considered control approaches are similar to those for the no-control case, i.e. there is no clear peak for densities. Moreover, it can be seen in Figures 3.12-3.13 that the speeds for all the considered approaches are also similar to those for the no-control case, i.e. the speed profiles are do not fluctuate heavily. Note that even the profiles of speeds and densities are similar to those for the no-control case, the control approaches based on multi-class METANET (Approaches A, B, E, and F) can still improve the control performance, e.g. for Approach F the performance for TTS and TE is improved by 4.2% without queue length constraint violation.

Overall conclusions for the case study

On the basis of all the simulation results, we can conclude that the approaches based on multi-class METANET combined with emission models can reduce the TTS and the TE in a balanced way; moreover, the multi-class METANET model captures the maximum queue dynamics better than FASTLANE although they are both based on the same queue model.

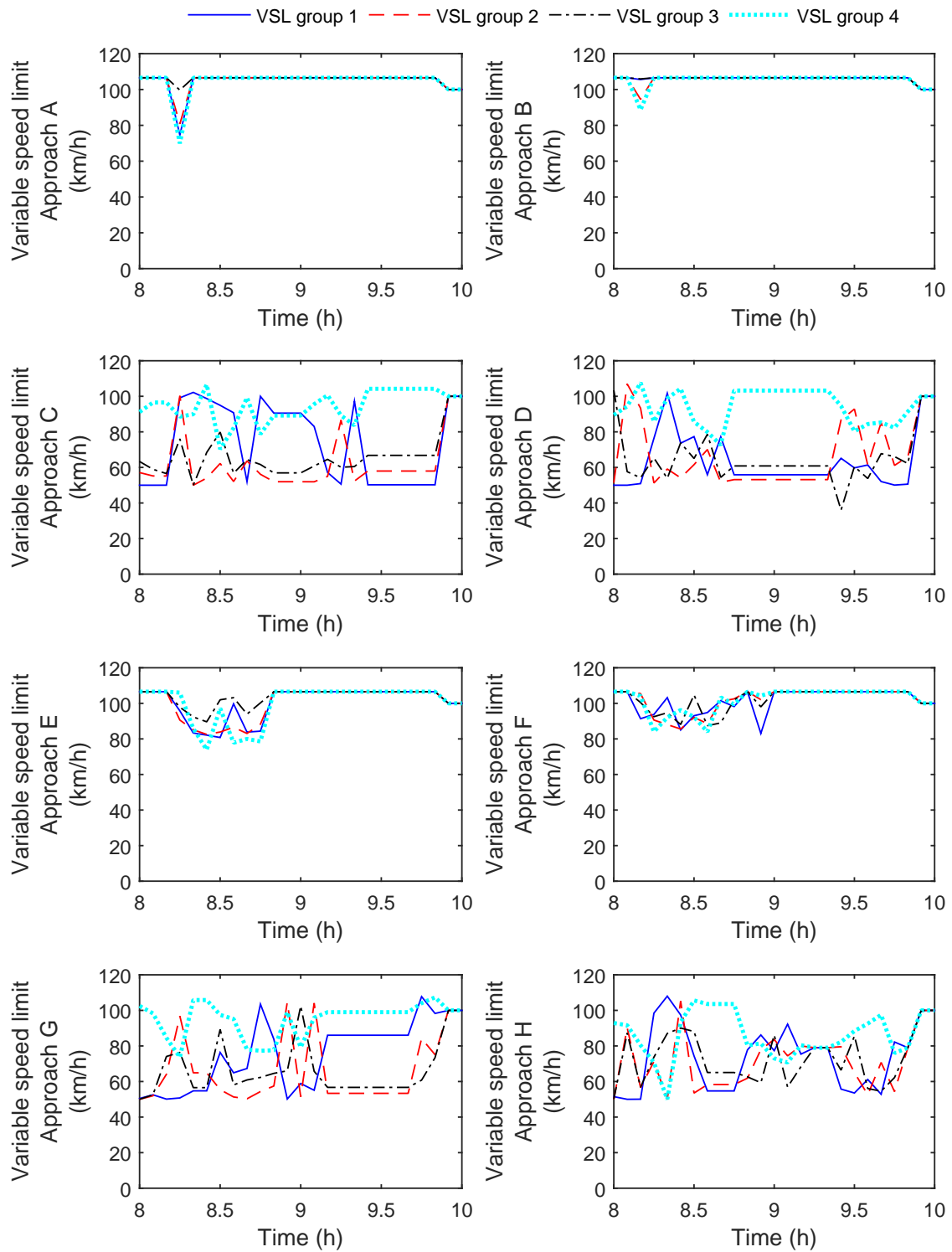


Figure 3.8: Variable speed limits

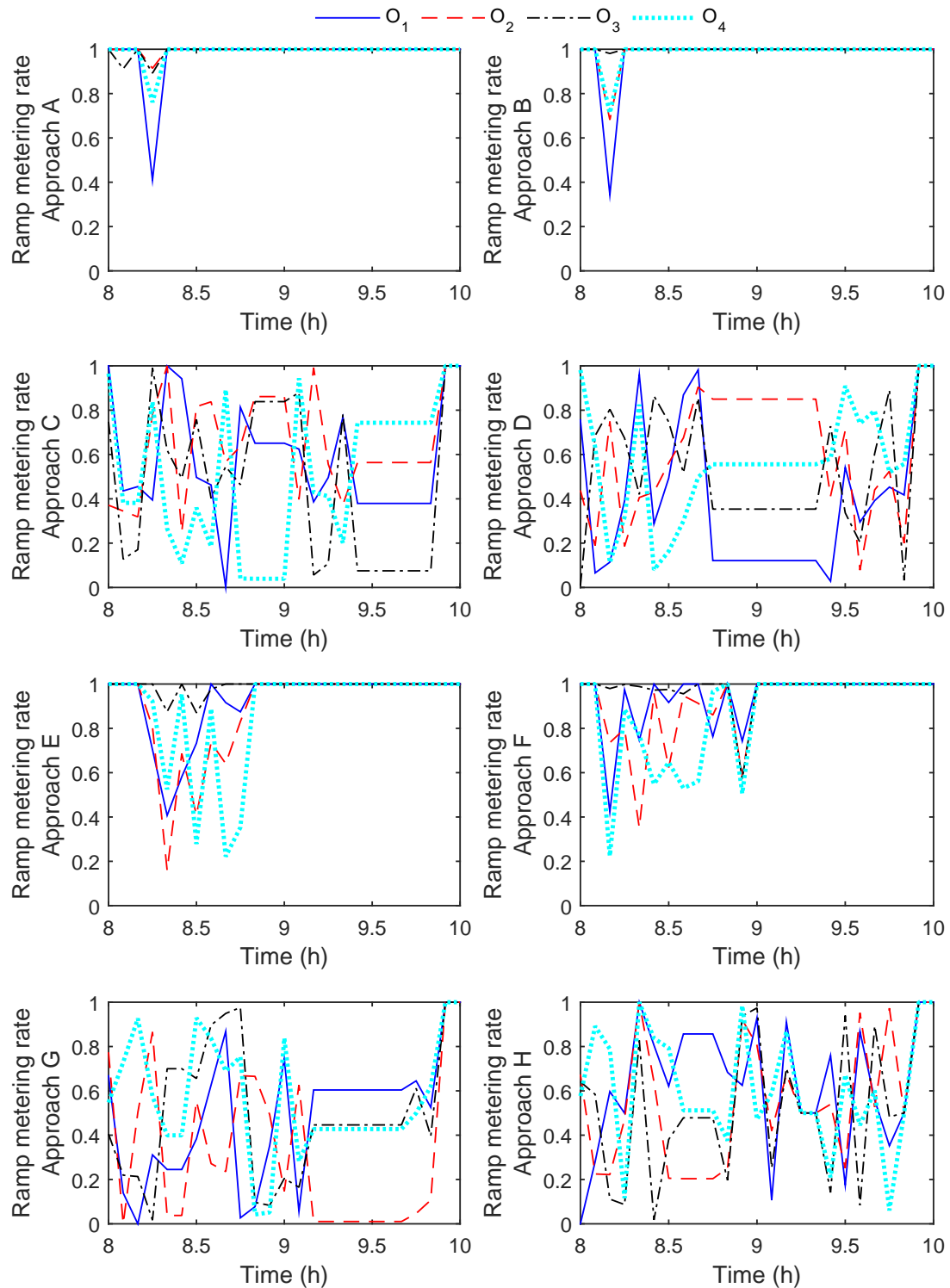


Figure 3.9: Ramp metering rates

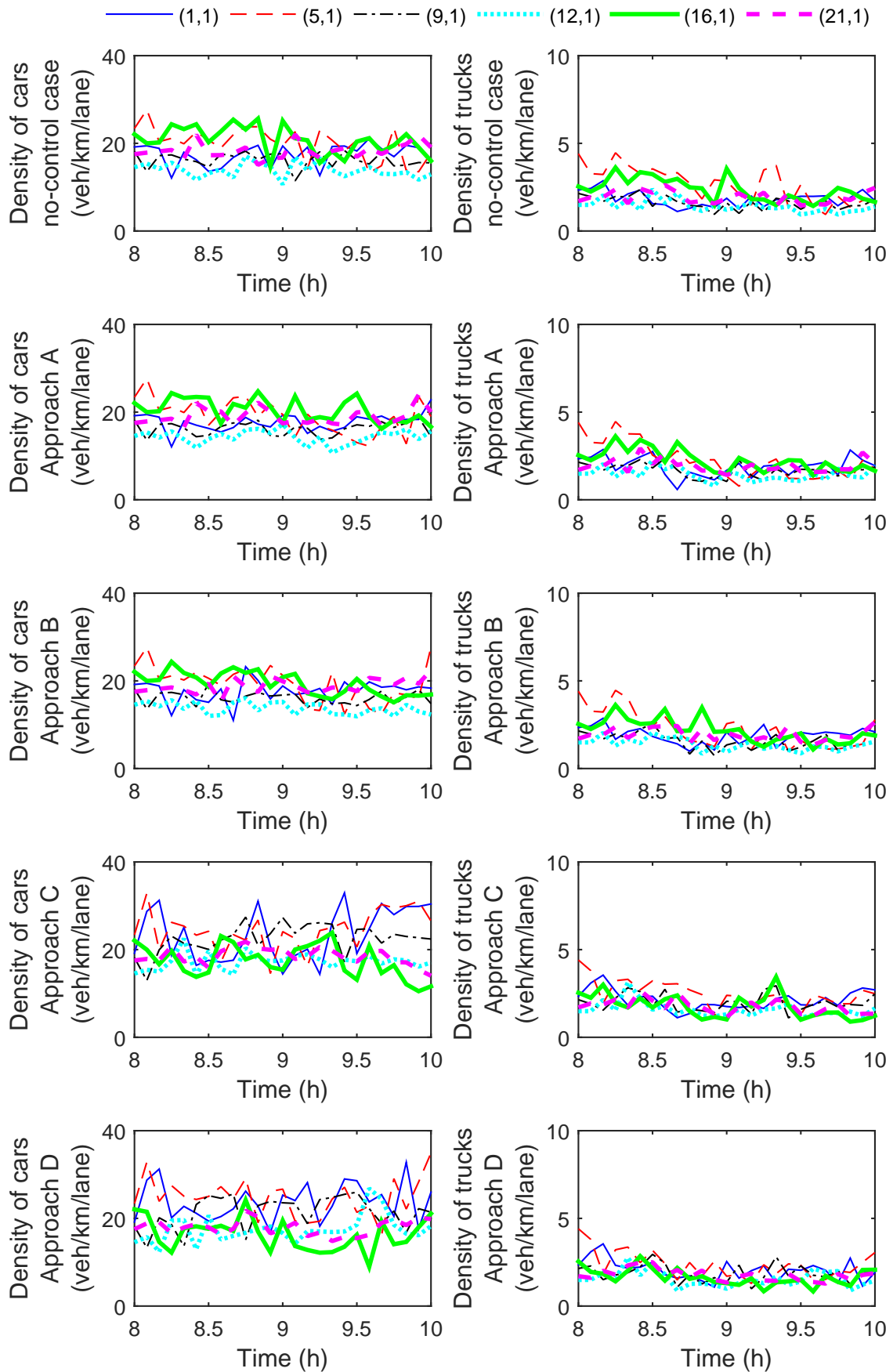


Figure 3.10: Densities of segments for the no-control case and Approaches A-D

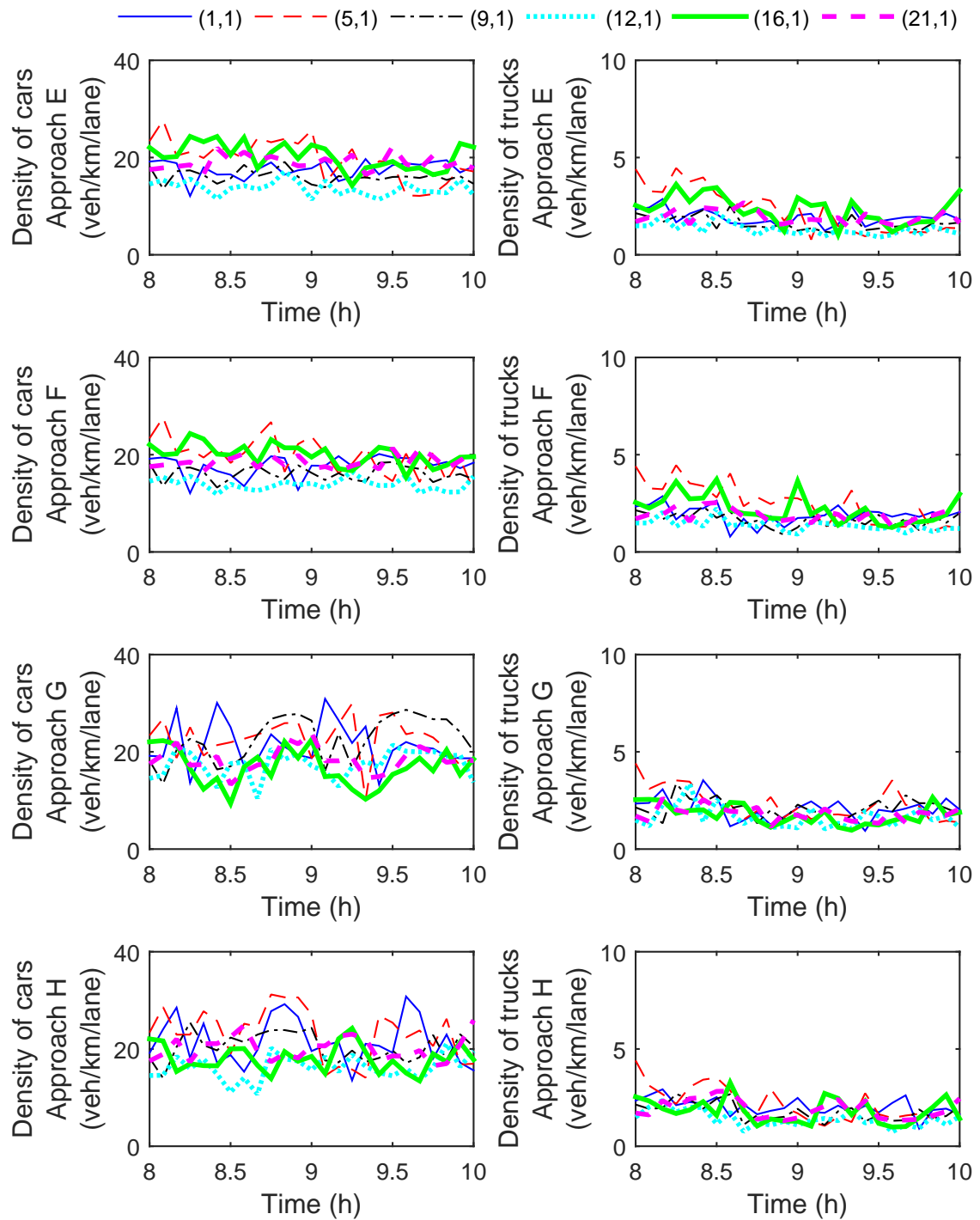


Figure 3.11: Densities of segments for Approaches E-H

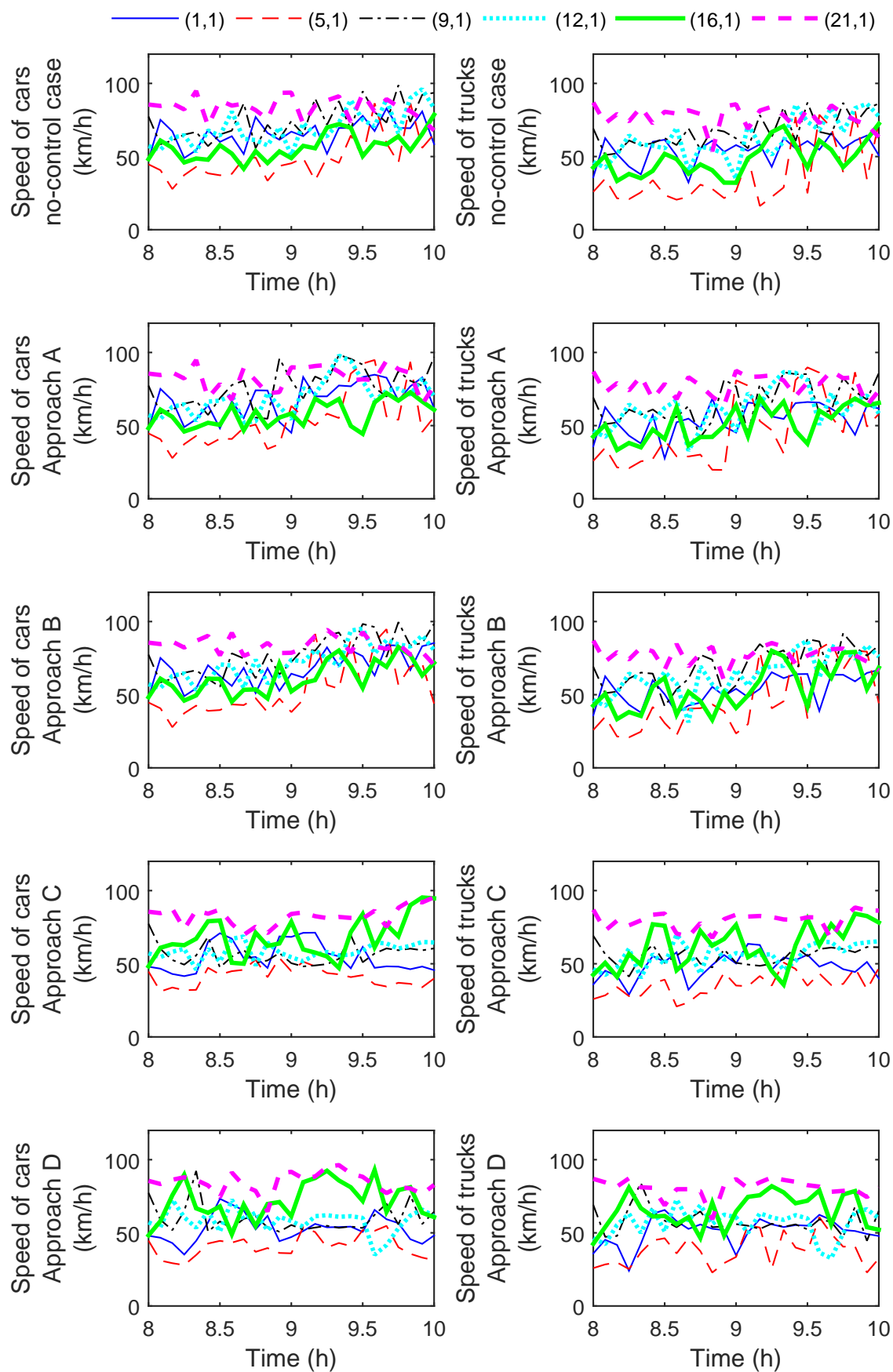


Figure 3.12: Speeds of segments for the no-control case and Approaches A-D

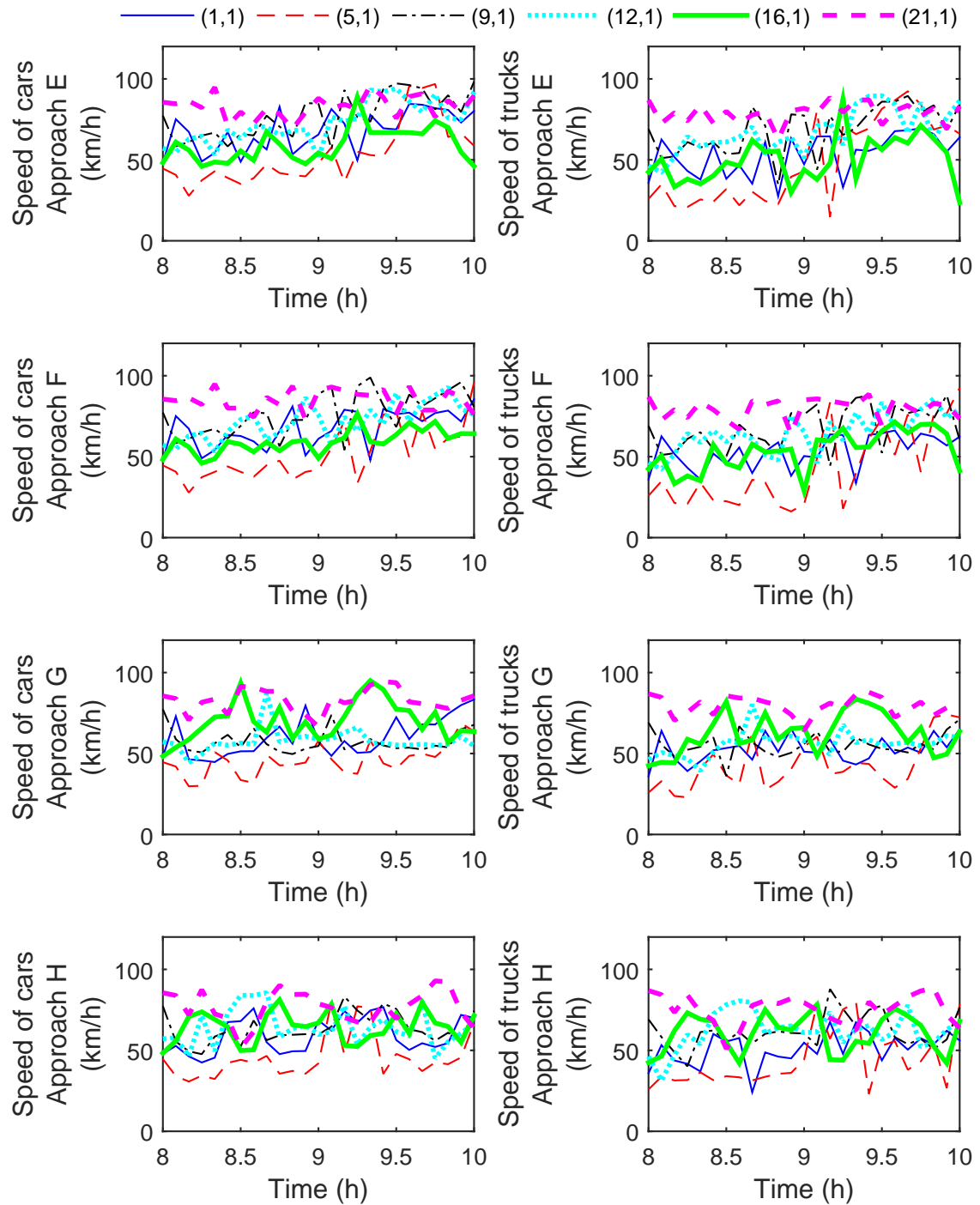


Figure 3.13: Speeds of segments for Approaches E-H

For the approaches based on multi-class METANET, including the end-point penalties can further improve the total performance. However, for the approaches based on FASTLANE, even though the end-point penalties are included, the performance for the TTS and the TE is still worse than that for the no-control case, and the queue length constraint violations are still large, probably because the end-point penalties cannot be appropriately estimated based on FASTLANE.

3.5 Summary

We have extended a second-order multi-class traffic flow model (multi-class METANET) and two multi-class traffic emission models (multi-class VERSIT+ and multi-class VT-macro). We have also incorporated variable speed limits and ramp metering in the first-order multi-class traffic flow model FASTLANE, to allow for a comparison with multi-class METANET in Model Predictive Control (MPC) for freeway networks. End-point penalties are proposed to account for the future evolution of the traffic system beyond the prediction period.

A simulation experiment has been implemented to compare these multi-class traffic flow models and traffic emission models, and to evaluate the effectiveness of the end-point penalties. Eight approaches have been considered for MPC for part of the Dutch freeway network A13, i.e., the four approaches based on the multi-class traffic flow models and traffic emission models, as well as these approaches with the end-point penalties. The results show that the approaches based on multi-class METANET can improve the performance for TTS and TE in a balanced way w.r.t. the no-control case with smaller queue length constraint violations than those for FASTLANE. For these approaches based on multi-class METANET, including end-point penalties can further improve the performance for TTS and TE and the total performance with a small sacrifice in the computational efficiency. On the other hand, for the given case study, the approaches based on FASTLANE lead to consistent queue length constraint violations, which may cause traffic jams upstream of the corresponding on-ramps; furthermore, for these approaches including end-point penalties cannot improve the total performance, probably due to the less reliable estimations of end-point penalties based on FASTLANE.

Chapter 4

Scenario-Based Receding-Horizon Parameterized Control for Traffic Networks

In this chapter, we propose a tractable scenario-based Receding-Horizon Parameterized Control (RHPC) approach for freeway networks. Some RHPC laws based on multi-class traffic models are developed; instead of the control inputs, only the parameters of these control laws are optimized in the control procedure. Thus the number of optimization variables in the optimization problem for determining the control inputs can be decreased w.r.t. conventional MPC, allowing us to reduce the computational burden. In the scenario-based RHPC approach, we use a scenario-based scheme together with a min-max scheme to deal with the robust control problem, considering a finite set of uncertainty scenarios to obtain the worst case of the sum of the control objective function and a constraint violation penalty.

4.1 RHPC Based on Multi-Class Traffic Models

In the RHPC approach [117, 130], the control inputs are parameterized as control laws depending on traffic states and outputs, and the parameters in these control laws are optimized instead of the full control input sequence $\tilde{u}(k_c)$. When multi-class traffic models are considered as prediction models, RHPC laws need to be extended to the multi-class case. As an extension of the single-class case of RHPC laws in [117, 130], in this chapter we develop several new RHPC laws for freeway networks, based on multi-class traffic flow models. Note that the RHPC laws developed in this chapter are independent from the multi-class traffic flow model that is considered. Even if the considered multi-class METANET model is replaced by some other multi-class traffic flow models, these RHPC laws can still be adopted.

4.1.1 RHPC Laws for Variable Speed Limits

Based on multi-class METANET, the following control laws for Variable Speed Limits (VSL) are proposed:

$$\begin{aligned}
v_{m,i}^{\text{ctrl}}(k_c + l + 1) &= \theta_{m,i,0}(k_c + l) v_{m,\max}^{\text{free}} \\
&+ \sum_{c=1}^{n_c} \left(\theta_{m,i,c,1}(k_c + l) \beta_{m,i,c}(k_c + l) \frac{v_{m,i+1,c}(k_c + l) - v_{m,i,c}(k_c + l)}{v_{m,i+1,c}(k_c + l) + \kappa_v} \right) \\
&+ \sum_{c=1}^{n_c} \left(\theta_{m,i,c,2}(k_c + l) \beta_{m,i,c}(k_c + l) \frac{\frac{\rho_{m,i+1,c}(k_c + l)}{\alpha_{m,i+1,c}(k_c + l)} - \frac{\rho_{m,i,c}(k_c + l)}{\alpha_{m,i,c}(k_c + l)}}{\frac{\rho_{m,i+1,c}(k_c + l)}{\alpha_{m,i+1,c}(k_c + l)} + \kappa_\rho} \right) \quad (4.1)
\end{aligned}$$

$$\begin{aligned}
v_{m,i}^{\text{ctrl}}(k_c + l + 1) &= \theta_{m,i,0}(k_c + l) v_{m,\max}^{\text{free}} \\
&+ \sum_{c=1}^{n_c} \left(\theta_{m,i,c,1}(k_c + l) \beta_{m,i,c}(k_c + l) \frac{V_{m,c}(\rho_{m,i,c}(k_c + l)) - v_{m,i,c}(k_c + l)}{V_{m,c}(\rho_{m,i,c}(k_c + l)) + \kappa_v} \right) \\
&+ \sum_{c=1}^{n_c} \left(\theta_{m,i,c,2}(k_c + l) \beta_{m,i,c}(k_c + l) \frac{\frac{\rho_{m,i+1,c}(k_c + l)}{\alpha_{m,i+1,c}(k_c + l)} - \frac{\rho_{m,i,c}(k_c + l)}{\alpha_{m,i,c}(k_c + l)}}{\frac{\rho_{m,i+1,c}(k_c + l)}{\alpha_{m,i+1,c}(k_c + l)} + \kappa_\rho} \right) \quad (4.2)
\end{aligned}$$

$$\begin{aligned}
v_{m,i}^{\text{ctrl}}(k_c + l + 1) &= \theta_{m,i,0}(k_c + l) v_{m,\max}^{\text{free}} \\
&+ \sum_{c=1}^{n_c} \left(\theta_{m,i,c,1}(k_c + l) \beta_{m,i,c}(k_c + l) \frac{v_{m,i+1,c}(k_c + l) \frac{\rho_{m,i+1,c}(k_c + l)}{\alpha_{m,i+1,c}(k_c + l)} - v_{m,i,c}(k_c + l) \frac{\rho_{m,i,c}(k_c + l)}{\alpha_{m,i,c}(k_c + l)}}{v_{m,i+1,c}(k_c + l) \frac{\rho_{m,i+1,c}(k_c + l)}{\alpha_{m,i+1,c}(k_c + l)} + \kappa_v \kappa_\rho} \right) \quad (4.3)
\end{aligned}$$

$$\begin{aligned}
v_{m,i}^{\text{ctrl}}(k_c + l + 1) &= v_{m,i}^{\text{ctrl}}(k_c + l) \\
&- \sum_{c=1}^{n_c} (\theta_{m,i,c,1}(k_c + l) \beta_{m,i,c}(k_c + l) (v_{m,i,c}(k_c + l) - v_{m,i,c}(k_c + l - 1))) \\
&+ \sum_{c=1}^{n_c} (\theta_{m,i,c,2}(k_c + l) \beta_{m,i,c}(k_c + l) (V_{m,c}(\rho_{m,i,c}(k_c + l)) - v_{m,i,c}(k_c + l))) \quad (4.4)
\end{aligned}$$

for $l = 0, \dots, N_p - 1$

where $\beta_{m,i,c}(k_c + l) = \frac{\rho_{m,i,c}(k_c + l)}{\sum_{j=1}^{n_c} \rho_{m,i,j}(k_c + l)}$ is the density fraction of vehicle class c in segment i of link m at control step $k_c + l$, κ_v and κ_ρ are small positive values to prevent the divisors to be 0, and $\theta_{m,i,0}$, $\theta_{m,i,c,1}$, and $\theta_{m,i,c,2}$ are the control parameters to be optimized in the control process.

The RHPC laws (4.1)–(4.4) are constructed based on the traffic states and outputs of the current segment (m, i) and the next segment $(m, i + 1)$, which reflect the future traffic situation that vehicles in the current segment will encounter. Inspired by the speed equation of multi-class METANET, Law (4.1) consists of the maximum free-flow speed among all vehicle classes, the relative variations in class-dependent speeds from the current segment to the next segment at control step $k_c + l$, and the relative variations in class-dependent equivalent densities from the current segment to the next segment at control step $k_c + l$. Compared with Law (4.1), the second term of Law (4.2) represents the relative differences between the class-dependent *desired* speeds and actual speeds in the

current segment at control step $k_c + l$. Law (4.3) includes the maximum free-flow speed among all vehicle classes and the relative variations in flows from the current segment to the next segment at control step $k_c + l$. With the class-dependent *desired* speeds and actual speeds as inputs, Law (4.4) is inspired by the PI-ALINEA law for ramp metering [126].

4.1.2 RHPC Laws for Ramp Metering Rates

Two control laws for Ramp Metering (RM) rates are developed based on multi-class METANET as follows:

$$r_o^{\text{ctrl}}(k_c + l + 1) = r_o^{\text{ctrl}}(k_c + l) + \sum_{c=1}^{n_c} \left(\theta_{o,c,1}(k_c + l) \beta_{m,1,c}(k_c + l) \frac{\rho_{m,c}^{\text{crit}} - \rho_{m,1,c}(k_c + l)}{\alpha_{m,1,c}(k_c + l)} \right) \quad (4.5)$$

$$\begin{aligned} r_o^{\text{ctrl}}(k_c + l + 1) = & r_o^{\text{ctrl}}(k_c + l) \\ & - \sum_{c=1}^{n_c} (\theta_{o,c,1}(k_c + l) \beta_{m,1,c}(k_c + l) (\rho_{m,1,c}(k_c + l) - \rho_{m,1,c}(k_c + l - 1))) \\ & + \sum_{c=1}^{n_c} (\theta_{o,c,2}(k_c + l) \beta_{m,1,c}(k_c + l) (\rho_{m,c}^{\text{crit}} - \rho_{m,1,c}(k_c + l))) \end{aligned} \quad (4.6)$$

$$\text{for } l = 0, \dots, N_p - 1$$

where the index m in (4.5) and (4.6) represents the link that is connected to on-ramp o , the index 1 represents the first segment of that link, and $\theta_{o,c,1}$ and $\theta_{o,c,2}$ are the control parameters to be optimized in the control process.

Law (4.5) is a generalization of the ALINEA law [96], and Law (4.6) is a generalization of the PI-ALINEA law [126].

4.1.3 Discussions on RHPC Laws

In (4.1)-(4.6), the control parameters can vary for the different control steps over the control period. Thus the control inputs can vary with both the control parameters and traffic states. The following alternatives about the control parameters can be considered:

- The control parameters ($\theta_{m,i,0}$, $\theta_{m,i,c,1}$, $\theta_{m,i,c,2}$, $\theta_{o,c,1}$, and $\theta_{o,c,2}$) in the RHPC laws are not necessarily optimized for every control step (i.e. every T_c). This will introduce a new time step (of which the length is different from T_c) for updating the control parameters for RHPC laws. In this case, the frequency of updating the control parameters can be reduced. However, for simplifying the exposition we just assume that the control parameters in the RHPC laws are optimized at every control step (i.e. every T_c) in this chapter.
- The control parameters ($\theta_{m,i,0}$, $\theta_{m,i,c,1}$, $\theta_{m,i,c,2}$, $\theta_{o,c,1}$, and $\theta_{o,c,2}$) do not necessarily vary for every control step (T_c) over the control period ($[k_c T_c, (k_c + N_c) T_c)$), i.e. they can vary with a different time step from T_c and the time step for updating the control parameters. In this case, the number of variables to be optimized over the control period can be smaller than that for standard MPC. For instance, the control

parameters can be assumed to be constant over the prediction period $((k_c T_c, (k_c + N_p) T_c))$, which covers the control period; thus the control inputs vary only with traffic states over the prediction period.

- The control parameters $(\theta_{m,i,c,1}, \theta_{m,i,c,2}, \theta_{o,c,1}, \text{ and } \theta_{o,c,2})$ can be assumed to be equal for different vehicle classes. Thus the variations in traffic states and outputs for different vehicle classes are combined based on density fractions for different vehicle classes, and the number of optimization variables in the RHPC optimization problem is reduced compared to the case with class-dependent control parameters.
- For a traffic network, the control parameters $(\theta_{m,i,0}, \theta_{m,i,c,1}, \theta_{m,i,c,2}, \theta_{o,c,1}, \text{ and } \theta_{o,c,2})$ for different segments and on-ramps can be grouped, e.g. the parameters for the segments of the same link can be assumed to be equal. Then the number of optimization variables in the RHPC optimization problem to be solved is reduced w.r.t. the case that the control parameters are not grouped.
- Apart from laws (4.1)-(4.6), other control laws can also be developed based on the evolution of traffic flows.

In addition, upper bounds and lower bounds for variable speed limits and ramp metering rates are guaranteed by finally applying the following saturated control inputs:

$$v_{m,i,\text{sat}}^{\text{ctrl}}(k_c) = \max(\min(v_{m,i}^{\text{ctrl}}(k_c), v_{\max,m}), v_{\min,m}) \quad (4.7)$$

$$r_{o,\text{sat}}^{\text{ctrl}}(k_c) = \max(\min(r_o^{\text{ctrl}}(k_c), r_{\max,o}), r_{\min,o}) \quad (4.8)$$

in which $v_{m,i,\text{sat}}^{\text{ctrl}}$ represents the saturated variable speed limit in segment i of link m , $r_{o,\text{sat}}^{\text{ctrl}}$ represents the saturated ramp metering rate at on-ramp o , $v_{\max,m}$ and $v_{\min,m}$ are respectively the upper bound and lower bound of the variable speed limits in link m , and $r_{\max,o}$ and $r_{\min,o}$ are respectively the upper bound and lower bound of the ramp metering rate at on-ramp o .

4.2 Scenario-Based RHPC

4.2.1 Uncertainties in Demands and Traffic Compositions for Traffic Networks

The uncontrollable inputs in on-line model-based control for freeway networks include mainstream demands, on-ramp demands, boundary conditions, etc. As an example, let us here consider uncertainties in traffic demands, including uncertainties in the total demands and uncertainties in the fractions of different classes of vehicles in the total demands. Note, however, that other types of uncertainties can also be dealt with using the proposed scenario-based RHPC approach.

According to the literature [12, 25, 100], A nominal demand profile can be estimated in various ways, based on historical data and on-line measurement data. An intuitive way is that the nominal demand is estimated as the average of historical data. The nominal demand can be separately estimated for different weekdays and weekends, so that the characteristics of different weekdays and weekends can be described more accurately. Moreover, if on-line measurements are available, shifting and scaling the nominal demand according to these

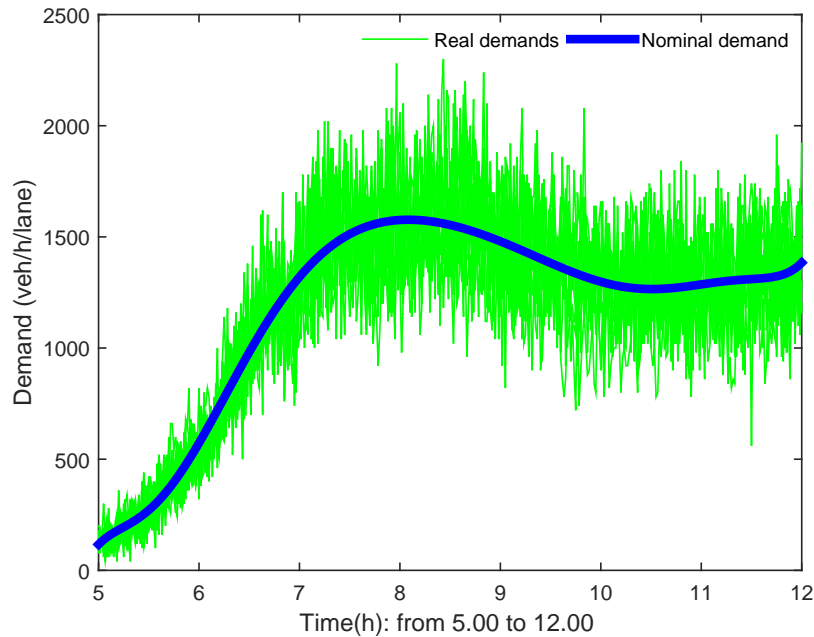


Figure 4.1: An example of real demands and nominal demand

measurements can also improve the estimation. In addition, another way is to build a library of possible uncertainties and their possibilities of appearances.

As an illustration, we consider here the Dutch freeway A13 near Rijswijk. In the direction of Rotterdam, the upstream boundary of the considered part of the A13 is seen as the mainstream origin. For the A13, the measurements for flows and speeds are available at "regiolab-delft.nl". Note that here we consider the measured flows at the mainstream origin to be the real demands, since for the chosen period (5.00-12.00 on several Fridays in 2013 and 2014) no congestion occurs, i.e. the measured speeds are close to the maximum speed for most of the time. The total mainstream demands of A13 for the considered period are shown in Figure 4.1. The real demands are plotted with the same linetype (normal line width) and these real demand profiles overlap with each other. A nominal demand profile is estimated as the average of these historical real demands and shown in Figure 4.1 with a different linetype (thickened line width). This figure shows that real demands fall within a confidence band around the nominal demand profile. Thus it makes sense to model uncertainties in the nominal demand profile as noise limited by a lower bound and an upper bound.

The estimations of the fractions of different vehicle classes (i.e. traffic compositions) can be obtained in a similar way as the estimation of the nominal demand profile. However, the estimations of these fractions ask for separate measurements for different vehicle classes, which can be obtained by cameras installed along freeway stretches, or by inductive loops when all data derived from GPS devices allows to identify the type of detected vehicles. In robust control for freeway networks based on multi-class traffic models, uncertainties in the estimations of the fractions of different vehicle classes are nonnegligible.

4.2.2 Motivation for Scenario-Based RHPC

With uncertainties included, it is assumed that a traffic network is described as a discrete-time nonlinear system of the following form¹⁰:

$$x_\omega(k+1) = f_\omega(x_\omega(k), u(k), D_\omega(k), \omega(k)) \quad (4.9)$$

$$y_\omega(k) = h(x_\omega(k)) \quad (4.10)$$

where f_ω represents the state function for the case with uncertainties, x_ω represents the state vector (containing e.g. densities and speeds) for the case with uncertainties, y_ω represents the output vector (containing e.g. flows) for the case with uncertainties, D_ω represents the uncontrollable input vector (containing e.g. demands) for the case with uncertainties, the vector ω contains the uncertainties of the traffic network, and u represents the control input vector (containing e.g. ramp metering rates and variable speed limits) for the traffic network.

The control input sequence vector $\tilde{u}(k)$ is given by (2.37). The predicted state vector ($\tilde{x}_\omega(k)$), the predicted output vector ($\tilde{y}_\omega(k)$), and the predicted uncontrollable input vector ($\tilde{D}_\omega(k)$) are defined as follows:

$$\tilde{x}_\omega(k) = [x_\omega^T(k+1), \dots, x_\omega^T(k+N_p)]^T \quad (4.11)$$

$$\tilde{y}_\omega(k) = [y_\omega^T(k+1), \dots, y_\omega^T(k+N_p)]^T \quad (4.12)$$

$$\tilde{D}_\omega(k) = [D_\omega^T(k), \dots, D_\omega^T(k+N_p-1)]^T \quad (4.13)$$

Since the uncontrollable inputs are usually assumed to be known nominal values in nominal RHPC, the predicted states yielded by the nonlinear prediction model are influenced by the realizations of the uncertainties over the prediction period, and one realization of the uncertainties is denoted by the vector $\tilde{\omega}(k)$:

$$\tilde{\omega}(k) = [\omega^T(k), \dots, \omega^T(k+N_p-1)]^T \quad (4.14)$$

In case the real values and the nominal values of the uncontrollable inputs are significantly different, the control decisions given by nominal RHPC may not result in an improvement of the control performance, while guaranteeing the constraints to be satisfied. However, the realizations of the uncertainties ($\tilde{\omega}(k)$) are not known a priori, and the robust control problem is a computationally hard problem. A min-max scheme [23] can be used for solving the robust control problem. The robust RHPC problem based on the min-max scheme can be formulated as follows:

$$\min_{\tilde{u}(k)} \max_{\tilde{\omega}(k) \in \tilde{\mathbb{W}}} J_\omega(\tilde{x}_\omega(k), \tilde{y}_\omega(k), \tilde{u}(k)) \quad (4.15)$$

$$\text{s.t. } x_\omega(k+l+1) = f_\omega(x_\omega(k+l), u(k+l), D_\omega(k+l), \omega(k+l)) \quad l = 0, \dots, N_p - 1 \quad (4.16)$$

$$y_\omega(k+l) = h(x_\omega(k+l)) \quad l = 1, \dots, N_p \quad (4.17)$$

$$x_\omega(k) = x_\omega^k \quad (4.18)$$

$$x_\omega(k+l) \in \mathbb{X}, \quad l = 1, \dots, N_p \quad (4.19)$$

$$y_\omega(k+l) \in \mathbb{Y}, \quad l = 1, \dots, N_p \quad (4.20)$$

¹⁰Note that in the current Section 4.2.2 we assume $T_c = T$ for the sake of simplicity of notation; for Section 4.1 and Sections 4.2.3-4.3, the general case $T_c \neq T$ is considered.

Equations (2.43) and (2.46)

for all $\tilde{\omega}(k) \in \tilde{\mathbb{W}}$

where J_ω represents the objective function for the case with uncertainties, x_ω^k represents the measured state vector at time step k for the case with uncertainties, $\tilde{\mathbb{W}}$ represents the set of all the possible realizations of uncertainties over the prediction period, and the uncertainty realizations in $\tilde{\mathbb{W}}$ are in general form.

For the robust control problem consisting of (2.43), (2.46), and (4.15)-(4.20), the computational complexity increases rapidly as the size of traffic network grows, making the problem intractable in practice. As a solution we propose a novel tractable scenario-based RHPC approach for freeway networks.

4.2.3 Scenario-Based RHPC Based on Multi-Class Traffic Models

In this chapter we use Total Time Spent (TTS) as the control performance index, but it is important to note that other control performance indices such as Total Emissions (TE) can also be included according to the aim of the traffic control. As an illustration, variable speed limits and ramp metering are chosen as control measures.

Without including uncertainties, the objective function can be defined as

$$J(k_c) = \xi_{\text{TTS}} \frac{\text{TTS}(k_c)}{\text{TTS}_{\text{nom}}} + \frac{\xi_{\text{ramp}}}{N_c N_{\text{RM}}} \sum_{j=k_c}^{k_c+N_c-1} \sum_{o \in O_{\text{ramp}}} \left\| r_o^{\text{ctrl}}(j) - r_o^{\text{ctrl}}(j-1) \right\|_2 + \frac{\xi_{\text{speed}}}{N_c N_{\text{VSL}}} \sum_{j=k_c}^{k_c+N_c-1} \sum_{(m,i) \in I_{\text{speed}}} \left\| \frac{v_{m,i}^{\text{ctrl}}(j) - v_{m,i}^{\text{ctrl}}(j-1)}{v_{m,\max}^{\text{free}}} \right\|_2 \quad (4.21)$$

where $r_o(k) = r_o^{\text{ctrl}}(k_c)$ and $v_{m,i}^{\text{SL}}(k) = v_{m,i}^{\text{ctrl}}(k_c)$ for $k = Mk_c + 1, \dots, M(k_c + 1)$. In (4.21), the first term is the performance index, and the second term and the third term are used for penalizing the variations of the control inputs.

In order to obtain the optimal control inputs in RHPC for freeway networks, traffic state variables need to be predicted with future demands as exogenous inputs. Nominal RHPC for freeway networks adopts nominal demands, which may be very different from real demands. The differences between nominal demands and real demands may affect the control performance and the satisfaction of constraints.

Here we propose a tractable scenario-based RHPC approach, aiming at improving the behavior of the controlled system by taking into account uncertainties. The scenario-based scheme is used for reducing the computational burden w.r.t. the case that all possible uncertainties are considered, making the robust control problem more tractable. Moreover, aiming at the satisfaction of the queue length constraints, we include a queue length constraint violation penalty; hence, the queue length constraints are treated as soft constraints, to avoid infeasible optimization problems under uncertainties.

The objective function for the tractable scenario-based RHPC approach is as follows¹¹:

$$J_{\max}(k_c) = \max_{\tilde{\omega}(k_c) \in \tilde{\Omega}(k_c)} \left(J_\omega(\tilde{x}_\omega(k_c), \tilde{y}_\omega(k_c), \tilde{u}(k_c)) \right)$$

¹¹As an illustration of how to include a constraint violation penalty, here we consider queue length constraints only. Note that constraints on outputs and other states can be dealt with in a similar way.

$$+ \gamma \max_{o \in O_{\text{ramp}}} \max \left(\max_{j=k_c M, \dots, (k_c + N_p)M - 1} \sum_{c=1}^{n_c} \frac{p_c w_{o,c}(j)}{w_{o,\text{efc}}^{\max}} - 1, 0 \right) \quad (4.22)$$

where $\tilde{\Omega}(k_c) = \{\tilde{\omega}_1(k_c), \dots, \tilde{\omega}_H(k_c)\} \subset \tilde{\mathbb{W}}$ represents the set of H possible scenarios that will be considered for the scenario-based RHPC approach for control time step k_c , $w_{o,\text{efc}}^{\max}$ is the maximum allowed queue length (in pce) for all vehicle classes at on-ramp o , and γ is a positive weight to penalize queue length constraint violation under uncertainties $\tilde{\omega}(k_c) \in \tilde{\Omega}(k_c)$.

The objective function J_{\max} represents the worst case of the chosen H possible uncertainty scenarios, and J_{\max} is minimized in the scenario-based RHPC approach. The scenario-based RHPC problem for freeway networks is defined as follows:

$$\min_{\tilde{u}(k_c)} J_{\max}(k_c) \quad (4.23)$$

s.t. Equations (2.43), (2.46), and (4.16) – (4.18)

for all $\tilde{\omega}(k_c) \in \tilde{\Omega}(k_c)$

In the above scenario-based RHPC problem, when the maximum queue length is smaller than the maximum permitted value, the queue length constraint violation penalty equals 0; thus the TTS is optimized. However, if the maximum queue length is larger than the maximum permitted value, the queue length constraint violation penalty will be taken into account. Due to the high weight γ for the queue length constraint violation penalty, the queue length will be in general optimized so that the maximum queue length is smaller than the maximum permitted value. The inner max operator of the queue length constraint violation penalty ensures that once the maximum queue length in the entire prediction period exceeds the maximum permitted value, the queue length constraint violation penalty will be taken into account.

4.3 Case Study: Assessments of Scenario-Based RHPC

4.3.1 Benchmark Network

The benchmark network shown in Figure 4.2, which has been simulated with other controllers in some papers [41, 50], is used for the case study. This network includes one mainstream origin, one on-ramp, one destination, and two links. Link 1 is 4 km long and divided into 4 segments with a length of 1 km. Link 2 is 2 km long and divided into 2 segments with a length of 1 km. Thus the length of the segments for both links is $L_m = 1$ km, for $m = 1, 2$. The on-ramp connects to the first segment of link 2. There are two lanes in the main road, and 1 lane in the on-ramp road. In the third and fourth segments of link 1 variable speed limits are present, and ramp metering is used at the on-ramp. It is assumed that the queue length at the origin is not limited, and the outflow at the destination is unrestricted. The multi-class METANET model that has been extended in Chapter 3 is used as both the simulation model and the prediction model.

We consider two classes of vehicles in the network: class 1 represents cars, and class 2 represents trucks. The parameters for these two classes of vehicles are as follows [50, 60, 76]: $v_{m,1}^{\text{free}} = 106$ km/h, $a_{m,1} = 1.6761$, $\delta_{m,1} = 0.12$, $\rho_{m,1}^{\text{crit}} = 35$ veh/km/lane, $\rho_{m,1}^{\text{max}} = 175$ veh/km/lane, $C_{\text{main},1} = 2034$ veh/h/lane, and $C_{\text{onramp},1} = 1934$ veh/h/lane for

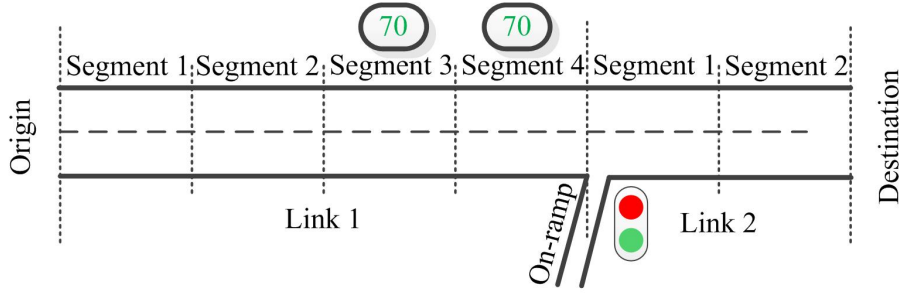


Figure 4.2: Benchmark network

$m = 1, 2$; $v_{m,2}^{\text{free}} = 83$ km/h, $a_{m,2} = 2.1774$, $\delta_{m,2} = 0.05$, $\rho_{m,2}^{\text{crit}} = 19$ veh/km/lane, $\rho_{m,2}^{\text{max}} = 75$ veh/km/lane, $C_{\text{main},2} = 990$ veh/h/lane, and $C_{\text{onramp},2} = 890$ veh/h/lane for $m = 1, 2$. Common parameters for cars and trucks are [50, 60]: $\tau_{m,c} = 18$ s, $\kappa_{m,c} = 40$ veh/h/km, and $\eta_{m,c} = 60$ km²/h for $c = 1, 2$ and $m = 1, 2$. The passenger car equivalents are $p_1 = 1$ and $p_2 = 7/3$. In order to avoid spill-back to the upstream stretch of the on-ramp, the total queue length of cars and trucks at the on-ramp is limited to 150 pce.

The simulation period covers 1 h, and the simulation time step is $T = 10$ s (according to (2.1), $T < \frac{L_m}{v_{m,1}^{\text{free}}} = 34$ s). As for other parameters, we select $\xi_{\text{TTS}} = 1$, $\xi_{\text{ramp}} = \xi_{\text{speed}} = 0.1$, $T_c = 60$ s, and $N_p = 7$. The control time step is 6 times larger than the simulation time step, because the control inputs should not be changed too frequently in practice. Here we suppose that the weights ξ_{TTS} , ξ_{ramp} , and ξ_{speed} are defined by policy makers. The control performance index TTS dominates in the objective function, and the penalties to avoid abrupt variations in control inputs are minor in comparison with the TTS. The control parameters for the RHPC laws depend on the future predictions. Hence, the prediction period is not too long to avoid large prediction errors under uncertainties. However, the prediction period cannot be too short either due to the requirement for crossing the considered traffic network within the prediction period. Thus the length of the prediction period is chosen according to the typical travel time through the considered network as suggested in [50].

4.3.2 Control Set-up

Nominal Demands and Uncertainties

The nominal demands at the mainstream origin and the on-ramp are shown in Figure 4.3. The nominal density fraction for trucks is $\beta_{\text{truck}} = 0.1$. The real demands are generated by adding random disturbances to the nominal demands. Here we consider two cases:

- Case 1: there are only uncertainties in the total demands;
- Case 2: there are uncertainties in both the total demands and the estimations of truck fractions.

The uncertainties in the total demand values are limited within 10% with a base value of 100 veh/h. As for the truck fractions, we assume that the range is from 0 to 0.3. Both uncertainties for the total demands and for the truck fractions are described as uniform random noise. For each case, 10 scenarios for uncertainties, corresponding to 10 realizations of real demands, are investigated to evaluate the effectiveness of the scenario-based RHPC approach.

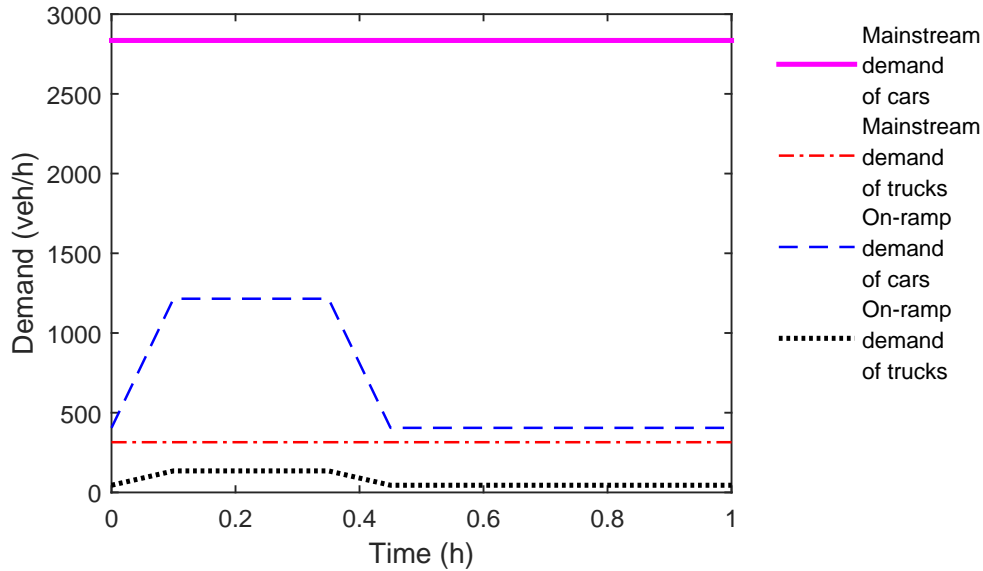


Figure 4.3: Nominal demands for the benchmark network

Both nominal RHPC and scenario-based RHPC are implemented for comparison. In scenario-based RHPC, 10 uniform random uncertainty scenarios are used for obtaining the worst-case objective function. These 10 uncertainty scenarios are different from the aforementioned 10 realizations of real demands. This is due to the fact that the real realizations of future demands are not known a priori and can thus not be used in the control procedure. However, the uncertainty scenarios used in scenario-based RHPC are generated in the same way as the aforementioned 10 realizations of real demands.

Control Approaches

As examples, the RHPC Laws (4.1) and (4.4) for variable speed limits, and (4.5) and (4.6) for ramp metering rates are adopted in the case study. We test and compare the following approaches for the aforementioned two cases of uncertainties:

- Nominal RHPC 1 (NRHPC 1): Law (4.1)+Law (4.5);
- Scenario-Based RHPC 1 (SRHPC 1): Law (4.1)+Law (4.5);
- Nominal RHPC 2 (NRHPC 2): Law (4.4)+Law (4.6);
- Scenario-Based RHPC 2 (SRHPC 2): Law (4.4)+Law (4.6);

Note that the number (100) of starting points for "fmincon" for every control step is chosen as the same for the above approaches.

For comparison, we also apply a standard control scheme for the combination: Law (4.4) + Law (4.6), which are PI-ALINEA-like laws. In the standard control scheme, the parameters for the control laws are constant for the entire simulation period, and they are determined beforehand. The following approaches based on the standard control scheme are tested:

- Standard Control 1 (SC 1): using nominal demands and fractions of cars and trucks, with the queue length constraint violation penalty;

- Standard Control 2 (SC 2): using 10 random scenarios for uncertainties, with the queue length constraint violation penalty;
- Standard Control 3 (SC 3): based on nominal demands and fractions of cars and trucks, with the queue length constraint violation penalty and a queue override scheme¹²;
- Standard Control 4 (SC 4): based on 10 random scenarios for uncertainties, with the queue length constraint violation penalty and a queue override scheme.

Note that (4.7) and (4.8) are also used for the standard control approaches.

The weight γ is tested for different values: 0.01, 0.1, 1, 10, 100. In this case study, we assume that the control parameters of the RHPC laws are the same for all vehicle classes, and that they are constant over the entire prediction period. Moreover, the control parameters are different for segment 3 and segment 4 of link 1. For the control parameters in the RHPC laws the control period covers 1 control step, while for the actual control inputs the control period covers 7 control steps, due to the variations of the traffic states used in the RHPC laws.

4.3.3 Simulation Results and Analysis

In the remainder of this section, $J_{\text{TTS}}^{\text{imp}}$ represents the relative improvement in the Total Time Spent (TTS) w.r.t. the no-control case, while J_{pen} represents the maximum relative queue length constraint violation that is defined as:

$$J_{\text{pen}} = \max \left(\max_{k=1, \dots, k_{\text{end}}} \frac{\sum_{c=1}^{n_c} (p_c w_{o,c}(k))}{w_{o,\text{efc}}^{\text{max}}} - 1, 0 \right) \quad (4.24)$$

where k_{end} is the last simulation time step of the entire simulation period, and the total performance J_{tot} is defined as

$$J_{\text{tot}} = \frac{\text{TTS}_{\text{tot}}}{\text{TTS}_{\text{nom}}} + \gamma J_{\text{pen}} \quad (4.25)$$

For each combination of the values of γ (5 values), the realizations of real demands (10 scenarios), and the control approaches (8 control approaches), the closed-loop simulation is repeated 10 times with different random seeds, which correspond to different starting points for "fmincon"¹³. The average of the results for the 10 repeated closed-loop simulations is considered as the result for a combination. The average control performance improvements, the average constraint violations, and the total performance of the results for 10 different realizations of real demands are listed in Tables 4.1-4.8. Furthermore, the standard deviations of the results for 10 different realizations are also included in Tables 4.1-4.8.

¹²In the queue override scheme [95], the ramp metering rate is set to be 1 if the maximum queue length exceeds the maximum permitted value.

¹³The optimization function "fmincon" in Matlab is used for solving optimization problems in the case study, based on the "active-set" algorithm.

Table 4.1: Simulation results for NRHPC 1 and SRHPC 1, Case 1

Approaches		NRHPC 1					SRHPC 1				
γ		0.01	0.1	1	10	100	0.01	0.1	1	10	100
Average	J_{TTS}^{imp}	7.4%	6.7%	6.5%	6.4%	6.2%	6.6%	6.1%	6.0%	5.9%	5.8%
	J_{pen}	25.5%	9.0%	7.7%	6.6%	5.5%	13.4%	2.3%	1.9%	1.8%	1.6%
	J_{tot}	15.4	15.6	15.6	16.3	21.2	15.6	15.7	15.7	15.9	17.3
Standard deviation	J_{TTS}^{imp}	0.3%	0.4%	0.4%	0.3%	0.2%	0.5%	0.4%	0.3%	0.3%	0.3%
	J_{pen}	2.5%	1.2%	1.3%	2.2%	2.1%	2.1%	0.4%	0.3%	0.2%	0.3%
	J_{tot}	0.2	0.3	0.3	0.5	2.3	0.3	0.3	0.3	0.3	0.4

Table 4.2: Simulation results for NRHPC 1 and SRHPC 1, Case 2

Approaches		NRHPC 1					SRHPC 1				
γ		0.01	0.1	1	10	100	0.01	0.1	1	10	100
Average	J_{TTS}^{imp}	6.1%	4.4%	4.7%	4.6%	4.6%	4.7%	4.3%	4.3%	4.2%	4.1%
	J_{pen}	53.4%	21.5%	12.7%	11.2%	10.6%	18.2%	2.5%	1.6%	1.2%	1.0%
	J_{tot}	18.9	20.9	19.3	20.3	29.7	19.1	19.2	19.3	19.4	20.3
Standard deviation	J_{TTS}^{imp}	0.3%	1.2%	0.3%	0.3%	0.3%	0.2%	0.2%	0.2%	0.2%	0.3%
	J_{pen}	4.0%	19.5%	4.2%	2.7%	2.8%	5.3%	1.0%	0.8%	0.7%	0.6%
	J_{tot}	0.4	5.6	0.4	0.5	3.0	0.4	0.4	0.4	0.4	0.7

Table 4.3: Simulation results for NRHPC 2 and SRHPC 2, Case 1

Approaches		NRHPC 2					SRHPC 2				
γ		0.01	0.1	1	10	100	0.01	0.1	1	10	100
Average	J_{TTS}^{imp}	9.5%	5.3%	5.1%	5.1%	5.0%	9.4%	5.0%	5.0%	5.2%	5.2%
	J_{pen}	70.0%	4.5%	3.0%	4.0%	3.8%	66.3%	0.8%	0.8%	0.8%	0.6%
	J_{tot}	15.0	15.8	15.8	16.2	19.7	15.1	15.8	15.9	16.0	16.4
Standard deviation	J_{TTS}^{imp}	0.9%	0.2%	0.3%	0.3%	0.2%	0.7%	0.2%	0.3%	0.3%	0.3%
	J_{pen}	8.4%	1.2%	1.5%	2.0%	1.1%	7.1%	0.6%	0.5%	0.3%	0.4%
	J_{tot}	0.3	0.3	0.2	0.2	1.1	0.3	0.2	0.2	0.6	0.5

Table 4.4: Simulation results for NRHPC 2 and SRHPC 2, Case 2

Approaches		NRHPC 2					SRHPC 2				
γ		0.01	0.1	1	10	100	0.01	0.1	1	10	100
Average	J_{TTS}^{imp}	7.2%	4.2%	4.0%	4.0%	4.0%	6.3%	3.9%	3.7%	3.7%	3.7%
	J_{pen}	125.7%	12.5%	10.1%	8.7%	9.1%	82.0%	2.7%	1.4%	1.0%	0.8%
	J_{tot}	18.7	19.3	19.4	20.1	28.4	18.8	19.3	19.4	19.5	20.2
Standard deviation	J_{TTS}^{imp}	0.5%	0.3%	0.2%	0.2%	0.2%	0.6%	0.2%	0.3	0.2%	0.2%
	J_{pen}	22.3%	5.4%	2.6%	2.9%	2.9%	17.5%	1.8%	0.8%	0.6%	0.3%
	J_{tot}	0.4	0.4	0.4	0.6	3.1	0.4	0.4	0.4	0.5	0.4

Table 4.5: Simulation results for SC 1 and SC 2, Case 1

Approaches		SC 1					SC 2				
	γ	0.01	0.1	1	10	100	0.01	0.1	1	10	100
Average	J_{TTS}^{imp}	6.1%	11.5%	2.2%	4.1%	6.0%	12.1%	12.1%	1.9%	1.6%	2.2%
	J_{pen}	114.2%	86.2%	62.6%	52.9%	70.0%	93.3%	90.0%	0%	0%	0.1%
	J_{tot}	29.8	14.8	16.9	21.3	85.6	14.7	14.7	16.3	16.4	16.4
Standard deviation	J_{TTS}^{imp}	1.6%	0.5%	2.8%	1.9%	0.3%	0.3%	0.4%	0.2%	0.2%	0.2%
	J_{pen}	18.9%	6.1%	45.5%	28.5%	8.9%	5.7%	5.8%	0%	0%	0.2%
	J_{tot}	44.8	0.2	0.5	2.6	9.1	0.2	0.3	0.2	0.2	0.4

Table 4.6: Simulation results for SC1 and SC2, Case 2

Approaches		SC 1					SC 2				
	γ	0.01	0.1	1	10	100	0.01	0.1	1	10	100
Average	J_{TTS}^{imp}	6.1%	8.7%	1.9%	2.6%	6.1%	9.3%	1.0%	0.9%	1.3%	0.4%
	J_{pen}	241.0%	167.9%	104.5%	82.1%	151.0%	173.2%	0%	0%	1.3%	1.1%
	J_{tot}	18.9	18.5	20.8	27.8	169.9	18.2	19.8	19.9	20.0	21.1
Standard deviation	J_{TTS}^{imp}	1.2%	0.4%	2.2%	0.6%	0.4%	0.6%	0.1%	0.2%	0.3%	0.4%
	J_{pen}	38.4%	35.0%	65.1%	25.4%	11.8%	31.0%	0%	0%	3.0%	3.1%
	J_{tot}	0.5	0.4	0.5	2.7	12.0	0.4	0.4	0.5	0.6	3.2

Table 4.7: Simulation results for SC3 and SC4, Case 1

Approaches		SC 3					SC 4				
	γ	0.01	0.1	1	10	100	0.01	0.1	1	10	100
Average	J_{TTS}^{imp}	2.0%	4.2%	-1.9%	1.0%	1.9%	4.6%	4.6%	2.8%	0.7%	2.3%
	J_{pen}	13.5%	12.2%	6.6%	6.7%	6.9%	7.9%	14.1%	0.6%	0.5%	0%
	J_{tot}	16.3	16.0	17.0	17.2	23.2	15.9	15.9	16.2	16.6	16.3
Standard deviation	J_{TTS}^{imp}	1.2%	0.2%	1.0%	0.4%	0.7%	1.0%	0.6%	0.7%	1.0%	0.2%
	J_{pen}	2.9%	3.8%	4.1%	3.5%	3.8%	4.0%	2.3%	1.9%	1.2%	0%
	J_{tot}	0.4	0.2	0.3	0.3	4.1	0.3	0.3	0.3	0.3	0.2

Table 4.8: Simulation results for SC3 and SC4, Case 2

Approaches		SC 3					SC 4				
	γ	0.01	0.1	1	10	100	0.01	0.1	1	10	100
Average	J_{TTS}^{imp}	1.1%	3.5%	-1.2%	0.6%	1.6%	3.8%	2.7%	1.8%	1.0%	1.5%
	J_{pen}	21.4%	26.2%	8.3%	10.1%	14.0%	27.7%	16.7%	0.4%	0%	0%
	J_{tot}	19.9	19.4	20.4	21.0	33.8	19.3	19.6	19.7	19.9	19.8
Standard deviation	J_{TTS}^{imp}	0.6%	0.3%	1.2%	0.3%	0.6%	0.4%	0.5%	0.3%	0.2%	0.2%
	J_{pen}	7.0%	7.8%	4.0%	4.9%	6.6%	4.1%	5.2%	1.3%	0%	0%
	J_{tot}	0.5	0.4	0.6	0.7	7.0	0.4	0.4	0.4	0.4	0.4

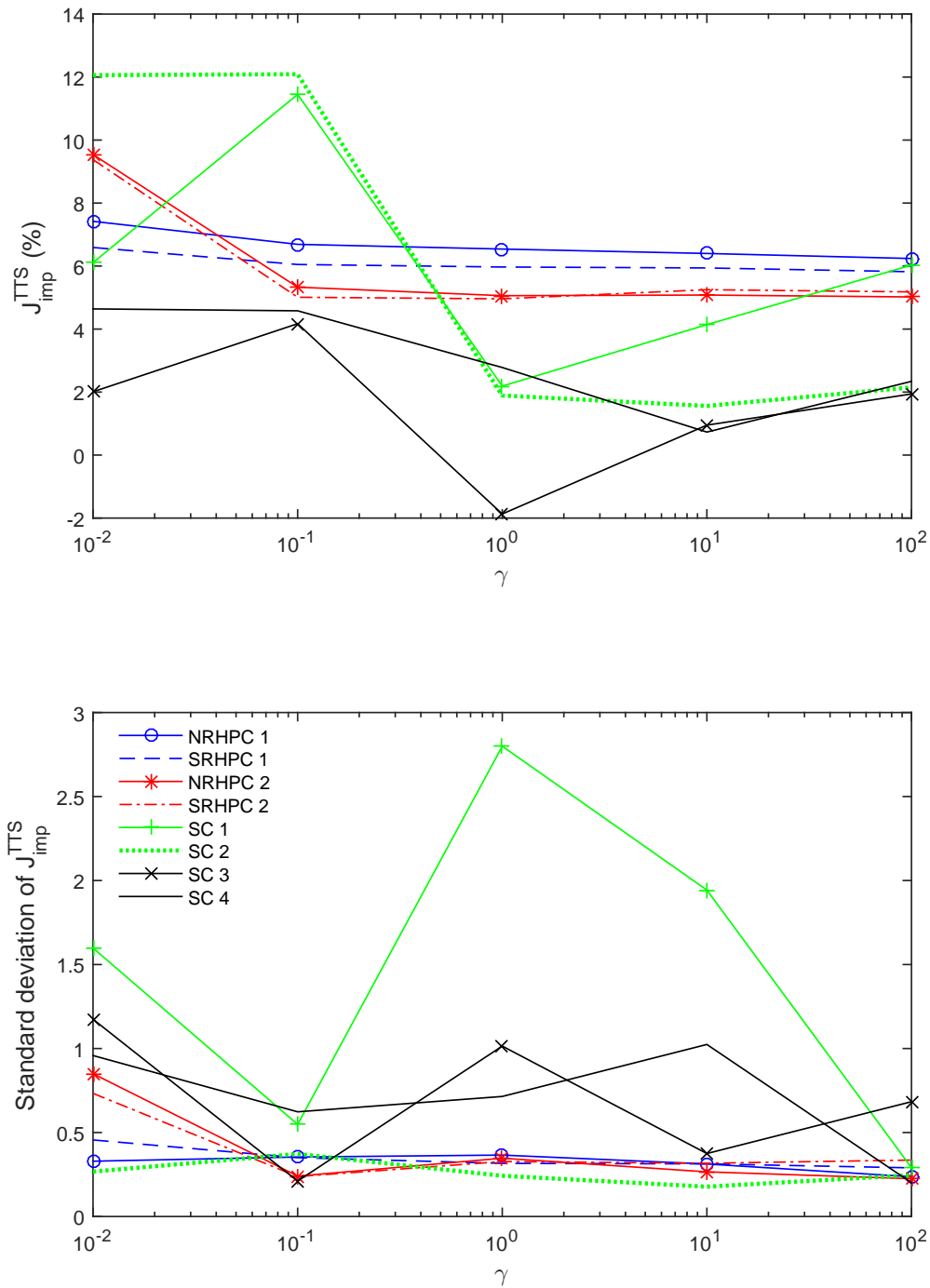


Figure 4.4: Relative control performance improvements, Case 1

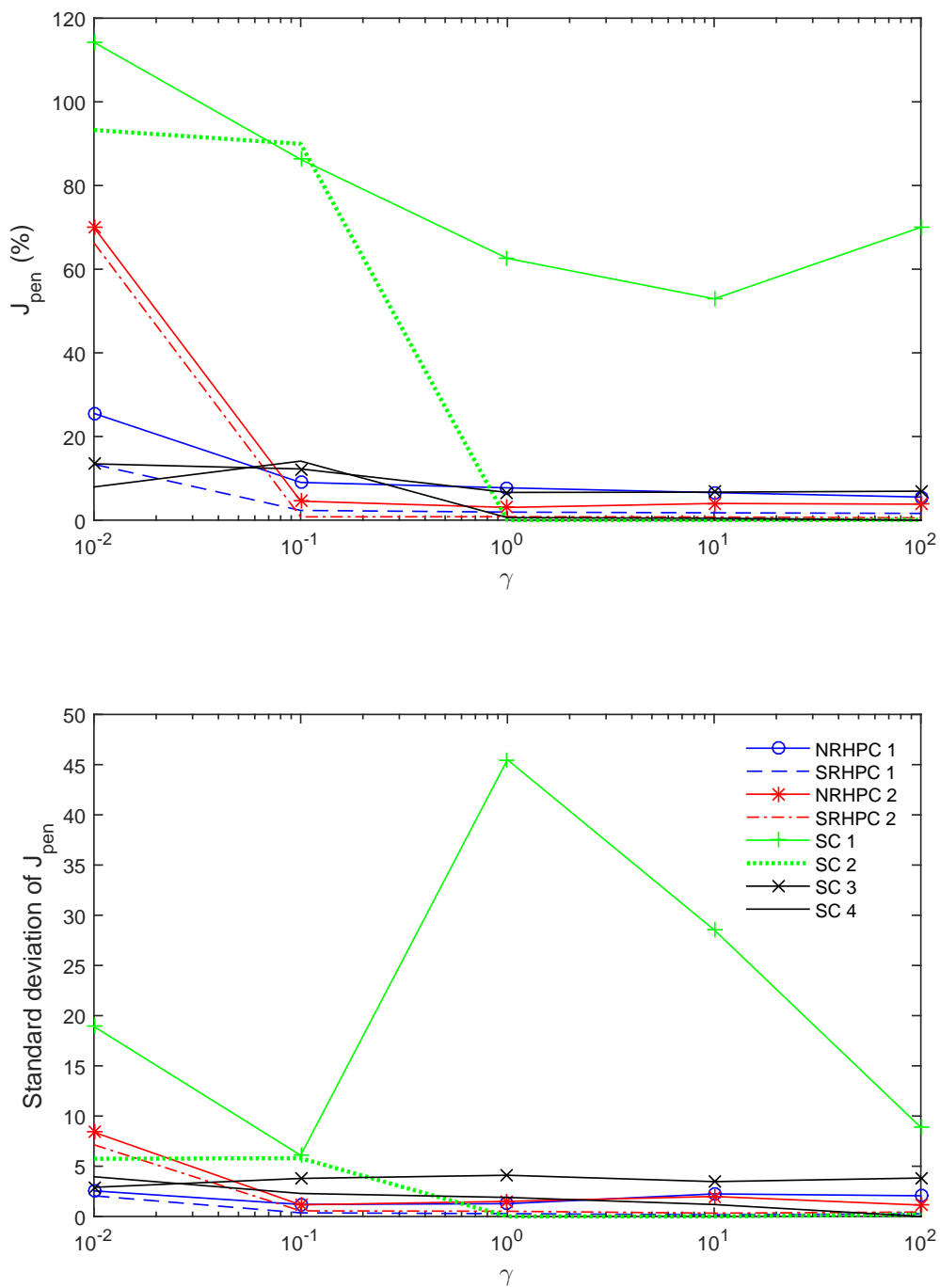


Figure 4.5: Constraint violations, Case 1

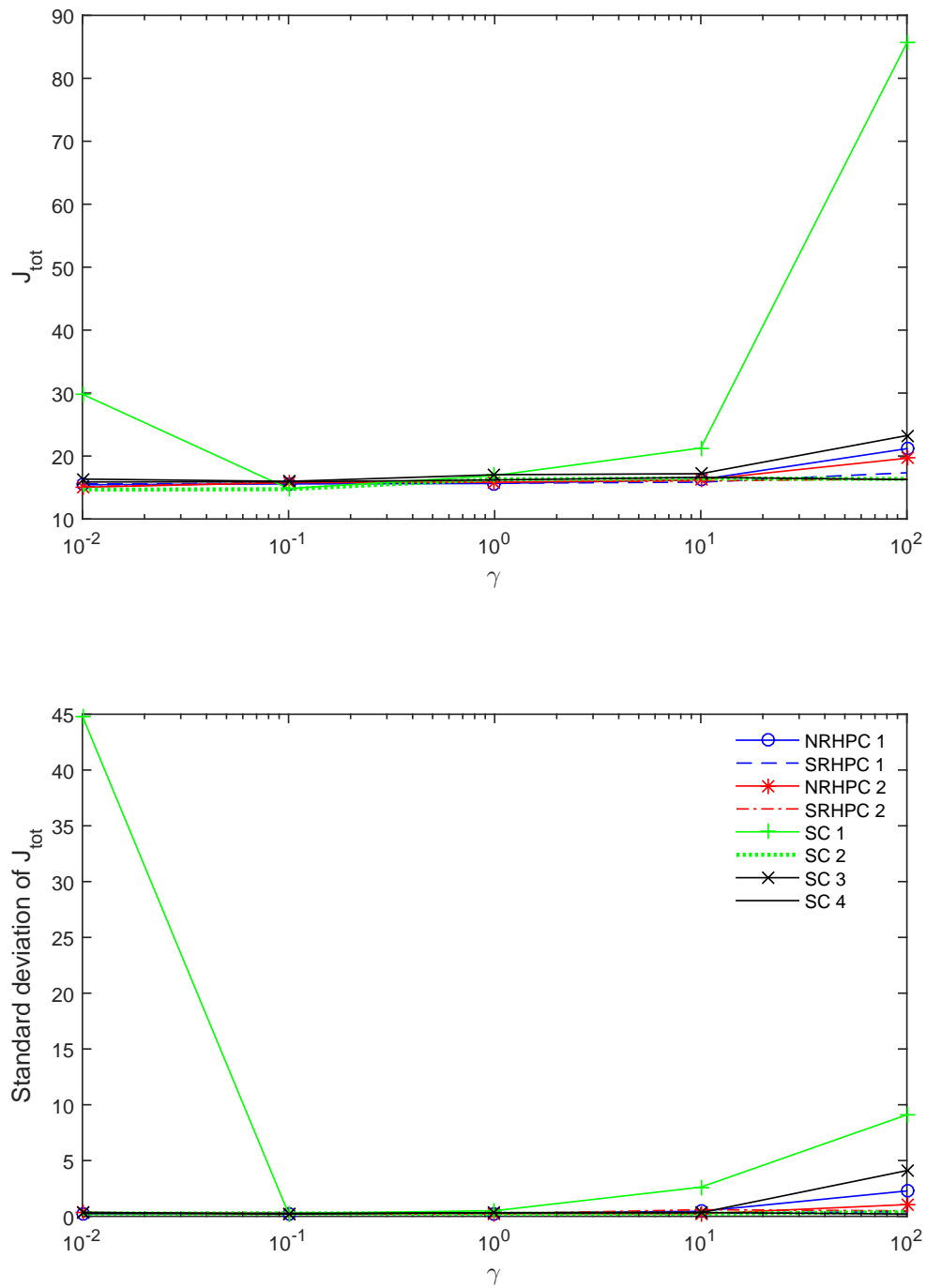


Figure 4.6: Total performance, Case 1

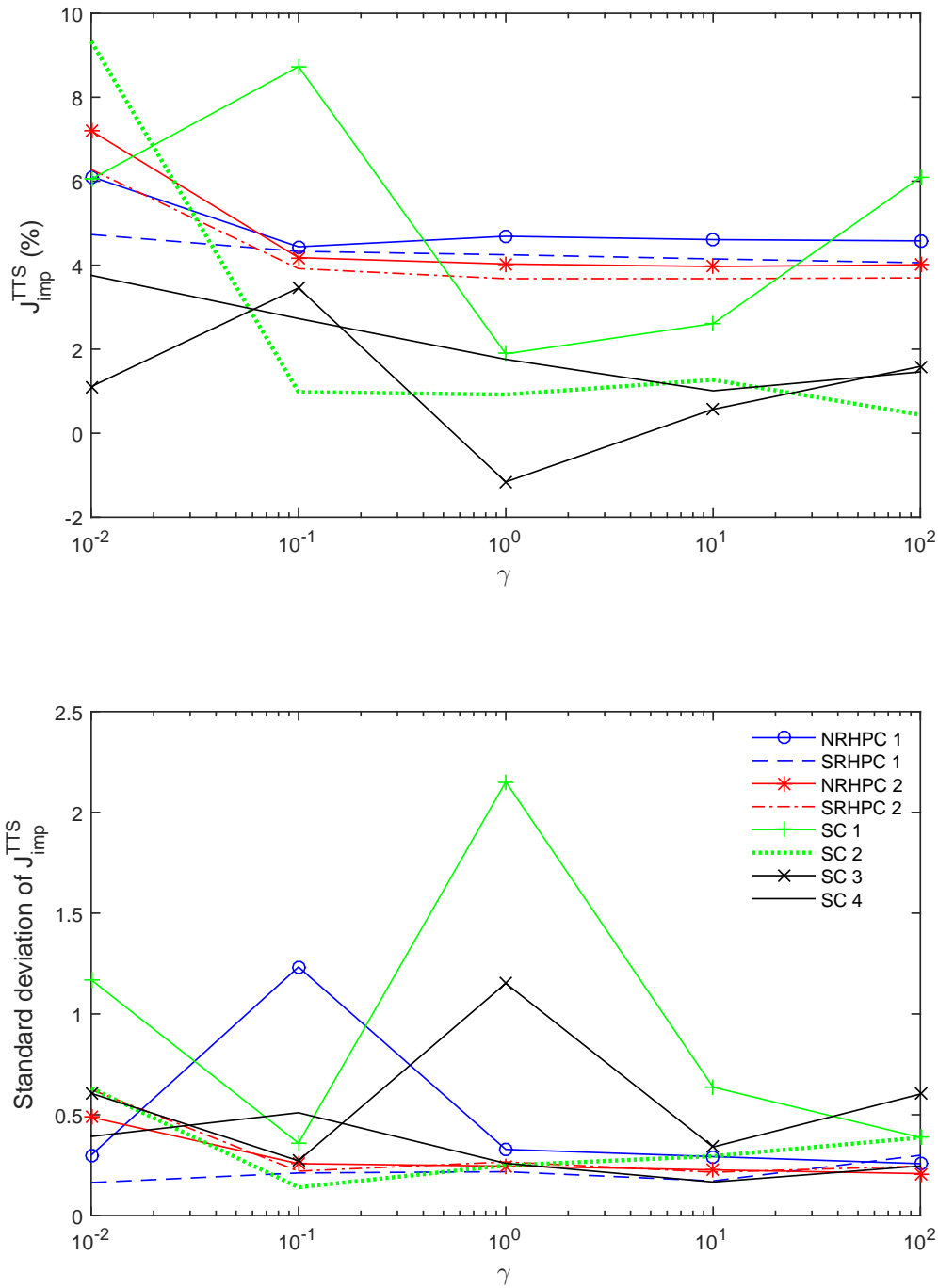


Figure 4.7: Relative control performance improvements, Case 2

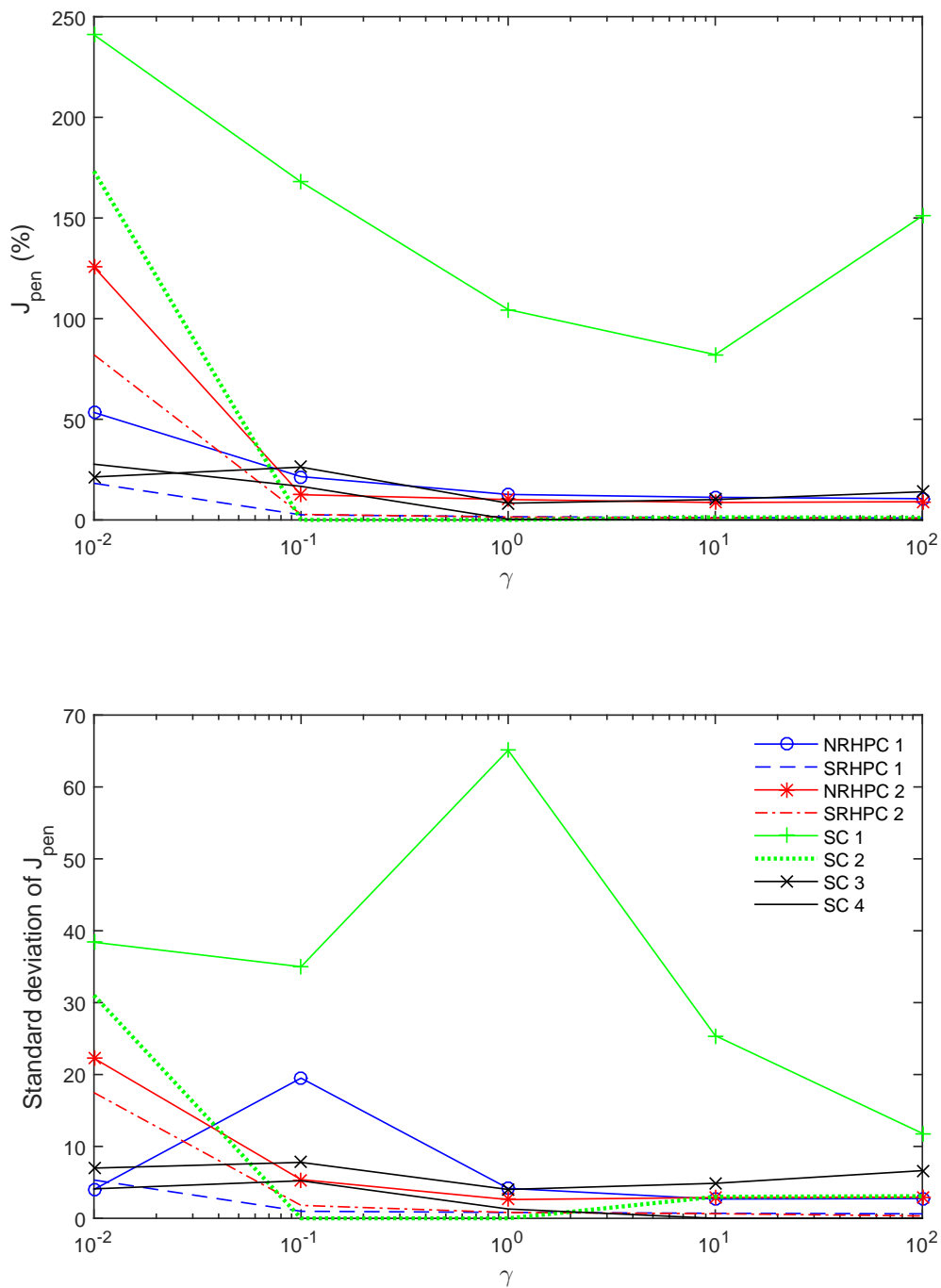


Figure 4.8: Constraint violations, Case 2

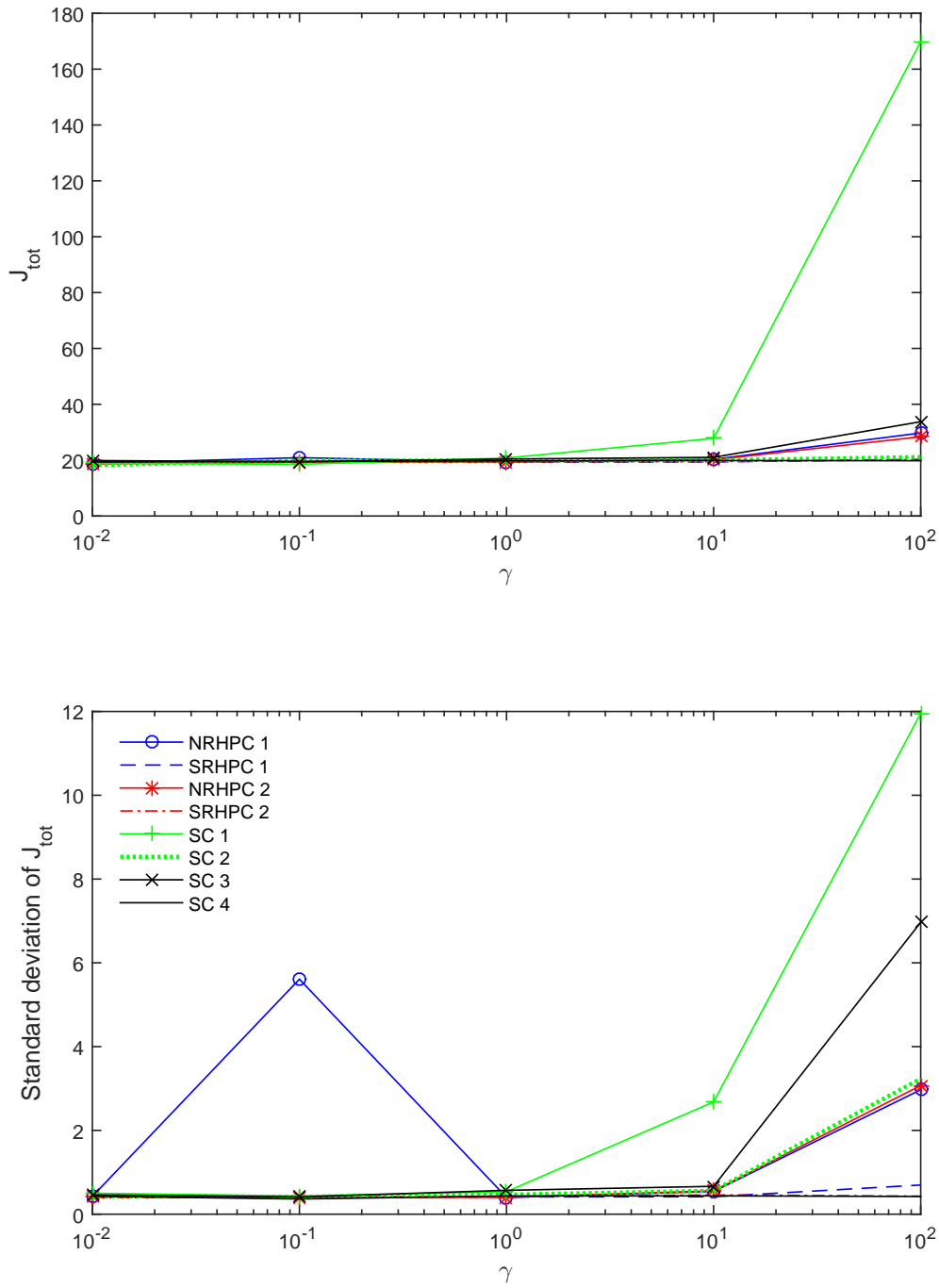


Figure 4.9: Total performance, Case 2

Comparison w.r.t. Performance and Constraint Violations

In this section, the approaches ignoring uncertainties are first compared to the corresponding approaches including uncertainties, i.e., NRHPC 1 w.r.t. SRHPC 1, NRHPC 2 w.r.t. SRHPC 2, SC 1 w.r.t. SC 2, and SC 3 w.r.t. SC 4. After that, all approaches are compared together based on Figures 4.4-4.9, which display the relative control performance improvements (i.e. the improvements on TTS), constraint violations, and the total performance.

1. Results for NRHPC 1 and SRHPC 1:

According to the results for Case 1 in Table 5.1, the control performance improvements for SRHPC 1 (5.8% – 6.6%) are less than the control performance improvements for NRHPC 1 (6.2% – 7.4%). However, NRHPC 1 leads to higher queue length constraint violations (5.5%–25.5%) than SRHPC 1 (1.6%–13.4%) for all values of γ considered. For SRHPC 1, the queue length constraint violations (1.6%–2.3%) are relatively small when $\gamma \in \{0.1, 1, 10, 100\}$. Comparing the values of J_{tot} , we find that SRHPC 1 (15.9 – 17.3) results in better total performance than NRHPC 1 (16.3 – 21.2) for $\gamma \in \{10, 100\}$. For both NRHPC 1 and SRHPC 1, the standard deviations of $J_{\text{TTS}}^{\text{imp}}$ and J_{tot} are small, and the standard deviations of J_{pen} are large.

The results for Case 2 are shown in Table 4.2. Just as for Case 1, the control performance improvements for SRHPC 1 (4.1% – 4.7%) are less than the control performance improvements for NRHPC 1 (4.4% – 6.1%). For NRHPC 1, the queue length constraint violations (10.6% – 53.4%) are higher than those for SRHPC 1 (1.0% – 18.2%) for all values of γ considered. For SRHPC 1, the queue length constraint violations (1.0% – 2.5%) are relatively small when $\gamma \in \{0.1, 1, 10, 100\}$; furthermore, for these values of γ , the total performance for SRHPC 1 (19.2 – 20.3) is not worse than the total performance for NRHPC 1 (19.3 – 29.7). The standard deviations of $J_{\text{TTS}}^{\text{imp}}$ and J_{tot} are small for both NRHPC 1 and SRHPC 1 except for NRHPC 1 with $\gamma = 0.1$. For both NRHPC 1 and SRHPC 1, the standard deviations of J_{pen} are large.

2. Results for NRHPC 2 and SRHPC 2:

The results for Case 1 are shown in Table 4.3. The control performance improvements for SRHPC 2 (5.0%–9.4%) are slightly less than the control performance improvements for NRHPC 2 (5.1% – 9.5%) when $\gamma \in \{0.01, 0.1, 1\}$. SRHPC 2 (5.2%) can even improve the control performance more than NRHPC 2 (5.0% – 5.1%) when $\gamma \in \{10, 100\}$. The queue length constraint violations for NRHPC 2 (3.0% – 70.0%) are higher than those for SRHPC 2 (0.6%–66.3%) for all the values of γ considered. For $\gamma \in \{0.1, 1, 10, 100\}$, the queue length constraint violations for SRHPC 2 (0.6% – 0.8%) are quite small. SRHPC 2 (16.0 – 16.4) results in a better total performance than NRHPC 2 (16.2 – 19.7) when $\gamma \in \{10, 100\}$. For both NRHPC 1 and SRHPC 1, the standard deviations of $J_{\text{TTS}}^{\text{imp}}$ and J_{tot} are small, and the standard deviations of J_{pen} are large.

The results for Case 2 are shown in Table 4.4. For all the values of γ considered, the control performance improvements for SRHPC 2 (3.7% – 6.3%) are less than the control performance improvements for NRHPC 2 (4.0% – 7.2%). However, NRHPC 2 leads to higher queue length constraint violations (9.1% – 125.7%) than SRHPC 2 (0.8%-82.0%) for all values of γ considered. When $\gamma \in \{0.1, 1, 10, 100\}$, SRHPC 2 can

reduce the queue length constraint violations (0.8% – 2.7%) to relatively low values; furthermore, for these values of γ , the total performance for SRHPC 2 (19.3 – 20.2) is not worse than the total performance for NRHPC 2 (19.3 – 28.4). For both NRHPC 1 and SRHPC 1, the standard deviations of J_{TTS}^{imp} and J_{tot} are small, and the standard deviations of J_{pen} are large.

3. Results for SC 1 and SC 2:

The results for Case 1 are shown in Table 4.5. For SC 1 with all values of γ considered and for SC 2 with $\gamma \in \{0.01, 0.1\}$, the control performance improvements are 2.2% – 12.1%, however, the queue length constraint violations (52.9% – 114.2%) are quite high. For SC 2 with $\gamma \in \{1, 10, 100\}$, the queue length constraint violations (0% – 0.1%) are small, but the control performance improvements (1.6% – 2.2%) are also small. For all the values of γ considered, the total performance for SC 2 (14.7 – 16.4) is better than the total performance for SC 1 (14.8 – 85.6). For SC 1, the standard deviations of J_{TTS}^{imp} and J_{pen} are large in general, and the standard deviations of J_{tot} are small except for $\gamma = 0.01$. For SC 2, the standard deviations of J_{TTS}^{imp} , J_{pen} , and J_{tot} are small except for the standard deviations of J_{pen} with $\gamma = 100$.

The results for Case 2 are shown in Table 4.6. For SC 1 with all values of γ considered and for SC 2 with $\gamma = 0.01$, the control performance improvements are 1.9% – 9.3%, with high queue length constraint violations (82.1% – 241.0%). When $\gamma \in \{0.1, 1, 10, 100\}$, the queue length constraint violations are reduced to 0% – 1.3% for SC 2, but the control performance improvements are quite small (0.4% – 1.3%). For $\gamma \in \{1, 10, 100\}$, the total performance for SC 2 (19.9 – 21.1) is better than the total performance for SC 1 (20.8 – 169.9). For SC 1 and SC 2, the standard deviations of J_{TTS}^{imp} and J_{pen} are large in general, and the standard deviations of J_{tot} are small in general.

4. Results for SC 3 and SC 4:

The results for Case 1 are shown in Table 4.7. For SC 3 with all values of γ considered and for SC 4 with $\gamma \in \{0.01, 0.1\}$, the control performance is changed by –1.9% – 4.6%, but the queue length constraint violations (6.6% – 14.1%) are still high, although they are reduced w.r.t. SC 1 without queue override scheme. This is due to the fact that when the mainstream is congested the vehicles at the on-ramp cannot enter the main road even if the ramp metering rate is 1. For SC 4 with $\gamma \in \{1, 10, 100\}$, the queue length constraint violations (0% – 0.6%) are small, while the control performance improvements (0.7% – 2.8%) are also small. For all the values of γ considered, the total performance for SC 4 (15.9 – 16.6) is better than the total performance for SC 3 (16.0 – 23.2). For SC 3 and SC 4, the standard deviations of J_{TTS}^{imp} and J_{pen} are large in general, and the standard deviations of J_{tot} are small in general.

The results for Case 2 are shown in Table 4.8. For SC 3 with all values of γ considered and for SC 4 with $\gamma \in \{0.01, 0.1\}$, the control performance is changed by –1.2% – 3.8%, with high queue length constraint violations (8.3% – 27.7%), which are reduced w.r.t. SC 1 without queue override scheme. For SC 4 with $\gamma \in \{1, 10, 100\}$, the queue length constraint violations are reduced to 0% – 0.4%. Nevertheless, the control performance improvements (1.0% – 1.8%) are also small. For $\gamma \in \{1, 10, 100\}$, the total performance for SC 4 (19.7 – 19.9) is better than the total performance for SC 3 (20.4 – 33.8). For

SC 3 and SC 4, the standard deviations of J_{TTS}^{imp} and J_{pen} are large in general, and the standard deviations of J_{tot} are small in general.

5. Overall comparison for all approaches:

The control performance improvements for TTS (J_{TTS}^{imp}), constraint violations (J_{pen}), and total performance (J_{tot}) for all approaches considered are plotted in Figures 4.4-4.9. In these figures, the lines with marker symbols correspond to the approaches ignoring uncertainties (NRHPC 1, NRHPC 2, SC 1, and SC 3), and the lines without marker symbols correspond to the approaches including uncertainties (SRHPC 1, SRHPC 2, SC 2, and SC 4).

For both cases of uncertainties (Case 1 and Case 2), the control performance improvements for TTS for SC 2, SC 3, and SC 4 are small in comparison with NRHPC 1, NRHPC 2, SRHPC 1, and SRHPC 2 when $\gamma \in \{1, 10, 100\}$. For SC 1, the queue length constraint violations are much higher than those for NRHPC 1 and NRHPC 2 for both cases of uncertainties (Case 1 and Case 2). Due to the inclusion of a queue override scheme, the queue length constraint violations for SC 3 are comparable with those for NRHPC 1 and NRHPC 2 for both cases of uncertainties (Case 1 and Case 2). The queue length constraint violations are reduced to low values for SRHPC 1, SRHPC 2, SC 2, and SC 4 when the weight γ for the queue length constraint violation penalty is large enough, e.g. $\gamma \in \{1, 10, 100\}$. In J_{tot} , a larger weight γ for the queue length constraint violation penalty corresponds to assigning more importance to satisfying the queue length constraint. When the weight γ is large enough (e.g. $\gamma \in \{10, 100\}$), the total performance for SRHPC 1, SRHPC 2, SC 2, and SC 4 is better than that for NRHPC 1, NRHPC 2, SC 1, and SC 3.

Control Inputs

One realization of uncertainties for Case 2 is chosen as an illustrative example for showing the control inputs. For $\gamma = 100$, the variable speed limits and ramp metering rates for all the considered control approaches with $\gamma = 100$ are respectively shown in Figures 4.10-4.11.

As shown in Figure 4.10, the variable speed limits of the nominal RHPC approaches (NRHPC 1 and NRHPC 2) are similar with those of the scenario-based RHPC approaches (SRHPC 1 and SRHPC 2), and there are no large fluctuations for either of them. However, the standard control approaches (SC 2, SC 3, and SC 4) except for SC 1 yield variable speed limits that fluctuate more than the nominal RHPC approaches (NRHPC 1 and NRHPC 2) and the scenario-based RHPC approaches (SRHPC 1 and SRHPC 2).

Figure 4.11 shows the ramp metering rates. The nominal RHPC approaches (NRHPC 1 and NRHPC 2) and the scenario-based RHPC approaches (SRHPC 1 and SRHPC 2) can appropriately address the variations in the demand for the on-ramp, i.e., the ramp metering rates increase when there is a peak in the on-ramp demand from $t=0.1$ h to $t=0.35$ h (as shown in Figure 4.3). However, for the standard control approaches the ramp metering rates do not increase in a similar way.

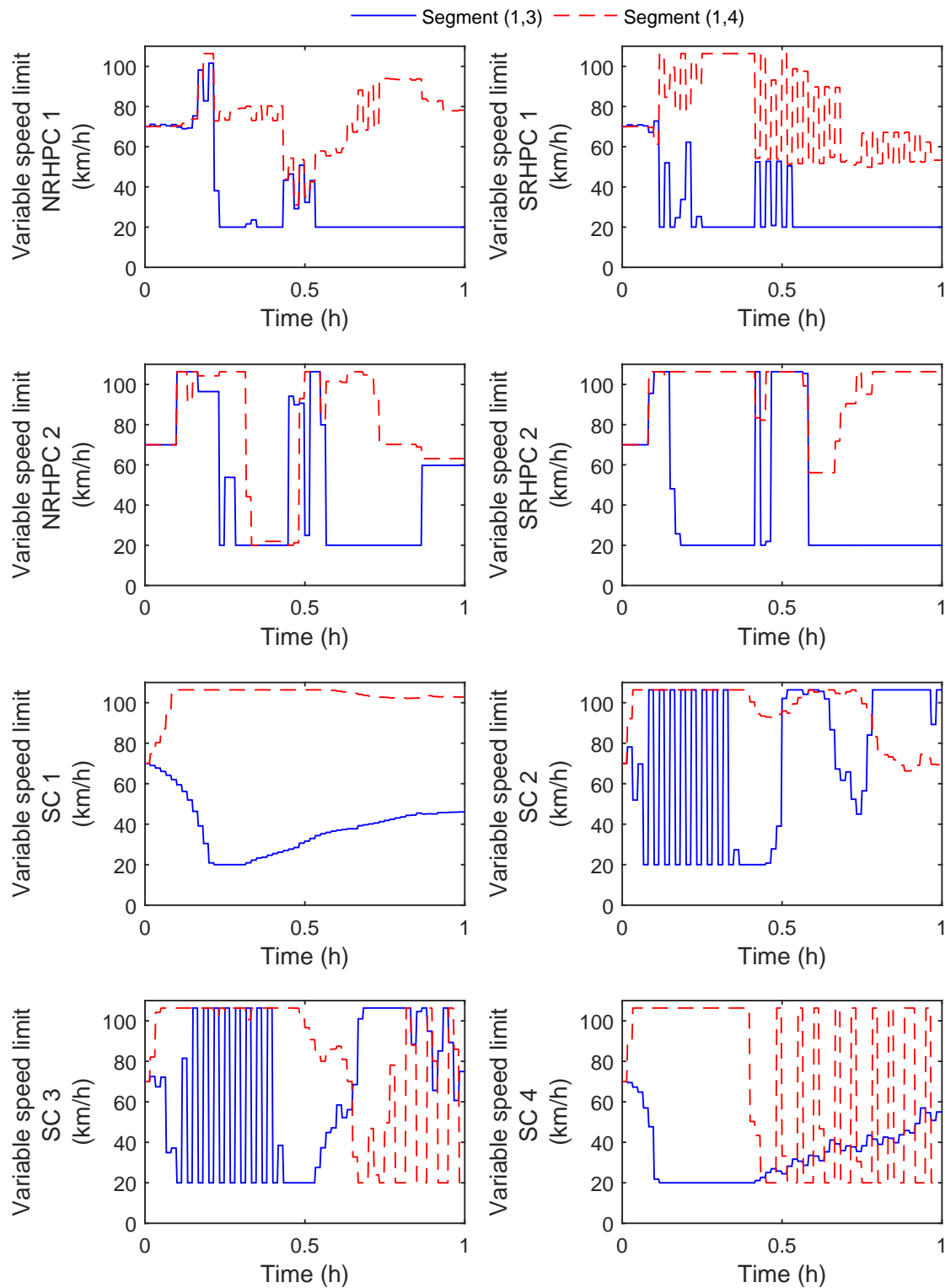


Figure 4.10: Variable speed limits (Case 2)

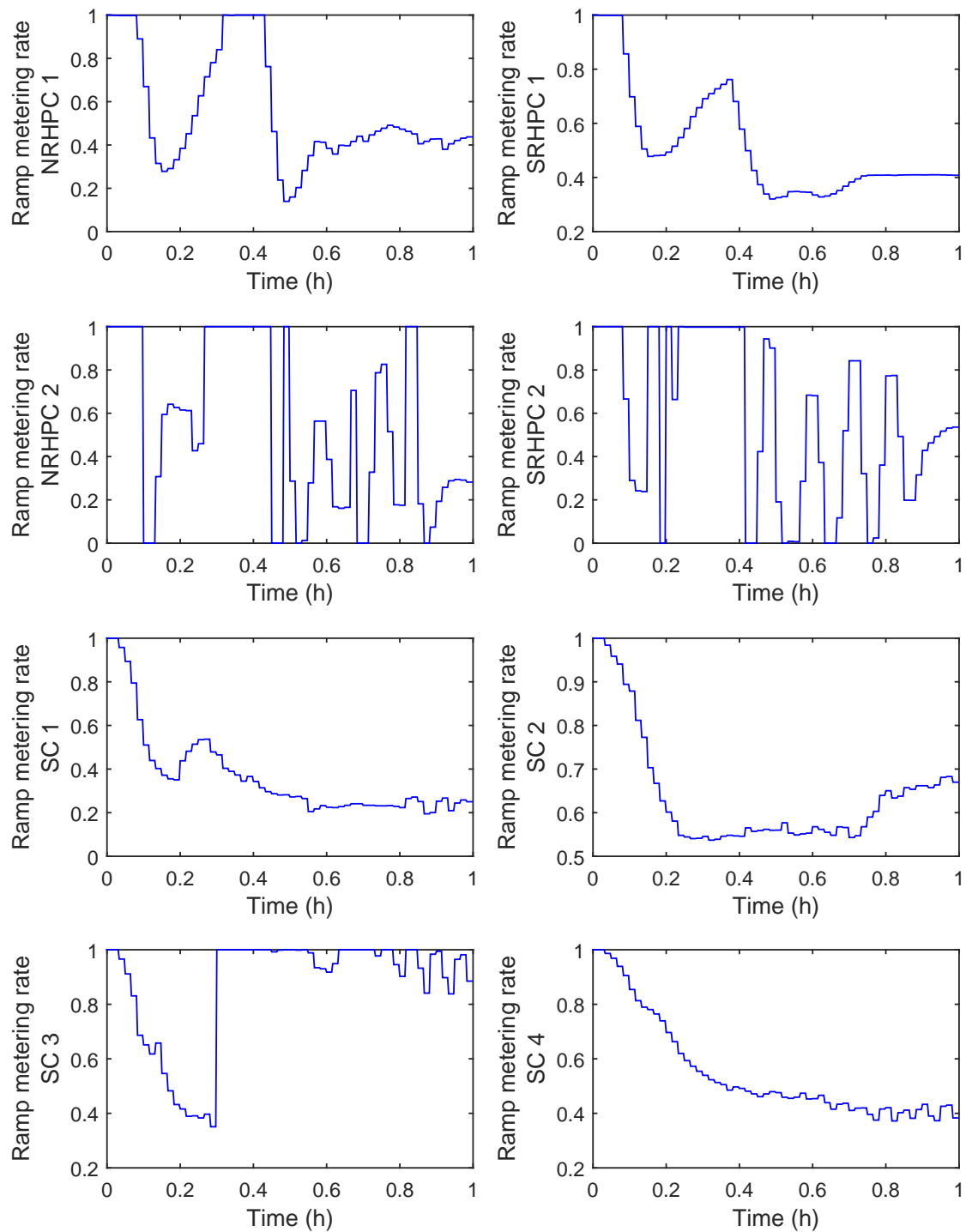


Figure 4.11: Ramp metering rates (Case 2)

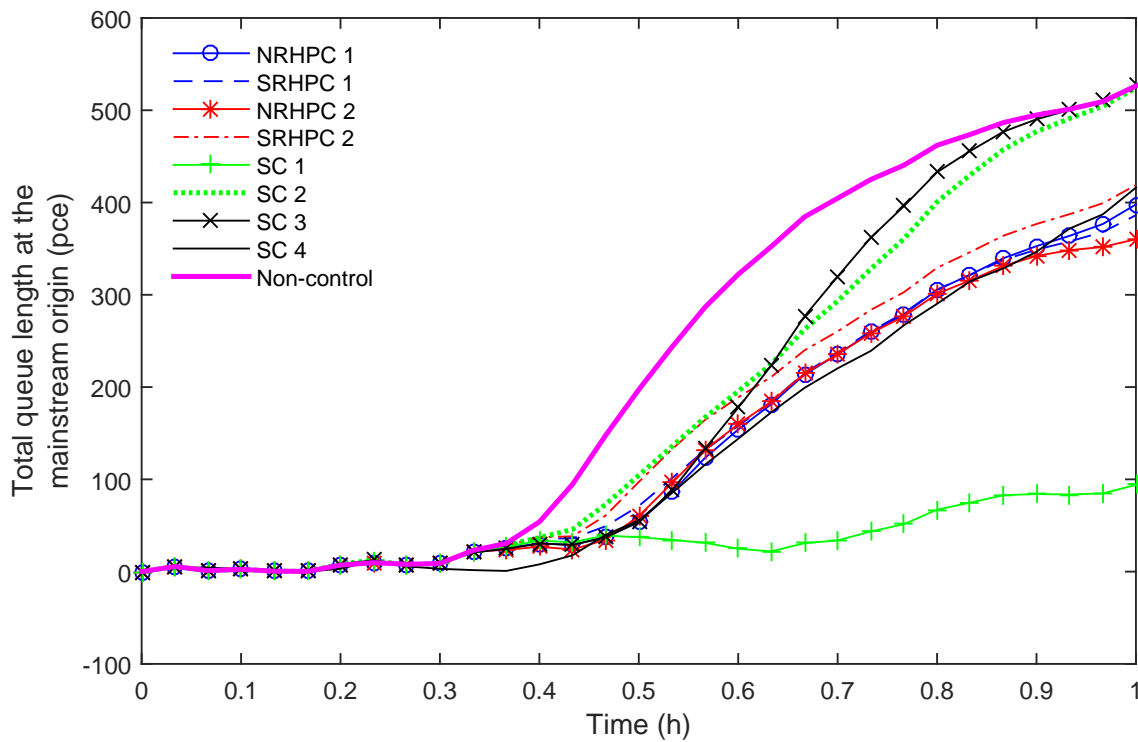


Figure 4.12: Queue lengths at the mainstream origin (Case 2)

Analysis of Traffic Behavior

For the same settings as Figures 4.10-4.11, the queue lengths at the mainstream origin and the on-ramp, and the densities and speeds for segments are plotted in Figures 4.12-4.17.

From Figure 4.12, it can be seen that the queue lengths at the mainstream origin are decreased w.r.t. the no-control case for both the nominal RHPC approaches (NRHPC 1 and NRHPC 2) and the scenario-based RHPC approaches (SRHPC 1 and SRHPC 2). In comparison with the no-control case, the queue lengths at the mainstream origin are also reduced for the standard control approaches (SC 1, SC 2, SC 3, and SC 4). From Figure 4.13, the control approaches ignoring uncertainties (NRHPC 1, NRHPC 2, SC1, and SC 3) lead to queue length constraint violations. These queue length constraint violations are effectively reduced by the control approaches considering uncertainties (SRHPC 1, SRHPC 2, SC 2, and SC 4).

From Figures 4.14-4.15, it can be noticed that the evolutions of the densities for segments are similar for all the considered approaches, and from an overview the peak values of densities during 0.2 h-0.6 h are reduced for all the considered approaches w.r.t. the no-control case.

From Figures 4.16-4.17, it can be seen that the speeds for the standard control approaches SC 2 and SC 3 fluctuate more than those for the RHPC approaches (NRHPC 1, NRHPC 2, SRHPC 1, and SRHPC 2). The fluctuations in speeds for segments correspond to variable speed limits shown in Figure 4.10.

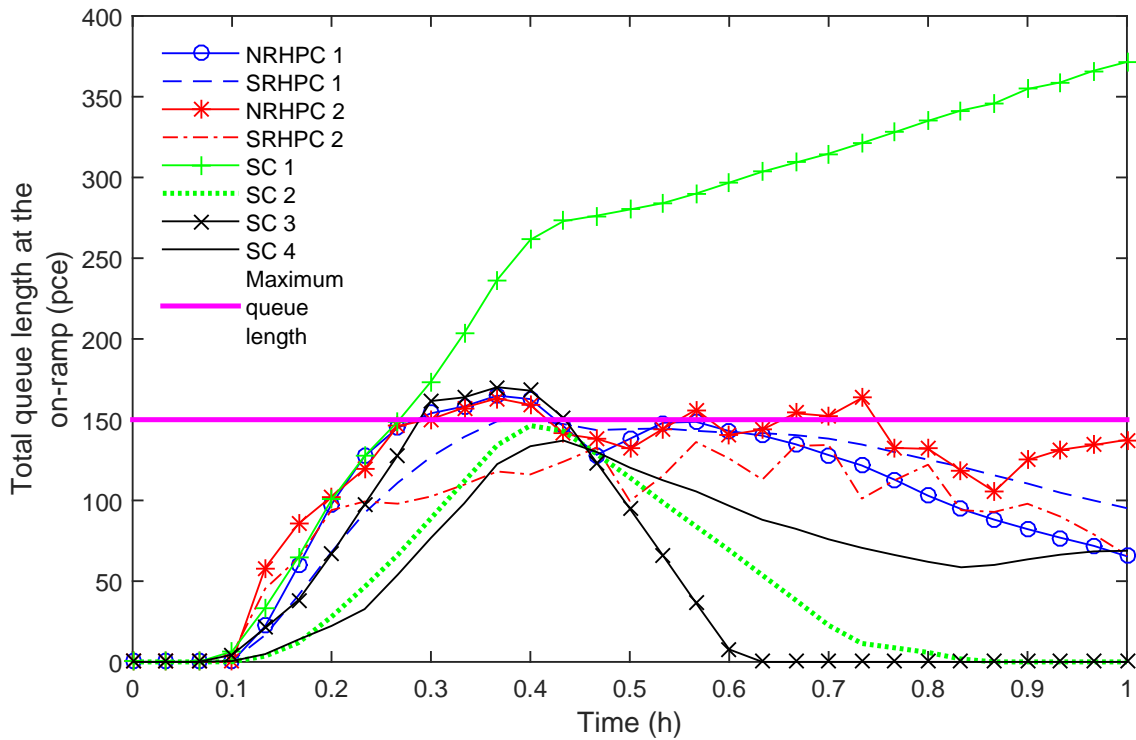


Figure 4.13: Queue lengths at the on-ramp (Case 2)

Overall Conclusions of Results

According to the results of the above simulation experiment, we can give the following conclusions:

1. The nominal RHPC approaches ignoring uncertainties (NRHPC 1 and NRHPC 2) can improve the control performance (i.e. the TTS) but with high queue length constraint violations for all the considered values of the weight γ for the queue length constraint violation penalty.
2. The scenario-based RHPC approaches including uncertainties (SRHPC 1 and SRHPC 2) can also improve the control performance, while there may be a small sacrifice in the control performance improvement compared to the nominal RHPC approaches ignoring uncertainties (NRHPC 1 and NRHPC 2). The queue length constraint violations are significantly reduced w.r.t. the nominal RHPC approaches ignoring uncertainties (NRHPC 1 and NRHPC 2) when the weight γ for the queue length constraint violation penalty is large enough.
3. The scenario-based RHPC approaches including uncertainties (SRHPC 1 and SRHPC 2) are more conservative in improving the control performance and satisfying the queue length constraints than the nominal RHPC approaches ignoring uncertainties (NRHPC 1 and NRHPC 2). This may be due to the fact that the scenario-based RHPC approaches including uncertainties (SRHPC 1 and SRHPC 2) are optimizing the worst case of the sum of the control objective function and the queue length constraint violation penalty among all the considered uncertainty scenarios.

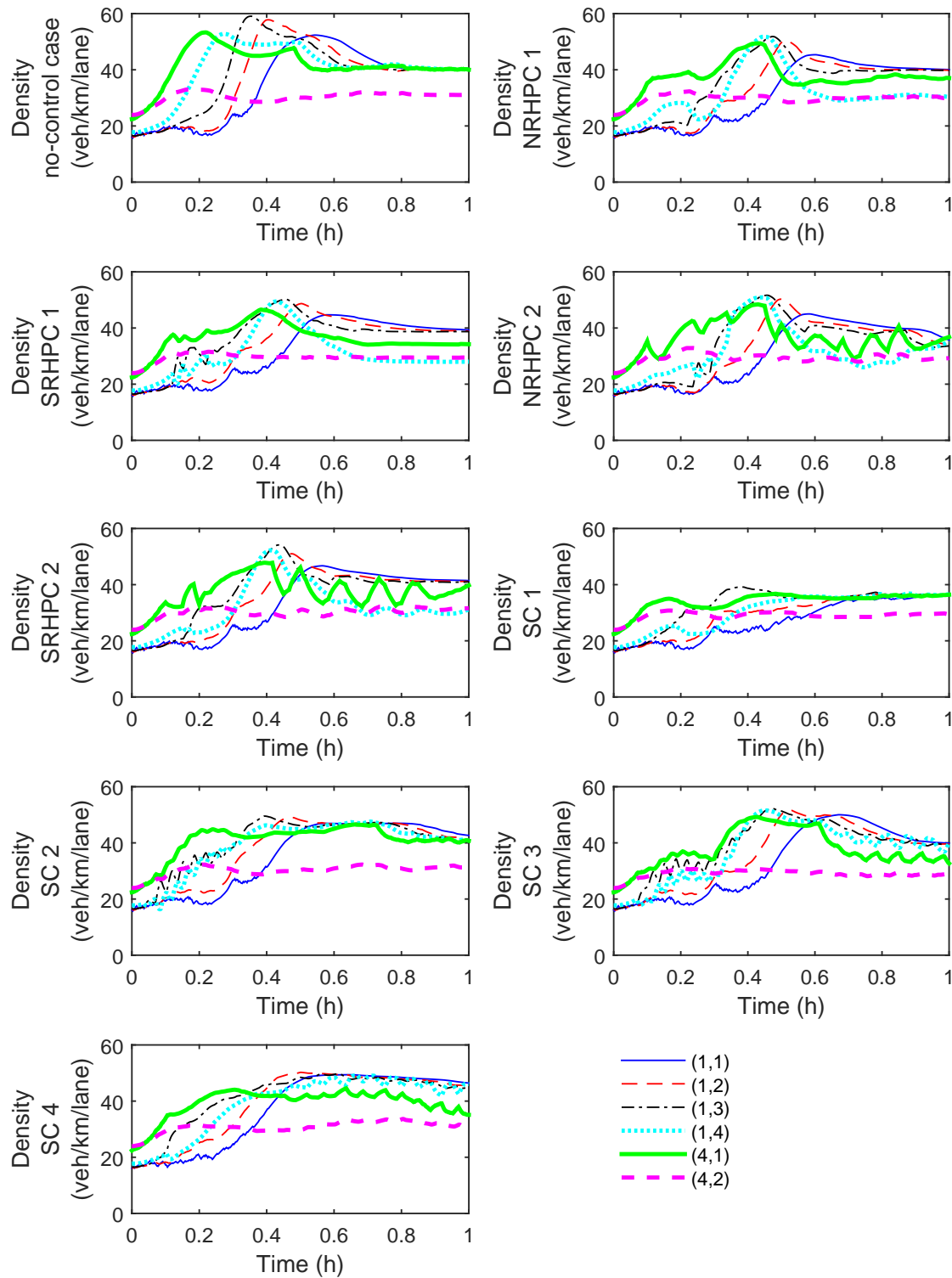


Figure 4.14: Densities of cars for segments (Case 2)

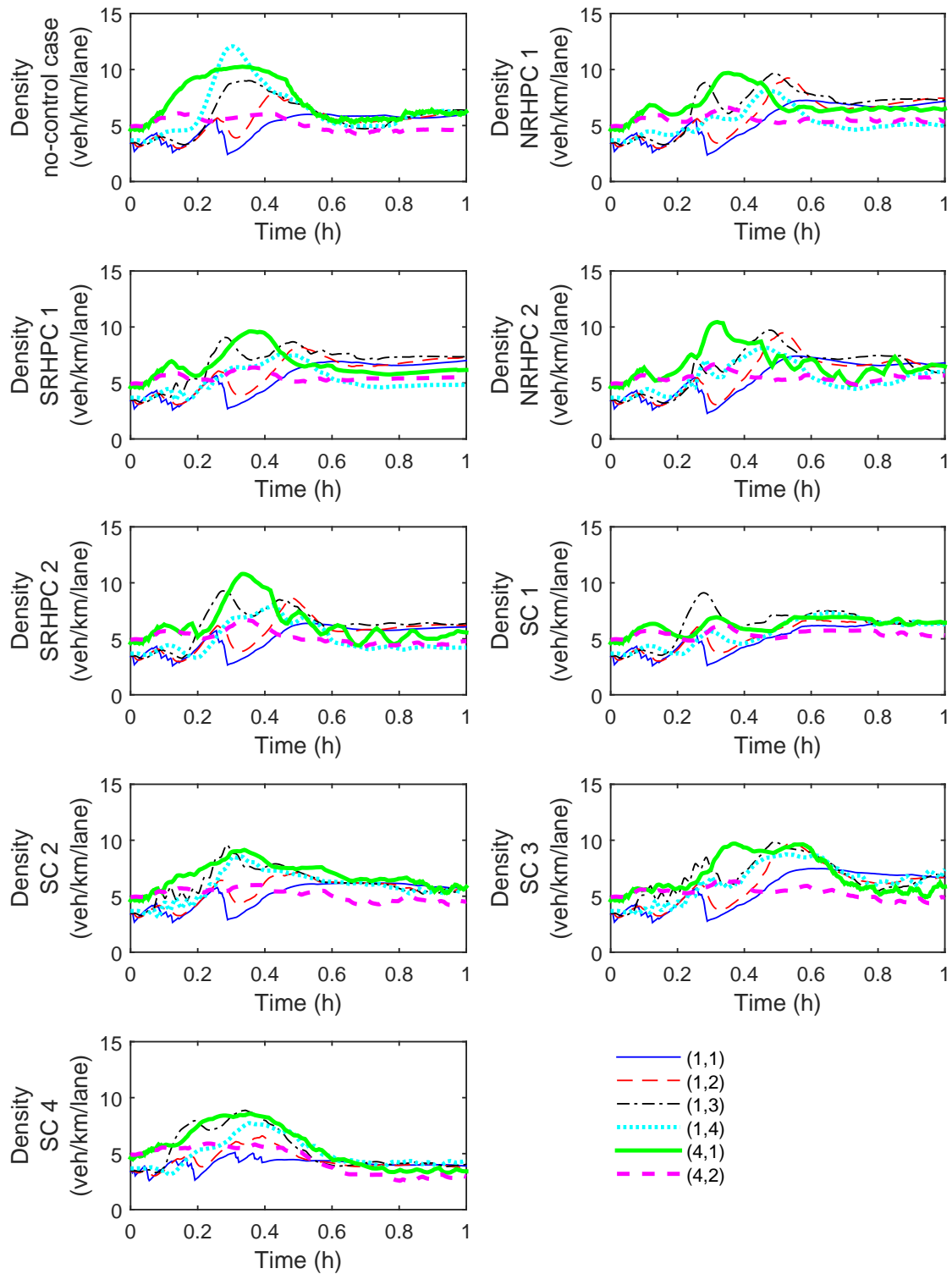


Figure 4.15: Densities of trucks for segments (Case 2)

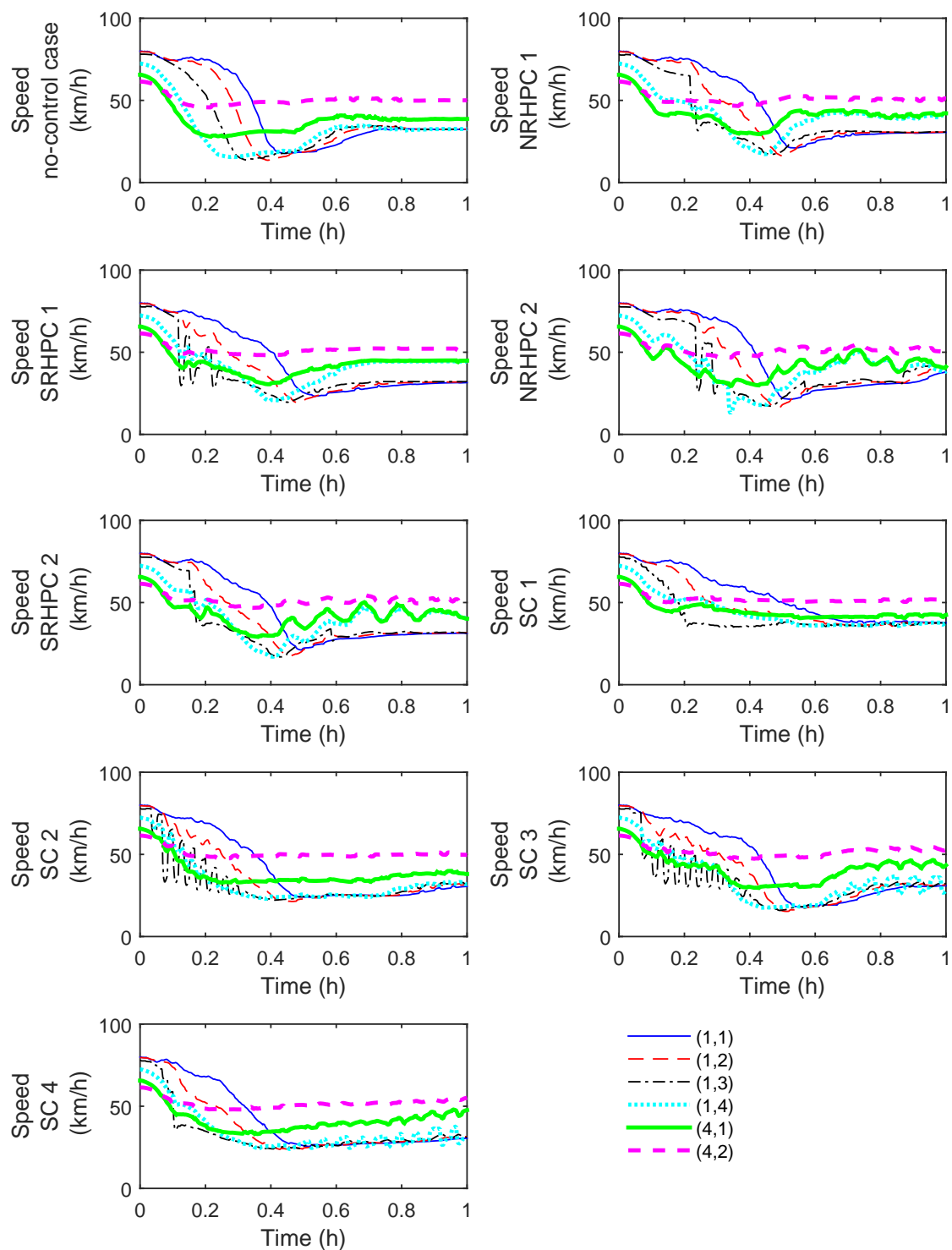


Figure 4.16: Speeds of cars for segments (Case 2)

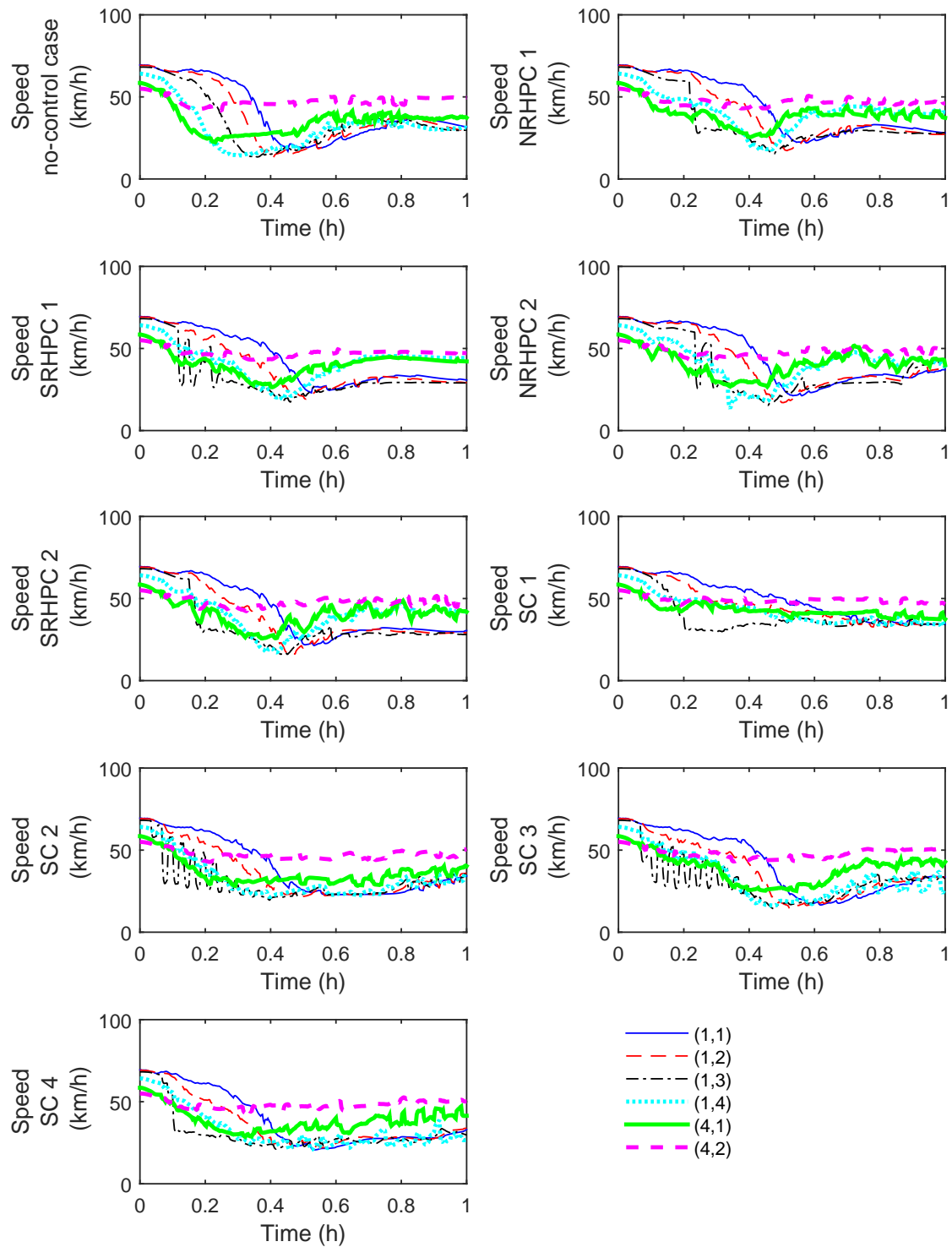


Figure 4.17: Speeds of trucks for segments (Case 2)

4. The standard control approach ignoring uncertainties (SC 1) can improve the control performance; however, the queue length constraint violations are quite high for all the considered values of the weight γ for the queue length constraint violation penalty. Even when a queue override scheme is included in the standard control approach ignoring uncertainties (SC 3), there are still high queue length constraint violations. This is due to the fact that when the mainstream is congested the vehicles at the on-ramp cannot enter the main road even if the ramp metering rate is 1.
5. The standard control approaches including uncertainties (SC 2 and SC 4) can significantly reduce the queue length constraint violations when the weight γ for the queue length constraint violation penalty is large enough. However, the control performance improvements for these approaches are less than those for the scenario-based RHPC approaches including uncertainties (SRHPC 1 and SRHPC 2).
6. When there are also uncertainties in truck fractions (Case 2), the queue length constraint violations may be even higher in comparison with the case that there are only uncertainties in the total demand (Case 1).
7. There are still small queue length constraint violations for the approaches including uncertainties (SRHPC 1, SRHPC 2, SC 2, and SC 4). This is probably due to the fact that we use only a limited number of scenarios for the uncertainties when solving the control problem.
8. When the weight γ for the queue length constraint violation penalty is large enough (in general, $\gamma = 1$ in our case study) for the approaches including uncertainties (SRHPC 1, SRHPC 2, SC 2, and SC 4), the queue length constraint violations are significantly reduced compared to the approaches ignoring uncertainties. Increasing the weight γ to be even larger ($\gamma \in \{10, 100\}$) does not significantly affect the control performance improvements and the ability of reducing queue length constraint violations. However, a larger weight γ for the queue length constraint violation penalty corresponds to putting more emphasis on satisfying the queue length constraint. For appropriate values of the weight γ (e.g. $\gamma \in \{10, 100\}$), the total performance for the approaches including uncertainties (SRHPC 1, SRHPC 2, SC 2, and SC 4) is better than that for the approaches ignoring uncertainties (NRHPC 1, NRHPC 2, SC 1, and SC 3).
9. According to standard deviations, the RHPC approaches (NRHPC 1, NRHPC 2, SRHPC 1, and SRHPC 2) are comparable for the different scenarios considered in control performance improvements, but they differ for the different scenarios considered in queue length constraint violations. Note that for the scenario-based RHPC approaches (SRHPC 1 and SRHPC 2), the queue length constraint violations are minor when the weight γ for the queue length constraint violation penalty is large enough; although the relative standard deviations are large, the actual variations in these violations are still small. The standard control approaches SC 1, SC 3, and SC 4 differ for the different scenarios considered in both control performance improvements and queue length constraint violations.
10. The variable speed limits of the standard control approaches SC 2, SC 3, and SC 4 fluctuate more than those of the RHPC approaches (NRHPC 1, NRHPC 2, SRHPC 1,

and SRHPC 2). This might be because control parameters that are constant over the entire simulation period cannot appropriately reflect the relation between the optimal variable speed limits and the variations in the traffic states. The RHPC approaches (NRHPC 1, NRHPC 2, SRHPC 1, and SRHPC 2) can appropriately address the peak in the on-ramp demand by increasing the ramp metering rates at corresponding time; however, the standard control approaches (SC 1, SC 2, SC 3, and SC4) do not increase the ramp metering rates in a similar way.

In conclusion, we can say that the scenario-based RHPC approaches are effective for satisfying queue length constraints, at the cost of a small sacrifice in the control performance. Note that avoiding high queue length constraint violations is significant for on-ramps with strict limits on queue lengths, e.g. the on-ramps that are connected to busy urban stretches or intersections in upstream. High queue length constraint violations at these on-ramps may cause spill-back to upstream stretches; thus, scenario-based RHPC is helpful for these on-ramps.

4.4 Summary

In this chapter, we have developed a scenario-based Receding-Horizon Parameterized Control (RHPC) approach for freeway networks. For the scenario-based RHPC approach, we have developed several RHPC laws for freeway networks based on multi-class METANET. In the analysis of uncertainties for freeway networks we have particularly considered uncertainties in traffic demands, consisting of the uncertainties in the total demands and the uncertainties in the estimations of the fractions of different vehicle classes. However, other types of uncertainties can also be dealt with using the proposed scenario-based RHPC approach. A queue length constraint violation penalty has been included in the objective function of scenario-based RHPC, to prevent infeasible optimization problems under uncertainties. In the scenario-based RHPC approach, the worst case of the sum of the control objective function and the queue length constraint violation penalty among a finite number of uncertainty scenarios is optimized in the control process.

A case study was implemented to assess the effectiveness of this newly proposed scenario-based RHPC approach. Two combinations of the RHPC laws for Variable Speed Limits (VSL) and Ramp Metering (RM) were considered: a VSL law based on the variations in the speeds and densities from one segment to the next in combination with an ALINEA-like RM law, and a PI-ALINEA-like VSL law in combination with a PI-ALINEA-like RM law, for which both nominal RHPC approaches and scenario-based RHPC approaches were implemented. Standard control approaches (PI-ALINEA-like) were implemented for comparison, and a queue override scheme was also considered as extra comparison. The results show that the nominal RHPC approaches may lead to high queue length constraint violations even if the weight for the queue length constraint violation penalty is high. The scenario-based RHPC approaches are more conservative than the nominal RHPC approaches, and they can significantly reduce the queue length constraint violations when the weight for the queue length constraint violation penalty is large enough, with small sacrifices in control performance improvements. The standard control approach ignoring uncertainties may lead to high queue length constraint violations, which are still high even when a queue override scheme is used. This is due to the fact that when the mainstream is

congested the vehicles at the on-ramp cannot enter the main road even if the ramp metering rate is 1. The standard control approaches including uncertainties can reduce the queue length constraint violations to a low level when the weight for the queue length constraint violation penalty is large enough; however, the control performance improvements are less than those for the scenario-based RHPC approaches. Overall, for the given case study we can conclude that scenario-based RHPC is capable of effectively improving the control performance without high queue length constraint violations.

Chapter 5

Scenario-Based Distributed Model Predictive Control for Traffic Networks

In this chapter a scenario-based Distributed Model Predictive Control (DMPC) approach based on a reduced scenario tree is developed for large-scale freeway networks. In the new scenario-based DMPC approach, the uncertainties in a large-scale freeway network are distinguished into two categories: global uncertainties for the overall network and local uncertainties applicable to subnetworks only. We propose to use a reduced scenario tree consisting of global scenarios and a reduced local scenario tree, instead of using a complete scenario tree consisting of global scenarios and all the combinations of the local scenarios for all subnetworks. Moreover, an expected-value setting and a min-max setting are considered for handling uncertainties in scenario-based DMPC. The results for a numerical experiment show that the new scenario-based DMPC approach is effective in improving the control performance while at the same time satisfying the queue length constraints in the presence of uncertainties. Additionally, the proposed approach results in with a relatively low computational burden compared to the case with the complete scenario tree.

5.1 Global Uncertainties and Local Uncertainties in Large-Scale Traffic Networks

5.1.1 Uncertainties in Large-Scale Traffic Networks

In large-scale freeway networks, uncertainties can be introduced through various sources, such as the measurements of traffic states, the external uncontrollable inputs, the parameters of prediction models, and so on. For example, uncertainties are usually introduced in the process of measuring traffic states due to factors like the accuracy of sensors. Similarly, uncertainties are often introduced in the procedure of estimating the external uncontrollable inputs, such as demands and boundary conditions. Furthermore, uncertainties are also introduced in the procedure of calibrating the parameters of the prediction models. More specifically, the accuracy of the parameters of the prediction models for freeway networks can be affected by various uncertain factors, such as weather conditions (e.g. sunny or rainy), traffic compositions (e.g. cars and trucks), and extra flows to some destinations caused by events (e.g. a pop concert or a soccer game). Particularly, the weather conditions can affect free-flow speeds; the traffic compositions can affect the

accuracy of most model parameters; extra flows to some destinations can affect turning rates at intersections.

The uncertainties for large-scale freeway networks can be described in different ways. For instance, uncertainties often fall within some confidence bands around the nominal profiles; thus uncertainties can be described by means of some bounded sets including all the possible values of the uncertainties. Uncertainties can also be described by building a library of the possible scenarios for the uncertainties, and the possibilities of the appearances for these scenarios can be estimated. Note that bounded sets can be used for describing an infinite number of realizations of uncertainties, while a library of scenarios can be used for describing a finite number of uncertainty scenarios. In this chapter, we assume that the uncertainties are described by means of a library consisting of finite sets that cover all possible scenarios of uncertainties. In this case, it is possible to use an expected-value setting (which is probabilistic) for robust control, based on the probabilities for uncertainty scenarios.

5.1.2 Global Uncertainties and Local Uncertainties

In order to develop a scenario-based DMPC approach for large-scale freeway networks, we divide the uncertainties in the considered overall network into two categories, i.e. global uncertainties and local uncertainties. The global uncertainties are those uncertainties that apply to the overall network, e.g. the uncertainties in network-wide global weather conditions. The local uncertainties are those uncertainties that apply to a single network, including the uncertainties in local weather conditions, local traffic compositions, local demands at origins, boundary conditions, the measurements of traffic states, and so on. We define a set for global scenarios and a set for local uncertainties. In particular, Ω_{glob} is defined as the set of all the possible global scenarios, and Ω_s^{loc} is defined as the set of all the possible local scenarios for subnetwork s . The global scenarios in Ω_{glob} apply to all subnetworks, while the local scenarios in Ω_s^{loc} only apply to subnetwork s .

Distinguishing global scenarios from local scenarios can reduce the size of the scenario tree w.r.t. the case that all uncertainties are considered in the same way. The number of combinations of the local scenarios for all subnetworks is the multiplication of the numbers of the local scenarios for individual subnetworks, i.e. $\prod_{s=1, \dots, N_{\text{sub}}} N_s^{\text{loc}}$, with N_{sub} the number of subnetworks and N_s^{loc} the number of the local scenarios for subnetwork s . If global uncertainties are considered in the same way as local uncertainties, there will be N_{glob} scenarios for each subnetwork corresponding to global uncertainties, and the number of possible combinations is $N_{\text{glob}}^{N_{\text{sub}}}$. Otherwise, if global uncertainties are considered to be the same for all subnetworks, there will be N_{glob} combinations for global uncertainties for all subnetworks. The total number of combinations for all uncertainty scenarios is equal to the number of combinations for local scenarios multiplied by the number of combinations for global scenarios. Therefore, when global uncertainties are treated in a different way from local uncertainties, the number of combinations for all uncertainty scenarios is significantly reduced in comparison with the case that they are not distinguished.

5.2 DMPC for Large-Scale Traffic Networks

5.2.1 Model Predictive Control for Large-Scale Traffic Networks

The prediction model METANET considered in this chapter is nonlinear and nonconvex, and therefore the resulting optimization problem for Model Predictive Control (MPC) is nonlinear and nonconvex. We consider a large-scale freeway network, which can be divided into several subnetworks. Couplings between subnetworks are described by means of interconnecting constraints for the subnetworks. The performance criteria are assumed to be additive for different subnetworks, i.e. the sum of the performance criteria for different subnetworks equals the performance criterion for the overall network. Thus, the centralized model predictive control problem can be formulated as follows:

$$\min_{\tilde{u}_1(k), \dots, \tilde{u}_{N_{\text{sub}}}(k)} \sum_{s=1}^{N_{\text{sub}}} J_s(\tilde{x}_s(k), \tilde{y}_s(k), \tilde{u}_s(k)) \quad (5.1)$$

$$\text{s.t. } x_s(k+z+1) = f_s(x_s(k+z), u_s(k+z), D_s^{\text{in}}(k+z), E_s^{\text{in}}(k+z)) \quad (5.2)$$

for $z = 0, \dots, N_p - 1$

$$y_s(k+z) = h_s(x_s(k+z)) \quad \text{for } z = 1, \dots, N_p \quad (5.3)$$

$$x_s^k(k) = x_s^k \quad (5.4)$$

$$u_s(k+z) = u_s(k+N_c-1) \quad \text{for } z = N_c, \dots, N_p - 1 \quad (5.5)$$

$$F_s(\tilde{x}_s(k), \tilde{y}_s(k), \tilde{u}_s(k)) \leq 0 \quad (5.6)$$

$$E_{j,s}^{\text{in}}(k+z) - E_{s,j}^{\text{out}}(k+z) = 0 \quad \text{for } j \in S_s^{\text{nb}}, z = 0, \dots, N_p - 1 \quad (5.7)$$

$$\text{for } s = 1, \dots, N_{\text{sub}}$$

where $\sum_{s=1}^{N_{\text{sub}}} J_s(\tilde{x}_s(k), \tilde{y}_s(k), \tilde{u}_s(k))$ represents the overall control objective function, J_s is the local control objective function of subnetwork s , f_s is the dynamic function of subnetwork s , h_s is the output function of subnetwork s , x_s represents the state vector of subnetwork s , x_s^k represents the measured state vector of subnetwork s at time step¹⁴ k , y_s represents the output vector of subnetwork s , u_s represents the control input vector for subnetwork s , F_s is a general constraint function¹⁵ on the states, outputs, and control inputs for subnetwork s over the prediction period, $S_s^{\text{nb}} = \{j_{s,1}, \dots, j_{s,N_s^{\text{nb}}}\}$ is the set of all the indices for the neighbors of subnetwork s , with N_s^{nb} the number of the neighbors of subnetwork s , D_s^{in} represents the external uncontrollable input vector for subnetwork s (e.g. demands for subnetwork s), $E_s^{\text{in}}(k) = [(E_{j_{s,1},s}^{\text{in}}(k))^T, \dots, (E_{j_{s,N_s^{\text{nb}},s}^{\text{in}}(k))^T]^T$ represents the interconnecting input vector (w.r.t. agent s) for subnetwork s from all neighbors at time step k , (5.7) represents the interconnecting constraints between subnetwork s and all neighbors, $E_{j,s}^{\text{in}}$ represents the interconnecting input vector (w.r.t. agent s) for subnetwork s from neighboring subnetwork j , $E_{s,j}^{\text{out}}$ represents the interconnecting output vector (w.r.t. agent j) from neighboring subnetwork j to subnetwork s , and $E_{s,j}^{\text{out}}(k) = K_{s,j}[x_j^T(k), y_j^T(k), u_j^T(k)]^T$, with $K_{s,j}$ the interconnecting output selection matrix from j to s . In addition, the vectors $\tilde{x}_s(k)$, $\tilde{y}_s(k)$,

¹⁴In Sections 5.2-5.5, we assume $T_c = T$ for the sake of simplicity of notation; in Section 5.6 the general case with $T_c \neq T$ is considered.

¹⁵Note that (5.6) comprises all equality and inequality constraints on the states, outputs, and control inputs, such as inequality constraints for limiting the maximum queue lengths at on-ramps.

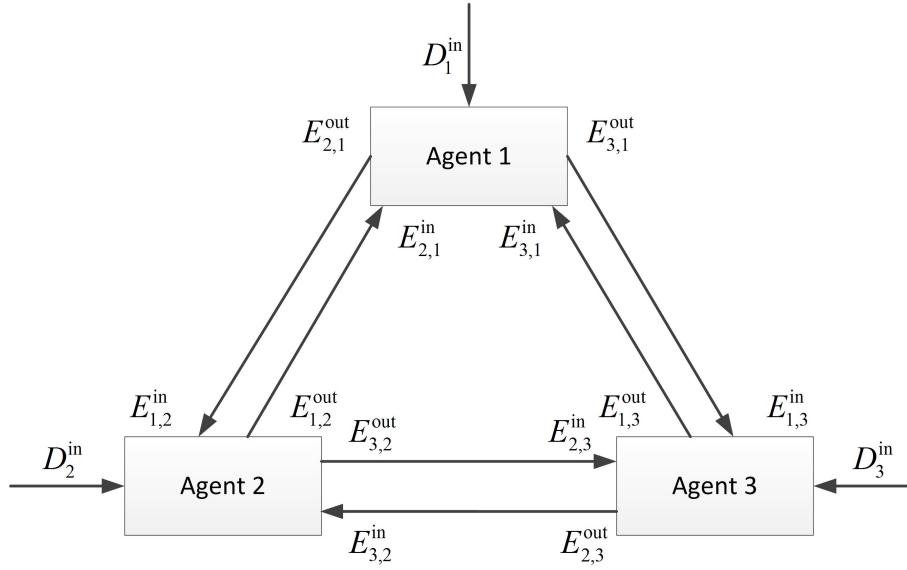


Figure 5.1: Uncontrollable inputs and interconnecting inputs and outputs for an example network

and $\tilde{u}_s(k)$ are defined as follows:

$$\tilde{x}_s(k) = [x_s^T(k+1), \dots, x_s^T(k+N_p)]^T \quad (5.8)$$

$$\tilde{y}_s(k) = [y_s^T(k+1), \dots, y_s^T(k+N_p)]^T \quad (5.9)$$

$$\tilde{u}_s(k) = [u_s^T(k), \dots, u_s^T(k+N_c-1)]^T \quad (5.10)$$

As an example, Figure 5.1 shows the uncontrollable inputs and the interconnecting inputs and outputs for a network including 3 subnetworks. For a subnetwork, both the uncontrollable inputs and the interconnecting inputs can affect the dynamics of that subnetwork. The interconnecting outputs of a subnetwork can affect the dynamics of the neighbors of that subnetwork. Note that in this chapter we only consider interconnecting *equality* constraints between individual subnetworks. However, it is possible to include other types of interconnecting constraints, such as interconnecting *inequality* constraints between individual subnetworks (e.g. an upper bound on the flow from an on-ramp to an adjacent stretch that belongs to another subnetwork).

The interconnecting constraints (i.e. (5.7)) can be merged into the overall control objective function in (5.1) by defining an augmented Lagrangian function as follows [14, 87]:

$$\begin{aligned} & L(\tilde{x}_1(k), \tilde{y}_1(k), \tilde{u}_1(k), \dots, \tilde{x}_{N_{\text{sub}}}(k), \tilde{y}_{N_{\text{sub}}}(k), \tilde{u}_{N_{\text{sub}}}(k), \tilde{\Lambda}^{\text{in}}(k)) \\ &= \sum_{s=1}^{N_{\text{sub}}} \left(J_s(\tilde{x}_s(k), \tilde{y}_s(k), \tilde{u}_s(k)) + \sum_{j \in S_s^{\text{nb}}} \left((\tilde{\lambda}_{j,s}^{\text{in}}(k))^T (\tilde{E}_{j,s}^{\text{in}}(k) - \tilde{E}_{s,j}^{\text{out}}(k)) \right. \right. \\ & \quad \left. \left. + \frac{e}{2} \left\| \tilde{E}_{j,s}^{\text{in}}(k) - \tilde{E}_{s,j}^{\text{out}}(k) \right\|_2^2 \right) \right) \end{aligned} \quad (5.11)$$

where $\tilde{\Lambda}^{\text{in}}(k) = [(\lambda_{j_1,1}^{\text{in}}(k))^T, \dots, (\lambda_{j_{N_{\text{sub}}}, N_{\text{sub}}}^{\text{in}}(k))^T]^T$, e is a positive constant, $\lambda_{j,s}^{\text{in}}$

represents the Lagrange multiplier vector corresponding to $E_{j,s}^{\text{in}}$, and $\tilde{\Lambda}^{\text{in}}(k)$, $\tilde{\lambda}_{j,s}^{\text{in}}(k)$, $\tilde{E}_{j,s}^{\text{in}}(k)$, and $\tilde{E}_{s,j}^{\text{out}}(k)$ are defined in a similar way to $\tilde{x}_s(k)$ (i.e. (5.8)) over the prediction period covering steps $k+z$, $z=0, \dots, N_p-1$.

According to duality theory [14, 16, 87], the dual problem associated with the original problem (defined by (5.1)-(5.7)) is defined as maximizing (5.11) over the Lagrange multipliers while minimizing (5.11) over the control inputs, i.e. as follows:

$$\begin{aligned} \max_{\tilde{\Lambda}^{\text{in}}(k)} \min_{\tilde{u}_1(k), \dots, \tilde{u}_{N_{\text{sub}}}(k)} L(\tilde{x}_1(k), \tilde{y}_1(k), \tilde{u}_1(k), \dots, \tilde{x}_{N_{\text{sub}}}(k), \tilde{y}_{N_{\text{sub}}}(k), \tilde{u}_{N_{\text{sub}}}(k), \tilde{\Lambda}^{\text{in}}(k)) \quad (5.12) \\ \text{s.t. (5.2) - (5.6) for } s = 1, \dots, N_{\text{sub}} \end{aligned}$$

Referring to [14, 24, 87], if the local control objective functions (i.e. J_s in (5.1)) and the inequality constraints (i.e. (5.6)) of subnetworks are convex and the equality constraints (i.e. (5.7)) of subnetworks are affine, the solution of the original problem (defined by (5.1)-(5.7)) can be obtained by iteratively solving the dual problem (defined by (5.2)-(5.6), and (5.12)). In the procedure for solving the dual problem, the Lagrange multipliers are fixed within one iteration, and for a given iteration they are estimated according to the solution for the previous iteration.

5.2.2 Decomposition of the MPC Problem for Large-Scale Traffic Networks

In order to solve the centralized control problem through DMPC, the augmented Lagrangian function (5.11), which is not separable due to the quadratic terms, needs to be distributed to local agents. In the literature [17, 59, 87], some approaches have been developed for decomposing the quadratic terms, such as block coordinate descent [87], dual ascent [17], and auxiliary problem principle [59]. With these approaches, the centralized control problem can be distributed to local agents, and a local agent iteratively solves the following problem with fixed Lagrange multipliers within one iteration:

$$\begin{aligned} \min_{\tilde{u}_s(k)} \left(J_s(\tilde{x}_s(k), \tilde{y}_s(k), \tilde{u}_s(k)) + \right. \\ \left. \tilde{E}_{j_{s,1},s}^{\text{in}}(k), \dots, \tilde{E}_{j_{s,N_{\text{nb}}},s}^{\text{in}}(k) \sum_{j \in S_s^{\text{nb}}} J_s^{\text{inter}}(\tilde{\lambda}_{j,s}^{\text{in}}(k), \tilde{\lambda}_{j,s}^{\text{out}}(k), \tilde{E}_{j,s}^{\text{in}}(k), \tilde{E}_{j,s}^{\text{out}}(k)) \right) \quad (5.13) \\ \tilde{E}_{j_{s,1},s}^{\text{out}}(k), \dots, \tilde{E}_{j_{s,N_{\text{nb}}},s}^{\text{out}}(k) \\ \text{s.t. (5.2) - (5.6) for } s = 1, \dots, N_{\text{sub}} \end{aligned}$$

in which J_s^{inter} is the function handling the interconnecting variables determined by agent s , $E_{j,s}^{\text{out}}$ represents the interconnecting output vector (w.r.t. agent s) from subnetwork s to neighboring subnetwork j , $\lambda_{j,s}^{\text{out}}$ represents the Lagrange multiplier vector corresponding to $E_{j,s}^{\text{out}}$, and $\tilde{\lambda}_{j,s}^{\text{out}}(k)$ and $\tilde{E}_{j,s}^{\text{out}}(k)$ are defined in a similar way to $\tilde{x}_s(k)$ (i.e. (5.8)) over the prediction period covering steps $k+z$, $z=0, \dots, N_p-1$.

5.3 Scenario-Based DMPC with Global Uncertainties

In this section, we include global uncertainties into the scenario-based DMPC problem. We consider an expected-value setting (which is probabilistic) and a min-max setting for

handling global uncertainties in the scenario-based DMPC problem. The symbols $x_{s,g}$, $y_{s,g}$, $J_{s,g}$, $f_{s,g}$, $F_{s,g}$, $J_{s,g}^{\text{inter}}$, $D_{s,g}^{\text{in}}$, $E_{s,g}^{\text{in}}$, $E_{j,s,g}^{\text{in}}$, $E_{s,j,g}^{\text{out}}$, $E_{j,s,g}^{\text{out}}$, Λ_g^{in} , $\lambda_{j,s,g}^{\text{in}}(k)$, and $\lambda_{j,s,g}^{\text{out}}$ have similar meanings to the corresponding symbols without subscript g in Section 5.2, but now they apply to the case with global uncertainties. In addition, $\tilde{x}_{s,g}(k)$ and $\tilde{y}_{s,g}(k)$ in a similar way to $\tilde{x}_s(k)$ (i.e. (5.8)) over the prediction period covering steps $k+z$, $z=1, \dots, N_p$; $\tilde{E}_{j,s,g}^{\text{in}}(k)$, $\tilde{E}_{s,j,g}^{\text{out}}(k)$, $\tilde{\Lambda}_g^{\text{in}}(k)$, $\tilde{\lambda}_{j,s,g}^{\text{in}}(k)$, and $\tilde{\lambda}_{j,s,g}^{\text{out}}(k)$ are defined similarly to $\tilde{x}_s(k)$ (i.e. (5.8)) over the prediction period covering steps $k+z$, $z=0, \dots, N_p-1$.

5.3.1 Scenario-Based DMPC with Global Uncertainties on the Basis of an Expected-Value Setting

For different scenarios for global uncertainties, the control input variable is uniformly defined, i.e. $\tilde{u}_s = \tilde{u}_{s,1} = \dots = \tilde{u}_{s,N_{\text{glob}}}$, with the subscripts $1, \dots, N_{\text{glob}}$ corresponding to global scenarios. This is because in our scenario-based DMPC approach each agent is assumed to deal with all the scenarios for one subnetwork. The centralized scenario-based MPC problem for the large-scale freeway network considered in Section 5.2 can be formulated as follows:

$$\min_{\tilde{u}_1(k), \dots, \tilde{u}_{N_{\text{sub}}}(k)} \sum_{g=1}^{N_{\text{glob}}} p_g \sum_{s=1}^{N_{\text{sub}}} J_{s,g}(\tilde{x}_{s,g}(k), \tilde{y}_{s,g}(k), \tilde{u}_s(k)) \quad (5.14)$$

$$\text{s.t. } x_{s,g}(k+z+1) = f_{s,g}(x_{s,g}(k+z), u_s(k+z), D_{s,g}^{\text{in}}(k+z), E_{s,g}^{\text{in}}(k+z), \omega_g(k+z)) \quad (5.15)$$

for $z=0, \dots, N_p-1$

$$y_{s,g}(k+z) = h_s(x_{s,g}(k+z)) \quad \text{for } z=1, \dots, N_p \quad (5.16)$$

$$x_{s,g}(k) = x_s^k \quad (5.17)$$

$$\omega_g(k+z) \in \Omega_{\text{glob}}(k+z) \quad \text{for } z=0, \dots, N_p-1 \quad (5.18)$$

$$F_{s,g}(\tilde{x}_{s,g}(k), \tilde{y}_{s,g}(k), \tilde{u}_s(k)) \leq 0 \quad (5.19)$$

$$E_{j,s,g}^{\text{in}}(k+z) - E_{s,j,g}^{\text{out}}(k+z) = 0 \quad \text{for } j \in S_s^{\text{nb}}, z=0, \dots, N_p-1 \quad (5.20)$$

Equation (5.5)

for $s=1, \dots, N_{\text{sub}}$, and $g=1, \dots, N_{\text{glob}}$

where $\sum_{g=1}^{N_{\text{glob}}} p_g \sum_{s=1}^{N_{\text{sub}}} J_{s,g}(\tilde{x}_{s,g}(k), \tilde{y}_{s,g}(k), \tilde{u}_s(k))$ represents the overall control objective function for scenario-based DMPC with global uncertainties, g is the index for the scenarios for global uncertainties, and p_g is the probability of global scenario g , ω_g represents scenario g for global uncertainties.

Referring to [14, 87], the augmented Lagrangian function with global uncertainties can be defined as follows:

$$\begin{aligned} & L_g(\tilde{x}_{1,1}(k), \tilde{y}_{1,1}(k), \tilde{u}_1(k), \dots, \tilde{x}_{N_{\text{sub}}, N_{\text{glob}}}(k), \tilde{y}_{N_{\text{sub}}, N_{\text{glob}}}(k), \tilde{u}_{N_{\text{sub}}}(k), \tilde{\Lambda}_g^{\text{in}}(k)) \\ &= \sum_{g=1}^{N_{\text{glob}}} p_g \sum_{s=1}^{N_{\text{sub}}} \left(J_{s,g}(\tilde{x}_{s,g}(k), \tilde{y}_{s,g}(k), \tilde{u}_s(k)) + \sum_{j \in S_s^{\text{nb}}} \left((\tilde{\lambda}_{j,s,g}^{\text{in}}(k))^T (\tilde{E}_{j,s,g}^{\text{in}}(k) - \tilde{E}_{s,j,g}^{\text{out}}(k)) \right. \right. \\ & \quad \left. \left. + \frac{e}{2} \left\| \tilde{E}_{j,s,g}^{\text{in}}(k) - \tilde{E}_{s,j,g}^{\text{out}}(k) \right\|_2^2 \right) \right) \end{aligned} \quad (5.21)$$

Each subnetwork is assigned a local agent, which determines the optimal local control inputs. For handling uncertainties in the joint constraint on the states, outputs, and control inputs, (5.19) can be incorporated into the local control objective functions via penalty terms. As described in Section 5.2, the quadratic terms in (5.21) can be decomposed for different subnetworks. Similarly to Section 5.2, we also let each local agent iteratively solve the following scenario-based control problem for a subnetwork

$$\begin{aligned}
& \min_{\substack{\tilde{u}_s(k) \\ \tilde{E}_{j_s,1,s,g}^{\text{in}}(k), \dots, \tilde{E}_{j_s, N_s^{\text{nb}}, s, g}^{\text{in}}(k) \\ \tilde{E}_{j_s,1,s,g}^{\text{out}}(k), \dots, \tilde{E}_{j_s, N_s^{\text{nb}}, s, g}^{\text{out}}(k)}}} \sum_{g=1}^{N_{\text{glob}}} p_g \left(J_{s,g}(\tilde{x}_{s,g}(k), \tilde{y}_{s,g}(k), \tilde{u}_s(k)) \right. \\
& \quad \left. + \Gamma \max(F_{s,g}(\tilde{x}_{s,g}(k), \tilde{y}_{s,g}(k), \tilde{u}_s(k)), 0) \right. \\
& \quad \left. + \sum_{j \in S_s^{\text{nb}}} J_{s,g}^{\text{inter}}(\tilde{\lambda}_{j,s,g}^{\text{in}}(k), \tilde{\lambda}_{j,s,g}^{\text{out}}(k), \tilde{E}_{j,s,g}^{\text{in}}(k), \tilde{E}_{j,s,g}^{\text{out}}(k)) \right) \quad (5.22) \\
& \text{s.t. (5.5), (5.15) – (5.18)}
\end{aligned}$$

in which Γ is a relatively high weight w.r.t. the weights for $J_{s,g}$ and $J_{s,g}^{\text{inter}}$. Moreover, the order of magnitude of Γ should be higher than those of the weights for $J_{s,g}$ and $J_{s,g}^{\text{inter}}$. Similarly to Section 5.2, the Lagrange multipliers are fixed within one iteration of solving the scenario-based control problem for each subnetwork, and they are computed based on the solutions of the previous iteration.

In the current Section 5.3 only global scenarios are considered; in the following Sections 5.4 to 5.6 local scenarios will also be included. We define the part after $\sum_{g=1}^{N_{\text{glob}}} p_g$ in (5.22) as the local *total objective function* for subnetwork s in global scenario g , and denote it as $J_{s,g}^{\text{tot}}$:

$$\begin{aligned}
& J_{s,g}^{\text{tot}}(\tilde{x}_{s,g}(k), \tilde{y}_{s,g}(k), \tilde{u}_s(k), \tilde{\lambda}_{j_s,1,s,g}^{\text{in}}(k), \tilde{\lambda}_{j_s,1,s,g}^{\text{out}}(k), \tilde{E}_{j_s,1,s,g}^{\text{in}}(k), \tilde{E}_{j_s,1,s,g}^{\text{out}}(k)) \\
& = J_{s,g}(\tilde{x}_{s,g}(k), \tilde{y}_{s,g}(k), \tilde{u}_s(k)) + \Gamma \max(F_{s,g}(\tilde{x}_{s,g}(k), \tilde{y}_{s,g}(k), \tilde{u}_s(k)), 0) \\
& \quad + \sum_{j \in S_s^{\text{nb}}} J_{s,g}^{\text{inter}}(\tilde{\lambda}_{j,s,g}^{\text{in}}(k), \tilde{\lambda}_{j,s,g}^{\text{out}}(k), \tilde{E}_{j,s,g}^{\text{in}}(k), \tilde{E}_{j,s,g}^{\text{out}}(k)) \quad (5.23)
\end{aligned}$$

For the sake of simplicity of notation, in the following descriptions, we do not include the inputs for $J_{s,g}^{\text{tot}}$, i.e. $\tilde{x}_{s,g}(k)$, $\tilde{y}_{s,g}(k)$, $\tilde{u}_s(k)$, $\tilde{\lambda}_{j_s,1,s,g}^{\text{in}}(k)$, $\tilde{\lambda}_{j_s,1,s,g}^{\text{out}}(k)$, $\tilde{E}_{j_s,1,s,g}^{\text{in}}(k)$, $\tilde{E}_{j_s,1,s,g}^{\text{out}}(k)$.

According to (5.22), the local *total objective function* $\sum_{g=1}^{N_{\text{glob}}} p_g J_{s,g}^{\text{tot}}$ is optimized by local agent s . Since global scenarios apply to all subnetworks, the sum of the local *total objective functions* for all subnetworks is the same as the overall *total objective function*, which is defined as the expected value of the overall *total objective function* values for all global scenarios:

$$\sum_{s=1}^{N_{\text{sub}}} \left(\sum_{g=1}^{N_{\text{glob}}} p_g J_{s,g}^{\text{tot}} \right) = \sum_{g=1}^{N_{\text{glob}}} p_g \left(\sum_{s=1}^{N_{\text{sub}}} J_{s,g}^{\text{tot}} \right) \quad (5.24)$$

Therefore, in the expected-value setting, the overall *total objective function* is jointly optimized by the local agents when only global uncertainties are included.

5.3.2 Scenario-Based DMPC with Global Uncertainties on the Basis of a Min-Max Setting

The scenario-based DMPC problem with global uncertainties on the basis of the min-max setting for a local agent s is defined as follows:

$$\begin{aligned} & \min_{\substack{\tilde{u}_s(k) \\ \tilde{E}_{j,s,1,s,g}^{\text{in}}(k), \dots, \tilde{E}_{j,s,N_{\text{pb}},s,g}^{\text{in}}(k) \\ \tilde{E}_{j,s,1,s,g}^{\text{out}}(k), \dots, \tilde{E}_{j,s,N_{\text{pb}},s,g}^{\text{out}}(k)}} \max_{g=1, \dots, N_{\text{glob}}} J_{s,g}^{\text{tot}} & (5.25) \\ & \text{s.t. (5.5), (5.15) – (5.18)} \end{aligned}$$

where $J_{s,g}^{\text{tot}}$ is defined in (5.23), and the local *total objective function* $\max_{g=1, \dots, N_{\text{glob}}} J_{s,g}^{\text{tot}}$ is optimized by local agent s .

The sum of the local *total objective functions* for all subnetworks is an upper bound of the overall *total objective function*, which is defined as the maximum overall *total objective function* value among all global scenarios:

$$\sum_{s=1}^{N_{\text{sub}}} \left(\max_{g=1, \dots, N_{\text{glob}}} J_{s,g}^{\text{tot}} \right) \geq \max_{g=1, \dots, N_{\text{glob}}} \left(\sum_{s=1}^{N_{\text{sub}}} J_{s,g}^{\text{tot}} \right) \quad (5.26)$$

This is because for defining the overall *total objective function*, all subnetworks correspond to the same global scenario; however, for defining local *total objective functions*, different subnetworks may correspond to different global scenarios. For subnetworks, the global scenarios that are considered to be the worst for local *total objective functions* are worse than or equal to the global scenario that is considered to be the worst for the overall *total objective function*. Therefore, in the min-max setting, an upper bound of the overall *total objective function* is jointly optimized by the local agents when only global uncertainties are included.

5.4 Scenario-Based DMPC on the Basis of a Reduced Scenario Tree of Global and Local Uncertainties

In this section, we include local uncertainties into the scenario-based DMPC problem by developing a reduced scenario tree. The expected-value setting (which is probabilistic) and the min-max setting are considered for handling local uncertainties in the scenario-based DMPC problem. The symbols $x_{s,g,l}$, $y_{s,g,l}$, $J_{s,g,l}$, $f_{s,g,l}$, $F_{s,g,l}$, $D_{s,g,l}^{\text{in}}$, and $E_{j,s,g,l}^{\text{out}}$ also have similar meanings to the corresponding symbols without subscripts g and l in Section 5.2, but now they apply to the case with global uncertainties and local uncertainties. In addition, $\tilde{x}_{s,g,l}(k)$ and $\tilde{y}_{s,g,l}(k)$ are defined in a similar way to $\tilde{x}_s(k)$ (i.e. (5.8)) over the prediction period covering steps $k+z$, $z=1, \dots, N_p$, and $\tilde{E}_{j,s,g,l}^{\text{out}}(k)$ is defined similarly to $\tilde{x}_s(k)$ (i.e. (5.8)) over the prediction period covering steps $k+z$, $z=0, \dots, N_p-1$.

5.4.1 Reduced Scenario Tree of Global and Local Uncertainties

For computing local *total objective functions*, local agents need interconnecting inputs from neighboring subnetworks. For a given global scenario for a subnetwork, the interconnecting inputs from neighboring subnetworks are considered to be predicted for the same given global scenario. However, local uncertainties only apply to certain subnetworks; thus, for a given subnetwork s , any local scenario in Ω_j^{loc} may occur for neighboring agent j .

When all the combinations of the local scenarios for all subnetworks are considered, i.e. a complete local scenario tree for local uncertainties is constructed, the total number of these combinations for a given global scenario is

$$N_{\text{com}} = \prod_{s=1, \dots, N_{\text{sub}}} N_s^{\text{loc}} \quad (5.27)$$

Thus the number of the combinations to be handled by a local agent is N_{com} for a given global scenario. In this case, the computational burden is large due to the large size of the complete local scenario tree.

In order to reduce the computational burden w.r.t. the complete local scenario tree, we propose a reduced local scenario tree, in which the interconnecting inputs for a subnetwork from neighboring subnetworks are assumed to be independent of the local scenarios for the neighboring subnetworks. The interconnecting inputs for a given subnetwork and the interconnecting outputs from the neighboring subnetworks to the given subnetwork describe the same physical quantities. Thus, the interconnecting outputs of a neighboring subnetwork are combined for all the local scenarios for that neighboring subnetwork, resulting in the combined interconnecting outputs corresponding to the interconnecting inputs for the given subnetwork.

We define the *reduced scenario tree* by combining all global scenarios and the reduced local scenario tree for the entire network. Similarly, we define the *complete scenario tree* by combining all global scenarios and the complete local scenario tree for the entire network. For subnetwork s , the number of combinations of global scenarios and local scenarios for the reduced scenario tree (i.e. $N_{\text{glob}} N_s^{\text{loc}}$) is smaller than that for the complete scenario tree (i.e. $N_{\text{glob}} N_{\text{com}}$). Therefore, the computational burden for processing the reduced scenario is relatively small w.r.t. that for processing the complete scenario tree.

5.4.2 Scenario-Based DMPC on the Basis of a Reduced Scenario Tree and an Expected-Value Setting

In the expected-value setting, the interconnecting outputs for a subnetwork are combined as follows:

$$\tilde{E}_{j,s,g}^{\text{out}}(k) = \sum_{l=l_{s,1}}^{l_{s,N_s^{\text{loc}}}} p_{s,l} \tilde{E}_{j,s,g,l}^{\text{out}}(k) \quad (5.28)$$

where l is the index for the local scenarios for a subnetwork, and $p_{s,l}$ is the probability of local scenario l for subnetwork s .

The scenario-based DMPC problem on the basis of the reduced scenario tree and the

expected-value setting for a local agent s is defined as follows:

$$\begin{aligned} \min_{\substack{\tilde{u}_s(k) \\ \tilde{E}_{j_s,1,s,g}^{\text{in}}(k), \dots, \tilde{E}_{j_s, N_s^{\text{nb}}, s, g}^{\text{in}}(k) \\ \tilde{E}_{j_s,1,s,g}^{\text{out}}(k), \dots, \tilde{E}_{j_s, N_s^{\text{nb}}, s, g}^{\text{out}}(k)}}} & \sum_{g=1}^{N_{\text{glob}}} p_g \left(\sum_{l=l_{s,1}}^{l_{s, N_s^{\text{loc}}}} p_{s,l} \left(J_{s,g,l}(\tilde{x}_{s,g,l}(k), \tilde{y}_{s,g,l}(k), \tilde{u}_s(k)) \right. \right. \\ & \left. \left. + \Gamma \max(F_{s,g,l}(\tilde{x}_{s,g,l}(k), \tilde{y}_{s,g,l}(k), \tilde{u}_s(k)), 0) \right) \right. \\ & \left. + \sum_{j \in S_s^{\text{nb}}} J_{s,g}^{\text{inter}}(\tilde{\lambda}_{j,s,g}^{\text{in}}(k), \tilde{\lambda}_{j,s,g}^{\text{out}}(k), \tilde{E}_{j,s,g}^{\text{in}}(k), \tilde{E}_{j,s,g}^{\text{out}}(k)) \right) \end{aligned} \quad (5.29)$$

$$\text{s.t. } x_{s,g,l}(k+z+1) = f_{s,g,l}(x_{s,g,l}(k+z), u_s(k+z), D_{s,g,l}^{\text{in}}(k+z), E_{s,g}^{\text{in}}(k+z), \omega_g(k+z), \omega_{s,l}(k+z)) \quad \text{for } z=0, \dots, N_p-1 \quad (5.30)$$

$$y_{s,g,l}(k+z) = h_s(x_{s,g,l}(k+z)) \quad \text{for } z=1, \dots, N_p \quad (5.31)$$

$$x_{s,g,l}(k) = x_s^k \quad (5.32)$$

$$\omega_{s,l}(k+z) \in \Omega_s^{\text{loc}}(k+z) \quad \text{for } z=0, \dots, N_p-1 \quad (5.33)$$

Equations (5.5) and (5.18)

for $g=1, \dots, N_{\text{glob}}$ and $l=1, \dots, N_s^{\text{loc}}$

where $\omega_{s,l}$ represents scenario l for the local uncertainties for subnetworks s .

Note that for the reduced scenario tree, the local *total objective function* ($J_{s,g}^{\text{tot}}$) for subnetwork s in global scenario g , which is introduced in Section 5.3, is redefined as the

part after $\sum_{g=1}^{N_{\text{glob}}} p_g$ in (5.29):

$$\begin{aligned} & J_{s,g}^{\text{tot}}(\tilde{x}_{s,g,l}(k), \tilde{y}_{s,g,l}(k), \tilde{u}_s(k), \tilde{\lambda}_{j,s,g}^{\text{in}}(k), \tilde{\lambda}_{j,s,g}^{\text{out}}(k), \tilde{E}_{j,s,g}^{\text{in}}(k), \tilde{E}_{j,s,g}^{\text{out}}(k)) \\ & = \sum_{l=l_{s,1}}^{l_{s, N_s^{\text{loc}}}} p_{s,l} \left(J_{s,g,l}(\tilde{x}_{s,g,l}(k), \tilde{y}_{s,g,l}(k), \tilde{u}_s(k)) \right. \\ & \quad \left. + \Gamma \max(F_{s,g,l}(\tilde{x}_{s,g,l}(k), \tilde{y}_{s,g,l}(k), \tilde{u}_s(k)), 0) \right) \\ & \quad + \sum_{j \in S_s^{\text{nb}}} J_{s,g}^{\text{inter}}(\tilde{\lambda}_{j,s,g}^{\text{in}}(k), \tilde{\lambda}_{j,s,g}^{\text{out}}(k), \tilde{E}_{j,s,g}^{\text{in}}(k), \tilde{E}_{j,s,g}^{\text{out}}(k)) \end{aligned} \quad (5.34)$$

5.4.3 Scenario-Based DMPC on the Basis of a Reduced Scenario Tree and a Min-Max Setting

In the min-max setting, the interconnecting outputs for a subnetwork can be combined as follows:

$$\tilde{E}_{j,s,g}^{\text{out}}(k) = \max_{l=l_{s,1}, \dots, l_{s, N_s^{\text{loc}}}} \left\| \tilde{E}_{j,s,g,l}^{\text{out}}(k) - \tilde{E}_{s,j,g}^{\text{in}}(k) \right\|_2^2 \quad (5.35)$$

which corresponds to the local scenario that leads to the maximum distance between $\tilde{E}_{j,s,g,l}^{\text{out}}(k)$ and $\tilde{E}_{s,j,g}^{\text{in}}(k)$. Note that other alternatives¹⁶ for defining $\tilde{E}_{j,s,g}^{\text{out}}$ can also be considered.

The scenario-based DMPC problem on the basis of the reduced scenario tree and the min-max setting for a local agent s is defined as follows:

$$\begin{aligned} & \min_{\tilde{u}_s(k)} \max_{g=1,\dots,N_{\text{glob}}} J_{s,g}^{\text{tot}} & (i.e. (5.25)) \\ & \tilde{E}_{j_{s,1},s,g}^{\text{in}}(k), \dots, \tilde{E}_{j_{s,N_s^{\text{nb}}},s,g}^{\text{in}}(k) \\ & \tilde{E}_{j_{s,1},s,g}^{\text{out}}(k), \dots, \tilde{E}_{j_{s,N_s^{\text{nb}}},s,g}^{\text{out}}(k) \end{aligned}$$

s.t. Equations (5.5), (5.18), and (5.30) – (5.33).

where the local *total objective function* ($J_{s,g}^{\text{tot}}$) for subnetwork s in global scenario g is defined as follows:

$$\begin{aligned} & J_{s,g}^{\text{tot}}(\tilde{x}_{s,g,l}(k), \tilde{y}_{s,g,l}(k), \tilde{u}_s(k), \tilde{\lambda}_{j,s,g}^{\text{in}}(k), \tilde{\lambda}_{j,s,g}^{\text{out}}(k), \tilde{E}_{j,s,g}^{\text{in}}(k), \tilde{E}_{j,s,g}^{\text{out}}(k)) \\ & = \max_{l=l_{s,1}, \dots, l_{s,N_s^{\text{loc}}}} \left(J_{s,g,l}(\tilde{x}_{s,g,l}(k), \tilde{y}_{s,g,l}(k), \tilde{u}_s(k)) \right. \\ & \quad \left. + \Gamma \max(F_{s,g,l}(\tilde{x}_{s,g,l}(k), \tilde{y}_{s,g,l}(k), \tilde{u}_s(k)), 0) \right) \\ & \quad + \sum_{j \in S_s^{\text{nb}}} J_{s,g}^{\text{inter}}(\tilde{\lambda}_{j,s,g}^{\text{in}}(k), \tilde{\lambda}_{j,s,g}^{\text{out}}(k), \tilde{E}_{j,s,g}^{\text{in}}(k), \tilde{E}_{j,s,g}^{\text{out}}(k)) \end{aligned} \quad (5.36)$$

5.5 Alternating Direction Method of Multipliers for Scenario-Based DMPC

The newly proposed scenario-based DMPC approach in this chapter is developed based on the dual decomposition method and the augmented Lagrangian relaxation method. As an illustration, the Alternating Direction Method of Multipliers (ADMM) [17] is chosen as the DMPC algorithm in this chapter. Note that the newly proposed scenario-based DMPC approach is independent of the considered DMPC algorithm, and it can be easily combined with other DMPC algorithms based on the dual decomposition method, such as the serial DMPC algorithm proposed in [87], accelerated gradient methods [43], etc.

In this section, we mainly apply ADMM to the new scenario-based DMPC approach developed in Section 5.4. More specifically, we adopt the "General Form Consensus Optimization" stated in Chapter 7.2 of [17], where the dual decomposition method and the augmented Lagrangian method are used for decomposing the overall optimization problem into local optimization problems.

¹⁶An alternative way to define $\tilde{E}_{j,s,g}^{\text{out}}(k)$ in the min-max setting can e.g. be

$$\tilde{E}_{j,s,g}^{\text{out}}(k) = \max_{l=l_{s,1}, \dots, l_{s,N_s^{\text{loc}}}} J_{s,g}^{\text{inter}}(\tilde{\lambda}_{j,s,g}^{\text{in}}(k), \tilde{\lambda}_{j,s,g}^{\text{out}}(k), \tilde{E}_{j,s,g}^{\text{in}}(k), \tilde{E}_{j,s,g,l}^{\text{out}}(k))$$

5.5.1 Couplings between Subnetworks in ADMM

In Chapter 7.2 of [17], global variables are used for describing couplings between subnetworks. The interconnecting inputs of agent s from agent j should ideally equal the interconnecting outputs of agent j to agent s , since they correspond to the same quantities. These interconnecting inputs and outputs for different agents corresponding to the same quantities should converge to the same global variables through negotiation iterations between agents. For a specific combination of global scenario and local scenario, the number (N_{gv}) of global variables is

$$N_{\text{gv}} = \sum_{s=1}^{N_{\text{sub}}} N_s^{\text{nb}} \quad (5.37)$$

Based on the setting in Sections 5.3 and 5.4, the overall global variable for global scenario g is defined as $G_g(k) = [(G_{g,1}(k))^T, \dots, (G_{g,N_{\text{gv}}}(k))^T]^T$. In order to apply ADMM, the interconnecting constraint (5.20) should be replaced with

$$\begin{cases} \tilde{E}_{j,s,g}^{\text{in}}(k) - \tilde{G}_{j,s,g}(k) = 0 \\ \tilde{E}_{s,j,g}^{\text{out}}(k) - \tilde{G}_{j,s,g}(k) = 0 \end{cases} \text{ for } j \in S_s^{\text{nb}} \quad (5.38)$$

in which $G_{j,s,g}$ is the global variable corresponding to the interconnecting variable from subnetwork j to subnetwork s for global scenario g , and $\tilde{G}_{j,s,g}(k)$ is defined as

$$\tilde{G}_{j,s,g}(k) = P_{j,s} \tilde{G}_g(k) \quad (5.39)$$

where $P_{j,s}$ is the matrix for selecting the global variable corresponding to the interconnecting variable from subnetwork j to subnetwork s , and $\tilde{G}_{j,s,g}(k)$ and $\tilde{G}_g(k)$ are defined in a similar way to $\tilde{x}_s(k)$ (i.e. (5.8)) over the prediction period covering steps $k+z$, $z = 0, \dots, N_p - 1$.

Note that if (5.35) is used for defining $\tilde{E}_{j,s,g}^{\text{out}}(k)$, $\tilde{E}_{s,j,g}^{\text{in}}(k)$ should be replaced by $\tilde{G}_{s,j,g}(k)$, since interconnecting variables should converge to global variables in ADMM:

$$\tilde{E}_{j,s,g}^{\text{out}}(k) = \max_{l=l_{s,1}, \dots, l_{s,N_s^{\text{loc}}}} \left\| \tilde{E}_{j,s,g,l}^{\text{out}}(k) - \tilde{G}_{s,j,g}(k) \right\|_2^2 \quad (5.40)$$

The function $J_{s,g}^{\text{inter}}$ is defined as follows:

$$\begin{aligned} & J_{s,g}^{\text{inter}}((\tilde{\lambda}_{j,s,g}^{\text{in}}(k))^\sigma, (\tilde{\lambda}_{j,s,g}^{\text{out}}(k))^\sigma, (\tilde{E}_{j,s,g}^{\text{in}}(k))^{\sigma+1}, (\tilde{E}_{j,s,g}^{\text{out}}(k))^{\sigma+1}) \\ &= \begin{bmatrix} (\tilde{\lambda}_{j,s,g}^{\text{in}}(k))^\sigma \\ (\tilde{\lambda}_{j,s,g}^{\text{out}}(k))^\sigma \end{bmatrix}^T \begin{bmatrix} (\tilde{E}_{j,s,g}^{\text{in}}(k))^{\sigma+1} \\ (\tilde{E}_{j,s,g}^{\text{out}}(k))^{\sigma+1} \end{bmatrix} + \frac{e}{2} \left\| \begin{bmatrix} (\tilde{E}_{j,s,g}^{\text{in}}(k))^{\sigma+1} - (\tilde{G}_{j,s,g}(k))^\sigma \\ (\tilde{E}_{j,s,g}^{\text{out}}(k))^{\sigma+1} - (\tilde{G}_{s,j,g}(k))^\sigma \end{bmatrix} \right\|_2^2 \end{aligned} \quad (5.41)$$

where σ represents the negotiation iteration number, and both $\lambda_{j,s,g}^{\text{in}}$ and $\lambda_{j,s,g}^{\text{out}}$ are determined by agent s .

5.5.2 Algorithm for Scenario-Based DMPC on the Basis of ADMM

The algorithm for the scenario-based DMPC approach on the basis of the reduced scenario tree is described as follows:

1. Initialization: let $\sigma = 1$ and $\epsilon^\sigma = \infty$, and set an appropriate value for e . For $s = 1, \dots, N_{\text{sub}}$, let $x_s(k)$ equal the measured state vector x_s^k ; let $u_s(k)$ equal the initial control input variable; estimate $\tilde{D}_{s,g,l}^{\text{in}}(k)$ according to historical data; let $(\tilde{\lambda}_{j,s,g}^{\text{in}}(k))^\sigma = 0$ and $(\tilde{\lambda}_{j,s,g}^{\text{out}}(k))^\sigma = 0$; and initialize $(\tilde{G}_{j,s,g}(k))^\sigma$ and $(\tilde{G}_{s,j,g}(k))^\sigma$ by a warm start¹⁷.
2. For $s = 1, \dots, N_{\text{sub}}$, in a parallel fashion or a serial fashion agent s determines $(\tilde{u}_s(k))^{\sigma+1}$, $(\tilde{E}_{j,s,g}^{\text{in}}(k))^{\sigma+1}$, and $(\tilde{E}_{j,s,g}^{\text{out}}(k))^{\sigma+1}$ for $j \in S_s^{\text{nb}}$ by solving the local problem defined by: (5.5), (5.18), (5.29)-(5.33), and (5.41).
3. For $s = 1, \dots, N_{\text{sub}}$, update the global variables for all pairs of s and $j \in S_s^{\text{nb}}$:

$$(\tilde{G}_{j,s,g}(k))^{\sigma+1} = \frac{1}{2}((\tilde{E}_{j,s,g}^{\text{in}}(k))^{\sigma+1} + (\tilde{E}_{s,j,g}^{\text{out}}(k))^{\sigma+1}) \quad (5.42)$$

$$(\tilde{G}_{s,j,g}(k))^{\sigma+1} = \frac{1}{2}((\tilde{E}_{s,j,g}^{\text{in}}(k))^{\sigma+1} + (\tilde{E}_{j,s,g}^{\text{out}}(k))^{\sigma+1}) \quad (5.43)$$

4. For $s = 1, \dots, N_{\text{sub}}$, update the Lagrange multipliers for all pairs of s and $j \in S_s^{\text{nb}}$:

$$(\tilde{\lambda}_{j,s,g}^{\text{in}}(k))^{\sigma+1} = (\tilde{\lambda}_{j,s,g}^{\text{in}}(k))^\sigma + e((\tilde{E}_{j,s,g}^{\text{in}}(k))^{\sigma+1} - (\tilde{G}_{j,s,g}(k))^{\sigma+1}) \quad (5.44)$$

$$(\tilde{\lambda}_{j,s,g}^{\text{out}}(k))^{\sigma+1} = (\tilde{\lambda}_{j,s,g}^{\text{out}}(k))^\sigma + e((\tilde{E}_{j,s,g}^{\text{out}}(k))^{\sigma+1} - (\tilde{G}_{s,j,g}(k))^{\sigma+1}) \quad (5.45)$$

5. Check the stopping condition:

$$\epsilon^{\sigma+1} = \left\| \left\| \begin{bmatrix} ((\tilde{\Lambda}_1^{\text{in}}(k))^{\sigma+1} - (\tilde{\Lambda}_1^{\text{in}}(k))^\sigma)^T \\ \vdots \\ ((\tilde{\Lambda}_{N_{\text{glob}}}^{\text{in}}(k))^{\sigma+1} - (\tilde{\Lambda}_{N_{\text{glob}}}^{\text{in}}(k))^\sigma)^T \\ ((\tilde{\Lambda}_1^{\text{out}}(k))^{\sigma+1} - (\tilde{\Lambda}_1^{\text{out}}(k))^\sigma)^T \\ \vdots \\ ((\tilde{\Lambda}_{N_{\text{glob}}}^{\text{out}}(k))^{\sigma+1} - (\tilde{\Lambda}_{N_{\text{glob}}}^{\text{out}}(k))^\sigma)^T \end{bmatrix} \right\| \right\|_\infty \quad (5.46)$$

where $\Lambda_g^{\text{out}}(k) = [(\lambda_{j_1,1,1,g}^{\text{out}}(k))^T, \dots, (\lambda_{j_{N_{\text{sub}}, N_{\text{sub}}^{\text{nb}}}, N_{\text{sub}}, g}^{\text{out}}(k))^T]^T$ for $g = 1, \dots, N_{\text{glob}}$. If $\epsilon^{\sigma+1} < \epsilon$ (ϵ : a small positive value), stop the optimization, and output $(\tilde{u}_s(k))^{\sigma+1}$. Otherwise, go to step 2.

¹⁷In the warm start, we assume that for the first control step the control inputs equal the initial control inputs over the prediction period, and that for other control steps the control inputs over the prediction period are estimated by shifting one step ahead the optimal control input sequence obtained at the previous control step, based on the receding-horizon scheme [22, 79].

5.6 Case Study: Assessment of Scenario-Based DMPC

5.6.1 Benchmark Network

We consider a freeway network as shown in Figure 5.2 for the case study. In this freeway network, there are 10 links ($m = 1, \dots, 10$), 1 mainstream origin (O_0), 1 unrestricted destination (D_0), 3 on-ramps (O_1 , O_2 , and O_3), and 3 unrestricted off-ramps (O_4 , O_5 , and O_6). In total, these 10 links are divided into 18 segments with equal length $L_m=1$ km. The mainstream stretch includes 2 lanes, and each on-ramp or each off-ramp includes 1 single lane. The positions of variable speed limits ($N_{VSL} = 6$) are shown in Figure 5.2, and all on-ramps are metered ($N_{RM} = 3$). The queue lengths at all on-ramps are limited within 100 veh for avoiding spill back to upstream stretches. The turning rates at all off-ramps are assumed to be fixed as 5% of the mainstream flow. For applying scenario-based DMPC, the network is divided into 3 subnetworks (S_1 , S_2 , and S_3), and each subnetwork includes 6 segments, 1 on-ramp, and 1 off-ramp.

The single-class traffic flow model METANET is used as both the process model and the prediction model. According to [50, 60], the nominal parameters for METANET are chosen as follows: $C_{\text{main}}=2100$ veh/h/lane, $C_{\text{onramp}}=2000$ veh/h/lane, $\tau=18$ s, $\eta=60$ km²/h, $\kappa=40$ veh/km/lane, $a_m=1.867$, $\delta_m=0.1$, $v_m^{\text{free}}=102$ km/h, $\rho_m^{\text{crit}}=33.5$ veh/km/lane, and $\rho_m^{\text{max}}=180$ veh/km/lane for $m = 1, \dots, 10$. The weights in local *total objective functions* are as follows: $\xi_{\text{TTS}} = 1$, $\xi_{\text{speed}} = 0.05$, $\xi_{\text{ramp}} = 0.05$, and $\Gamma = 100$. The simulation time interval is $T = 10$ s, and the control time interval¹⁴ is $T_c = 180$ s. As suggested in [50], the prediction horizon is chosen according to the average time needed for a vehicle to go through the considered subnetwork: this leads to $N_p = 3$, and the control horizon is chosen to be smaller than N_p : $N_c = 2$. The considered simulation period is 2.5 h, and Figure 5.3 shows the nominal demands for the mainstream origin and on-ramps.

5.6.2 Control Settings

Uncertainty Scenarios

- *Uncertainty Scenarios for the Simulations*

Uncertainties in weather conditions (sunny or rainy) are considered as global uncertainties for the overall network. We suppose that the model parameter τ and the free-flow speed v_m^{free} are affected by weather conditions. For sunny days, τ and v_m^{free} are considered to be nominal values given in Section 5.6.1. For rainy days, τ is considered to be 5% larger than the corresponding nominal value, i.e. $\tau=18.9$ s, and v_m^{free} is considered to be 5% smaller than the corresponding nominal value, i.e. $v_m^{\text{free}}=96.9$ km/h. The probability for sunny days is assumed to be 0.8, and the probability for rainy days is assumed to be 0.2.

Uncertainties in demands are considered as local uncertainties for subnetworks. Based on nominal demands, three base demand scenarios over the entire simulation period are considered for constructing scenarios for simulations and scenario-based DMPC:

- Base demand scenario 1: nominal demands with a probability of 0.7;
- Base demand scenario 2: 90% of nominal demands with a probability of 0.1;

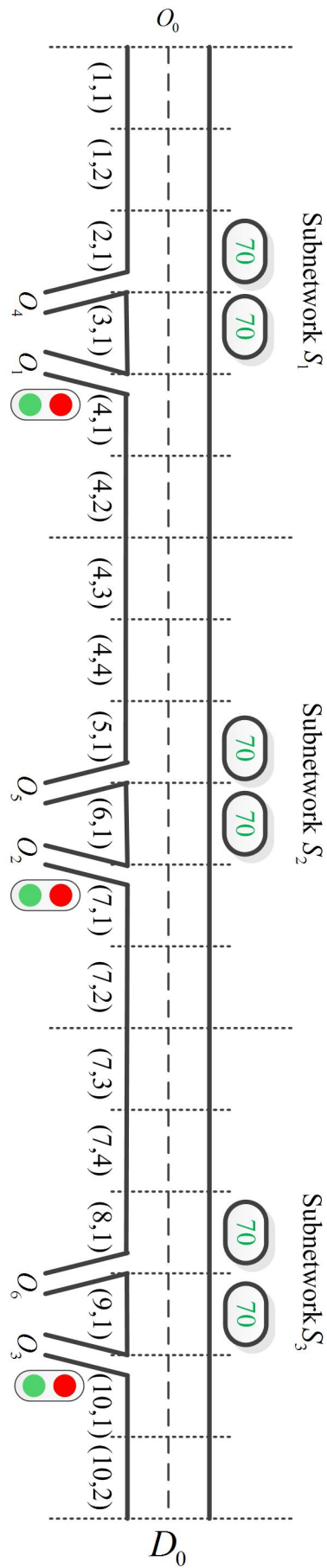


Figure 5.2: The Freeway network used for the case study

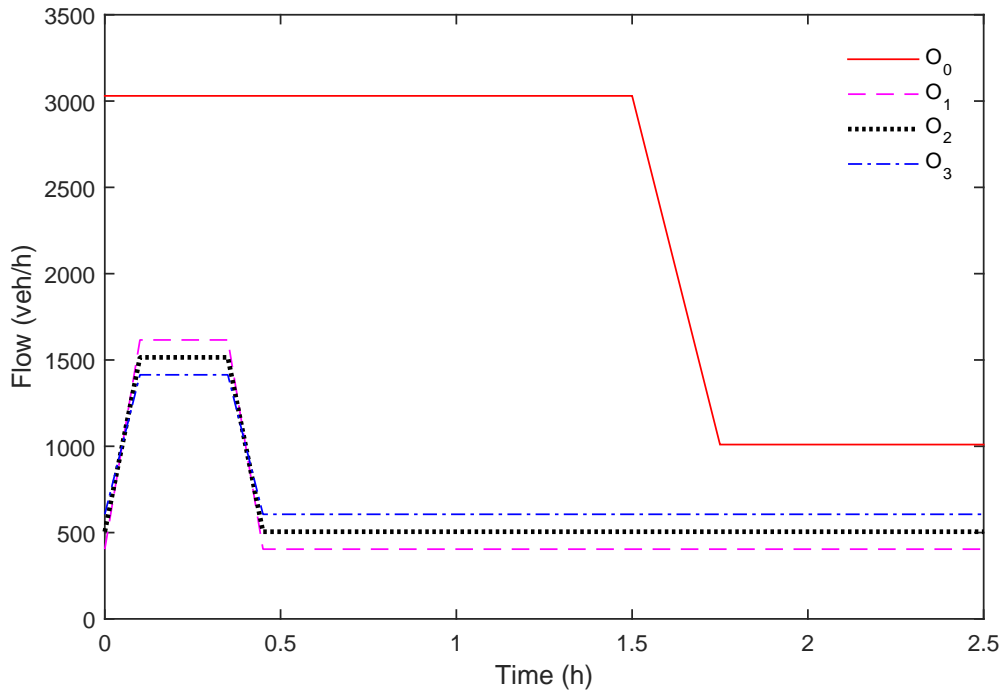


Figure 5.3: Nominal demands for the mainstream origin and on-ramps

- Base demand scenario 3: 110% of nominal demands with a probability of 0.2.

In this case study, we consider 10 demand scenarios for the simulations, of which the sampling step length is assumed to be equal to the control time step interval. Each of these 10 demand scenarios is constructed as follows: for each origin and at every sampling step the demand is randomly set to be one of the 3 base demand scenarios with the corresponding probabilities (i.e., 0.7, 0.1, 0.2). In the considered 10 demand scenarios for the simulations, 8 are for sunny days, and the remaining 2 are for rainy days.

- *Uncertainty Scenarios for Scenario-Based DMPC*

For scenario-based DMPC, global scenarios include sunny days and rainy days; demand scenarios (i.e. local scenarios) are constructed on the basis of the base demand scenarios. If all the possible combinations of the 3 base demand scenarios are considered, then for a given origin and for a given control step, there are 27 (i.e. $(3 \text{ base scenarios})^{N_p}$) possible demand scenarios over the prediction period. The probability of each of these 27 demand scenarios is obtained by multiplying the probabilities of the selected base demand scenarios for all sampling steps over the prediction period. Next, we ignore the demand scenarios with probabilities lower than 0.02, which leaves 10 demand scenarios over the prediction period for each origin at every control step, of which the total probability is 0.868. Thus the number of the considered demand scenarios for each origin at each control step is significantly reduced, while the total probability is still large. Note that in the expected-value setting the probability for each of the remaining 10 demand scenarios needs to be divided by 0.868, so that the equivalent total probability equals 1. The same 10 demand scenarios are also considered in the min-max setting.

Control Approaches

The following control approaches are considered:

- Nominal DMPC: based on nominal parameters and nominal demands;
- Scenario-Based DMPC 1: based on the reduced scenario tree and the expected-value setting;
- Scenario-Based DMPC 2: based on the reduced scenario tree and the min-max setting.

For scenario-based DMPC 2, (5.40) is used for determining interconnecting outputs for global scenarios.

All approaches are implemented in a serial scheme, i.e. local agents solve local optimization problems in a serial fashion, taking into account the latest information of neighboring local agents [87]. For all approaches, we set a fixed CPU time for all computations including negotiation iterations between agents for every control step (note that in this case the stopping condition (5.46) is not used). Two cases are considered, for one case the fixed CPU time for every control step for all control approaches is set to be 3 minutes, and for the other case the fixed CPU time for every control step for all control approaches is set to be 10 minutes¹⁸. All optimization problems are solved by the "fmincon" function based on the "active-set" algorithm in MATLAB, with the prediction model METANET coded in C. All simulations are implemented on a computer with 2 Intel(R) Xeon(R) CPU E5-1620 v3 @3.50GHz processors.

Performance Index

In the case study, the single-class METANET model is used as the prediction model, and TTS is considered as the performance criterion. For single-class traffic flows, TTS is defined as follows:

$$\text{TTS}(k_c) = T \sum_{z=k_c M}^{(k_c + N_p)M - 1} \left(\sum_{(m,i) \in I_{\text{all}}} \rho_{m,i}(z) L_m \mu_m + \sum_{o \in O_{\text{all}}} w_o(z) \right) \quad (5.47)$$

The objective function for a subnetwork is the same as (4.21), but TTS is computed for single class traffic flows as in (5.47).

5.6.3 Results and Analysis

Performance

For a simulation scenario, the simulation with a control approach is repeated 10 times for different random seeds corresponding to different random starting points for "fmincon", and the average of the results for the 10 repetitions is considered as the result for that simulation scenario. In Tables 5.1-5.2, for a control approach, the average and the standard deviation of the results for all simulation scenarios are listed.

¹⁸Note that in this chapter we make the CPU time for different approaches equal for fair comparison. In practice, the CPU time for each control step is required to be less than or equal to T_c , and this can e.g. be realized by means of fast implementation or parallel implementation, which are outside the scope of this chapter.

Table 5.1: Simulation results, CPU time for every control step: 3 minutes.

Approaches		Nominal DMPC	Scenario-Based DMPC 1	Scenario-Based DMPC 2
Average	J_{TTS}^{imp}	6.9%	5.2%	4.6%
	J_{pen}	12.0%	0%	0%
	J_{tot}^{imp}	-6.1%	5.2%	4.6%
Standard deviation	J_{TTS}^{imp}	0.8%	0.7%	0.5%
	J_{pen}	4.5%	0%	0%
	J_{tot}^{imp}	4.8%	0.7%	0.5%

Table 5.2: Simulation results, CPU time for every control step: 10 minutes.

Approaches		Nominal DMPC	Scenario-Based DMPC 1	Scenario-Based DMPC 2
Average	J_{TTS}^{imp}	6.9%	6.0%	5.5%
	J_{pen}	12.4%	0%	0%
	J_{tot}^{imp}	-6.6%	6.0%	5.5%
Standard deviation	J_{TTS}^{imp}	0.8%	0.7%	0.6%
	J_{pen}	4.7%	0%	0%
	J_{tot}^{imp}	5.1%	0.7%	0.6%

In Tables 5.1-5.2, J_{TTS}^{imp} represents the relative improvement in TTS w.r.t. the no-control case over the entire simulation period, J_{pen} represents the maximum of the relative queue length constraint violations for all on-ramps over the entire simulation period:

$$J_{pen} = \max \left(\max_{k=1, \dots, k_{end}} \frac{w_o(k)}{w_o^{max}} - 1, 0 \right) \quad (5.48)$$

where k_{end} represents the last simulation time step of the entire simulation period, and w_o^{max} represents the maximum permitted queue length for on-ramp o . The symbol J_{tot}^{imp} represents the relative improvement in the total performance w.r.t. the no-control case, and the total performance is defined as

$$J_{tot} = \frac{TTS_{total}}{TTS_{nom}} + \Gamma J_{pen} \quad (5.49)$$

with TTS_{total} the total time spent over the entire simulation period in a closed-loop simulation.

From Tables 5.1-5.2 we can see that for nominal DMPC the total performance is worse than that for the no-control case, while for scenario-based DMPC the total performance is improved w.r.t. the case without control. More specifically, the TTS can be improved by nominal DMPC, but the queue length constraints are not satisfied, leading to a worse total performance than the no-control case. For scenario-based DMPC, the TTS is improved less than nominal DMPC, but the queue length constraints are satisfied, resulting in an improvement of the total performance.

When the CPU time for every control step is increased from 3 minutes to 10 minutes,

the total performance is further improved by scenario-based DMPC; however, this not the case for nominal DMPC. This is probably due to the fact that nominal DMPC does not take into account uncertainties; thus longer CPU time can lead to control inputs corresponding to a better total performance for the nominal model parameters and the nominal demands. However, due to the presence of uncertainties, these control inputs in general may result in a worse total performance.

Moreover, the standard deviations of J_{TTS}^{imp} , J_{pen} , and J_{tot}^{imp} are all small for scenario-based DMPC. However, the standard deviations of J_{pen} and J_{tot}^{imp} are relatively large for nominal DMPC. This shows that scenario-based DMPC results in a more stable total performance than nominal DMPC.

Comparing scenario-based DMPC for the expected-value setting (scenario-based DMPC 1) with scenario-based DMPC for the min-max setting (scenario-based DMPC 2), we can see that for this case study using the expected-value setting can improve the total performance more than using the min-max setting. This is probably due to the fact that the same uncertainty scenarios are used for the expected-value setting and the min-max setting. For the min-max setting the worst case of the total performance among all the considered uncertainty scenarios is optimized, resulting in more conservative control inputs than those for the expected-value setting.

Control inputs

For one realization of uncertainties and the case that the CPU time for every control step is fixed as 10 minutes, the variable speed limits and the ramp metering rates for all the considered approaches are plotted in Figures 5.4-5.9.

From Figures 5.4-5.6 we can see that the variable speed limits determined by scenario-based DMPC are more fluctuating than those determined by nominal DMPC. Similarly, from Figures 5.7-5.9 we can see that the ramp metering rates determined by scenario-based DMPC are more fluctuating than those determined by nominal DMPC at on-ramp O_1 . For the other two on-ramps (O_2 and O_3) the ramp metering rates determined by scenario-based DMPC slightly fluctuate in comparison with those determined by nominal DMPC.

The fluctuations in the control inputs determined by scenario-based DMPC are probably due to the fact that scenario-based DMPC takes into account uncertainties. The predictions for the dynamics of the considered freeway network are fluctuating due to the uncertainties, and this makes the control inputs determined by scenario-based DMPC fluctuating. Another reason might be that when applying the new scenario-based DMPC approach for a nonlinear nonconvex freeway network, the convergence between neighboring subnetworks is not easy to be obtained. Besides, since we have a nonlinear-nonconvex problem, at every control step the solutions of the local controllers in general converge to local optima instead of a global optimum of the centralized control problem; this could also lead to fluctuations in the control inputs.

The ramp metering rates plotted in Figures 5.8-5.9 are optimal for the given setting of the case study. In practice, zero capacities for on-ramps can be avoided by limiting the minimum permitted metering rates or by penalizing the number of stops of vehicles at on-ramps.

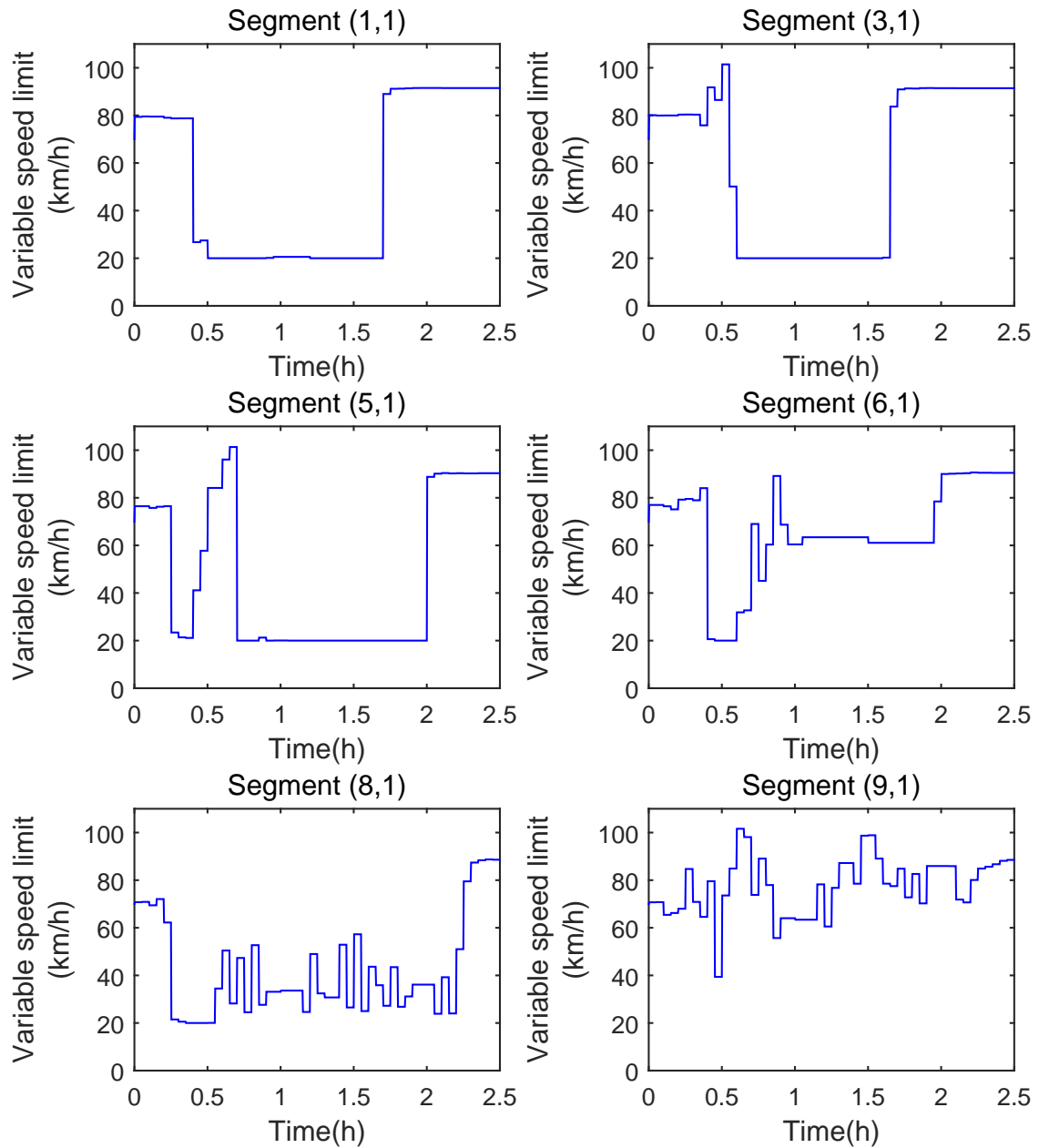


Figure 5.4: Variable speed limits for Nominal DMPC

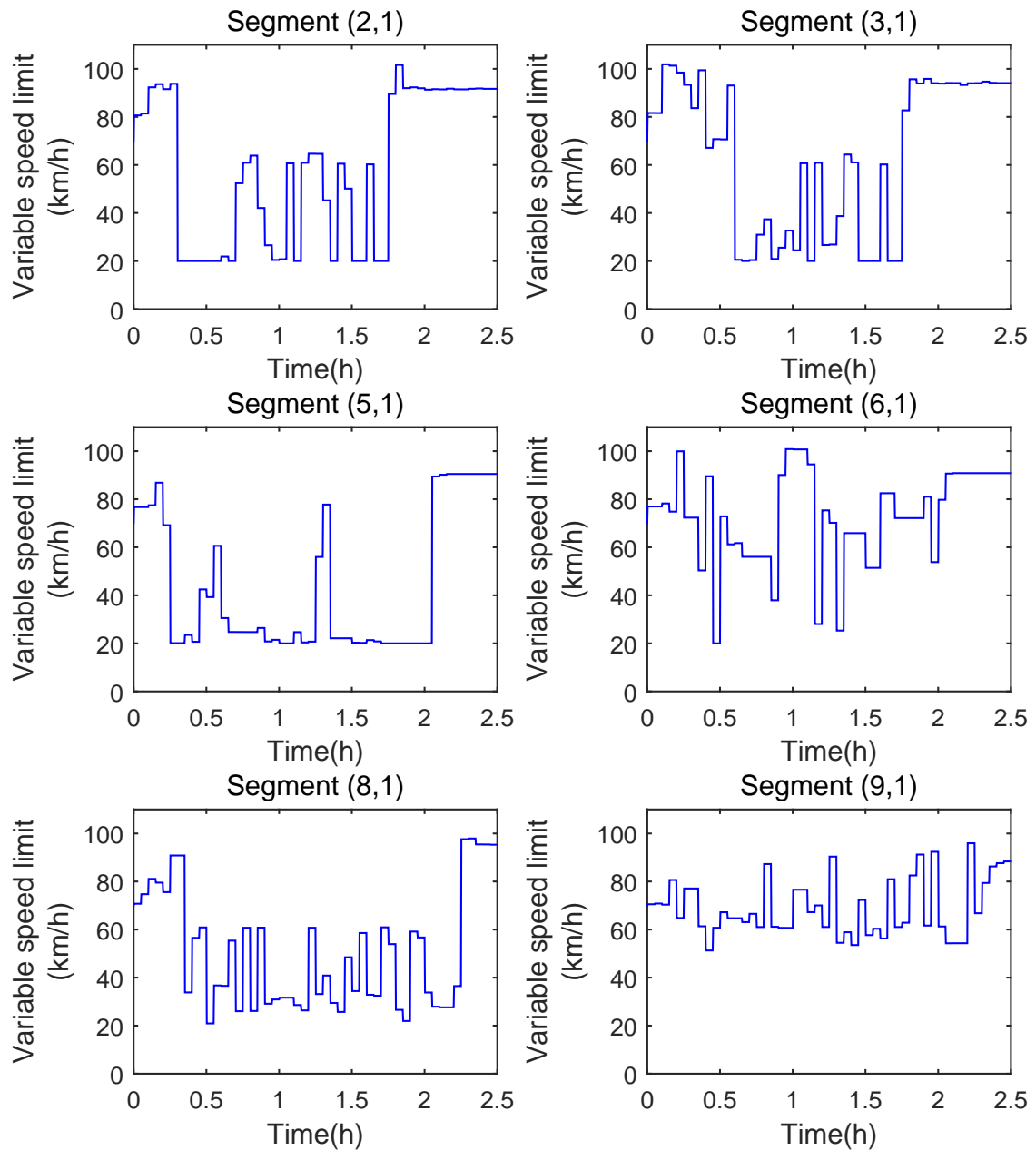


Figure 5.5: Variable speed limits for scenario-based DMPC 1

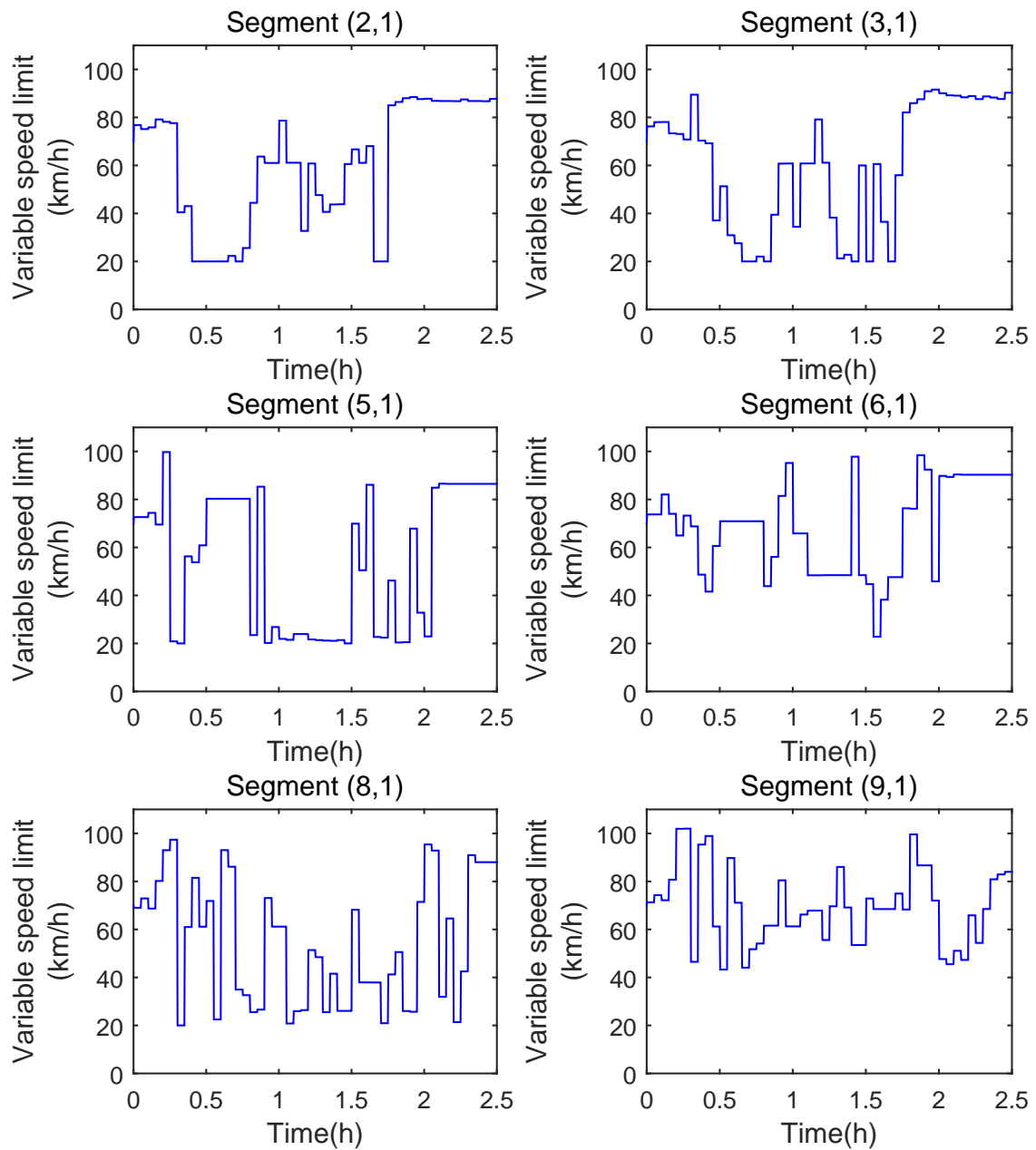


Figure 5.6: Variable speed limits for scenario-based DMPC 2

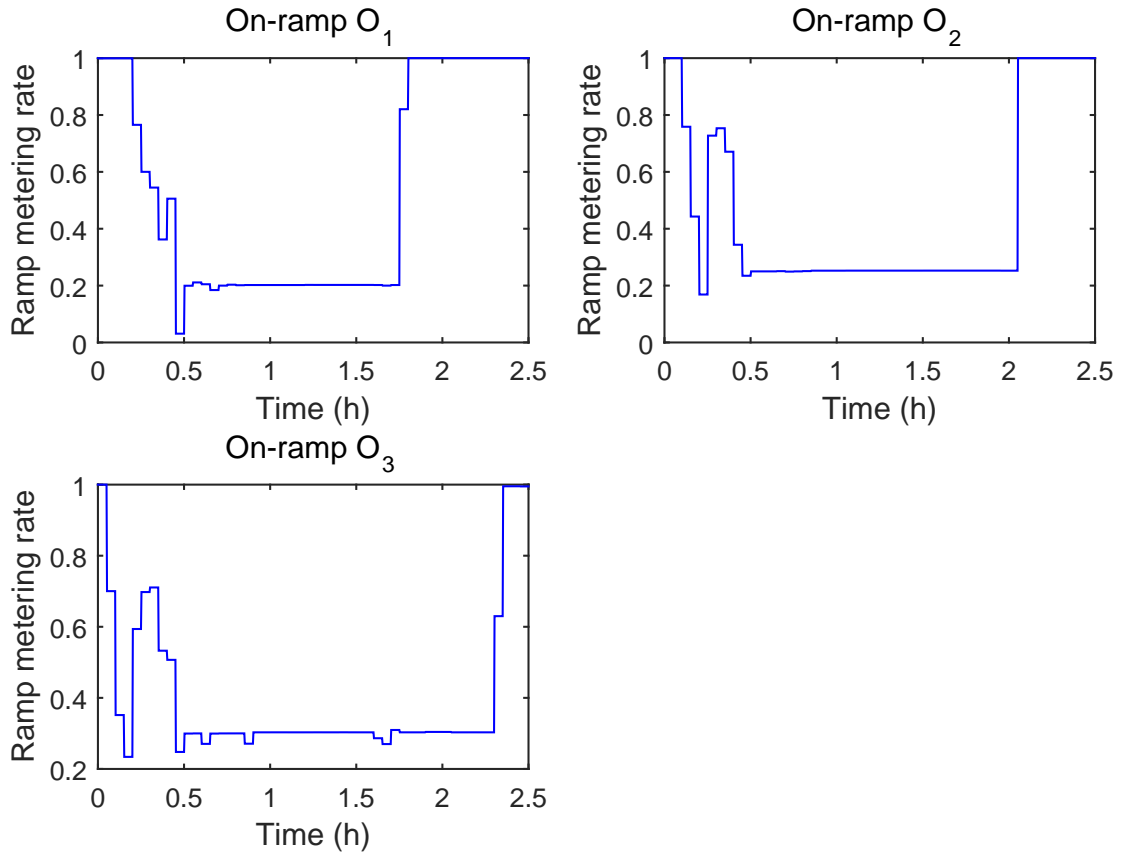


Figure 5.7: Ramp metering rates for Nominal DMPC

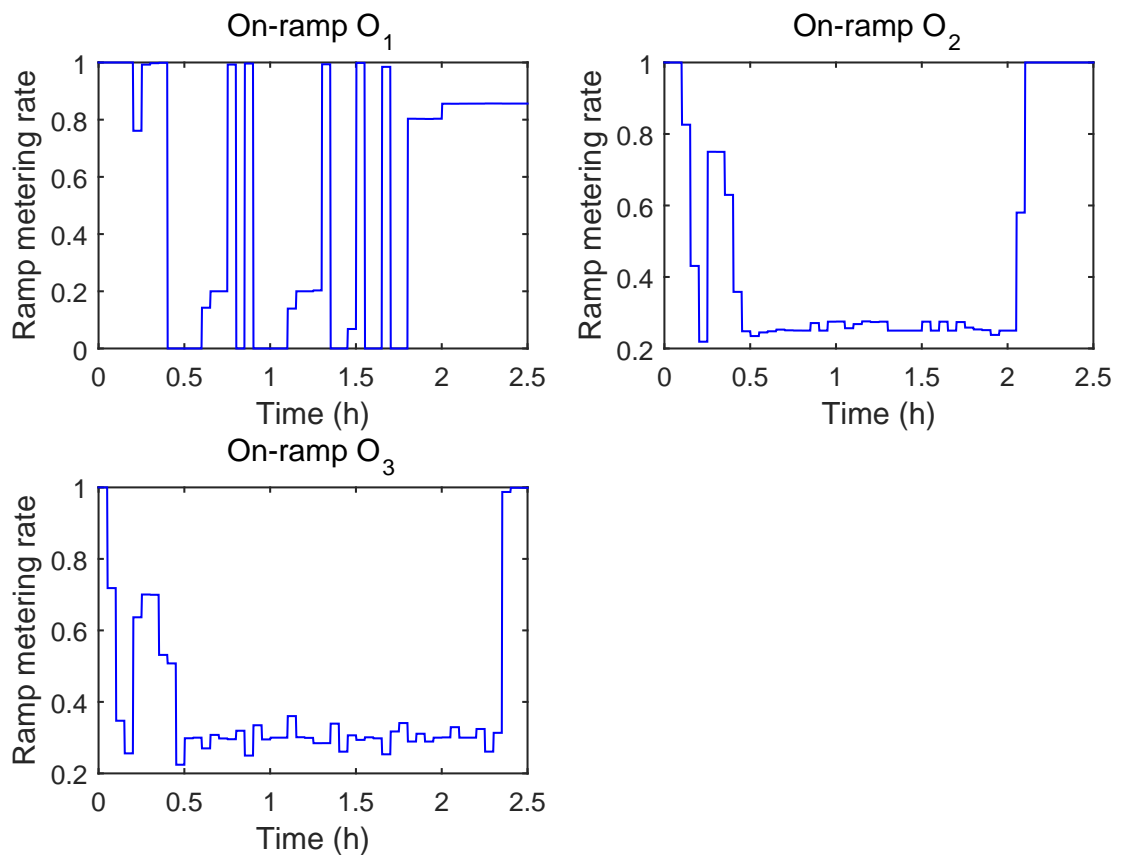


Figure 5.8: Ramp metering rates for scenario-based DMPC 1

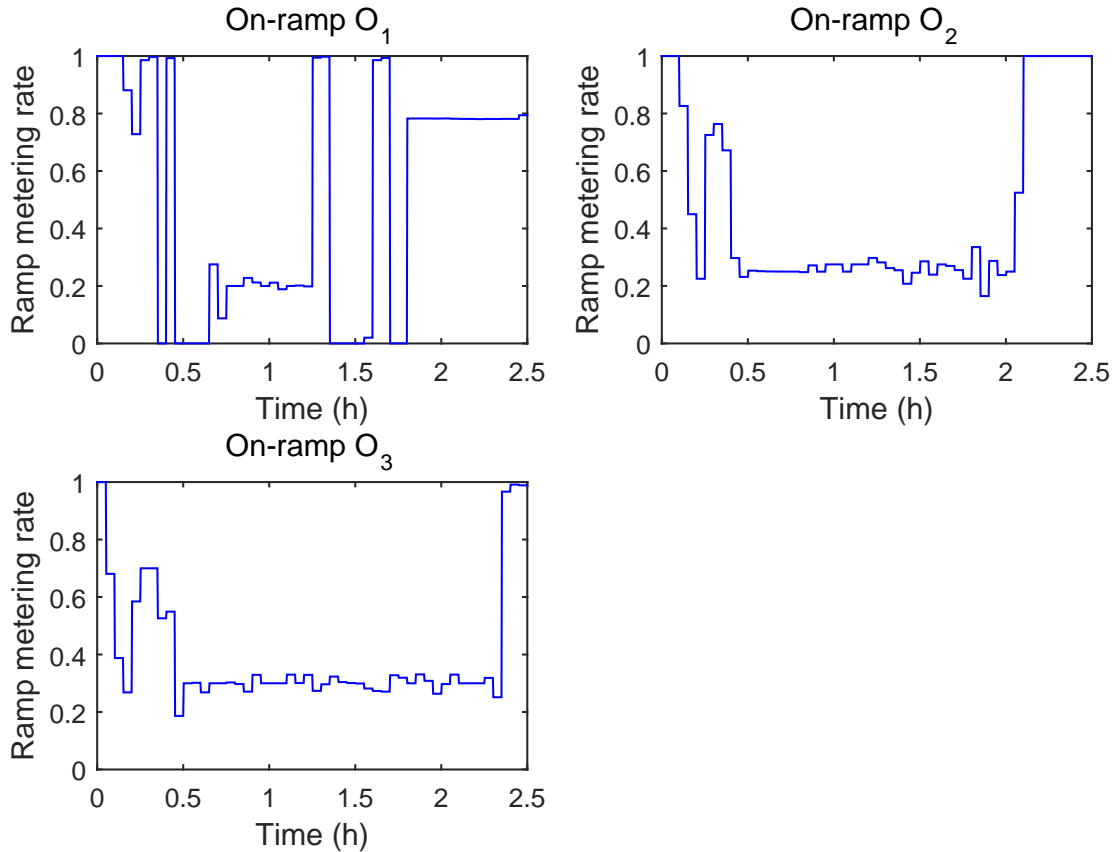


Figure 5.9: Ramp metering rates for scenario-based DMPC 2

Analysis of Traffic Behavior

For the same realization of uncertainties and settings as Figures 5.4-5.9, the densities and speeds of segments for all the considered control approaches are plotted in Figures 5.10-5.16.

From Figure 5.10, it can be noticed that the queue length at the mainstream origin is reduced to 0 by both nominal DMPC and scenario-based DMPC. Nominal DMPC can lead to queue length constraint violations (up to 20%) at on-ramps, while scenario-based DMPC do not lead to queue length constraint violations.

From Figures 5.11-5.13, for the period (0.3h-0.7h) corresponding to the peaks of densities in the no-control case, the densities are more clearly reduced by both nominal DMPC and scenario-based DMPC for segments (e.g. segments (1,1)-(4,2)) which are closer to the mainstream origin.

From to Figures 5.14-5.16, it can be seen that for the period (0.3 h-0.7 h) corresponding to the peaks of densities in the no-control case, the speeds are more clearly increased by both nominal DMPC and scenario-based DMPC for segments (e.g. segments (1,1)-(4,2)) which are closer to the mainstream origin.

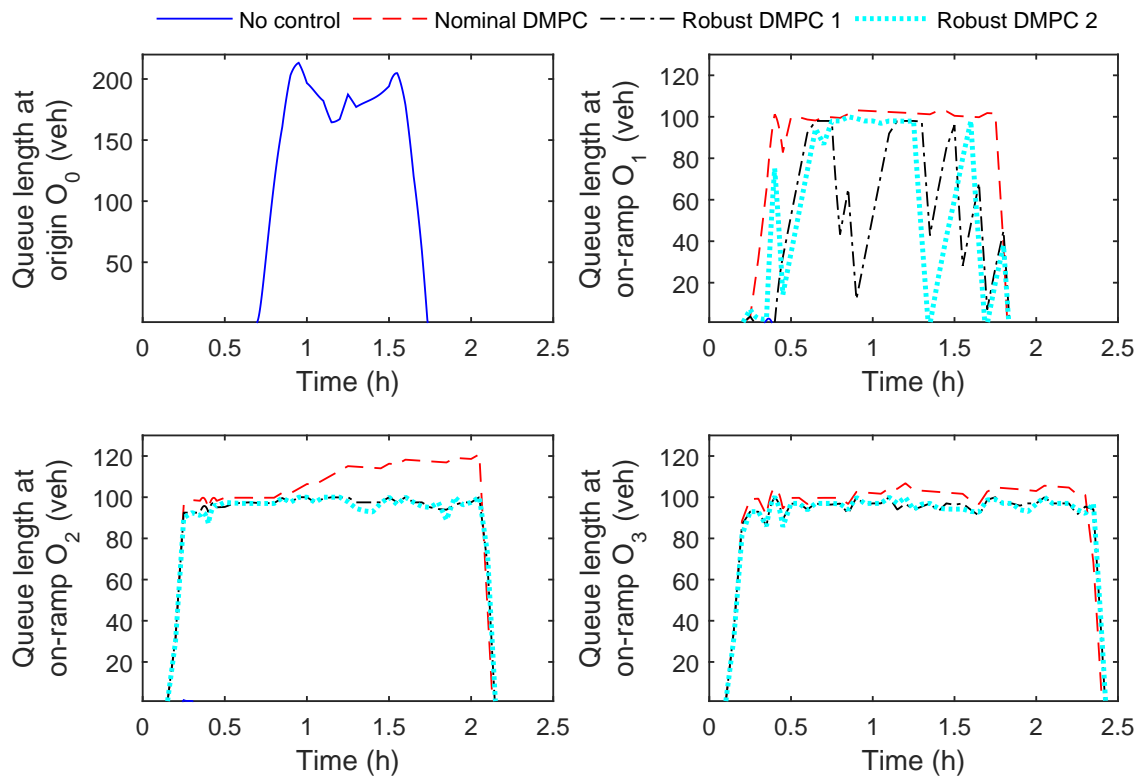


Figure 5.10: Queue lengths for the mainstream origin and on-ramps

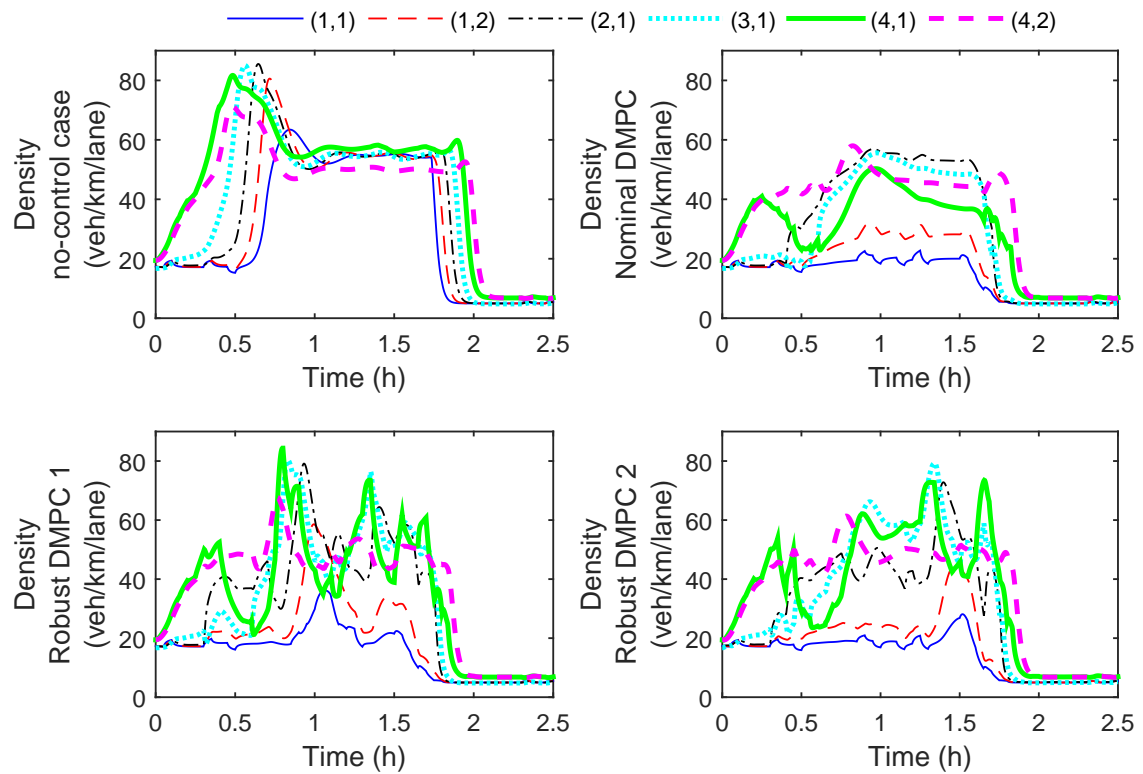


Figure 5.11: Densities for segments (1,1)-(4,2)

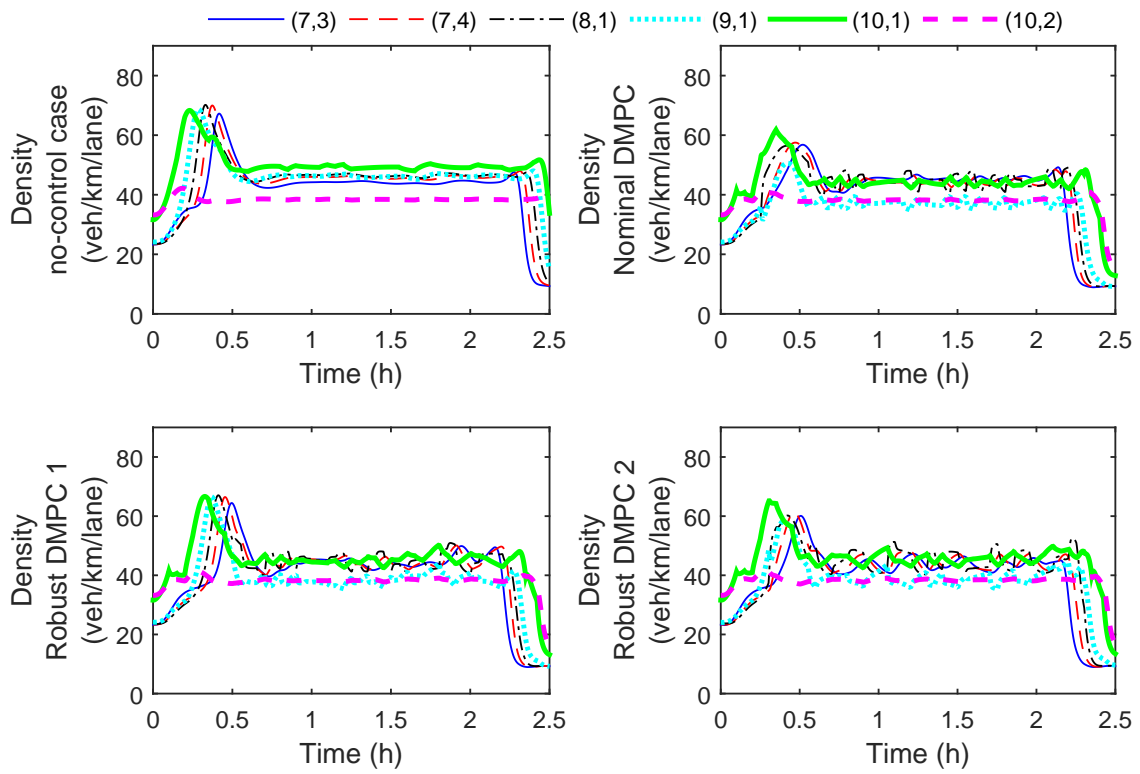


Figure 5.12: Densities for segments (4,3)-(7,2)

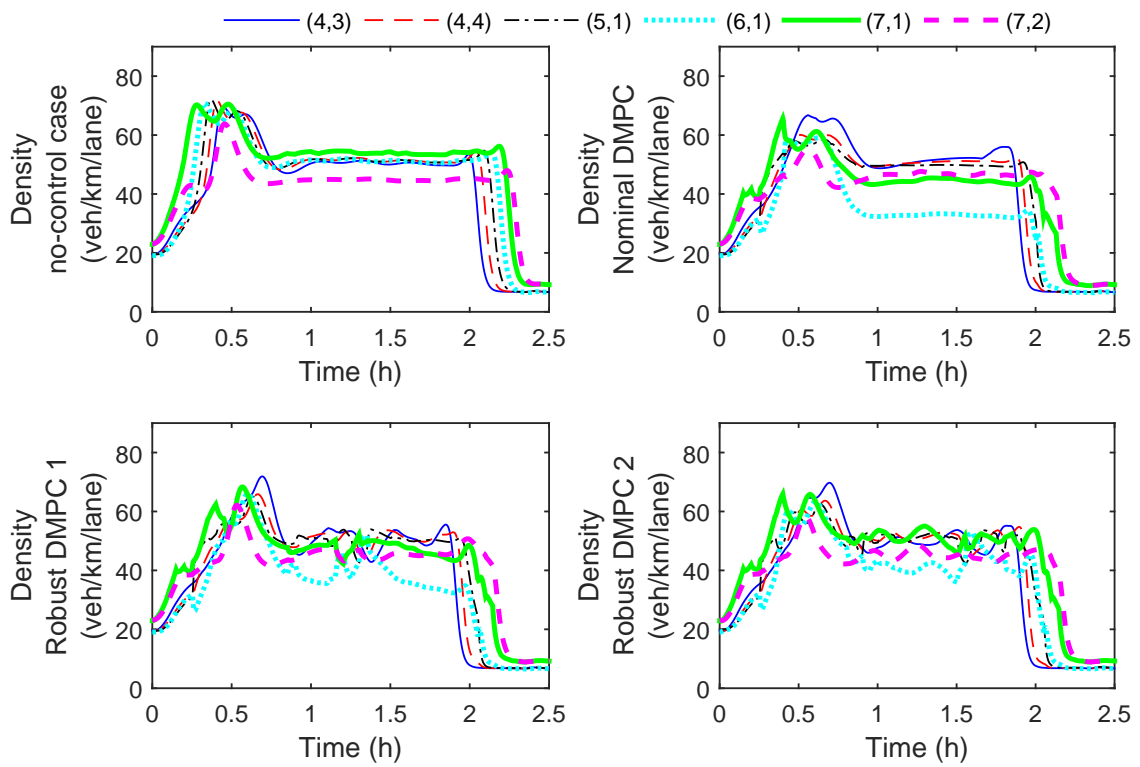


Figure 5.13: Densities for segments (7,3)-(10,2)

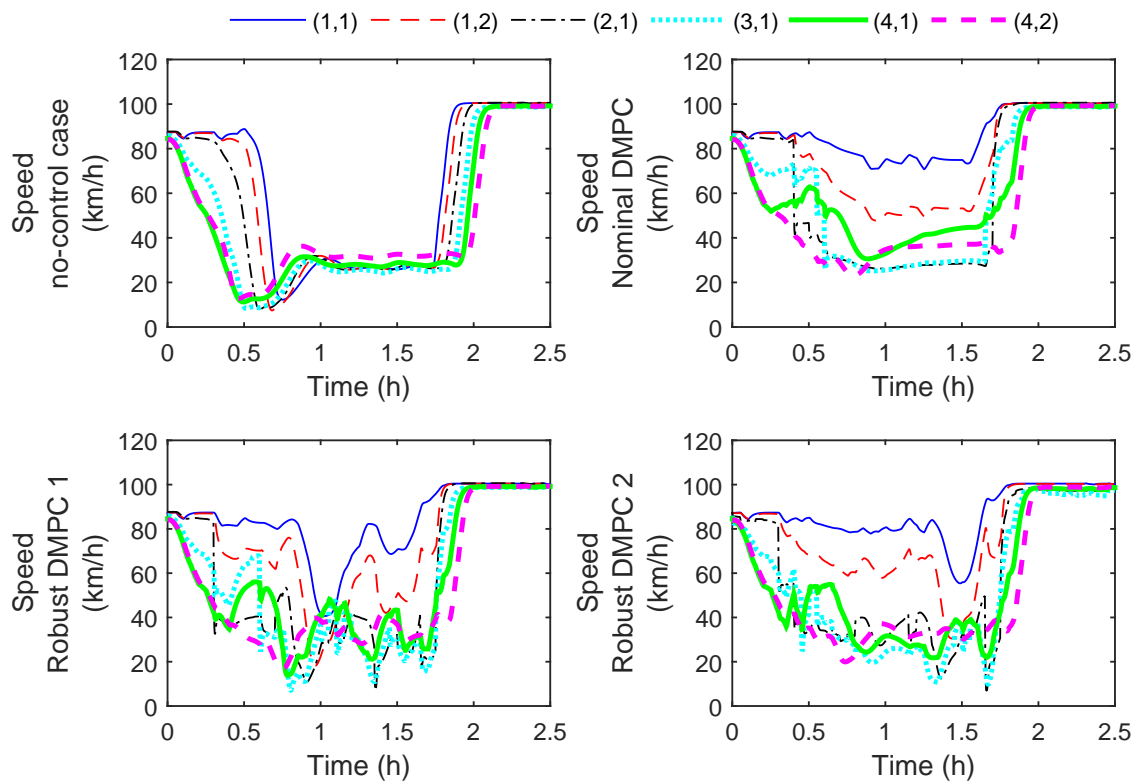


Figure 5.14: Speeds for segments (1,1)-(4,2)

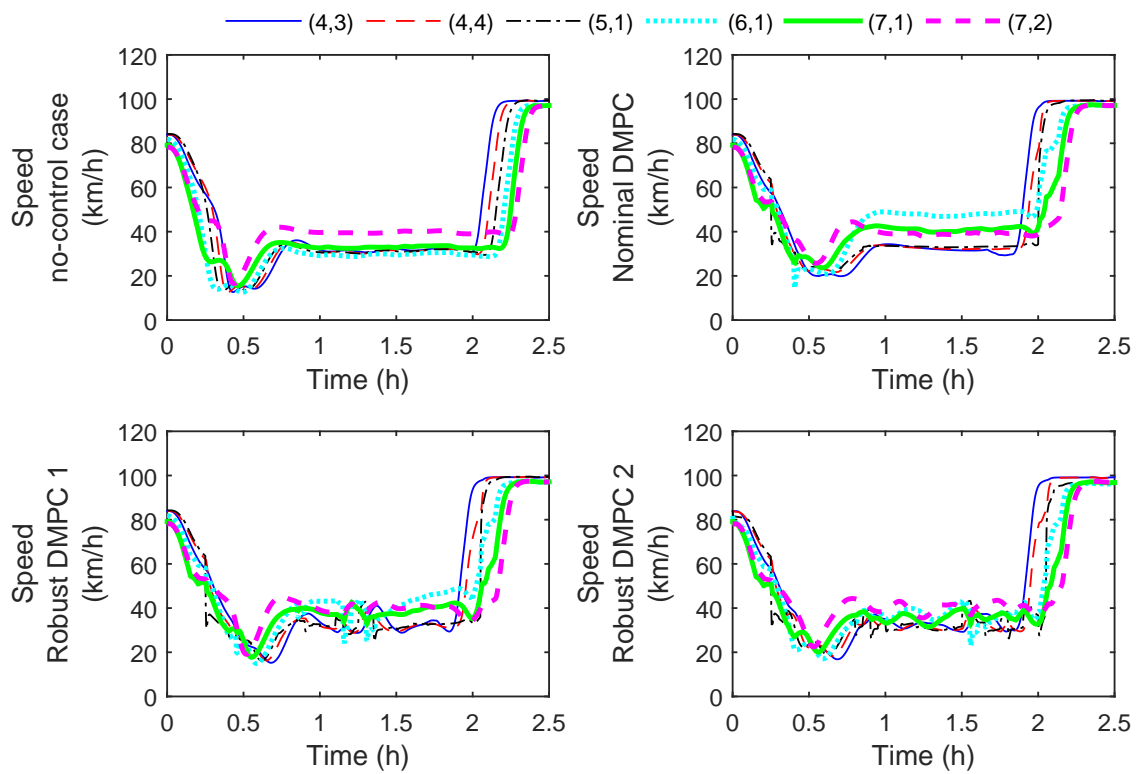


Figure 5.15: Speeds for segments (4,3)-(7,2)

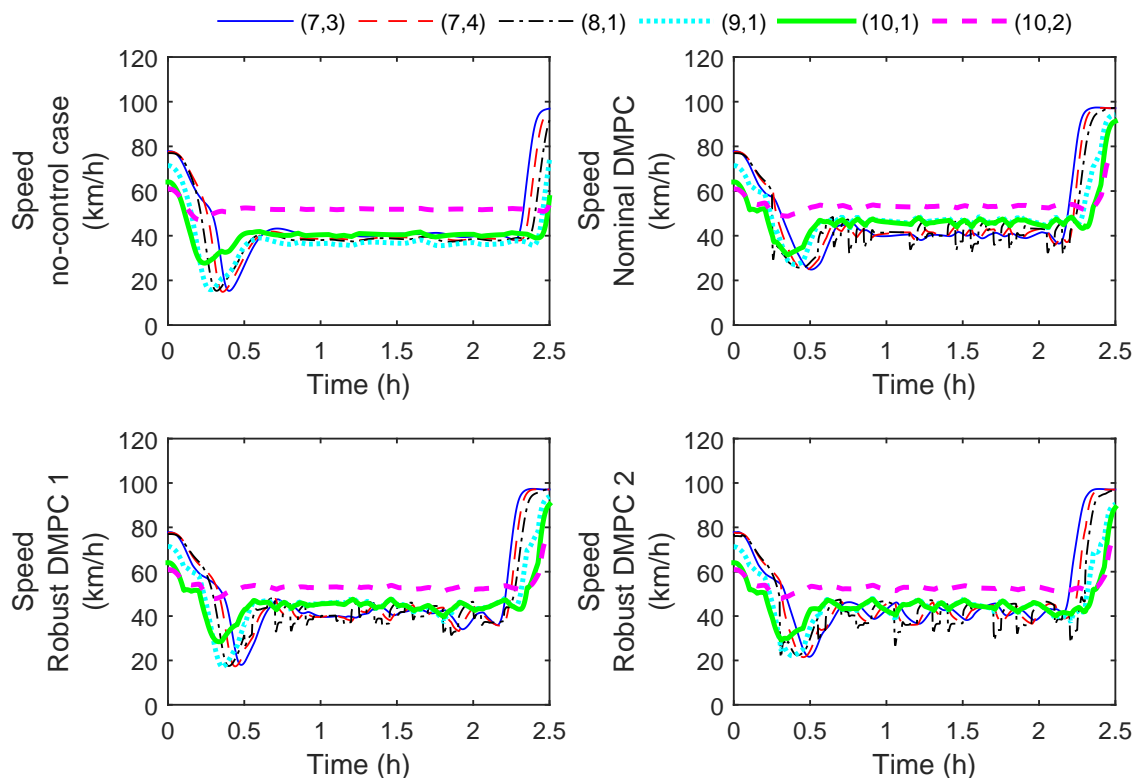


Figure 5.16: Speeds for segments (7,3)-(10,2)

Computational Efficiency w.r.t. the Complete Scenario Tree

In the case study, we did not apply scenario-based DMPC on the basis of the complete scenario tree. For evaluating the computational efficiency, we select the scenario-based DMPC approach on the basis of the complete scenario tree and the expected-value setting as a reference case. This approach is described in Appendix B.

By a numerical test we find that for scenario-based DMPC on the basis of the complete scenario tree, a local agent takes about 28 minutes on average to solve the local optimization problem once for one starting point at a given control step; this is much longer than the fixed CPU time for a control step for scenario-based DMPC on the basis of the reduced scenario tree. However, we can estimate the total time needed for scenario-based DMPC on the basis of the complete scenario tree to finish the same number of negotiation iterations as for scenario-based DMPC on the basis of the reduced scenario tree. For the case that the CPU time for every control step is fixed as 3 minutes, the total number of negotiation iterations for a single run for scenario-based DMPC on the basis of the reduced scenario tree is about 500. According to the test, it takes roughly 14 hours for finishing one negotiation iteration for scenario-based DMPC on the basis of the complete scenario tree; hence, it would take about 7000 hours for finishing 500 negotiation iterations.

According to the above discussion we can confirm that the computational efficiency of scenario-based DMPC on the basis of the reduced scenario tree is much higher than that of scenario-based DMPC on the basis of the complete scenario tree.

5.7 Summary

In this chapter, we have developed a new scenario-based DMPC approach for freeway networks by distinguishing global uncertainties for the overall network from local uncertainties for particular subnetworks only. Instead of constructing a complete scenario tree with all the combinations of the local scenarios for all subnetworks considered, we have proposed to construct a reduced scenario tree by combining the interconnecting outputs for a subnetwork for all the local scenarios for that subnetwork. To reduce the computational burden, in the new scenario-based DMPC approach, an expected-value setting (which is probabilistic) and a min-max setting are considered for combining local scenarios and for defining *total objective functions* for subnetworks, which include both control performance indices and constraint violation penalties.

We have illustrated by a numerical experiment that for scenario-based DMPC on the basis of the reduced scenario tree the total performance can be improved compared to the no-control case, with the queue length constraints satisfied; while for nominal DMPC, the total performance could not be improved w.r.t. to the no-control case, due to the violation of the queue length constraints. The experiment also showed that both the expected-value setting and the min-max setting are effective in improving the total performance.

Chapter 6

Conclusions and Future Work

Aiming at improving the control performance, reducing constraint violations, and improving the computational efficiency, in this thesis we have extended several multi-class macroscopic traffic flow models and traffic emission models, evaluated the effectiveness of end-point penalties in model predictive control for freeway networks, and developed a scenario-based receding-horizon parameterized control approach and a scenario-based distributed model predictive control approach for freeway networks. In this chapter, we first give conclusions of the thesis; next, we present some recommendations for future work.

6.1 Conclusions of the Thesis

The contributions of the thesis are concluded as follows:

- **Several multi-class macroscopic traffic flow models and traffic emission models have been extended and evaluated.**

The effectiveness of Model Predictive Control (MPC) for traffic networks relies to a large extent on the models that are used for predicting the evolution of traffic dynamics. In order to reduce the computational load, usually macroscopic prediction models are used. In single-class macroscopic traffic flow models and traffic emission models, all vehicles in the considered traffic network are aggregated in space and time, without including the differences between different classes of vehicles, such as cars, vans, buses, and trucks. Extending multi-class macroscopic traffic flow models and traffic emission models by taking into account the differences between different classes of vehicles is a way to improve the accuracy of prediction models for MPC for traffic networks.

In Chapter 3, we have extended several multi-class macroscopic traffic flow models and traffic emission models. In particular, we have extended the second-order single-class METANET model to a multi-class version, by considering three traffic regimes: free flow, semi-congestion, and congestion. Based on the traffic regimes, we define road space fractions for different vehicle classes, which reflect interactions between different vehicle classes. It is assumed that a vehicle class is constrained within its assigned road space specified by the road space fraction for that vehicle class, and that a vehicle class is subject to the fundamental diagram of that vehicle class. Moreover, for comparison with the extended multi-class METANET model, we

have incorporated variable speed limits and ramp metering into the first-order multi-class traffic flow model FASTLANE. For estimating traffic emissions in the multi-class setting, we have integrated the macroscopic emission model VT-macro with multi-class traffic flow models, and have extended the microscopic emission model VERSIT+ to be a multi-class macroscopic version.

We implemented a case study for comparing the above mentioned multi-class macroscopic traffic flow models and traffic emission models. In the case study, both the Total Time Spent (TTS) and the Total Emissions (TE) were included in the objective function for MPC. A microscopic traffic flow simulator VISSIM and a microscopic traffic emission simulator EnViver were used as simulation models. All the four possible combinations for the above multi-class macroscopic traffic flow models and traffic emission models were used for predicting future traffic dynamics: multi-class METANET and multi-class VERSIT+, multi-class METANET and multi-class VT-macro, FASTLANE and multi-class VERSIT+, and FASTLANE and multi-class VT-macro. It was shown by the case study that combining the extended multi-class METANET model with the multi-class VT-Macro model or the multi-class VERSIT+ model can improve the TTS and the TE in a balanced way, and that the extended multi-class METANET model can better describe on-ramp queues than FASTLANE. The results suggest that the extended multi-class METANET model, which is a second-order model, can be a better choice for jointly reducing traffic congestion and traffic emissions than the first-order FASTLANE model.

- **The effectiveness of end-point penalties in MPC for freeway networks has been evaluated.**

The prediction period length for MPC for traffic networks relates to the size of the controlled network. For achieving appropriate performance, larger traffic networks require longer prediction periods, leading to higher computational complexity. Instead of directly increasing the prediction period length, a way to extend the period covered by MPC for determining the control inputs is to include penalties in the control objective function, estimating the performance beyond the prediction period.

In Chapter 3, we have proposed end-point penalties corresponding to the TTS and the TE for the vehicles that are present in the considered traffic network at the end of the prediction period. By including the end-point penalties corresponding to the TTS and the TE in the objective function for MPC, the performance beyond the prediction period can be taken into account.

In the case study in Chapter 3, the four approaches for the extended multi-class macroscopic traffic flow models and traffic emission models were also used for the case with end-point penalties. The simulation results show that including end-point penalties in MPC based on the extended multi-class METANET model can further improve the control performance (about 2% better than the case without the end-point penalties), with the queue length constraints being satisfied. However, this is not the case for FASTLANE, probably due to the first-order characteristics of FASTLANE, which can lead to unreliable estimations for the end-point penalties. In general, the results indicate that including well-estimated end-point penalties in MPC for traffic networks can further improve the control performance, with the queue length constraints being satisfied.

- **A scenario-based receding-horizon parameterized control approach for freeway networks has been developed.**

Uncertainties occurring in the procedure of implementing MPC for traffic networks will affect the control effectiveness, including the improvement of control performance, the satisfaction of constraints on states and outputs, etc. Thus, the control effectiveness of MPC for traffic networks can be improved by developing robust MPC approaches, which take into account uncertainties. In general the computational burden for robust MPC approaches will increase compared to the case that uncertainties are not included. Parameterized MPC laws can be considered for reducing the computational burden, since in the control procedure instead of the control inputs only the parameters of MPC laws are optimized, making it possible to reduce the number of optimization variables to be determined w.r.t. standard MPC.

In Chapter 4, we have proposed a scenario-based Receding-Horizon Parameterized Control (RHPC) approach for freeway networks. Particularly, several RHPC laws for variable speed limits and ramp metering rates have been developed for the multi-class traffic setting. In the scenario-based RHPC approach, the constraints on the lengths of on-ramp queues are incorporated into the control objective function via a queue length constraint violation penalty, to avoid infeasible optimization problems. To deal with uncertainties, we have considered a scenario-based scheme with a finite set of uncertainty scenarios in combination with a min-max setting. The motivation for applying the scenario-based scheme is to reduce the computational load in comparison with the case that all the possible uncertainty realizations are considered. The motivation for adopting the min-max setting is to minimize the worst-case control performance over the finite set of scenarios considered, and to guarantee satisfaction of the queue length constraints for the finite set of scenarios considered.

A numerical experiment was implemented for illustrating the effectiveness of the scenario-based RHPC approach. Scenario-based RHPC was compared with nominal RHPC and standard control (i.e. feedback control). For standard control, the following four settings were considered for determining the parameters for the control laws: ignoring uncertainties¹⁹; ignoring uncertainties and adopting a queue override scheme; accounting for uncertainties¹⁹; accounting for uncertainties and adopting a queue override scheme. For appropriate weights for the queue length constraint violation penalty, the simulation results are summarized as follows. Scenario-based RHPC can effectively reduce the TTS (3.7% – 6.0%) with low queue length constraint violations (0.6% – 1.9%). In contrast to scenario-based RHPC, nominal RHPC can reduce the TTS (4.0 – 6.5%) a bit more, but the queue length constraint violations are higher (3.0% – 12.7%). When uncertainties are not taken into account for determining the parameters for the control laws, standard control can lead to high queue length constraint violations (52.9% – 151.0%); but even when a queue override scheme is adopted, there are still queue length constraint violations (6.6% – 14.0%). When uncertainties are taken into account for determining the parameters for the control

¹⁹For standard control in this case study, ignoring uncertainties means that nominal demands and nominal fractions of different vehicle classes are used for determining the parameters for the control laws; accounting for uncertainties means that 10 random scenarios for demands and fractions of different vehicle classes are used for determining the parameters for the control laws.

laws, standard control can lead to small queue length constraint violations (0% – 1.3%), while the reductions of the TTS (0.4% – 2.8%) are also small compared to scenario-based RHPC. In comparison with other considered approaches, scenario-based RHPC can both effectively improve the control performance and keep the queue length constraint violations at a low level.

- **A scenario-based distributed model predictive control approach for freeway networks has been developed.**

Due to the computational complexity, it is hard to control a large-scale traffic network by means of centralized MPC. Distributed Model Predictive Control (DMPC) can be used for controlling a large-scale traffic network, by dividing it into subnetworks and distributing the control problems for the subnetworks to local agents. In general, there are couplings between neighboring subnetworks, so the control effectiveness for a subnetwork can also be affected by the uncertainties for the neighboring subnetworks. Scenario-based DMPC controls a large-scale traffic network through collaborative local agents, with uncertainties taken into account²⁰ for determining the control actions.

In Chapter 5, we have developed a scenario-based DMPC approach for a large-scale freeway network including multiple subnetworks based on a scenario tree for uncertainties. We distinguish global uncertainties (which apply to the overall network) from local uncertainties (which only apply to individual subnetworks), and assume that all these uncertainties are described by finite sets of scenarios. A straightforward way of combining the local scenarios for different subnetworks is to consider all the combinations of the local scenarios (i.e. to construct a complete local scenario tree); however, the computational load will be large in this case. Therefore, we have proposed to construct a reduced local scenario tree for the entire network for combining the local scenarios for different subnetworks. In the reduced local scenario tree, the dynamics of a subnetwork are predicted for different local scenarios for that subnetwork by assuming that the interconnecting inputs for that subnetwork from neighboring subnetworks are independent of the local scenarios for the neighboring subnetworks. Afterwards, a reduced scenario tree for the entire network can be defined by combining global scenarios with the reduced local scenario tree. Moreover, we consider an expected-value setting and a min-max setting for combining local scenarios for each subnetwork and for defining total objective functions that include both performance indicators and queue penalties for subnetworks.

A numerical experiment was executed for evaluating the scenario-based DMPC approach based on the reduced scenario tree. Scenario-based DMPC based on the reduced scenario tree was compared with nominal DMPC (which is based on a nominal prediction model) for the expected-value setting and the min-max setting. The simulation results show that the total performance including the TTS and the queue length constraint violation penalty can be improved by scenario-based DMPC based on the reduced scenario tree (4.6% – 5.2%), and the total performance can be further improved (5.5% – 6.0%) when the allowed CPU time for every control step is increased from 3 minutes to 10 minutes. Moreover, for scenario-based DMPC based

²⁰Uncertainties can e.g. be taken into account by using a scenario-based approach.

on the reduced scenario tree, both the expected-value setting and the min-max setting are effective in improving the total performance. However, the total performance is worse than the no-control case for nominal DMPC (-6.1%), and by increasing the allowed CPU time for every control step from 3 minutes to 10 minutes the total performance becomes even worse (-6.6%). This might be because of that for longer allowed CPU time nominal DMPC can result in the control inputs leading to a better total performance estimated based on the nominal prediction model, but in general these control inputs lead to a worse total performance due to uncertainties.

6.2 Recommendations for Future Work

In this section, we present several possible topics for future research.

- **Further assessment of the approaches developed in this thesis based on case studies:**
 - For the extended multi-class traffic flow models and traffic emission models in Chapter 3, the model parameters can be identified for more scenarios, or by means of other algorithms such as a stochastic genetic algorithm [105]. The model parameters for the extended multi-class traffic flow models can also be identified to fit the measured flows and densities to the predicted flows and densities.
 - The impact of end-point penalties on the control effectiveness for MPC can be further investigated by testing suitable weights for the end-point penalties in different control conditions, and by comparing the case including the end-point penalties with the case that longer prediction periods are considered.
 - The way for choosing uncertainty scenarios for scenario-based RHPC and scenario-based DMPC can be further investigated.
 - The impact of data coverage (availability) and data type on the approaches developed in this thesis can be investigated.
 - The effectiveness of the extended multi-class traffic flow models and traffic emission models, the scenario-based RHPC approach, and the scenario-based DMPC approach based on the reduced scenario tree can be investigated for networks with different layouts and for a wide range of traffic scenarios. For instance, the effectiveness of the scenario-based RHPC approach can be investigated for uncertainties with different distributions and different skewness factors.
- **Fast MPC based on multi-class prediction models:**

For on-line applications of real traffic networks, a fast MPC scheme [67] can be combined with multi-class traffic models. In the fast MPC scheme, the control inputs for a given control step are obtained by re-adjusting the control inputs pre-computed before that control step, according to the measured states at that control step. The challenges for developing fast MPC approaches based on multi-class prediction models involve obtaining the optimal control inputs within the available time interval (i.e. the control sampling time interval), and analyzing the sensitivities of the control inputs w.r.t. the multi-class traffic states. For obtaining the optimal control inputs

within the available time interval, one option is to reduce the number of optimization variables in the optimization problems to be solved; this can e.g. be realized by parameterizing the control input variables via parameterized control laws.

- **Robust MPC based on model bias correction:**

The idea behind the model bias correction approach in [55], i.e. using the measurements to adjust the model, can be considered for developing robust MPC approaches for freeway networks. For example, the latest measurements can be used to adjust prediction models, or to adjust the control inputs generated based on nominal prediction models. The challenges here are to find suitable compensation laws, and to obtain appropriate parameters for the compensation laws.

- **Robust event-triggered MPC for freeway networks:**

Event-triggered MPC [37] only optimizes the control inputs when some specified conditions (i.e. triggering rules) are satisfied, instead of at every control step. The triggering rules are usually constructed based on checking the errors between predicted states and measured states. By adopting event-triggered MPC, the frequency of solving optimization problems for obtaining the optimal control inputs can be reduced. In general, event-triggered MPC is applied for systems without significant uncertainties. For systems with uncertainties, robust event-triggered MPC [64] can be developed. For determining the control inputs, uncertainties can be taken into account by developing robust MPC approaches. The main challenge is then to account for uncertainties when defining triggering rules. The triggering rules could be designed by linearizing traffic models and applying the approach of [64]. Another way is to first develop robust triggering rules for the nonlinear or piecewise-affine case, and next apply them to traffic models; for the piecewise-affine case, the traffic models then need to be first transformed to the piecewise-affine form (see e.g. [44]).

- **Scenario-based hierarchical MPC for freeway networks:**

For scenario-based DMPC for a large-scale traffic network with global uncertainties distinguished from local uncertainties, an alternative is to consider a hierarchical scheme, in which two or more control layers are present: one or more high-layer coordinators and low-layer local controllers. The main challenge is to combine global uncertainties and local uncertainties in the hierarchical scheme, which is different from the distributed MPC scheme considered in this thesis. One option for combining global uncertainties with local uncertainties in the hierarchical scheme is as follows.

On the basis of global uncertainties, the high-layer coordinators estimate interconnecting variables, which are considered as reference quantities for local controllers. A local controller obtains the optimal control inputs by minimizing a local objective function that is defined based on local traffic states and interconnecting variables for all global uncertainties and local uncertainties for that subnetwork. With the optimal control inputs used for estimating interconnecting variables by the coordinators, the above procedure is repeated until a stopping condition is satisfied. The stopping condition can be defined as a threshold on the differences in Lagrange multipliers between two adjacent iterations, or it can be defined as a limitation on the CPU time.

Appendix A

Computation of Jerks for Multi-Class Macroscopic Traffic Flow Models

The equations for computing jerks for multi-class traffic flows are developed based on the multi-class METANET model of Chapter 3; however, the equations can also be used for other multi-class macroscopic traffic flow models. As shown in Figure A.1, there are three types of jerks (i.e. derivatives of accelerations) in segment i of link m at time step k :

- Segment $i - 1 \rightarrow$ segment $i - 1 \rightarrow$ segment i : this kind of jerk corresponds to those vehicles moving within segment $i - 1$ from time step $k - 2$ to $k - 1$, and moving from segment $i - 1$ to i from time step $k - 1$ to k :

$$\begin{aligned} j_{m,i,c,1}(k) &= \frac{a_{(m,i-1),(m,i),c}^{\text{cross}}(k) - a_{m,i-1,c}^{\text{inter}}(k-1)}{T} \\ &= \frac{v_{m,i,c}(k) - 2v_{m,i-1,c}(k-1) + v_{m,i-1,c}(k-2)}{T^2} \end{aligned} \quad (\text{A.1})$$

- Segment $i - 1 \rightarrow$ segment $i \rightarrow$ segment i : this kind of jerk corresponds to those vehicles moving from segment $i - 1$ to i from time step $k - 2$ to $k - 1$, and moving within segment i from $k - 1$ to k :

$$j_{m,i,c,2}(k) = \frac{a_{m,i,c}^{\text{inter}}(k) - a_{(m,i-1),(m,i),c}^{\text{cross}}(k-1)}{T}$$

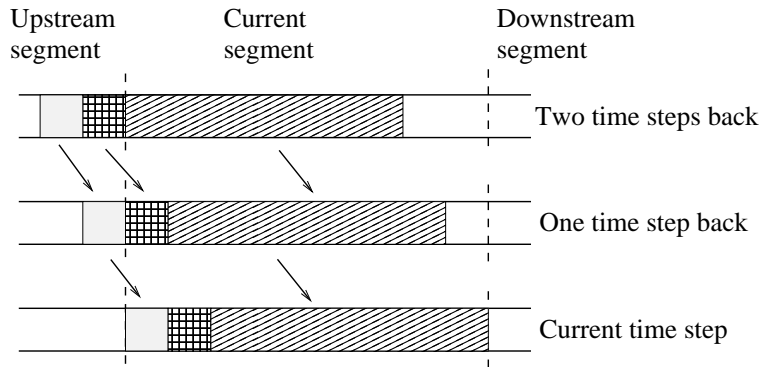


Figure A.1: Jerk: derivative of acceleration

$$= \frac{v_{m,i,c}(k) - 2v_{m,i,c}(k-1) + v_{m,i-1,c}(k-2)}{T^2} \quad (\text{A.2})$$

- Segment $i \rightarrow$ segment $i \rightarrow$ segment i : this kind of jerk corresponds to those vehicles moving within segment i from time step $k-2$ to $k-1$, i.e.

$$\begin{aligned} j_{m,i,c,3}(k) &= \frac{a_{m,i,c}^{\text{inter}}(k) - a_{m,i,c}^{\text{inter}}(k-1)}{T} \\ &= \frac{v_{m,i,c}(k) - 2v_{m,i,c}(k-1) + v_{m,i,c}(k-2)}{T^2} \end{aligned} \quad (\text{A.3})$$

Appendix B

Scenario-Based DMPC on the Basis of a Complete Scenario Tree and an Expected-Value Setting

The scenario-based DMPC problem based on the complete scenario tree and the expected-value setting (which is probabilistic) for a local agent s is defined as follows:

$$\begin{aligned} \min_{\substack{\tilde{u}_s(k) \\ \tilde{E}_{j_s,1,s,g,\ell}^{\text{in}}(k), \dots, \tilde{E}_{j_s, N_s^{\text{nb}}, s, g, \ell}^{\text{in}}(k) \\ \tilde{E}_{j_s,1,s,g,\ell}^{\text{out}}(k), \dots, \tilde{E}_{j_s, N_s^{\text{nb}}, s, g, \ell}^{\text{out}}(k)}}} \sum_{g=1}^{N_{\text{glob}}} p_g \left(\sum_{\ell=1}^{N_{\text{com}}} p_\ell \left(J_{s,g,\ell}(\tilde{x}_{s,g,\ell}(k), \tilde{y}_{s,g,\ell}(k), \tilde{u}_s(k)) \right. \right. \\ \left. \left. + \gamma \max(F_{s,g,\ell}(\tilde{x}_{s,g,\ell}(k), \tilde{y}_{s,g,\ell}(k), \tilde{u}_s(k)), 0) \right. \right. \\ \left. \left. + \sum_{j \in S_s^{\text{nb}}} J_{s,g,\ell}^{\text{inter}}(\tilde{\lambda}_{j,s,g,\ell}^{\text{in}}(k), \tilde{\lambda}_{j,s,g,\ell}^{\text{out}}(k), \tilde{E}_{j,s,g,\ell}^{\text{in}}(k), \tilde{E}_{j,s,g,\ell}^{\text{out}}(k)) \right) \right) \quad (\text{B.1}) \end{aligned}$$

$$\text{s.t. } x_{s,g,\ell}(k+z+1) = f_{s,g,\ell}(x_{s,g,\ell}(k+z), u_s(k+z), D_{s,g,\ell}^{\text{in}}(k+z), E_{s,g,\ell}^{\text{in}}(k+z), \omega_\ell(k+z), \omega_\ell(k+z)) \quad \text{for } z = 0, \dots, N_p - 1 \quad (\text{B.2})$$

$$y_{s,g,\ell}(k+z) = h_s(x_{s,g,\ell}(k+z)) \quad \text{for } z = 1, \dots, N_p \quad (\text{B.3})$$

$$x_{s,g,\ell}(k) = x_s^k \quad (\text{B.4})$$

$$\omega_\ell(k+z) \in \Omega_1^{\text{loc}}(k+z) \times \dots \times \Omega_{N_{\text{sub}}}^{\text{loc}}(k+z) \quad \text{for } z = 0, \dots, N_p - 1 \quad (\text{B.5})$$

Equations (5.5) and (5.18)

for $g = 1, \dots, N_{\text{glob}}$, and $l = 1, \dots, N_{\text{com}}$

where ω_ℓ represents a combined local uncertainty scenario for all subnetworks in the complete scenario tree, and p_ℓ is the probability for ω_ℓ . The symbols $x_{s,g,\ell}$, $y_{s,g,\ell}$, $J_{s,g,\ell}$, $F_{s,g,\ell}$, $J_{s,g,\ell}^{\text{inter}}$, $f_{s,g,\ell}$, $\lambda_{j,s,g,\ell}^{\text{in}}$, $\lambda_{j,s,g,\ell}^{\text{out}}$, $E_{j,s,g,\ell}^{\text{in}}$, $E_{j,s,g,\ell}^{\text{out}}$, $D_{s,g,\ell}^{\text{in}}$, and $E_{s,g,\ell}^{\text{in}}$ have similar meanings to corresponding symbols without subscripts g and ℓ in Section 5.2, but now they are for the case with global uncertainties and combined local uncertainty scenarios for all subnetworks. In addition, $\tilde{x}_{s,g,\ell}(k)$ and $\tilde{y}_{s,g,\ell}(k)$, are defined in similarly to $\tilde{x}_s(k)$ (i.e. (5.8)) over the prediction horizon covering steps $k+z$, $z = 1, \dots, N_p$; $\tilde{\lambda}_{j,s,g,\ell}^{\text{in}}(k)$, $\tilde{\lambda}_{j,s,g,\ell}^{\text{out}}(k)$, $\tilde{E}_{j,s,g,\ell}^{\text{in}}(k)$, and $\tilde{E}_{j,s,g,\ell}^{\text{out}}(k)$ are defined in a similar way to $\tilde{x}_s(k)$ (i.e. (5.8)) over the prediction horizon covering steps $k+z$, $z = 0, \dots, N_p - 1$.

Bibliography

- [1] In *INFRAS. HBEFA web site, 2011.*
- [2] K. Aboudolas, M. Papageorgiou, A. Kouvelas, and E. Kosmatopoulos. A rolling-horizon quadratic-programming approach to the signal control problem in large-scale congested urban road networks. *Transportation Research Part C: Emerging Technologies*, 18(5):680–694, October 2010.
- [3] K. Ahn and H. Rakha. The effects of route choice decisions on vehicle energy consumption and emissions. *Transportation Research Part D: Transport and Environment*, 13(3):151–167, May 2008.
- [4] K. Ahn, A. A. Trani, H. Rakha, and M. Van Aerde. Microscopic fuel consumption and emission models. In *Proceedings of the 78th Annual Meeting of the Transportation Research Board*, Washington DC, USA, January 1999. CD-ROM.
- [5] A. Alessandri, A. Di Febbraro, A. Ferrara, and E. Punta. Optimal control of freeways via speed signalling and ramp metering. *Control Engineering Practice*, 6(6):771–780, June 1998.
- [6] F. An, M. Barth, J. Norbeck, and M. Ross. Development of comprehensive modal emissions model: Operating under hot-stabilized conditions. *Transportation Research Record*, 1587:52–62, 1997.
- [7] A. Aw and M. Rascle. Resurrection of "second order" models of traffic flow. *SIAM Journal on Applied Mathematics*, 60(3):916–938, 2000.
- [8] R. Balakrishna, C. Antoniou, M. Ben-Akiva, H. N. Koutsopoulos, and Y. Wen. Calibration of microscopic traffic simulation models: Methods and application. *Transportation Research Record*, 1999:198–207, 2007.
- [9] D. Banister. *Transport Policy and the Environment*. Alexandrine Press, Oxford, United Kingdom, 2002.
- [10] J. Barceló. *Fundamentals of Traffic Simulation, Volume 145 of International Series in Operations Research & Management Science*. Springer Science&Business Media, New York, USA, 2010.
- [11] M. Behrisch, L. Bieker, J. Erdmann, and D. Krajzewicz. SUMO-simulation of urban mobility. In *Proceedings of the Third International Conference on Advances in System Simulation*, pages 63–68, Barcelona, Spain, October 2011.

- [12] S. Bera and K. V. Krishna Rao. Estimation of origin-destination matrix from traffic counts: the state of the art. *European Transport\Trasporti Europei*, 49:3–23, December 2011.
- [13] D. Bernardini and A. Bemporad. Scenario-based model predictive control of stochastic constrained linear systems. In *Proceedings of the Joint 48th IEEE Conference on Decision and Control and 28th Chinese Control Conference*, pages 6333–6338, Shanghai, China, December 2009.
- [14] D. P. Bertsekas. *Constrained Optimization and Lagrange Multiplier Methods*. Academic Press, London, United Kingdom, 1982.
- [15] H. H. J. Bloemen, T. J. J. van den Boom, and H. B. Verbruggen. Optimizing the end-point state-weighting matrix in model-based predictive control. *Automatica*, 38(6): 1061–1068, June 2002.
- [16] S. Boyd and L. Vandenberghe. *Convex Optimization*. Cambridge University Press, Cambridge, United Kingdom, 2004.
- [17] S. Boyd, N. Parikh, E. Chu, B. Peleato, and J. Eckstein. Distributed optimization and statistical learning via the alternating direction method of multipliers. *Foundations and Trends in Machine Learning*, 3(1):1–122, January 2011.
- [18] E. Brockfeld, R. D. Kühne, and P. Wagner. Calibration and validation of microscopic traffic flow models. *Transportation Research Record*, 1876:62–70, 2004.
- [19] G. C. Calafiore and M. C. Campi. The scenario approach to robust control design. *IEEE Transactions on Automatic Control*, 51(5):742–753, May 2006.
- [20] G. C. Calafiore and L. Fagiano. Robust model predictive control via scenario optimization. *IEEE Transactions on Automatic Control*, 58(1):219–224, January 2013.
- [21] C. Caligaris, S. Sacone, and S. Siri. Multi-class freeway traffic: Model predictive control and microscopic simulation. In *Proceedings of the 16th Mediterranean Conference on Control and Automation*, pages 1862–1867, Ajaccio, France, June 2008.
- [22] E. F. Camacho and C. Bordons. *Model Predictive Control*. Springer-Verlag, London, United Kingdom, 2007.
- [23] P. J. Campo and M. Morari. Robust model predictive control. In *Proceedings of the American Control Conference*, pages 1021–1026, Minneapolis, USA, June 1987.
- [24] E. Camponogara, D. Jia, B. H. Krogh, and S. Talukdar. Distributed model predictive control. *IEEE Control Systems Magazine*, 22(1):44–52, February 2002.
- [25] E. Cascetta, A. Papola, V. Marzano, F. Simonelli, and I. Vitiello. Quasi-dynamic estimation of o-d flows from traffic counts: Formulation, statistical validation and performance analysis on real data. *Transportation Research Part B: Methodological*, 55:171–187, September 2013.

- [26] H. Chen and F. Allgöwer. A quasi-infinite horizon nonlinear model predictive control scheme with guaranteed stability. In *Proceedings of the European Control Conference*, pages 1421–1426, Brussels, Belgium, July 1997.
- [27] P. D. Christofides, R. Scattolini, D. M. de la Peña, and J. Liu. Distributed model predictive control: A tutorial review and future research directions. *Computers & Chemical Engineering*, 51:21–41, April 2013.
- [28] R. Courant, K. Friedrichs, and H. Lewy. On the partial difference equations of mathematical physics. *IBM Journal of Research and Development*, 11(2):215–234, March 1967.
- [29] A. Csikós and I. Varga. Real-time modeling and control objective analysis of motorway emissions. *Procedia - Social and Behavioral Sciences*, 54:1027–1036, October 2012.
- [30] C. F. Daganzo. The cell transmission model: A dynamic representation of highway traffic consistent with the hydrodynamic theory. *Transportation Research Part B: Methodological*, 28(4):269–287, August 1994.
- [31] C. F. Daganzo. The cell transmission model, part II: Network traffic. *Transportation Research Part B: Methodological*, 29(2):79–93, April 1995.
- [32] C. F. Daganzo. A behavioral theory of multi-lane traffic flow. Part I: Long homogeneous freeway sections. *Transportation Research Part B: Methodological*, 36(2):131–158, February 2002.
- [33] G. De Nicolao, L. Magni, and R. Scattolini. Stabilizing receding-horizon control of non-linear time-varying systems. *IEEE Transactions on Automatic Control*, 43(7):1030–1036, July 1998.
- [34] L. del Re, F. Allgöwer, L. Glielmo, C. Guardiola, and I. Kolmanovsky. *Automotive Model Predictive Control: Models, Methods and Applications*. Springer-Verlag, Berlin Heidelberg, Germany, 2010.
- [35] P. Deo, B. De Schutter, and A. Hegyi. Model predictive control for multi-class traffic flows. In *Proceedings of the 12th IFAC Symposium on Transportation Systems*, pages 25–30, Redondo Beach, California, USA, September 2009.
- [36] J. Doblás and F. G. Benitez. An approach to estimating and updating origin-destination matrices based upon traffic counts preserving the prior structure of a survey matrix. *Transportation Research Part B: Methodological*, 39(7):565–591, August 2005.
- [37] A. Ferrara, S. Sacone, and S. Siri. Event-triggered model predictive schemes for freeway traffic control. *Transportation Research Part C: Emerging Technologies*, 58(Special Issue: Advanced Road Traffic Control):554–567, September 2015.
- [38] A. Ferrara, A. Nai Oleari, S. Sacone, and S. Siri. Freeways as systems of systems: A distributed model predictive control scheme. *IEEE Systems Journal*, 9(1):312–323, March 2015.

- [39] J. R. D. Frejo and E. F. Camacho. Global versus local MPC algorithms in freeway Traffic control with ramp metering and variable speed limits. *IEEE Transactions on Intelligent Transportation Systems*, 13(4):1556–1565, December 2012.
- [40] J. R. D. Frejo, A. Núñez, B. De Schutter, and E. F. Camacho. Model predictive control for freeway traffic using discrete speed limit signals. In *Proceedings of the European Control Conference*, pages 4033–4038, Zürich, Switzerland, July 2013.
- [41] J. R. D. Frejo, A. Núñez, B. De Schutter, and E. F. Camacho. Hybrid model predictive control for freeway traffic using discrete speed limit signals. *Transportation Research Part C: Emerging Technologies*, 46:309–325, September 2014.
- [42] P. Giselsson. Output feedback distributed model predictive control with inherent robustness properties. In *Proceedings of the American Control Conference*, pages 1691–1696, Washington, DC, USA, June 2013.
- [43] P. Giselsson, M. D. Doan, T. Keviczky, B. De Schutter, and A. Rantzer. Accelerated gradient methods and dual decomposition in distributed model predictive control. *Automatica*, 49(3):829–833, March 2013.
- [44] N. Groot, B. De Schutter, and H. Hellendoorn. Integrated model predictive traffic and emission control using a piecewise-affine approach. *IEEE Transactions on Intelligent Transportation Systems*, 14(2):587–598, June 2013.
- [45] J. K. Gruber, D. R. Ramírez, D. Limon, and T. Alamo. Computationally efficient nonlinear min-max model predictive control based on Volterra series models-Application to a pilot plant. *Journal of Process Control*, 23(4):543–560, April 2013.
- [46] M. Hadiuzzaman and T. Z. Qiu. Cell transmission model based variable speed limit control for freeways. *Canadian Journal of Civil Engineering*, 40(1):46–56, January 2013.
- [47] M. Hasan, M. Jha, and M. Ben-Akiva. Evaluation of ramp control algorithms using microscopic traffic simulation. *Transportation Research Part C: Emerging Technologies*, 10(3):229–256, 2002.
- [48] M. L. Hazelton. Statistical inference for time varying origin-destination matrices. *Transportation Research Part B: Methodological*, 42(6):542–552, July 2008.
- [49] A. Hegyi. *Model Predictive Control For Integrating Traffic Control Measures*. PhD thesis, Delft University of Technology, Delft, Netherlands, February 2004.
- [50] A. Hegyi, B. De Schutter, and J. Hellendoorn. Model predictive control for optimal coordination of ramp metering and variable speed limits. *Transportation Research Part C: Emerging Technologies*, 13(3):185–209, June 2005.
- [51] D. Helbing and A. F. Johansson. On the controversy around Daganzo’s requiem for and Aw-Rasclé’s resurrection of second-order traffic flow models. *The European Physical Journal B*, 69(4):549–562, June 2009.
- [52] D. Helbing, A. Hennecke, and M. Treiber. Phase diagram of traffic states in the presence of inhomogeneities. *Physical Review Letters*, 82(21):4360–4363, May 1999.

- [53] S. Hoogendoorn and R. Hoogendoorn. Calibration of microscopic traffic-flow models using multiple data sources. *Philosophical Transactions of the Royal Society of London A: Mathematical, Physical and Engineering Sciences*, 368(1928):4497–4517, October 2010.
- [54] S. P. Hoogendoorn. *Multiclass Continuum Modelling of Multiclass Traffic Flow*. PhD thesis, Delft University of Technology, Delft, The Netherlands, December 1999.
- [55] W. Huang, F. Viti, and C. M. J. Tampère. Repeated anticipatory network traffic control using iterative optimization accounting for model bias correction. *Transportation Research Part C: Emerging Technologies*, 67:243–265, June 2016.
- [56] L. K. Jones, R. Deshpande, N. H. Gartner, C. Stamatiadis, and F. Zou. Robust controls for traffic networks: The near-Bayes near-Minimax strategy. *Transportation Research Part C: Emerging Technologies*, 27:205–218, February 2013.
- [57] P. Kachroo and K. Özbay. *Feedback Control Theory for Dynamic Traffic Assignment*. Springer Science&Business Media, London, Uinites Kingdom, 1999.
- [58] A. Karimi, A. Hegyi, B. De Schutter, H. Hellendoorn, and F. Middelham. Integration of dynamic route guidance and freeway ramp metering using model predictive control. In *Proceedings of the American Control Conference*, pages 5533–5538, Boston, USA, July 2004.
- [59] B. H. Kim and R. Baldick. Coarse-grained distributed optimal power flow. *IEEE Transactions on Power Systems*, 12(2):932–939, May 1997.
- [60] A. Kotsialos, M. Papageorgiou, C. Diakaki, Y. Pavlis, and F. Middelham. Traffic flow modeling of large-scale motorway networks using the macroscopic modeling tool METANET. *IEEE Transactions on Intelligent Transportation Systems*, 3(4):282–292, December 2002.
- [61] A. Kotsialos, M. Papageorgiou, M. Mangeas, and H. Haj-Salem. Coordinated and integrated control of motorway networks via non-linear optimal control. *Transportation Research Part C: Emerging Technologies*, 10(1):65–84, February 2002.
- [62] C. Leidereiter, A. Potschka, and H. G. Bock. Dual decomposition for QPs in scenario tree NMPC. In *Proceedings of the European Control Conference*, pages 1608–1613, Linz, Austria, July 2015.
- [63] H. Li and Y. Shi. Robust distributed model predictive control of constrained continuous-time nonlinear systems: A robustness constraint approach. *IEEE Transactions on Automatic Control*, 59(6):1673–1678, June 2014.
- [64] H. Li and Y. Shi. Event-triggered robust model predictive control of continuous-time nonlinear systems. *Automatica*, 50(5):1507–1513, May 2014.
- [65] M. J. Lighthill and G. B. Whitham. On kinematic waves. II. A theory of traffic flow on long crowded roads. *Proceedings of the Royal Society of London. Series A, Mathematical and Physical Sciences*, 229(1178):317–345, May 1955.

- [66] N. E. Ligterink, R. De Lange, and E. Schoen. Refined vehicle and driving-behavior dependencies in the VERSIT+ emission model. In *Proceedings of the ETTAP Symposium*, pages 177–186, Toulouse, France, June 2009.
- [67] S. Lin, B. De Schutter, Y. Xi, and J. Hellendoorn. Fast model predictive control for urban road networks via MILP. *IEEE Transactions on Intelligent Transportation Systems*, 12(3):846–856, September 2011.
- [68] S. Liu, B. De Schutter, and J. Hellendoorn. Multi-class traffic flow and emission control for freeway networks. In *Proceedings of the 16th International IEEE Conference on Intelligent Transportation Systems*, pages 1334–1339, The Hague, The Netherlands, October 2013.
- [69] S. Liu, B. De Schutter, and J. Hellendoorn. Integrated traffic flow and emission control based on FASTLANE and the multi-class vt-macro model. In *Proceedings of the 2014 European Control Conference*, pages 2908–2913, Strasbourg, France, June 2014.
- [70] S. Liu, B. De Schutter, and J. Hellendoorn. Model predictive traffic control based on a new multi-class METANET model. In *Proceedings of the 19th World Congress of the International Federation of Automatic Control*, pages 8781–8786, Cape Town, South Africa, August 2014.
- [71] S. Liu, J. R. D. Frejo, A. Núñez, B. De Schutter, A. Sadowska, J. Hellendoorn, and E. F. Camacho. Tractable robust predictive control approaches for freeway networks. In *Proceedings of the 17th International Conference on Intelligent Transportation Systems*, pages 1857–1862, Qingdao, China, October 2014.
- [72] S. Liu, H. Hellendoorn, and B. De Schutter. Model predictive control for freeway networks based on multi-class traffic flow and emission models. Technical Report 15-020, Delft Center for Systems and Control, Delft University of Technology, Delft, The Netherlands, August 2015. Accepted for Publication in *IEEE Transactions on Intelligent Transportation Systems*.
- [73] S. Liu, A. Sadowska, J.R.D. Frejo, A. Núñez, E.F. Camacho, H. Hellendoorn, and B. De Schutter. Robust receding horizon parameterized control for multi-class freeway networks: A tractable scenario-based approach. *International Journal of Robust and Nonlinear Control*, 26(6):1211–1245, April 2016.
- [74] S. Liu, A. Sadowska, H. Hellendoorn, and B. De Schutter. A robust distributed model predictive control approach for freeway networks. Technical report, Delft Center for Systems and Control, Delft University of Technology, Delft, The Netherlands, February 2016. Submitted to *IEEE Transactions on Control Systems Technology*.
- [75] S. Logghe. *Dynamic Modeling of Heterogeneous Vehicular Traffic*. PhD thesis, Katholieke Universiteit Leuven, Leuven, Belgium, June 2003.
- [76] S. Logghe and L. H. Immers. Multi-class kinematic wave theory of traffic flow. *Transportation Research Part B: Methodological*, 42(6):523–541, July 2008.

- [77] X. Lu, P. Varaiya, R. Horowitz, D. Su, and S. E. Shladover. Novel freeway traffic control with variable speed limit and coordinated ramp metering. *Transportation Research Record*, 2229:55–65, 2011.
- [78] J. D. Lundgren and A. Peterson. A heuristic for the bilevel origin-destination-matrix estimation problem. *Transportation Research Part B: Methodological*, 42(4):339–354, May 2008.
- [79] J. M. Maciejowski. *Predictive Control: with Constraints*. Person Education, London, United Kingdom, 2002.
- [80] J. M. Maestre, L. Raso, P. J. van Overloop, and B. De Schutter. Distributed tree-based model predictive control on an open water system. In *Proceedings of the American Control Conference*, pages 1985–1990, Montréal, Canada, June 2012.
- [81] L. Maggi, S. Sacone, and S. Siri. Freeway traffic control considering capacity drop phenomena: Comparison of different mpc schemes. In *Proceedings of the 18th International Conference on Intelligent Transportation Systems*, pages 457–462, Las Palmas de Gran Canaria, Spain, September 2015.
- [82] R. Martí, S. Lucia, D. Sarabia, R. Paulen, S. Engell, and C. de Prada. An efficient distributed algorithm for multi-stage robust nonlinear predictive control. In *Proceedings of the European Control Conference*, pages 2664–2669, Linz, Austria, July 2015.
- [83] D. Q. Mayne, E. C. Kerrigan, E. J. van Wyk, and P. Falugi. Tube-based robust nonlinear model predictive control. *International Journal of Robust and Nonlinear Control*, 21(11):1341–1353, July 2011.
- [84] A. Messmer and M. Papageorgiou. METANET: A macroscopic simulation program for motorway networks. *Traffic Engineering and Control*, 31(8–9):466–470, 1990.
- [85] M. Morari, J. H. Lee, C. E. Garcia, and D. M. Prett. *Model Predictive Control*. Prentice-Hall, Englewood Cliffs, NJ, USA, 1993.
- [86] G. J. L. Naus, J. Ploeg, M. J. G. Van de Molengraft, W. P. M. H. Heemels, and M. Steinbuch. Design and implementation of parameterized adaptive cruise control: An explicit model predictive control approach. *Control Engineering Practice*, 18(8):882–892, August 2010.
- [87] R. R. Negenborn, B. De Schutter, and J. Hellendoorn. Multi-agent model predictive control for transportation networks: Serial versus parallel schemes. *Engineering Applications of Artificial Intelligence*, 21(3):353–366, April 2008.
- [88] Y. M. Nie and H. M. Zhang. A variational inequality formulation for inferring dynamic origin-destination travel demands. *Transportation Research Part B: Methodological*, 42(7–8):635–662, August 2008.
- [89] C. Ocampo-Martinez, S. Bovo, and V. Puig. Partitioning approach oriented to the decentralised predictive control of large-scale systems. *Journal of Process Control*, 21(5):775–786, June 2011.

- [90] Optimal Control of Freeway Corridors. Y. Stephanedes and K. Chang. *Journal of Transportation Engineering*, 119(4):504–514, 1993.
- [91] K. W. Ogden. *Safer Roads: A Guide to Road Safety Engineering*. Ashgate Publishing Ltd, Melbourne, Australia, 1996.
- [92] M. Papageorgiou. *Applications of Automatic Control Concepts to Traffic Flow Modeling and Control*. Springer-Verlag, New York, USA, 1983.
- [93] M. Papageorgiou. Some remarks on macroscopic traffic flow modeling. *Transportation Research Part A: Policy and Practice*, 32(5):323–329, September 1998.
- [94] M. Papageorgiou and A. Kotsialos. Freeway ramp metering: An overview. *IEEE Transactions on Intelligent Transportation Systems*, 3(4):271–281, December 2002.
- [95] M. Papageorgiou, J. M. Blosseville, and H. Haj-Salem. Modelling and real-time control of traffic flow on the southern part of Boulevard Périphérique in Paris: Part II: Coordinated on-ramp metering. *Transportation Research Part A: General*, 24(5):361–370, September 1990.
- [96] M. Papageorgiou, H. Haj-Salem, and J. M. Blosseville. ALINEA: A local feedback control law for on-ramp metering. *Transportation Research Record*, 1320:58–64, 1991.
- [97] M. Papageorgiou, C. Diakaki, V. Dinopoulou, A. Kotsialos, and Y. Wang. Review of road traffic control strategies. *Proceedings of the IEEE*, 91(12):2043–2067, December 2003.
- [98] I. Papamichail, A. Kotsialos, I. Margonis, and M. Papageorgiou. Coordinated ramp metering for freeway networks – A model-predictive hierarchical control approach. *Transportation Research Part C: Emerging Technologies*, 18(3):311–331, June 2010.
- [99] T. Parisini and R. Zoppoli. A receding horizon regulator for nonlinear systems and a neural approximation. *Automatica*, 31(10):1443–1451, October 1995.
- [100] K. Parry and M. Hazelton. Estimation of origin-destination matrices from link counts and sporadic routing data. *Transportation Research Part B: Methodological*, 46(1):175–188, January 2012.
- [101] C. Pasquale, S. Liu, S. Siri, S. Saccone, and B. De Schutter. A new emission model including on-ramps for two-class freeway traffic control. In *Proceedings of the 18th IEEE International Conference on Intelligent Transportation Systems*, pages 1143–1149, Las Palmas de Gran Canaria, Spain, September 2015.
- [102] C. Pasquale, I. Papamichail, C. Roncoli, S. Saccone, S. Siri, and M. Papageorgiou. Two-class freeway traffic regulation to reduce congestion and emissions via nonlinear optimal control. *Transportation Research Part C: Emerging Technologies*, 55:85–99, June 2015.
- [103] H. J. Payne. Models of freeway traffic and control. *Mathematical Models of Public Systems*, 1:51–61, 1971.

- [104] G. Pinto and M. T. Oliver-Hoyo. Using the relationship between vehicle fuel consumption and CO₂ emissions to illustrate chemical principles. *Journal of Chemical Education*, 85(2):218–220, February 2008.
- [105] A. J. Poole and A. Kotsialos. Metanet model validation using a genetic algorithm. *Control in Transportation Systems*, 13(1):7–12, September 2012.
- [106] V. Punzo, M. Montanino, and B. Ciuffo. Do we really need to calibrate all the parameters? variance-based sensitivity analysis to simplify microscopic traffic flow models. *IEEE Transactions on Intelligent Transportation Systems*, 16(1):184–193, February 2015.
- [107] H. Rakha, K. Ahn, and A. Trani. Comparison of MOBILE5a, MOBILE6, VT-MICRO, and CMEM models for estimating hot-stabilized light-duty gasoline vehicle emissions. *Canadian Journal of Civil Engineering*, 30(6):1010–1021, December 2003.
- [108] A. Richards and J. P. How. Robust distributed model predictive control. *International Journal of Control*, 80(9):1517–1531, September 2007.
- [109] P. I. Richards. Shock waves on the highway. *Operations Research*, 4(1):42–51, February 1956.
- [110] M. Rinaldi, W. Himpe, and C. M. J. Tampère. A sensitivity-based approach for adaptive decomposition of anticipatory network traffic control. *Transportation Research Part C: Emerging Technologies*, 66:150–175, May 2016.
- [111] G. Schildbach, L. Fagiano, C. Frei, and M. Morari. The scenario approach for stochastic model predictive control with bounds on closed-loop constraint violations. *Automatica*, 50(12):3009–3018, December 2014.
- [112] T. Schreiter, R. L. Landman, J. W. C. van Lint, A. Hegyi, and S. Hoogendoorn. Vehicle class-specific route guidance of freeway traffic by model-predictive control. *Transportation Research Record*, 2324:53–62, 2012.
- [113] P. O. M. Scokaert, J. B. Rawlings, and E. S. Meadows. Discrete-time stability with perturbations: Application to model predictive control. *Automatica*, 33(3):463–470, March 1997.
- [114] M. Slinn, P. Guest, and P. Matthews. *Traffic Engineering Design, Second Edition: Principles and Practice*. Butterworth Heinemann Ltd, Oxford, United Kingdom, 2005.
- [115] R. Smit, R. Smokers, and E. Schoen. VERSIT+ LD: Development of a new emission factor model for passenger cars linking real-world emissions to driving cycle characteristics. In *Proceedings of the 14th Symposium on Transport and Air Pollution*, pages 177–186, Graz, Austria, June 2005.
- [116] S. Smulders. Control of freeway traffic flow by variable speed signs. *Transportation Research Part B: Methodological*, 24(2):111–132, April 1990.
- [117] J. 't Hart. Comparison of conventional and parameterized MPC for traffic control: A case study. Master's thesis, Delft University of Technology, Delft, Netherlands, April 2011.

- [118] M. Taieb-Maimon and D. Shinar. Minimum and comfortable driving headways: Reality versus perception. *The Journal of the Human Factors and Ergonomics Society*, 43(1):159–172, 2001.
- [119] T. Tettamanti, T. Luspay, B. Kulcsár, T. Péni, and I. Varga. Robust control for urban road traffic networks. *IEEE Transactions on Intelligent Transportation Systems*, 15(1): 385–398, February 2014.
- [120] M. Treiber and A. Kesting. *Traffic Flow Dynamics: Data, Models and Simulation*. Springer-Verlag, Berlin Heidelberg, Germany, 2010.
- [121] S. V. Ukkusuri, G. Ramadurai, and G. Patil. A robust transportation signal control problem accounting for traffic dynamics. *Computers & Operations Research*, 37(5): 869–879, May 2010.
- [122] J. W. C. Van Lint, S. P. Hoogendoorn, and A. Hegyi. Dual EKF state and parameter estimation in multi-class first-order traffic flow models. In *Proceedings of the 17th World Congress of the International Federation of Automatic Control*, pages 14078–14083, Seoul, Korea, July 2008.
- [123] J. W. C. van Lint, S. P. Hoogendoorn, and M. Schreuder. Fastlane: New multiclass first-order traffic flow model. *Transportation Research Record*, 2088:177–187, 2008.
- [124] G. B. Whitham. *Linear and Nonlinear Waves*. Wiley-Interscience, New York, USA, 1974.
- [125] G. C. K. Wong and S. C. Wong. A multi-class traffic flow model—an extension of LWR model with heterogeneous drivers. *Transportation Research Part A: Policy and Practice*, 36(9):827–841, November 2002.
- [126] M. Papageorgiou Y. Wang, J. Gaffney, I. Papamichail, G. Rose, and W. Young. Local ramp metering in random-location bottlenecks downstream of metered on-ramp. *Transportation Research Record*, 2178:90–100, 2010.
- [127] L. Yu, Y. Xu, G. Song, Y. Hao, S. Guo, and Q. Shi. Development and application of macroscopic emission model for china. *Transportation Research Record*, 2123:66–75, 2009.
- [128] T. Zachariadis and Z. Samaras. An integrated modeling system for the estimation of motor vehicle emissions. *Journal of the Air and Waste Management Association*, 49(9): 1010–1026, September 1999.
- [129] S. K. Zegeye. *Model-Based Traffic Control for Sustainable Mobility*. PhD thesis, Delft University of Technology, The Netherlands, October 2011.
- [130] S. K. Zegeye, B. De Schutter, J. Hellendoorn, E. A. Breunese, and A. Hegyi. A predictive traffic controller for sustainable mobility using parameterized control policies. *IEEE Transactions on Intelligent Transportation Systems*, 13(3):1420–1429, September 2012.
- [131] X. Zhang, G. Schildbach, D. Sturzenegger, and M. Morari. Scenario-based MPC for energy-efficient building climate control under weather and occupancy uncertainty. In *Proceedings of the European Control Conference*, pages 1029–1034, Zürich, Switzerland, July 2013.

-
- [132] R. X. Zhong, A. Sumalee, T. L. Pan, and W. H. K. Lam. Optimal and robust strategies for freeway traffic management under demand and supply uncertainties: An overview and general theory. *Transportmetrica A: Transport Science*, 10(10):849–877, January 2014.
- [133] Z. Zhou, S. Lin, and Y. Xi. A fast network partition method for large-scale urban traffic networks. *Journal of Control Theory and Applications*, 11(3):359–366, August 2013.

Glossary

List of Symbols

The most frequently used symbols in this thesis are listed by chapters as follows.

Chapter 2

Traffic Flow Models

m	index for link
i	index for segment/cell
o	index for origin
L_m	segment/cell length of link m
μ_m	number of lanes of link m
t	time instant
T	simulation time step length
k	simulation time step counter
$q_{m,i}$	flow in segment/cell (m, i)
$\rho_{m,i}$	density in segment/cell (m, i)
$v_{m,i}$	speed in segment/cell (m, i)
V_m	desired speed function for link m
ρ_m^{crit}	critical density in link m
v_m^{free}	free-flow speed in link m
$\tau_m, \eta_m, \kappa_m, a_m$	model parameters in link m for METANET
δ_m	$1 + \delta_m$ is the non-compliance factor of vehicles in link m
$v_{m,i}^{\text{SL}}$	speed limit that is applied in segment/cell (m, i)
q_o	flow at origin o
d_o	external demand at origin o
w_o	queue length at origin o
r_o	ramp metering rate that is applied at on-ramp o
C_o	capacity of on-ramp o
ρ_m^{max}	maximum density of link m
$q_{m,1}^{\text{lim}}$	maximal inflow for the first segment of link m that is connected to the origin
$v_{m,1}^{\text{lim}}$	speed that limits the flow in segment $(m, 1)$
c	index for vehicle class
n_c	total number of vehicle classes
$\Theta_{m,i,c}$	dynamic passenger car equivalents for vehicle class c in cell (m, i)

s_c	gross stopping distance of vehicle class c
$T_{h,c}$	minimum time headway of vehicle class c
$v_{m,i,c}$	speed of vehicle class c in segment/cell (m, i)
$\rho_{m,i}^{\text{efc}}$	effective density in cell (m, i)
$\rho_{m,i,c}$	density of vehicle class c in segment/cell (m, i)
$q_{m,i,c}$	flow of vehicle class c in segment/cell (m, i)
$q_{m,c}^{i,i+1}$	flow of vehicle class c from cell i to cell $i + 1$ of link m
$V_{m,c}$	desired speed function for vehicle class c in link m
$v_{m,c}^{\text{free}}$	free-flow speed of vehicle class c in link m
$v_{m,jt}^{\text{crit}}$	joint critical speed for all vehicle classes in link m
$\rho_{m,jt}^{\text{crit}}$	joint critical density for all vehicle classes in link m
$\rho_{m,\text{efc}}^{\text{max}}$	effective maximum density in link m
$\lambda_{m,i,c}$	flow ratio of vehicle class c in cell (m, i)
$D_{m,i,c}$	demand of vehicle class c in cell (m, i)
$S_{m,i}$	supply for all vehicle classes in cell (m, i)
I_{link}	set including all the links

Traffic Emission and Fuel Consumption Models

y	index for emission (fuel) category
EM_y	emission rate (expressed in g/s) of emission category y for a single vehicle
$u_{0,y}, \dots, u_{9,y}$	model parameters for emission category y for VERSIT+
v	speed of a single vehicle
a	acceleration of a single vehicle
$a_{m,i}^{\text{inter}}$	inter-segment/inter-cell acceleration of vehicles in segment/cell (m, i)
$a_{\alpha,\beta}^{\text{cross}}$	cross-segment/cross-cell acceleration of vehicles from segment/cell α to segment/cell β
$n_{m,i}^{\text{inter}}$	number of vehicles corresponding to $a_{m,i}^{\text{inter}}$
$n_{\alpha,\beta}^{\text{cross}}$	number of vehicles corresponding to $a_{\alpha,\beta}^{\text{cross}}$
v_α	speed of vehicles in segment/cell/origin α
q_α	flow of vehicles in segment/cell/origin α
$EM_{y,m,i}^{\text{inter}}$	emission (fuel consumption) rate of emission (fuel) category y corresponding to $a_{m,i}^{\text{inter}}$
$EM_{y,\alpha,\beta}^{\text{cross}}$	emission (fuel consumption) rate of emission (fuel) category y corresponding to $a_{\alpha,\beta}^{\text{cross}}$
P_y	parameter matrix for emission (fuel consumption) rates for emission (fuel) category y
$EM_{\text{CO}_2,m,i}$	emission rate for CO ₂ in segment/cell (m, i)
$EM_{\text{fuel},m,i}$	fuel consumption rate in segment/cell (m, i)
$EM_{\text{fuel},m,i}^{\text{inter}}$	fuel consumption rate corresponding to $a_{m,i}^{\text{inter}}$
$EM_{\text{fuel},\alpha,(m,i)}^{\text{cross}}$	fuel consumption rate corresponding to $a_{\alpha,(m,i)}^{\text{cross}}$
γ_1, γ_2	model parameters for transferring the fuel consumption rate to the emission rate for CO ₂

$I_{m,i}^{\text{up}}$ set including all the upstream segments/cells and origins that connect to segment/cell (m, i)

Model Predictive Control

J objective function
 f state function
 h output function
 x state vector
 y output vector
 u control input vector
 D uncontrollable input vector
 x_k measured state vector at time step k
 \mathbb{X} set of all the feasible states
 \mathbb{Y} set of all the feasible outputs
 \mathbb{U} set of all the feasible control inputs
 N_p prediction horizon length
 N_c control horizon length

Chapter 3

Multi-Class Macroscopic Traffic Flow Models

$w_{o,c}$ queue length of vehicle class c at origin o
 $d_{o,c}$ external demand of vehicle class c at origin o
 $q_{o,c}$ flow of vehicle class c at origin o
 $\delta_{m,c}$ $1 + \delta_{m,c}$ is the non-compliance factor of vehicle class c in link m
 $\Theta_{o,c}$ dynamic passenger car equivalents for vehicle class c at origin o
 $D_{o,c}$ total demand of vehicle class c at origin o
 $\lambda_{o,c}$ share for vehicle class c among the total demand at on-ramp o
 C_o^{efc} effective capacity for on-ramp o
 C_{m-1}^{efc} effective capacity for the upstream link $m-1$ of the link m that connects to on-ramp o
 Λ_o proportion of effective capacities: $\frac{C_o^{\text{efc}}}{C_o^{\text{efc}} + C_{m-1}^{\text{efc}}}$
 $\alpha_{m,i,c}$ road space fraction of vehicle class c in segment (m, i)
 Q_c flow function of vehicle class c
 $\tau_{m,c}, \eta_{m,c}, \kappa_{m,c}$ model parameters for vehicle class c in link m for multi-class METANET
 $a_{m,c}$
 $\rho_{m,c}^{\text{crit}}$ critical density of vehicle class c in link m
 $\rho_{m,c}^{\text{max}}$ theoretical maximum density of link m if there would be only vehicle class c
 $C_{o,c}$ theoretical maximum capacity of on-ramp o if there would be only vehicle class c

$q_{m,1,c}^{\text{lim}}$	maximal inflow of vehicle class c for the first segment of link m that is connected to the origin
$v_{m,1,c}^{\text{lim}}$	speed that limits the flow for vehicle class c in segment $(m, 1)$
c_m^*	vehicle class with the slowest desired speed in free-flow regime
$\rho_{m,c}^{\text{crit}*}$	parameter of vehicle class c in link m for determining the boundary condition for the semi-congestion regime
$S_{m,i}^{\text{free}}$	set of all vehicle classes that are in free-flow mode in segment (m, i)
$S_{m,i}^{\text{cong}}$	set of all vehicle classes that are in congested mode in segment (m, i)

Multi-Class Macroscopic Traffic Emission Models

$a_{m,i,c}^{\text{inter}}$	inter-segment/inter-cell acceleration of vehicle class c in segment/cell (m, i)
$a_{\alpha,\beta,c}^{\text{cross}}$	cross-segment/cross-cell acceleration of vehicle class c from segment/cell α to segment/cell β
$n_{m,i,c}^{\text{inter}}$	number of vehicles corresponding to $a_{m,i,c}^{\text{inter}}$
$n_{\alpha,\beta,c}^{\text{cross}}$	number of vehicles corresponding to $a_{\alpha,\beta,c}^{\text{cross}}$
$v_{\alpha,c}$	speed of vehicle class c in segment/cell/origin α
$q_{\alpha,c}$	flow of vehicle class c in segment/cell/origin α
$EM_{y,m,i,c}^{\text{inter}}$	emission (fuel consumption) rate of emission (fuel) category y corresponding to $a_{m,i,c}^{\text{inter}}$
$EM_{y,\alpha,\beta,c}^{\text{cross}}$	emission (fuel consumption) rate of emission (fuel) category y corresponding to $a_{\alpha,\beta,c}^{\text{cross}}$
$\gamma_{1,c}, \gamma_{2,c}$	class-dependent model parameters for transferring the fuel consumption rate to the emission rate for CO ₂
$P_{y,c}$	class-dependent parameter matrix of vehicle class c for emission (fuel) category y in multi-class VT-macro
$u_{0,y,c}, \dots, u_{9,y,c}$	model parameters of vehicle class c for emission category y in multi-class VERSIT+

MPC with End-Point Penalties

TTS	total time spent
k_c	control time step counter
T_c	control time step length
M	positive integer defined by $M = T_c / T$
p_c	fixed passenger car equivalents for vehicle class c
I_{all}	set of all pairs of link and segment/cell indices (m, i)
O_{all}	set of the indices of all origins
TE_y	total emissions of emission category y
$EM_{y,o,c}^{\text{inter}}$	emission (fuel consumption) rate of emission (fuel) category y for vehicles in queue at origin o
P_{all}	set of all pairs of adjacent segments (cells) and origins

TTS^{end}	end-point penalty for total time spent
$t_{m,i,c}^{\text{rem}}$	time that a vehicle of class c that is present in segment/cell (m, i) at time step $(k_c + N_p)M$ would on the average need to get to its destination
$t_{m,i,c}^{\text{rem}}$	time that a vehicle of class c that is present in segment/cell (m, i) at time step $(k_c + N_p)M$ would on the average need to get to its destination
$t_{o,c}^{\text{rem}}$	time that a vehicle of class c present in queue at origin o at time step $(k_c + N_p)M$ would on the average need to get to its destination
TE_y^{end}	end-point penalty for total emissions of category y
$TE_{y,m,i,c}^{\text{rem}}$	emissions that a vehicle of class c present in segment/cell (m, i) at time step $(k_c + N_p)M$ would on the average generate before leaving the network
$TE_{y,o,c}^{\text{rem}}$	emissions that a vehicle of class c present in queue at origin o at time step $(k_c + N_p)M$ would on the average generate before leaving the network
TTS_{nom}	nominal total time spent
$TE_{y,\text{nom}}$	nominal total emissions of category y
$TTS_{\text{nom}}^{\text{end}}$	nominal end-point penalty for total time spent
$TE_{y,\text{nom}}^{\text{end}}$	nominal end-point penalty for total emissions of category y
$v_{m,\text{max}}^{\text{free}}$	free-flow speed of the fastest vehicle class in link m
$v_{m,i}^{\text{ctrl}}$	speed limit in segment/cell (m, i) for a given control step
r_o^{ctrl}	ramp metering rate of on-ramp o for a given control step
N_{VSL}	number of groups of variable speed limits
N_{RM}	number of groups of metered on-ramps
$\xi_{\text{TTS}}, \xi_{TE,y}, \xi_{\text{ramp}}, \xi_{\text{speed}}, \xi_{\text{TTS}}^{\text{end}}, \xi_{TE,y}^{\text{end}}$	nonnegative weights
O_{ramp}	set of all metered on-ramps
I_{speed}	set of all segments/cells with speed limits.

Chapter 4

RHPC Based on Multi-Class Traffic Models

$\theta_{m,i,0}, \theta_{m,i,c,1}$	control parameters for the RHPC laws for variable speed limits
$\theta_{m,i,c,2}$	
$\theta_{o,c,1}, \theta_{o,c,2}$	control parameters for the RHPC laws for ramp metering rates
κ_v, κ_ρ	small positive values to prevent the divisors to be 0
$\beta_{m,i,c}$	density fraction of vehicle class c in segment i of link m
$v_{m,i,\text{sat}}^{\text{ctrl}}$	saturated variable speed limit in segment i of link m
$r_{o,\text{sat}}^{\text{ctrl}}$	saturated ramp metering rate at on-ramp o
$v_{\text{max},m}$	upper bound of the variable speed limits in link m
$v_{\text{min},m}$	lower bound of the variable speed limits in link m
$r_{\text{max},o}$	upper bound of the ramp metering rate at on-ramp o
$r_{\text{min},o}$	lower bound of the ramp metering rate at on-ramp o

Scenario-Based RHPC

x_ω	state vector for the case with uncertainties
y_ω	output vector for the case with uncertainties
D_ω	uncontrollable input vector for the case with uncertainties
ω	vector containing the uncertainties
f_ω	state function for the case with uncertainties
J_ω	objective function for the case with uncertainties
x_ω^k	measured state vector at time step k for the case with uncertainties
\tilde{W}	set of all the possible realizations of uncertainties over the prediction period
J_{\max}	objective function for the scenario-based RHPC approach
$\tilde{\Omega}$	set of possible scenarios that will be considered for the scenario-based RHPC approach
γ	positive weight to penalize queue length constraint violation under uncertainties
$w_{o,efc}^{\max}$	maximum allowed queue length (in pce) for all vehicle classes at on-ramp o

Chapter 5

Global Uncertainties and Local Uncertainties in Large-Scale Traffic Networks

s	index for subnetwork
N_{sub}	number of subnetworks
Ω_{glob}	set of all the possible global uncertainty scenarios for all subnetworks
Ω_s^{loc}	set of all the possible local uncertainty scenarios for subnetwork s
N_s^{loc}	total number of the local uncertainty scenarios for subnetwork s
N_{glob}	total number of the global uncertainty scenarios for all subnetworks

DMPC for Large-Scale Traffic Networks

J_s	local control objective function of subnetwork s
f_s	dynamic function of subnetwork s
h_s	output function of subnetwork s
x_s	state vector of subnetwork s
x_s^k	measured state vector of subnetwork s at time step k
y_s	output vector of subnetwork s
u_s	control input vector for subnetwork s
F_s	general constraint function on the states, outputs, and control inputs for subnetwork s over the prediction period
S_s^{nb}	set of all the indices for the neighbors of subnetwork s
N_s^{nb}	number of the neighbors of subnetwork s
D_s^{in}	external uncontrollable input vector for subnetwork s
E_s^{in}	interconnecting input vector (w.r.t. agent s) for subnetwork s from all neighbors

$E_{j,s}^{\text{in}}$	interconnecting input vector (w.r.t. agent s) for subnetwork s from neighboring subnetwork j
$E_{s,j}^{\text{out}}$	interconnecting output vector (w.r.t. agent j) from neighboring subnetwork j to subnetwork s
$K_{s,j}$	interconnecting output selection matrix from j to s
L	augmented Lagrangian function
e	a positive constant
$\lambda_{j,s}^{\text{in}}$	Lagrange multiplier vector corresponding to $E_{j,s}^{\text{in}}$
Λ^{in}	vector comprises of $\lambda_{j,s}^{\text{in}}$ for $s = 1, \dots, N_{\text{sub}}$ and $j = j_{s,1}, \dots, j_{s,N_s^{\text{nb}}}$
J_s^{inter}	function handling the interconnecting variables determined by agent s
$\lambda_{j,s}^{\text{out}}$	Lagrange multiplier vector corresponding to $E_{j,s}^{\text{out}}$

Scenario-Based DMPC with Global Uncertainties

g	index for the scenarios for global uncertainties
$x_{s,g}$	state vector of subnetwork s for the case with global uncertainties
$y_{s,g}$	output vector of subnetwork s for the case with global uncertainties
$J_{s,g}$	local control objective function of subnetwork s for the case with global uncertainties
$f_{s,g}$	dynamic function of subnetwork s for the case with global uncertainties
$F_{s,g}$	general constraint function on the states, outputs, and control inputs for subnetwork s over the prediction period for the case with global uncertainties
$J_{s,g}^{\text{inter}}$	function handling the interconnecting variables determined by agent s for the case with global uncertainties
Γ	relatively high weight for the penalty term of the joint constraint on states, outputs, and control inputs w.r.t. the weights for $J_{s,g}$ and $J_{s,g}^{\text{inter}}$
$D_{s,g}^{\text{in}}$	external uncontrollable input vector for subnetwork s for the case with global uncertainties
$E_{s,g}^{\text{in}}$	interconnecting input vector (w.r.t. agent s) for subnetwork s from all neighbors for the case with global uncertainties
$E_{j,s,g}^{\text{in}}$	interconnecting input vector (w.r.t. agent s) for subnetwork s from neighboring subnetwork j for the case with global uncertainties
$E_{s,j,g}^{\text{out}}$	interconnecting output vector (w.r.t. agent j) from neighboring subnetwork j to subnetwork s for the case with global uncertainties
$\lambda_{j,s,g}^{\text{in}}$	Lagrange multiplier vector corresponding to $E_{j,s,g}^{\text{in}}$
$\lambda_{j,s,g}^{\text{out}}$	Lagrange multiplier vector corresponding to $E_{j,s,g}^{\text{out}}$
Λ_g^{in}	vector comprises of $\lambda_{j,s,g}^{\text{in}}$ for $s = 1, \dots, N_{\text{sub}}$ and $j = j_{s,1}, \dots, j_{s,N_s^{\text{nb}}}$
p_g	probability of global uncertainty scenario g
ω_g	scenario g for global uncertainties
L_g	augmented Lagrangian function for the case with global uncertainties
$J_{s,g}^{\text{tot}}$	total objective function for subnetwork s in global uncertainty scenario g

Scenario-Based DMPC on the Basis of a Reduced Scenario Tree of Global and Local Uncertainties

l	index for the local scenarios for a subnetwork
$x_{s,g,l}$	state vector of subnetwork s for the case with global uncertainties and local uncertainties
$y_{s,g,l}$	output vector of subnetwork s for the case with global uncertainties and local uncertainties
$J_{s,g,l}$	local control objective function of subnetwork s for the case with global uncertainties and local uncertainties
$f_{s,g,l}$	dynamic function of subnetwork s for the case with global uncertainties and local uncertainties
$F_{s,g,l}$	general constraint function on the states, outputs, and control inputs for subnetwork s over the prediction period for the case with global uncertainties and local uncertainties
$D_{s,g,l}^{\text{in}}$	external uncontrollable input vector for subnetwork s for the case with global uncertainties and local uncertainties
$E_{j,s,g,l}^{\text{out}}$	interconnecting output vector (w.r.t. agent s) from subnetwork s to neighboring subnetwork j for the case with global uncertainties and local uncertainties
N_{com}	number of all the combinations of local uncertainty scenarios for all subnetworks for a given global uncertainty scenario
$p_{s,l}$	probability of local uncertainty scenario l for subnetwork s
$\omega_{s,l}$	scenario l for the local uncertainties for subnetwork s

Alternating Direction Method of Multipliers for Scenario-Based DMPC

N_{gv}	number of global variables for a specific combination of global scenario and local scenario
G_g	overall global variable for global scenario g
$G_{j,s,g}$	global variable corresponding to the interconnecting variable from subnetwork j to subnetwork s for global scenario g
$P_{j,s}$	matrix for selecting the global variable corresponding to the interconnecting variable from subnetwork j to subnetwork s
σ	negotiation iteration number
Λ_g^{out}	vector comprises of $\lambda_{j,s,g}^{\text{out}}$ for $s = 1, \dots, N_{\text{sub}}$ and $j = j_{s,1}, \dots, j_{s,N_s^{\text{nb}}}$
ϵ	a small positive value

Summary

Modeling, Robust and Distributed Control for Freeway Networks

In Model Predictive Control (MPC) for traffic networks, traffic models are crucial since they are used as prediction models for determining the optimal control actions. In order to reduce the computational complexity of MPC for traffic networks, macroscopic traffic models are often used instead of microscopic traffic models. These macroscopic traffic models can be divided into homogeneous, single-class models and heterogeneous, multi-class models. In general, multi-class models are more accurate than single-class models, without increasing the computational complexity significantly. In MPC a more accurate model in general implies a better prediction of the controlled system, providing the controller more accurate information for determining the control actions. Therefore, developing and using multi-class traffic models is one way to improve the effectiveness of MPC. Apart from the above characteristics of traffic models, other factors such as uncertainties in external inputs and model parameters can also affect the accuracy of predictions. Thus another way for improving the effectiveness of MPC is to take into account the effects of these uncertainties and to develop robust MPC approaches for handling these uncertainties. Apart from improving the effectiveness of MPC, making MPC feasible for large-scale traffic networks is also important, due to the rapid increase of the computational complexity of the MPC optimization problem with the size of the controlled system. For large-scale systems, Distributed Model Predictive Control (DMPC) is often considered for making the control approach computationally feasible. Moreover, robust DMPC can be developed for ensuring both feasibility and robustness. In this context, the following three topics are studied in this thesis:

- Several multi-class macroscopic traffic flow models and traffic emission models are extended.
- A scenario-based Receding-Horizon Parameterized Control (RHPC) approach is proposed.
- A scenario-based DMPC approach with global uncertainties and local uncertainties distinguished is developed.

First, we propose new multi-class macroscopic traffic flow and emission models including a new multi-class METANET model, and two new multi-class emissions models: multi-class VT-macro and multi-class VERSIT+. To allow comparison with the new multi-class METANET model, we also extend the first-order multi-class traffic flow model

FASTLANE with variable speed limits and ramp metering. These new multi-class macroscopic traffic flow and emission models are used as prediction models in MPC for freeway networks. In addition, end-point penalties are included to account for the behavior of traffic flows beyond the prediction period. Through numerical experiments we show that the new multi-class METANET model combined with the extended emission models can reduce the total time spent and the total emissions in a balanced way w.r.t. the non-control case. The experiments also show that the new multi-class METANET model captures the maximum queue length dynamics better than FASTLANE although they are both based on the same queue model. Moreover, the experiments indicate that including end-point penalties can further improve the performance for the MPC approaches based on the new multi-class METANET model, but not for the MPC approaches based on FASTLANE.

Next, we propose a scenario-based Receding-Horizon Parameterized Control (RHPC) approach. In this approach, we use a scenario-based scheme to deal with the robust control problem for traffic networks, considering a limited set of scenarios for the uncertainties. The worst case of the considered scenarios is actually optimized in a min-max setting. In contrast to MPC, in RHPC only the parameters of control laws are optimized, instead of all the control inputs. As a result, the number of variables in the optimization problem can be decreased w.r.t. conventional MPC, allowing us to reduce the computational burden. Several RHPC laws are developed based on multi-class traffic flow models. We illustrate through simulation experiments that nominal RHPC approaches ignoring uncertainties may lead to high queue length constraint violations, and that scenario-based RHPC performs best as it is capable of improving the control performance without resulting in high queue length constraint violations.

At last, we develop a scenario-based DMPC approach with global uncertainties and local uncertainties distinguished. For a large-scale traffic network consisting of multiple subnetworks, two types of uncertainties can be distinguished: global uncertainties and local uncertainties. We assume that all these uncertainties are described through finite sets of scenarios. Thus, a tree based on the considered uncertainty scenarios can be built. An intuitive way of combining the local scenarios for different subnetworks is to consider all the combinations of the local scenarios (i.e. to construct a complete scenario tree). However, the computational burden will be very large in this case. Therefore, we propose to construct a reduced scenario tree for combining the local scenarios for different subnetworks, in which the interconnecting outputs of one subnetwork are combined for all the local scenarios for that subnetwork. Furthermore, two settings are considered for the new approach, i.e. an expected-value setting and a min-max setting. The numerical experiments show that the new scenario-based DMPC approach based on the reduced scenario tree is effective in improving the control performance while at the same time satisfying the constraints in the presence of uncertainties, with a relatively low computational burden compared to the case with the complete scenario tree.

Samenvatting

Modellering en Robuuste en Gedistribueerde Regeling voor Snelwegnetwerken

Verkeersmodellen zijn cruciaal voor modelgebaseerde voorspellende regeling (in het Engels: *Model Predictive Control* (MPC)) in verkeersnetwerken: zij worden gebruikt als voorspellende modellen om de optimale regelacties te bepalen. Om de rekencomplexiteit van MPC voor verkeersnetwerken te reduceren worden vaak macroscopische in plaats van microscopische modellen gebruikt. Deze macroscopische verkeersmodellen kunnen worden opgedeeld in homogene, eenklassige modellen en heterogene, meerklassige modellen. In het algemeen zijn meerklassige modellen nauwkeuriger dan eenklassige modellen, zonder dat zij significant meer rekencomplexiteit vereisen. Een nauwkeuriger model in MPC betekent in het algemeen een betere voorspelling van het te regelen systeem: de regelaar krijgt dan immers meer nauwkeurige informatie om regelacties te bepalen. Daarom is het ontwikkelen en gebruiken van meerklassige modellen een van de methodes om MPC-regelaars effectiever te laten functioneren. Naast de bovengenoemde eigenschappen van verkeersmodellen spelen andere factoren, zoals onzekerheden in externe ingangen en modelparameters, een rol in de nauwkeurigheid van de voorspellingen. Daarom bestaat een andere methode om de effectiviteit van MPC te verhogen erin de gevolgen van deze onzekerheden mee te nemen en robuuste MPC-methodes te ontwikkelen die met deze onzekerheden om kunnen gaan. Naast het verbeteren van de effectiviteit van MPC moet MPC ook geschikt gemaakt worden voor grootschalige verkeersnetwerken, dit vanwege de snelle toename van de rekencomplexiteit door de groei van de omvang van het aan te sturen systeem. Voor grote systemen wordt vaak overwogen gebruik te maken van gedistribueerde MPC (in het Engels: *Distributed Model Predictive Control* (DMPC)), omdat dat de regelaanpak qua rekentijd beheersbaar maakt. Daarnaast kan voor het garanderen van zowel haalbaarheid als robuustheid robuuste DMPC worden ontwikkeld. Vanuit deze overwegingen worden in dit proefschrift de volgende drie onderwerpen behandeld:

- het uitbreiden van diverse meerklassige macroscopische verkeersstroom- en verkeersuitstootmodellen,
- het voorstellen van een scenario-gebaseerde, verschuivende-horizon, geparametriseerde regelmethode,
- het ontwikkelen van een scenario-gebaseerde DMPC-methode met zowel algemene onzekerheden als plaatselijke onzekerheden.

Wij stellen ten eerste nieuwe meerclassige macroscopische verkeersmodellen voor waaronder een nieuw meerklassig METANET-model en twee meerclassige uitstootmodellen, nl. meerklassig VT-macro en meerklassig VERSIT+. Om de vergelijking met het nieuwe meerclassige METANET-model mogelijk te maken, breiden we ook het eerste-orde meerclassige verkeerstroombelastingmodel FASTLANE uit met variabele snelheidslimieten en toeritdosering. Deze nieuwe meerclassige macroscopische verkeersstroom- en uitstootmodellen worden gebruikt als voorspellingsmodel in MPC voor snelwegnetwerken. Daarnaast worden eindpuntermen toegevoegd aan de doelfunctie om rekening te houden met het gedrag van de verkeersstromen na de voorspeltijd. We laten met behulp van numerieke experimenten zien dat het meerclassige METANET-model gecombineerd met de uitgebreide uitstootmodellen de tijd die voertuigen in het netwerk doorbrengen en de totale uitstoot op een evenwichtige manier kunnen verminderen in vergelijking met de niet-geregelde situatie. Ook laten de experimenten zien dat het nieuwe meerclassige METANET-model de dynamiek van de maximale wachtrijlengte beter aankan dan FASTLANE, hoewel beide gebaseerd zijn op hetzelfde wachtrijmodel. Verder tonen de experimenten aan dat het toevoegen van eindpuntermen de prestaties van MPC met het nieuwe meerclassige METANET-model verder kan verbeteren, dit in tegenstelling tot methodes die met FASTLANE werken.

Verder stellen we een scenario-gebaseerde, verschuivende-horizon, geparametriseerde regelmethode (in het Engels: *Receding Horizon Parameterized Control* (RHPC)) voor. Voor deze methode maken we gebruik van een scenario-gebaseerde benadering om het robuuste regelprobleem aan te pakken. Het slechtste geval van de beschouwde scenario's wordt nu geoptimaliseerd in een min-max kader. In tegenstelling tot MPC worden in RHPC alleen de parameters van de regelwetten geoptimaliseerd en niet alle regelingen. Daardoor kan het aantal variabelen in het optimalisatieprobleem worden verminderd ten opzichte van conventionele MPC, wat de rekentijd verkort. Diverse RHPC-wetten worden ontworpen op basis van meerclassige verkeerstroombelastingmodellen. Door middel van simulatie-experimenten tonen we aan dat nominale RHPC-methodes, die onzekerheden negeren, kunnen leiden tot schending van de randvoorwaarden voor de wachtrijlengte, en dat scenario-gebaseerde RHPC het best functioneert en in staat is om de regelkwaliteit te verbeteren zonder de randvoorwaarde voor de wachtrijlengte te schenden.

Ten slotte ontwerpen we een scenario-gebaseerde DMPC-methode met aparte algemene onzekerheden en plaatselijke onzekerheden. Twee soorten onzekerheden voor grootschalige verkeersnetwerken bestaande uit verscheidene subnetwerken kunnen worden onderscheiden: algemene onzekerheden voor het hele netwerk en plaatselijke onzekerheden voor de individuele subnetwerken. We nemen aan dat al deze onzekerheden kunnen worden beschreven door eindige verzamelingen scenario's. Daardoor kan een boom die gebaseerd is op de betreffende onzekerheden, worden gebouwd. Een intuïtieve manier waarop de plaatselijke scenario's voor diverse subnetwerken kunnen worden onderscheiden, is door alle combinaties van de plaatselijke scenario's te beschouwen (d.w.z. door een complete scenarioboorn op te stellen). De rekentijd in dit geval zal echter zeer lang zijn. Daarom stellen we voor om een gereduceerde scenarioboorn op te stellen voor het combineren van plaatselijke scenario's voor diverse subnetwerken, waarin de verbindende uitgangen van een subnetwerk gecombineerd worden voor alle plaatselijke scenario's voor dat subnetwerk. Verder worden twee varianten voor de nieuwe aanpak beschouwd, nl. een verwachte-waarde variant en een min-max variant. De numerieke experimenten tonen aan dat de nieuwe scenario-gebaseerde DMPC-methode, die gebruik

maakt van de gereduceerde scenarioboorn, effectief de regelkwaliteit verbetert en ondanks de aanwezigheid van onzekerheden tegelijkertijd voldoet aan de randvoorwaarden, met een relatief lage rekentijd in vergelijking tot de methode gebaseerd op de complete scenarioboorn.

Shuai Liu

Curriculum Vitae

Shuai Liu was born in September 1988, Zhoukou, Henan Province, China. In 2009, she received the B.Sc degree from College of Aerospace Science and Engineering in National University of Defense Technology, China. Afterwards, she became a master student in the same college of the same university. In 2011, she obtained the M.Sc degree of Aeronautical and Astronautical Science and Technology.



In December 2011, she got a scholarship from the China Scholarship Council and became a Ph.D candidate at the Delft Center for Systems and Control, Delft University of Technology, the Netherlands. Under the supervision of Prof. Bart De Schutter and Prof. Hans Hellendoorn, in her Ph.D project she worked on multi-class macroscopic traffic flow and emission models, scenario-based model predictive control, and scenario-based distributed model predictive control for freeway networks.

TRAIL Thesis Series

The following list contains the most recent dissertations in the TRAIL Thesis Series. For a complete overview of more than 150 titles see the TRAIL website: www.rsTRAIL.nl.

The TRAIL Thesis Series is a series of the Netherlands TRAIL Research School on transport, infrastructure and logistics.

Liu, S., *Modeling, Robust and Distributed Model Predictive Control for Freeway Networks*, T2016/7, May 2016, TRAIL Thesis Series, the Netherlands

Calvert, S. C., *Stochastic Macroscopic Analysis and Modelling for Traffic Management*, T2016/6, May 2016, TRAIL Thesis Series, the Netherlands

Sparing, D., *Reliable Timetable Design for Railways and Connecting Public Transport Services*, T2016/5, May 2016, TRAIL Thesis Series, the Netherlands

Rasouli, S., *Uncertainty in Modeling Activity-Travel Demand in Complex Urban Systems*, T2016/4, March 2016, TRAIL Thesis Series, the Netherlands

Vries, J. de, *Behavioral Operations in Logistics*, T2016/3, February 2016, TRAIL Thesis Series, the Netherlands

Goñi-Ros, B., *Traffic Flow at Sags: Theory, Modeling and Control*, T2016/2, March 2016, TRAIL Thesis Series, the Netherlands

Khademi, E., *Effects of Pricing Strategies on Dynamic Repertoires of Activity-Travel Behaviour*, T2016/1, February 2016, TRAIL Thesis Series, the Netherlands

Cong, Z., *Efficient Optimization Methods for Freeway Management and Control*, T2015/17, November 2015, TRAIL Thesis Series, the Netherlands

Kersbergen, B., *Modeling and Control of Switching Max-Plus-Linear Systems: Rescheduling of railway traffic and changing gaits in legged locomotion*, T2015/16, October 2015, TRAIL Thesis Series, the Netherlands

Brands, T., *Multi-Objective Optimisation of Multimodal Passenger Transportation Networks*, T2015/15, October 2015, TRAIL Thesis Series, the Netherlands

Ardıç, Özgül, *Road Pricing Policy Process: The interplay between policy actors, the media and public*, T2015/14, September 2015, TRAIL Thesis Series, the Netherlands

Xin, J., *Control and Coordination for Automated Container Terminals*, T2015/13, September

2015, TRAIL Thesis Series, the Netherlands

Anand, N., *An Agent Based Modelling Approach for Multi-Stakeholder Analysis of City Logistics Solutions*, T2015/12, September 2015, TRAIL Thesis Series, the Netherlands

Hurk, E. van der, *Passengers, Information, and Disruptions*, T2015/11, June 2015, TRAIL Thesis Series, the Netherlands

Davydenko, I., *Logistics Chains in Freight Transport Modelling*, T2015/10, May 2015, TRAIL Thesis Series, the Netherlands

Schakel, W., *Development, Simulation and Evaluation of In-car Advice on Headway, Speed and Lane*, T2015/9, May 2015, TRAIL Thesis Series, the Netherlands

Dorsser, J. C. M. van, *Very Long Term Development of the Dutch Inland Waterway Transport System: Policy analysis, transport projections, shipping scenarios, and a new perspective on economic growth and future discounting*, T2015/8, May 2015, TRAIL Thesis Series, the Netherlands

Hajiahmadi, M., *Optimal and Robust Switching Control Strategies: Theory, and applications in traffic management*, T2015/7, April 2015, TRAIL Thesis Series, the Netherlands

Wang, Y., *On-line Distributed Prediction and Control for a Large-scale Traffic Network*, T2015/6, March 2015, TRAIL Thesis Series, the Netherlands

Vreeswijk, J. D., *The Dynamics of User Perception, Decision Making and Route Choice*, T2015/5, February 2015, TRAIL Thesis Series, the Netherlands

Lu, R., *The Effects of Information and Communication Technologies on Accessibility*, T2015/4, February 2015, TRAIL Thesis Series, the Netherlands

Ramos, G. de, *Dynamic Route Choice Modelling of the Effects of Travel Information using RP Data*, T2015/3, February 2015, TRAIL Thesis Series, the Netherlands

Sierzchula, W. S., *Development and Early Adoption of Electric Vehicles: Understanding the tempest*, T2015/2, January 2015, TRAIL Thesis Series, the Netherlands

Vianen, T. van, *Simulation-integrated Design of Dry Bulk Terminals*, T2015/1, January 2015, TRAIL Thesis Series, the Netherlands

Risto, M., *Cooperative In-Vehicle Advice: A study into drivers' ability and willingness to follow tactical driver advice*, T2014/10, December 2014, TRAIL Thesis Series, the Netherlands

Djukic, T., *Dynamic OD Demand Estimation and Prediction for Dynamic Traffic Management*, T2014/9, November 2014, TRAIL Thesis Series, the Netherlands

Chen, C., *Task Complexity and Time Pressure: Impacts on activity-travel choices*, T2014/8, November 2014, TRAIL Thesis Series, the Netherlands

Wang, Y., *Optimal Trajectory Planning and Train Scheduling for Railway Systems*, T2014/7, November 2014, TRAIL Thesis Series, the Netherlands

Wang, M., *Generic Model Predictive Control Framework for Advanced Driver Assistance Systems*, T2014/6, October 2014, TRAIL Thesis Series, the Netherlands